The background image shows the deck of a research vessel at sunset. In the foreground, there are large red pipes and a complex metal structure, likely part of a deep-sea sampling system. The sea is dark with whitecaps, and the sky is a mix of orange, pink, and blue. A person in an orange safety vest is visible on the left side of the deck.

Paleo-Water Column Structure In The South Pacific: Evidence from Foraminiferal $\delta^{18}\text{O}$ and Mg/Ca

Raúl Iván Tapia Arroyo

Dissertation

Kiel, 2016

Paleo-Water Column Structure In The South Pacific: Evidence from Foraminiferal $\delta^{18}\text{O}$ and Mg/Ca

Dissertation

in fulfilment of the requirements of the degree “Dr. rer. nat.” of the Faculty of
Mathematics and Natural Sciences at the Kiel University

submitted by

Raúl Iván Tapia Arroyo

Kiel, 2016

First referee: Prof. Dr. Dirk Nürnberg
Second referee: Dr. Katharina Pahnke

Date of the oral examination: 29. April 2016
Approved for publication : 18. July 2016

Signed: Prof. Dr. Wolfgang J. Duschl, Dean

Erklärung

Name: Raúl Iván Tapia Arroyo

Anschrift: Damsgårdsveien 88, 5058 Bergen, Norway

Hiermit versichere ich, dass ich (1) die Arbeit ohne unerlaubte fremde Hilfe angefertigt habe, (2) keine anderen als die von mir angegebenen Quellen und Hilfsmittel benutzt habe und (3) die den benutzten Werken wörtlich oder inhaltlich entnommenen Stellen als solche kenntlich gemacht habe.

Kiel, 5th March 2016

Raúl Iván Tapia Arroyo

*“Como no estás experimentado en las cosas del mundo,
todas las cosas que tienen algo de dificultad te parecen
imposibles.”*

*“Confía en el tiempo, que suele dar dulces salidas a muchas
amargas dificultades.”*



El Ingenioso Hidalgo Don Quijote de la Mancha
Miguel de Cervantes Saavedra (1547-1616)

Abstract

The South Pacific represents the largest sector of the Southern Ocean. Here lies the major intermediate and bottom water formation region, rendering it a key area for studies of intermediate-deep water masses such as Subantarctic Mode Water (SAMW) and Antarctic Intermediate Water (AAIW). The intermediate waters formed in the Southern Ocean (e.g. AAIW and SAMW) sequester significant quantities of anthropogenic CO₂ and other atmospheric gases in the ocean interior. These processes have been suggested to play an important role in modulating climatic variability at glacial-interglacial time scales. The AAIW and SAMW ventilate the thermocline of the oceanic gyres as well as form the link between the Southern Ocean and the tropics, via mechanisms such as “oceanic tunneling” that transport climatic signals (e.g. temperature and salinity) and nutrients across latitudes. The active participation of the AAIW and SAMW in the heat, freshwater and carbon transports at global scale renders their role relevant in climate modulation.

The central South Pacific is still poorly understood, as previous paleoceanographic reconstructions are mostly limited to the outer rim of the SPG, i.e. equatorial Pacific or close to the continental margin of South America and New Zealand. In addition, a limit in temporal coverage is evident since a large number of the reconstructions in the domain of the SPG are either time slices (Holocene-Last Glacial Maximum), or not extending beyond ~100 kyr. Therefore, the climatic history of the central South Pacific prior to MIS 5 is virtually unknown. Despite the large volume of intermediate waters formed in the South Pacific and the extensive area that the SPG covers, information regarding past changes in the formation of AAIW-SAMW and its impact on the South Pacific Gyre (SPG)'s thermocline is basically absent.

Chapter 3 of this thesis presents the first multi-species record of paired Mg/Ca ratios and stable oxygen isotope ($\delta^{18}\text{O}$) in the SPG (~ 44° S) that covers two glacial-interglacial cycles. The species selected are characterized by well-known water depth distribution, the surface dweller *Globigerina bulloides* and deep-dwellers *Globorotalia inflata* and *Globorotalia truncatulinoides*. On average, the Mg/Ca-derived sea surface temperatures (*Globigerina bulloides*) show similar conditions during the LGM and Marine Isotope Stage (MIS) 6 i.e. 9.4 °C versus 9.8 °C. On the other hand, the subsurface temperatures derived from the Mg/Ca values of *Globorotalia inflata* and *Globorotalia truncatulinoides* suggest that LGM is ~3 to ~2 °C colder than MIS 6. Furthermore, at subsurface depths the reconstructed $\delta^{18}\text{O}_{\text{sw-ivc}}$ record (proxy for relative local salinity changes) suggests opposite glacial conditions, with slightly saltier-than-Holocene waters during MIS 6, and fresher-than-Holocene waters during LGM. Contrasting glacial scenarios, plausibly due to changes in the presence of SOIWs at the

study site, suggest variable formation and/or advection of intermediate water formed in the Southern Ocean (e.g. AAIW and SAMW) to the SPG during different glacial stages.

Chapter 4 uses paired Mg/Ca-temperature, stable carbon and oxygen isotope records from surface-dwelling and deep-dwelling planktic foraminifera, *Globigerina bulloides* and *Globorotalia inflata*, to infer changes in the water column structure for the last 260 kyr in the central south Pacific (54°S). The focus of this study is to reconstruct the variability controlled by Antarctic Intermediate Water, which was subducted at the Subantarctic Front during the Last Glacial Maximum (LGM; ~29–17ka) and the Penultimate Glacial Maximum (PGM; ~180–150ka). At the study site, colder and fresher conditions at the subsurface glacial ocean suggest an enhanced presence of Antarctic Intermediate Water during glacials compared to the Holocene. At the sea surface (*Globigerina bulloides*), our data suggest comparable cooling during both glacials, however the PGM shows saltier conditions compared to the LGM. A 0.35‰ depletion in $\delta^{13}\text{C}$ from the LGM to the PGM at subsurface suggests glacial differences in the contribution of “old” low $\delta^{13}\text{C}$ deep waters to the study site. Multiple proxy records during glacial stages indicate changes in the convection depth of Antarctic Intermediate Water in the central South Pacific. Latitudinal comparisons between 54°S and 44°S (Chapter 3) suggest water column conditions (e.g. thermal gradient, mixed layer depth) that resemble the effects of climatic modes controlling the intensity of the South Westerly Winds, such as the effects of Southern Annular Mode (SAM) have on the ocean.

Chapter 5 reconstructs surface and subsurface conditions at the SPG during the last 600 kyr using paired Mg/Ca and stable isotopes. The reconstructed sea surface temperatures are characterized by small glacial-interglacial amplitude, exceptionally warm conditions are observed during MIS 15, MIS 13 and MIS 11. The evolution of the temperature and paleosalinity at subsurface ocean suggests two main stages of the presence/advection of SAMW-AAIW to the subsurface SPG, shifting from colder/fresher to warmer/saltier conditions at 320–360 kyr. This finding substantially differs from the typical SAMW-AAIW glacial-interglacial cyclicity associated with the air-sea forcing. We discuss several possible mechanisms that could lead to this difference, and the most likely explanation is a shift in the rotational speed of the SPG due to the enhanced intensity of the easterly winds during the Mid-Pleistocene Transition.

Zusammenfassung

Der Südpazifik repräsentiert den größten Teil des Südozeans. Hier befinden sich die bedeutendsten Intermediäre- und Tiefwasser Bildungsregionen, was dies zu einem Schlüsselgebiet dient um Intermediäre Wassermassen zu studieren, wie das Subantarktische Mittelwasser (SAMW) und das Antarktische Zwischenwasser (AAIW). Diese speichern bedeutsame Mengen an anthropogenen CO₂ - sowie auch andere atmosphärische Gase - im Ozeans Inneren. Diese Prozesse sollen eine wichtige Rolle spielen in der modulierung der Klimatischen Variabilität in Glazial-Interglaziale Zeitskalen. SAMW und AAIW versorgen Sauerstoff in die Thermokline und zusätzlich verlinken sie den Südozean mit den Tropischen Bereichen durch Prozesse wie das ‚oceanic tunneling‘, dass klimatische Signale (wie zum Beispiel Temperatur und Salinität) sowie Nährstoffe durch verschiedene Breiten transportieren. Die aktive Teilnahme von SAMW und AAIW in der Zufuhr von Wärme, Süßwasser und Kohlenstoff weltweit bedeutet dass diese Wassermassen eine sehr wichtige Rolle spielen in der Modulation des Klimas auf der Erde.

Der zentrale Südpazifik ist bis jetzt wenig erforscht worden, da sich die meisten Studien bis jetzt an den äußeren Rahmen des South Pacific Gyre (SPG) konzentriert haben, wie zum Beispiel im Äquatorialen Pazifik oder nah an den kontinentalrändern vor Süd Amerika oder Neuseeland. Dazu kommt ein limitiertes zeitlichen Rahmen in den bisherigen SPG Studien, die sich entweder an bestimmten Zeitscheiben konzentrieren (Holozän und letztes Glazial Maximum (LGM)), oder sich nicht vor den letzten ~100 tausend Jahren erstrecken. Demnach ist die klimatische Geschichte vom zentralen S Pazifik vor Marine Isotope Stage (MIS) 5 praktisch unbekannt. Trotz des hohen Wasservolumen der, im S Pazifik gebildeten, intermediären Wassermassen und des umfangreiches Gebietes des SPG, ist die Kenntnis über vergangene Änderungen in der Bildung von SAMW und AAIW, sowie deren Einfluss an der Thermokline des SPG, bis jetzt ungeklärt.

Im Kapitel 3 dieser These werden die ersten multi-Spezies Ergebnisse von gepaarten Mg/Ca Verhältnisse und stabile Sauerstoffisotope ($\delta^{18}\text{O}$) der letzten zwei Glazial-Interglazialzyklen des SPG (~ 44°S) präsentiert. Die gewählten Spezies charakterisieren sich für ihre bekannte Tiefenverteilung, nämlich der Oberflächen Bewohner *Globigerina bulloides* und die Tief Bewohnern *Globorotalia inflata* und *Globorotalia truncatulinoides*. Im Durchschnitt, die Mg/Ca abgeleitete Oberflächen Temperaturen (*Globigerina bulloides*) zeigen ähnliche Zustände für das LGM sowie für MIS 6, und zwar 9,4°C beziehungsweise 9,8°C. Andererseits zeigen die unter-Oberflächen abgeleiteten Mg/Ca Temperaturen (*Globorotalia inflata* und *Globorotalia truncatulinoides*) dass das LGM zwischen 2 und 3 °C kälter als MIS 6 gewesen sein soll. Außerdem, bei unter-Oberflächen Tiefen, zeigt das rekonstruierte $\delta^{18}\text{O}_{\text{sw-ivc}}$ Rekord

(ein Proxy für relative lokale Salinitätsänderungen) entgegengesetzten Glazialen Bedingungen. Diese weisen leicht salzigere Gewässer als im Holozän während MIS 6 und süßere Gewässer als im Holozän für das LGM. Diese Gegensätzliche Szenarien - durchaus möglich wegen Änderungen in der Präsenz von SOIW's - deuten unterschiedliche Bildung und/oder Advektion von intermediären Wassermassen an, die im Südozean entstanden und zum SPG geflossen seien während unterschiedliche Glazialzeiten.

Im Kapitel 4 werden gepaarte Mg/Ca abgeleiteten Temperaturen und stabile Kohlenstoff und Sauerstoffisotopen Rekorder von Oberflächen und Tief Bewohnern *Globigerina bulloides* und *Globorotalia inflata* präsentiert, um Änderungen in der Wassersäulenstruktur der letzten 260 tausend Jahre des zentralen S Pazifik (54°S) aufzuklären. Der Mittelpunkt dieser Studie sind Änderungen angetrieben von AAIW, die im Subantarktischen Front im LGM (~29-17 ka) sowie auch im vorletzten Glazialen Maximum (PGM: ~180-150 ka) subduziert wurde. Kühlere und süßere Bedingungen in unter-Oberflächen Bereiche während glazial Zeiten deuten zu einer verstärkte Präsenz von AAIW in diesen Perioden im Vergleich zum Holozän. In der Oberfläche, unsere Daten zeigen ähnliche Abkühlung während beide Glaziale, obwohl das PGM salzigere Bedingungen als das LGM andeutet. Ein Schwund von 0,35‰ im $\delta^{13}\text{C}$ Rekord vom LGM zum PGM im unter-Oberflächen Bereich, regt glaziale Unterschiede an in den Beitrag von alten, niedrigen $\delta^{13}\text{C}$ Gewässern im Untersuchungsgebiet. Mehrfache Proxy Rekorder während Glazialzeiten zeigen Änderungen in der Konvektionstiefe von AAIW im zentralen S Pazifik. Latitudinale Vergleiche zwischen 54°S und 44°S (Kapitel 3) deuten an Wassersäulenbedingungen (z. B. thermischer Gradient, Mischschichtstiefe) die von klimatisch bedingten Effekte in der Intensität von den Südlichen West Winde kontrolliert sind, wie zum Beispiel das Effekt von ‚Southern Annual Mode (SAM)‘ in den Ozean.

Kapitel 5 rekonstruiert Oberflächen und unter-oberflächen Bedingungen im SPG während der letzten 600 tausend Jahre mittels gepaarte Mg/Ca isotonen Verhältnissen. Die dadurch rekonstruierten Oberflächentemperaturen charakterisieren sich durch kleine glazial-interglaziale Amplituden, mit besonders Warme Bedingungen während MIS 15, MIS 13 und MIS 11. Die Entwicklung von Temperaturen und Paläo-salinitäten im unter-oberflächen Bereich des SPG deuten zur Präsenz von SAMW-AAIW während des Zeitraumes von 320 bis 360 ka, mit einer Verschiebung von kühleren/süßeren zu wärmeren/salzigere Bedingungen. Diese ergebnisse unterscheiden sich erheblich von der typischen SAMW-AAIW glazial-interglazialen Zyklizität verbunden mit dem Luft-Meer Zwingen. Wir diskutieren hier verschiedene Mechanismen die zu diesem Unterschied führen haben könnten. Die einleuchtende Erklärung ist eine Wechsel in der Drehzahl des SPG durch die erhöhten Intensität der Ostwinde während der Mid-Pleistocene Transition

Acknowledgments

I would like to thank to my supervisor Dirk Nürnberg for giving me the opportunity to carry out this research, particularly for his free reign-style supervision that gave me plenty of freedom to plan and carry out my research as independently as possible, as well as for his terrific help during my first days in Kiel. Special thanks goes to Martin Frank for his support during my time at GEOMAR.

I am thankful to Katharina Pahnke as well as all the members of my committee for reviewing this thesis. I would like to thank to Rainer Gersonde and Frank Lamy (AWI) for providing sediment samples, without which the project would have not been possible. I want to thank N. Gehre and L. Haxhijaj for their technical support at GEOMAR. Also, I would like to thank my colleagues Thomas Ronge, Johannes Ullermann (AWI), Mariem Saavedra-Pellitero, Jeroen Groeneveld (University of Bremen), Sergio Contreras (Universidad Católica de la Santísima Concepción), Mario Molina-Kescher (GEOMAR) for providing stimulating discussions. I want to give special acknowledgment to Ines Staben (GEOMAR-Human Resources) for her endless patience at the moment to deal with me and my questions about the administrative system.

I want to thank my family for their unconditional support and especially to my wife Ling, without whom this thesis would not exist. She helped by reading and critically commenting on the manuscripts, as well as giving moral support and encouragements during the endless writing time.

This PhD project was funded by the project SOPATRA (SOuth PACific paleoceanographic TRAnsect) funded by the German Ministry of Education and Research (BMBF) through grant No. 03G0213B and GEOMAR – Helmholtz Centre for Ocean Research Kiel.

Table of Contents

ERKLÄRUNG	IV
ABSTRACT	VI
ZUSAMMENFASSUNG	VIII
ACKNOWLEDGMENTS	X
TABLE OF CONTENTS	XI
LIST OF FIGURES	XV
LIST OF TABLES	XXII
CONTRIBUTIONS TO THIS THESIS AND RESULTING PUBLICATIONS	XXIII
CHAPTER 1	25
INTRODUCTION	25
1.1 GENERAL INTRODUCTION	26
1.2 TEMPERATURE IN THE UPPER OCEAN	26
1.3 SOUTHERN OCEAN	27
1.4 SURFACE OCEAN CIRCULATION IN THE SOUTH PACIFIC	28
1.4 INTERMEDIATE WATERS IN THE SOUTH PACIFIC	30
1.5 RELATIONSHIP BETWEEN INTERMEDIATE WATERS AND OCEANIC FRONTAL SYSTEM IN THE SOUTHERN OCEAN	33
1.6 OUTSTANDING RESEARCH ISSUES	35
1.7 REFERENCES	37
CHAPTER 2	44
GENERAL APPROACH AND METHODOLOGY	44
2.1 PROXY BACKGROUND	45
2.1.1 <i>Planktic Foraminiferal $\delta^{18}O$ and $\delta^{13}C$ as Paleo Proxies</i>	46
<i>Stable Oxygen Isotopes ($\delta^{18}O$)</i>	46
<i>Carbon Stable Isotopes ($\delta^{13}C$)</i>	48
2.1.2 <i>Planktic Foraminiferal Mg/Ca as a Paleothermometer</i>	48
2.2 MATERIALS AND METHODOLOGY	54
2.2.1 <i>Planktic Foraminifera Used for Geochemical Analyses</i>	55
2.2.2 <i>Stratigraphic Framework of Sediment Samples</i>	56
2.2.3 <i>Measuring Trace Elements and Stable Isotopes in Foraminifera</i>	57
2.3 THESIS OBJECTIVE AND OUTLINE	59
2.4. THESIS OUTLINE	60

2.5 REFERENCES	61
CHAPTER 3	70
<i>DISPARITIES IN GLACIAL ADVECTION OF SOUTHERN INTERMEDIATE WATER TO THE SOUTH PACIFIC GYRE</i>	70
ABSTRACT	70
3.1 INTRODUCTION	71
3.2 MATERIAL AND METHODS	72
3.3 RESULTS	77
3.3.1 Planktic Foraminiferal Mg/Ca-Temperatures	77
3.3.2 Planktic Foraminifera Stable Oxygen Isotopes and Relative Salinity Reconstruction	79
3.4 DISCUSSION	80
3.4.1 Assessing the Impact of Dissolution on Mg/Ca-Derived Temperatures in the South Pacific ..	80
3.4.2 Evolution of Water Column Structure in the South Pacific	82
3.4.3 Enhanced Pacific Intermediate Mode Water Formation	85
3.4.4 Glacial Variability of SOIW	86
3.5 CONCLUSIONS	89
3.6 ACKNOWLEDGMENTS	89
3.7 REFERENCES	89
CHAPTER 4	98
<i>GLACIAL SIGNATURE OF ANTARCTIC INTERMEDIATE WATER AT THE CENTRAL SOUTH PACIFIC: IMPLICATIONS FOR SUBSURFACE TRANSFER OF CLIMATIC SIGNAL</i>	98
ABSTRACT	98
4.1 INTRODUCTION	99
4.2 MATERIAL AND METHODS	102
4.2.1 Stable Isotopes and Mg/Ca paleothermometry	102
4.2.2 Seawater $\delta^{18}\text{O}$ and Relative Salinity Calculation	103
4.3 RESULTS	104
4.3.1 Planktic Foraminiferal Mg/Ca-Temperature	104
4.3.2 Foraminiferal $\delta^{18}\text{O}$ and Relative Salinity at Surface and Subsurface	105
4.3.3 Planktic Foraminiferal $\delta^{13}\text{C}$	105
4.4. DISCUSSION	107
4.4.1 Past Sea Surface Temperatures in the Central South Pacific	107
4.4.2 Vertical T and S Structure: Frontal Migration or Wind Intensity?	108
4.4.3 SOIWs Presence and Transport in the South Pacific During Glacials	110
4.4.4 Glacial Changes in Upwelling Strength Indicated by $\delta^{13}\text{C}$ Variability	112

4.4.5 Southern Annular Mode–like during LGM and PGM?	113
4.5 SUMMARY	115
4.6 ACKNOWLEDGMENTS.....	116
4.7 REFERENCES	116
SUPPLEMENTARY MATERIAL	121
S1. Age Model and Chronology.....	121
S2. Assessing cleaning efficiency.....	121
S3. Assessing the impact of dissolution on Mg/Ca–derived temperatures	122
S4. Estimated vertical distribution of <i>G. bulloides</i> and <i>G. inflata</i>	122
S. References	123
CHAPTER 5	125
<i>EVOLUTION OF THE SOUTH PACIFIC GYRE’S THERMOCLINE DURING THE LAST 600 KYR.....</i>	125
ABSTRACT.....	125
5.1 INTRODUCTION	126
5.2 MATERIAL AND METHODS	128
5.2.2 Foraminiferal Mg/Ca-temperatures and salinity approximation.....	128
5.3 RESULTS	131
5.3.1 Planktic foraminiferal Mg/Ca-temperature.....	131
5.3.2 Oxygen stable isotopes in planktic foraminifera and relative salinity reconstructions.....	131
5.4. DISCUSSION.....	132
5.4.1 Assessing the sea surface and subsurface Mg/Ca-temperature reconstructions in the SPG.	132
.....	132
5.4.2 Past surface conditions at the South Pacific	133
5.4.3 Subsurface south Pacific and SAMW-AAIW variability.....	135
5.4.4 Air-sea forcing and SAMW-AAIW formation.....	136
5.5 CONCLUSIONS.....	138
5.6. ACKNOWLEDGMENTS.....	138
5.7 REFERENCES	138
CHAPTER 6	148
SUMMARY AND CONCLUSION	148
6.1 GENERAL CONCLUSIONS	149
6.2 FUTURE PERSPECTIVES FOR FUTURE WORKS.....	151
6.3 DATA HANDLING.....	152
6.4 REFERENCES	152
APPENDIX 1	154

EVOLUTION OF THE SEA SURFACE TEMPERATURE AND $\Delta^{18}\text{O}$ IN THE CENTRAL SOUTH PACIFIC DURING THE PAST 500 KA: IMPLICATIONS ON OCEAN CIRCULATION	154
ABSTRACT.....	154
APPENDIX 2	155
REDUCED ADMIXTURE OF NORTH ATLANTIC DEEP WATER TO THE DEEP CENTRAL SOUTH PACIFIC DURING THE LAST TWO GLACIAL PERIODS	155
ABSTRACT.....	155
APPENDIX 3	156
DATA COMPILATION	156
GLACIAL SIGNATURE OF ANTARCTIC INTERMEDIATE WATER AT THE CENTRAL SOUTH PACIFIC: IMPLICATIONS FOR SUBSURFACE TRANSFER OF CLIMATIC SIGNAL.....	156
EVOLUTION OF THE SOUTH PACIFIC GYRE'S THERMOCLINE DURING THE LAST 600 KYR.....	167
EVOLUTION OF THE SEA SURFACE TEMPERATURE AND $\Delta^{18}\text{O}$ IN THE CENTRAL SOUTH PACIFIC DURING THE PAST 500 KA: IMPLICATIONS ON OCEAN CIRCULATION.....	175

List of Figures

- Figure 1.1 Differences on heat content in the upper ocean (700 meters) during 2014 relative to the average from 1993-2014. Locations below-average and above-average are denoted in blue and orange, respectively (from NOAA; www.climate.gov). 26
- Figure 1.2 A schematic view of the (a) major ocean currents of the Southern Hemisphere oceans south of 20° S and (b) meridional circulation, fronts and relevant zones in the Southern Ocean. An upper circulation cell is formed by northward Ekman transport beneath the westerly winds belt and southward eddy transport in the Upper Circumpolar Deep Water layer. The lower circulation cell is driven primarily by formation of dense AABW near the Antarctic continent. Continental shelf water (CSW), Antarctic surface water (ASSW), Subantarctic mode water (SAMW), Antarctic Intermediate water (AAIW), Subantarctic surface water (SASW), subtropical surface water (STSW), Antarctic slope front (ASF), Southern Boundary (SB), Southern ACC front (SACCF), Polar front (PF), Subantarctic front (SAF) and subtropical front (STF) [modified from Talley et al., 2011]. 22
- Figure 1.3 Ekman spiral occurs as consequence of the Coriolis force. The average flow over the full spiral is call Ekman transport, and is at 90° to the direction of the wind. (from NOAA, www.oceanservice.noaa.gov). 23
- Figure 1.4 (a) Mean austral summer (DJF) winds in ms^{-1} based on 12 year of CCMP data (2000-2011). The white dotted contour indicates the mean position of the maximum westerlies (~55° S) [from Carranza and Gille, 2015]. 24
- Figure 1.5 Schematic of the various processes involve in the formation of SAMW in the SE-Pacific [from Holte et al., 2013]. 25
- Figure 1.6 Colour chart denoting the subsurface salinity (300 water depth m), and the inferred subduction areas (shaded ellipses) with their respective maximum export path (green arrows) related to SAMW and AAIW in the Pacific sector of the Southern Ocean [Sallée et al., 2010; Hartin et al., 2011; Herraiz-Borreguero and Rintoul, 2011; Bostock et al., 2013]. 32
- Figure 1.7 (a) Averaged salinity values between 2004 and 2012 at 32° S. Trajectory-based transport (2004 to 2012) for the section 180° to 94.4° W (b) separated into 1°C by 1 psu bins, (c) per unit of temperature (°C) summed across all the salinities, and (d) per 1 psu of salinity summed across the temperatures [modified from Zilberman et al., 2014]. 27
- Figure 1.8 Bathymetric chart showing the location of sites relevant to this thesis. Sea surface temperature reconstructions in the south Pacific can be categorized in continuous records (in orange) and Holocene-LGM time-slices (in green). Records used to reconstruct intermediate waters (in yellow) are restricted to the continental margins [Luz, 1977; Mashiotta et al., 1999; Bostock et al., 2004; Pahnke and Zahn, 2005; Loubere and Bennett, 2008; Pena et al., 2008; De Pol-Holz et al., 2010; Muratli et al., 2010; Rose et al., 2010; Caniupán et al., 2011; Ho et al., 2012; Martínez-

List of Figures

- Méndez et al., 2013; Pena et al., 2013; Schiraldi et al., 2014; Elmore et al., 2015; Ronge et al., 2015]. The position of the SAF is denoted by blue line. 34
- Figure 2.1 Idealized scheme of the habitat of SST signal carriers. Corals and phytoplankton grow only in the photic zone, which normally overlaps with the mixed layer, however some species of planktic foraminifera can live below the photic zone and record deeper water temperatures (i.e. thermocline) [modified from Kucera, 2009]. 39
- Figure 2.2 Illustration of the Rayleigh distillation process on the $\delta^{18}\text{O}$ values as clouds move over land and into the polar regions. Decreasing air temperatures cause moisture to rain/snow out of the cloud. Fractionation of the oxygen isotopes during condensation further decreases values. By the point that a cloud reaches the high latitudes, less than 10% of the original water vapor remains. Snowfall on Antarctica has values between -20 and 60‰. The average $\delta^{18}\text{O}$ for ice on Antarctica \sim -40‰, modified from Rohling and Cooke [1999]. 47
- Figure 2.3 Mg/Ca calibration for several species of planktic foraminifera, temperatures were isotopically derived [Anand et al., 2003]. The data can be describe by a single equation [modified from Baker et al., 2005]. 50
- Figure 2.4 Location of the sediment samples (red) used; SO213-59 (chapters 3), PS75/059-2, (chapters 4, Appendix 1), SO213-60 (chapters 5, Appendix 2), PS75/034-1, PS75/051-2, PS75/056-2, PS75/076-1 and PS75/079-2 (Appendix 1). Main oceanographic features in the South Pacific ACC front (SACCF), Polar front (PF), Subantarctic front (SAF) and Subtropical front (STF) are denoted by lines. 54
- Figure 2.5 SEM from the planktic species selected in this thesis. Surface dweller *G. bulloides* (a), the deep-dwellers *G. inflata* (b) and *G. truncatulinoides* (c). (Hayward [2015]; www.marinespecies.org). 56
- Figure 3.1 (a) Chart showing salinity (colours) and temperature (white contour lines; WOA09) at 150 m water. The location of the core SO213-59-2 and reference sites MD97-2120 [Pahnke et al., 2003], EC11-2 [Mashiotta et al., 1999], GeoB3327-5 [Ho et al., 2012], ODP 1233 [Muratli et al., 2010] and GeoB15016 [Martínez-Méndez et al., 2013] are indicated by diamonds. The main SOIW formation area and dispersal path are marked by white area and arrows [after Hartin et al., 2011; Herraiz-Borreguero and Rintoul, 2011b]. Dashed lines denote the oceanographic frontal boundaries: the Subtropical Front (STF, grey), the Subantarctic Front (SAF, yellow), and the Polar Front (PF, red) [Orsi et al., 1995]. (b) Vertical profile of the annual mean, the seasonal mean, the minimum and the maximum summer temperature of the upper 600 m of the water column at the core location (WOA09). The average Holocene Mg/Ca–temperature for *G. bulloides* (1), *G. inflata* (2) and *G. truncatulinoides* (3) are plotted against the estimated habitat water depth of each species. The depth ranges of *G. bulloides* (< 50 m), *G. inflata* (~50 – 100 m) and *G. truncatulinoides* (> 150 m) are used to define “surface water”, “thermocline water” and “deep–thermocline water”. Boxes mark ranges of Mg/Ca–temperatures from surface sediments + Holocene sediments. (c) Detail of the S-N transect denoted in (a; vertical bar), indicating the vertical distribution of SAMW (26.6 – 27 kgm^{-3} ; ~100 – 600 m) and AAIW (> 27 kgm^{-3} ; > 600 m) [Tsuchiya and Talley, 1998; Hanawa and

Talley, 2001]. Numbers in the white boxes correspond to the assumed habitat depth range of the planktic foraminifera species analyzed as in (b). Open circle with dot denotes eastward directed flow of the maximum SWW. Colour-coded arrows mark oceanic fronts depicted in (a).

73

Figure 3.2 Mg/Ca plotted against (a) Mn/Ca and (b) Fe/Ca, low values and lack of covariance indicate that contamination has not controlled Mg/Ca variability

69

Figure 3.3 Foraminiferal (isotope) geochemical data of core SO213-59-2. (a) Age model for core SO213-59-2 based on the correlation of the benthic foraminiferal $\delta^{18}\text{O}$ record (blue curve) to the benthic $\delta^{18}\text{O}$ stack LR04 (grey curve) [Lisiecki and Raymo, 2005]. Auxiliary AMS¹⁴C age control points are indicated by black triangles (Table 2). Shaded bars indicate glacial intervals; black numbers in the bars represent the Marine Isotope Stages (MIS). Calculated seawater Mg/Ca-temperatures (red circles, red curve illustrates 3-points running average) and $\delta^{18}\text{O}$ (blue circles, blue curve illustrates 3-points running average) derived from (b) *G. bulloides*, (c) *G. inflata* and (d) *G. truncatulinoides*. SST_{Mg/Ca} = seasurface temperature, TT_{Mg/Ca} = thermocline temperature, DTT_{Mg/Ca} = deep-thermocline temperature. Surface sediment data from MUC SO213-59-1 are indicated by grey squares. Continuous grey lines denote average temperatures computed per each isotopic stage (MIS 1 to MIS 6). Orange arrows indicate the summer ocean temperature at 50 m (b, assumed mean living depth of *G. bulloides*), 75 m (c, assumed mean living depth of *G. inflata*) and 300 m (d, assumed mean living depth of *G. truncatulinoides*) water depth (WOA09); cyan arrows denote the modern temperature of SOIWs in the SEP (4-5 °C)[Hartin et al., 2011]. The downcore SST_{Mg/Ca} and $\delta^{18}\text{O}$ record of core SO213-59-2 shows smaller variability than the high resolution SST_{Mg/Ca} and $\delta^{18}\text{O}$ record (*G. bulloides*) reconstruction from the MD97-2120 (thin grey line) at 45° S [Pahnke et al., 2003; Cléroux et al., 2007].

78

Figure 3.4 Comparison of (a) mean ocean $\delta^{18}\text{O}_{\text{sw}}$ and the reconstructed local salinity anomalies for (b) Chatham Rise core MD97-2120 [Pahnke et al., 2003] and our study site SO213-59-2 in the SPG at (c) surface, (d) thermocline and (e) deep-thermocline level. Grey continuous lines denote species-specific mean Holocene values (surface sediments plus 0 – 10 ka). Continuous lines are the 3 points running average of the raw data (circles). Black dashed lines denote average values computed per each isotopic stage (MIS 1 to MIS 6).

80

Figure 3.5 (a) Random selection of shell weights plotted against Mg/Ca in *G. bulloides* and *G. truncatulinoides*, in both cases the coefficient of correlation (R^2) is < 0.1, discarding dissolution as the main factor controlling Mg/Ca variability. Calcite saturation horizon (CSH, $\Omega_{\text{CALCITE}} = 1$ for transects P16S 2005 (b) and P06 2003 (c), calculated from the DIC and alkalinity in the CARINA database [Brown and Elderfield, 1996; Key et al., 2010]. Location of the transects and the core SO213-59-2 (red diamond) is shown on the maps.

81

Figure 3.6 (a) Salinity and temperature differences ($\Delta\delta^{18}\text{O}_{\text{sw-ivc}}$ and ΔT) during LGM (blue) and MIS 6 (red) in comparison with mean Holocene values at surface (circle), thermocline (square) and deep-thermocline (triangle). Colder- and fresher-than-Holocene subsurface waters characterize LGM.

MIS 6 conditions are saltier-than-Holocene and warmer-than-LGM subsurface waters. (b) Scheme illustrating the water column conditions during MIS 6 (red) and LGM (blue) with different positions of the thermocline and different strengths of SOIW advection. $\Delta T_{\text{SST-DTT}}$ marks the temperature gradient between $\text{SST}_{\text{Mg/Ca}}$ of *G. bulloides* and $\text{DTT}_{\text{Mg/Ca}}$ of *G. truncatulinoides*, and $\Delta T_{\text{TT-DTT}}$ marks the temperature gradient between $\text{TT}_{\text{Mg/Ca}}$ of *G. inflata* and $\text{DTT}_{\text{Mg/Ca}}$ of *G. truncatulinoides*.

84

Figure 3.7 (a) Vertical temperature gradient in the water column. Orange line indicates the temperature gradient between sea surface ($\text{SST}_{\text{Mg/Ca}}$) and the deep-thermocline ($\text{DTT}_{\text{Mg/Ca}}$). Blue line denotes the temperature gradient between thermocline ($\text{TT}_{\text{Mg/Ca}}$) and deep-thermocline ($\text{DTT}_{\text{Mg/Ca}}$). (b) Calculated seawater isotopic differences ($\Delta\delta^{18}\text{O}_{\text{sw}}$). Purple colour lines indicate the $\Delta\delta^{18}\text{O}_{\text{sw}}$ between *G. bulloides* and *G. truncatulinoides* (Gb–Gt). Green colour lines denote $\Delta\delta^{18}\text{O}_{\text{sw}}$ between *G. inflata* and *G. truncatulinoides* (Gi–Gt). Thicker continuous lines denote average values computed per each isotopic stage (MIS 1 to MIS 6). (c) The $\delta^{13}\text{C}$ gradient between GeoB15016 and the Pacific Deep Water (PDW) stack ($\Delta\delta^{13}\text{C}_{\text{DIC}}$). Positive $\Delta\delta^{13}\text{C}_{\text{DIC}}$ values indicate measurable presence of AAIW, dashed cyan line denotes the modern $\Delta\delta^{13}\text{C}_{\text{DIC}}$ (0.4‰) for site GeoB15016 [Martínez-Méndez et al., 2013]. (d) Insoluble dust flux in EPICA Dome C ice core (blue) [Lambert et al., 2008] and the long-chain odd carbon-numbered n-alkanes (brown) and Fe flux (red) at core location PS2489–2/ODP1090 [Martínez-García et al., 2009]

88

Figure 4.1 (a) Bathymetric chart of the South Pacific showing the studied sediment core PS75/059-2 and reference sites discussed in the text: MD97-2120 [Pahnke et al., 2003], SO213-59-2 [Tapia et al., 2015], E20-18, RC12-225, E11-1 [Luz, 1977], E11-2 [Mashiotta et al., 1999], GeoB15016 [Martínez-Méndez et al., 2013], ODP1233 [Muratli et al., 2010], GeoB3327-5 and PS75/034-1 [Ho et al., 2012]. Major currents and oceanographic fronts [Orsi et al., 1995] are indicated: Subtropical Front (STF, yellow), Polar Front (PF, black) and Subantarctic Front (SAF, dotted), which separates cold and fresher polar surface waters from the warmer and saltier surface waters to the north. Subantarctic Mode Water (SAMW) forms north of the SAF (shaded area denotes the surface density of $\sigma_{\theta} = 26.6 \text{ kgm}^{-3}$ at 75 m); denser Antarctic Intermediate Water (AAIW) forms south of the SAF and north of the PF, and flows northwards below SAMW (arrows). (b) Temperature ($^{\circ}\text{C}$), density (σ_{θ} in kgm^{-3} ; dashed grey contours) and salinity (black contours) profile along the transect denoted in (a), clarifying the vertical distribution of SAMW, AAIW, and Upper Circumpolar Deep Water (UCDW). UCDW brings low $\delta^{13}\text{C}$ to the surface south of the PF. Open circle with dot denotes eastward-directed flow of the maximum SWW [Carranza and Gille, 2015]. Coloured arrows mark core positions and oceanic fronts (SAF and PF).

100

Figure 4.2 Foraminiferal proxy data of core PS75/059-2: (a) Benthic foraminiferal $\delta^{18}\text{O}$ record (blue) from core PS75/059-2 in comparison to the EPICA Dome C ice core Deuterium record (δD ; grey) displaying relative air temperature variations over East Antarctica (Antarctic Plateau) [Jouzel et al., 2007]. Records of planktic foraminifers *G. bulloides* (red) and *G. inflata* (blue): (b) Calculated Mg/Ca-temperatures, (c) $\delta^{18}\text{O}$ and (d) $\delta^{13}\text{C}$; $\delta^{13}\text{C}$ values were corrected according to Schiraldi et al.

List of Figures

[2014]. For comparison Mg/Ca-temperatures and $\delta^{18}\text{O}$ values from *N. pachyderma* (green) at site E11-2 at 56°S are added [Mashiotta et al., 1999]. Shaded bars mark the Last Glacial Maximum (LGM, ~29–17 ka) and the Penultimate Last Glacial Maximum (PGM, ~180–150 ka). Dashed (*G. bulloides*) and continuous (*G. inflata*) grey lines denote averaged values per each isotopic stage; symbols denote the averaged temperatures and $\delta^{13}\text{C}$ values during LGM and PGM for *G. bulloides* (orange) and *G. inflata* (light blue). Grey arrows denote $\delta^{13}\text{C}$ *G. inflata* minima. For comparison, the high resolution subsurface $\delta^{13}\text{C}$ record from the Equatorial Pacific [Pena et al., 2008] is provided (thin black line). The resemblance, timing and prominence of the CIMEs [Spero and Lea, 2002] suggest that the light $\delta^{13}\text{C}$ -signals in core PS75/059-2 represent large-scale water mass signatures. Coloured arrows on y-axes denote the averaged Holocene (0–8 ka) values for each species. 106

Figure 4.3 (a) Mean ocean $\delta^{18}\text{O}_{\text{SW}}$ (grey line) [Waelbroeck et al., 2002] in comparison to the benthic isotopic foraminiferal record at site PS75/059-2 (thin black line). Reconstructed local subsurface salinity anomaly ($\Delta\delta^{18}\text{O}_{\text{SW-IVC}}$) derived from *G. inflata* at the SPG (45° S) core site SO213-59-2 [Tapia et al., 2015] (b, green), and at the central south Pacific study site PS75/059-2 (54° S) (c, blue). In addition, the local surface $\Delta\delta^{18}\text{O}_{\text{SW-IVC}}$ record derived from *G. bulloides* (d, red) is shown. Shaded bars mark LGM (~29–17 ka) and PGM (~180–150 ka). Continuous black lines denote species-specific mean Holocene $\Delta\delta^{18}\text{O}_{\text{SW-IVC}}$ values for cores PS75/059-2 (< 8ka) and SO213-59-2 (< 10ka), dashed lines denoted averaged values per isotopic stage, averaged values during LGM and PGM are denoted by coloured symbols. 108

Figure 4.4 Surface (circle) and subsurface (square) differences in Mg/Ca_{Temperature} (a) and $\delta^{13}\text{C}$ (b) relative to the Holocene (0–8 ka) versus salinity ($\Delta\delta^{18}\text{O}_{\text{SW-IVC}}$) at the core site PS75/059-2 during the LGM (blue) and PGM (red). The LGM and PGM time slices are characterized by colder- and fresher-than-Holocene subsurface waters. At surface LGM and PGM show comparable cooling and contrasting salinities. The $\Delta\delta^{13}\text{C}$ data during the LGM and the PGM are characterized by comparable values at surface and large discrepancy at subsurface. 111

Figure 4.5 Subsurface temperatures and $\delta^{18}\text{O}_{\text{SW-IVC}}$ at cores SO213-59-2 (45°S; triangle) and PS75/059-2 (54°S; hexagon) during the PGM (dark red) and the LGM (blue). 111

Figure 4.6 Schematic diagram showing the response of the ocean to the high index-polarity of the Southern Annular Mode [Thompson et al., 2011; Ayers and Strutton, 2013; Tapia et al., 2015]. The past change in mixed-layer depth (MLD) is inferred from the vertical thermal gradient (ΔT , continuous lines) between Mg/Ca-temperatures from *G. bulloides* ($\text{SST}_{\text{Mg/Ca } G.\text{bulloides}}$) and *G. inflata* ($\text{SubST}_{\text{Mg/Ca } G.\text{inflata}}$) and inferred surface- and subsurface- $\delta^{18}\text{O}_{\text{SW}}$ ($\Delta\delta^{18}\text{O}_{\text{SW}}$, dashed lines) (see text for details), differentiated for the LGM (green) and the PGM (pink) at 45° S and 54° S, respectively. Arrows indicate inferred horizontal and vertical water mass migration. Colour coding (red to blue) corresponds to either increased or decreased temperatures/heat content. 115

Figure S1 Stratigraphic framework of core PS75/059-2. (a) The $\delta^{18}\text{O}$ record of the benthic foraminifer *Cibicidoides* spp (blue curve) was correlated to the benthic $\delta^{18}\text{O}$ reference stack LR04 of Lisiecki

List of Figures

- and Raymo [2005](grey curve) using the program using the software “Match” [Lisiecki and Lisiecki, 2002]. Black triangles mark the stratigraphic tie lines between both records. (b) Linear sedimentation rates of sediment core PS75/059-2, ranging between 2 and 6 cm per 1000 years [Ullermann, 2015]. 121
- Figure S2 Mg/Ca plotted against (a) Fe/Ca, (b) Mn/Ca and (c) Al/Ca, low values (<0.14 mmolmol⁻¹) and lack of evident correlation with Mg/Ca ($R^2 < 0.3$) suggest that contamination has not controlled Mg/Ca variability in *G. bulloides* (red) and *G. inflata* (blue). 121
- Figure S3 Shell weights plotted against Mg/Ca in *G. bulloides*, the coefficient of correlation (R^2) is <0.1, discards dissolution as the main factor controlling Mg/Ca variability. 122
- Figure S4 Vertical profile of the minimum and the maximum summer temperature WOA09, CTD cast and WOCE P17E of the upper 600 – 700 m of the water column; averaged Mg/Ca-temperature for *G. bulloides* (circle) and *G. inflata* (square) from upper most sediments sites PS75/059-2 and PS75/056-1. Colored boxes mark inferred vertical distribution assuming an error of $\pm 1^\circ\text{C}$. The inlet shows detail of the selected water column station WOA09 (pink square), CTD cast (green circle) and WOCE stations cruise P17E (yellow box) and study site (red diamond). 123
- Figure 5.1 Circulation pattern in the South Pacific and location of the sediment core site SO213-60-1 as well as the reference cores discussed in this study. Surface water circulation includes Antarctic Circumpolar Current (ACC); Humboldt Current System (HCS), South Equatorial Current (SEC), East Australian Current (EAC). Shaded areas show the location of the Subtropical Mode Water (STMW), Subantarctic Mode Water (SAMW) and Antarctic Intermediate Water (AAIW). Subantarctic front (SAF; blue line) [Orsi et al., 1995] divides the Arrows denote the flow of the SAMW and AAIW. 127
- Figure 5.2 Correlation of benthic $\delta^{18}\text{O}$ signal from the core SO213-60-1 (*U. peregrina*) (blue) and the core ODP 1123 (gray). The linear sedimentation rate (green) is on average is 1.78 cmkyr⁻¹; ranging from 0.2 to 7.9 cmkyr⁻¹. 128
- Figure 5.3 Mg/Ca plotted against (a) Fe/Ca, (b) Mn/Ca and (c) Al/Ca, low values and lack of covariance indicates that contamination has not controlled Mg/Ca variability of *G. bulloides* (red) and *G. inflata* (blue). 130
- Figure 5.4 Foraminiferal Mg/Ca ratios for *G. bulloides* (orange) and *G. inflata* (blue) for the core SO213-60-1 (circle), surface samples SO213-60-2 (triangle) and SO213-59-1 (square) [Tapia et al., 2015]. Shaded bars indicate glacial intervals; black numbers in the bars represent the Marine Isotope Stages (MIS). 131
- Figure 5.5a) Calculated seawater Mg/Ca-temperatures at sea surface (orange) and subsurface (blue). Red dashed lines denote the G-IG amplitude ($\sim 3^\circ\text{C}$) at surface; blue dashed line highlights two main stages of the subsurface temperatures (warmer/colder than $\sim 7^\circ\text{C}$). b) Stable isotopic ($\delta^{18}\text{O}$) record of *G. bulloides* (red) and *G. inflata* (blue). The subsurface dweller *G. inflata* displays an increasing $\delta^{18}\text{O}$ -amplitude toward present, although surface dweller *G. bulloides* shows a relatively constant $\delta^{18}\text{O}$ -amplitude ($\sim 0.7\text{‰}$) along the core, the section prior to 320-360 ka is characterized

List of Figures

- by heavier values than the younger section. c) Paleosalinity reconstructions (expressed as $\delta^{18}\text{O}_{\text{SW-IVC}}$) are characterized by low amplitude at surface (red), on the other hand at subsurface (blue) the $\delta^{18}\text{O}_{\text{SW-IVC}}$ suggest two stages shifting from fresher conditions to saltier conditions at ~300-360 kyr (reddish bar). Shaded bars indicate glacial intervals; black numbers in the bars represent the Marine Isotope Stages (MIS). 134
- Figure 5.6 Vertical gradients in the water column in green thermal ($\Delta T_{\text{SST-SubST}}$) and in orange the seawater isotopic composition ($\Delta\delta^{18}\text{O}_{\text{SW G.bulloides-G.inflata}}$). 136
- Figure 6.1 Bathymetric chart showing (shaded area) a possible area of interest to future studies regarding the evolution of the intermediates water formed at SEP. 152

List of Tables

Table 2.1 Summary of published Mg/Ca-temperature calibrations for single and multiple species of planktic, a very good agreement has been achieved between all three approaches [<i>Lea et al., 1999; Elderfield and Ganssen, 2000; Dekens et al., 2002; Anand et al., 2003; Barker et al., 2005; McConnell and Thunell, 2005; Greaves, 2008; Cléroux et al., 2013</i>].	50
Table 2.2 List of sediment samples selected for this study. Surface samples were collected with Multicore (MUC), meanwhile downcore were collected through Gravity core (GC) and Piston core (PC).	54
Table 2.3 AMS ¹⁴ C ages analyzed on planktic foraminifera and calibrated ages.	57
Table 2.4 List of species and calibration used in the differents chapters of this thesis.	59
Table 3.1 Acronyms and abbreviations.	72
Table 3.2 AMS ¹⁴ C ages analyzed on planktic foraminifera and calibrated ages at the site SO213-59 (45°49` S, 116°52` W).	74
Table 3.3 Values of “Vital Effects” reported in the literature.	76

Contributions to this Thesis and Resulting Publications

This thesis is part of project SOPATRA (South Pacific paleoceanographic TRAnsect). The project SOPATRA written by Martin Frank and Dirk Nürnberg was funded by the *Bundesministerium für Forschung und Bildung* (BMBF), through the grant No. 03G0213B. The material used as substrate for the analysis presented in the different chapters that compose this were collected during the cruise SOPATRA (coded SO213) onboard the *R/V Sonne*, in which one I participated, and the cruise ANT-XXVI/2 (coded PS75) onboard the *R/V Polarstern*.

Manuscript 1 Chapter 3

This chapter was published in *Earth Planetary Science Letters* (volume 410, pages 152 – 164, doi 10.1016/j.epsl.2014.11.031) authored by **R. Tapia**, D. Nürnberg, T. Ronge and R. Tiedemann under the title of “*Disparities in glacial advection of Southern Ocean Intermediate Water to the South Pacific Gyre*”.

R. Tiedemann and D. Nürnberg provided the sedimentological material. I performed the foraminiferal species selection, planktic foraminiferal picking, weighting, and preparation of the material (surface sediments and core sediments) for Mg/Ca and stable isotopic analysis, as well as the selection of the material for surface analysis of ^{14}C . T. Ronge provided the age model of the core SO213-59-2. I wrote the manuscript, D. Nürnberg and T. Ronge commented on the manuscript.

Manuscript 2 Chapter 4

This chapter is for submission to *Earth Planetary Science Letters* authored by **R. Tapia**, D. Nürnberg, J. Ullerman, F. Lamy, S. L. Ho, R. Gersonde and R. Tiedemann under the title of “*Glacial signature of southern ocean intermediate water: subsurface transfer of southern climatic signals into the central South Pacific*”.

I performed the manual extraction, preparation of the material (surface sediments and core sediments) for Mg/Ca and stable isotopic analysis of *G. inflata*. J. Ullermann provided the Mg/Ca and stable isotopic data for the planktic foraminifera *G. bulloides*. F. Lamy and J. Ullermann provided the age model of the core PS75/059-2. I wrote the manuscript, D. Nürnberg, S. L. Ho, F. Lamy, R. Gersonde and J. Ullermann commented on the manuscript.

Manuscript 3 Chapter 5

I wrote this chapter to be submitted to *Paleoceanography* under the title of “*Evolution of the South Pacific Gyre’s thermocline in the past 600 kyr*”. I performed the foraminiferal picking, the preparation of the material (surface sediments and core sediments) for Mg/Ca

and stable isotopic analysis, the age model of the core SO213-60-1. D. Nürnberg commented on the manuscript.

Appendix 1

The manuscript entitled “Evolution of the sea surface temperature and salinity in the central South Pacific during the past 500 ka: Implications on ocean circulation” authored by J. Ullermann, **R. Tapia**, F. Lamy, D. Nürnberg, R. Gersonde and R. Tiedemann is in preparation to be submitted to Quaternary Science Reviews. For this manuscript, I measured the Mg/Ca and stable isotopic records from the planktic foraminifera *G. bulloides* (core PS75/056-1), and contributed in the interpretation and discussion of this manuscript.

Appendix 2

This manuscript is under review in Paleooceanography under the title “Changes of the deep-water circulation in the central South Pacific during the last two glacial-interglacial cycles” authored by M. Molina-Kescher, M. Frank, **R. Tapia**, T. Ronge, D. Nürnberg and R. Tiedemann. For this manuscript, I measured the stable isotopic record ($\delta^{18}\text{O}$ and $\delta^{13}\text{C}$) of sediment core SO213-60-1, established the age model for the afore mentioned sediment core and commented on the manuscript written by M. Molina-Kescher.



INTRODUCTION

CHAPTER 1

1.1 General Introduction

Temperature is one of the physical parameters of the climate system. Knowledge of oceanic temperatures is critical for a better understanding of the global climate system because the ocean represents one of the largest reservoirs of latent heat on Earth. Ocean currents are the major means of heat redistribution at the Earth's surface (Figure 1.1), influencing climate change on timescales of greater than a few hundred years [Kucera, 2009; Hartin *et al.*, 2011; Gupta and McNeil, 2012; Bostock *et al.*, 2013]. Therefore, the acquisition of quantitative data of the oceans' temperature, both in space and time, is a crucial step in building realistic numerical climate models for future climate projection.

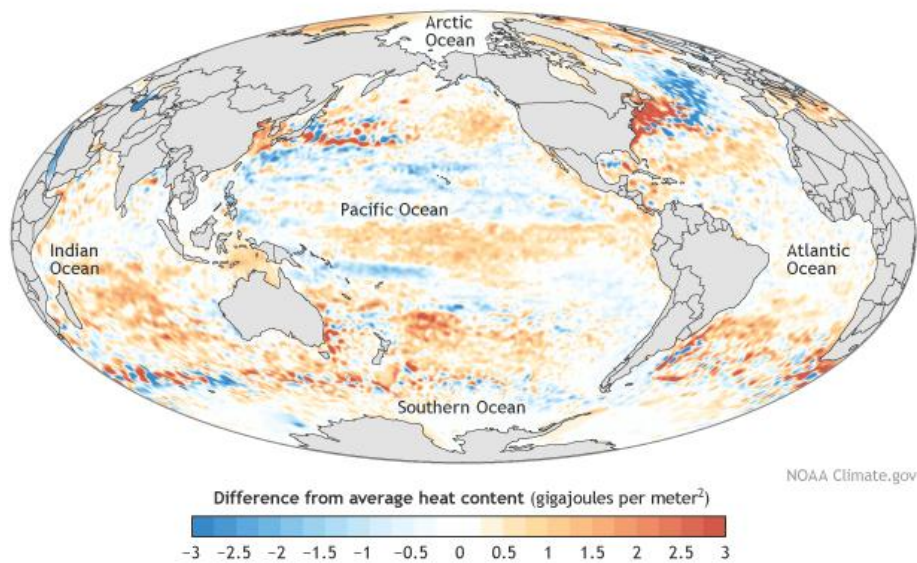


Figure 1.1 Differences on heat content in the upper ocean (700 meters) during 2014 relative to the average from 1993-2014. Locations below-average and above-average are denoted in blue and orange, respectively (from NOAA; www.climate.gov).

1.2 Temperature in the Upper Ocean

The surface ocean derives its temperature from solar insolation, whereas the temperature of the deep (intermediate) waters is relatively constant and preserves the temperature signature at the place of their origin [Talley *et al.*, 2011]. The upper ocean interacts with the wind and waves, mixing the water and distributing the warmth. This results in a body of waters with nearly uniform physical properties, known as the mixed layer. The depth of the mixed layer typically ranges from 50 to 100 m. However, it can also be as thin as a few metres during calm weather and intense heating (summer), and exceeding 400 m in windy conditions such as in the Southern Ocean [Dong *et al.*, 2008]. The state of oceanic stratification is diagnostic of large atmospheric circulation patterns, such as the Walker

circulation [McClymont and Rosell-Melé, 2005], water formation [Dong et al., 2008; Holte et al., 2012; 2013] and critical in regulating southern hemisphere's climatic modes such as the "El Niño" events [McPhaden et al., 2006; Merkel et al., 2010].

1.3 Southern Ocean

The Southern Ocean (SO) is the most important connection between the Atlantic, Indian and Pacific Ocean basins, playing an essential role in the redistribution of heat, salt, nutrients, gases and other properties throughout the global ocean (Figure 1.2) [Sloyan and Rintoul, 2001b; Tomczak and Godfrey, 2001; Sarmiento et al., 2004; Metzl et al., 2006; Loubere and Bennett, 2008; Talley et al., 2011]. Old, cold, nutrient-rich water upwells to the surface of the SO and enhances biological productivity along the main oceanic fronts [Anderson et al., 2009]. Thus the SO acts as an important biogeochemical exchange venue, orchestrating the transfer of nutrients between deep and surface waters, as well as the exchange of carbon between the ocean and atmosphere, via the biological pump and direct sea-air exchange [Sabine et al., 2004; Verdy et al., 2007; Carter et al., 2014]. In fact, 40% of the global oceanic uptake of anthropogenic CO₂ (~0.7 – ~1.2 Pg C yr⁻¹, 1Pg = 10¹⁵ g) is sequestered in the SO south of 35° S [Brown et al., 2015; Xue et al., 2015]. As such, it plays a significant role in slowing the accumulation of CO₂ in the atmosphere and in regulating the Earth's climate system [Sabine et al., 2004; Lovenduski et al., 2007; Sallée et al., 2012]

As a result, increasing scientific attention is being paid to the SO. Over the years, efforts have been made to evaluate past oceanographic changes here, via models, observations and proxy reconstructions. One major scientific interest is in the evolution of the water masses formed in the SO, given their role in connecting the deep ocean and the atmosphere, and ventilating the intermediate and abyssal depths of much of the world oceans [Rosenthal et al., 2000; Anderson et al., 2002; Ninnemann and Charles, 2002; Robinson et al., 2007; Loubere and Bennett, 2008; Anderson et al., 2009; Labracherie et al., 2010; Burke and Robinson, 2012].

The South Pacific represents the largest sector of the SO. Here lies the major intermediate and bottom water formation regions [McCartney, 1977; Hartin et al., 2011; Talley et al., 2011; Tomczak and Godfrey, 2013], rendering it a key area for studies of intermediate-deep water masses. However, the central South Pacific (~100° to 140° W) is still poorly understood, as previous paleoceanographic reconstructions are mostly limited to Holocene/Last Maximum Glacial time slices [e.g. Luz, 1977; Gersonde et al., 2003; 2005], and continuous reconstruction does not extend further than ~100 kyr [e.g. Mashiotta et al., 1999; Loubere and Bennett, 2008].

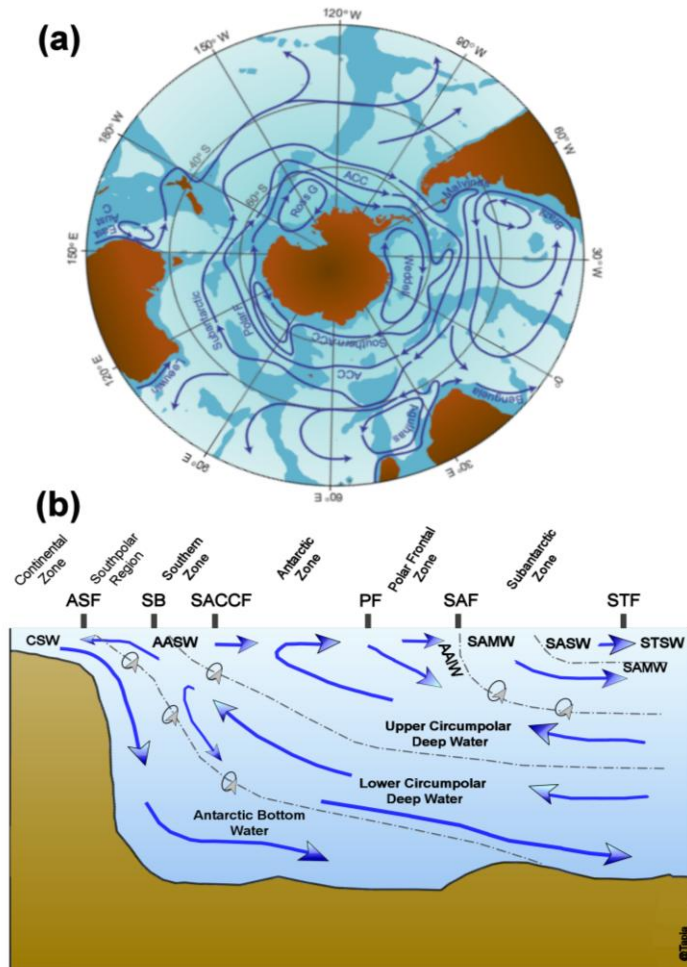


Figure 1.2 A schematic view of the (a) major ocean currents of the Southern Hemisphere oceans south of 20° S and (b) meridional circulation, fronts and relevant zones in the Southern Ocean. An upper circulation cell is formed by northward Ekman transport beneath the westerly winds belt and southward eddy transport in the Upper Circumpolar Deep Water layer. The lower circulation cell is driven primarily by formation of dense AABW near the Antarctic continent. Continental shelf water (CSW), Antarctic surface water (ASW), Subantarctic mode water (SAMW), Antarctic Intermediate water (AAIW), Subantarctic surface water (SASW), subtropical surface water (STSW), Antarctic slope front (ASF), Southern Boundary (SB), Southern ACC front (SACCF), Polar front (PF), Subantarctic front (SAF) and subtropical front (STF) [modified from Talley et al., 2011].

1.4 Surface Ocean Circulation in the South Pacific

Ocean currents redistribute the heat on Earth, both at the surface and at depths. Circulations in the ocean are controlled by wind (wind-driven circulation) and density differences (thermohaline circulation). Although different in their physical mechanism, wind-driven and thermohaline circulations are not independent from each other [Talley et al., 2011]. The currents generated by these processes are further modified by factors as deep waters, seafloor topography (e.g. shape of the basin) and Earth's rotation. Wind-driven circulation is more energetic than thermohaline circulation, and affects the upper layers of the ocean (upper 2 km) [Jones and Toba, 2001].

Although the surface currents are primarily dependent on the blowing wind (e.g. direction, intensity), the apparent direction of any ocean current results from the interplay between the wind stress and Coriolis force, which causes the deflection of any moving body on Earth. The wind blowing across the ocean drags the water immediately underneath, initiating motion in the upper layer. This process is then propagated downward in the water

column (Ekman layer) [Tomczak and Godfrey, 2001], with motion of water layers dragging the layer directly underneath it. Once the internal friction reduces the motion started by the wind, Coriolis force becomes more relevant; and the deflection is more “efficient” with the depth (Ekman spiral) (Figure 1.3). Because of the deflection by Coriolis force the net transport of the water is 90° to wind’s direction (Ekman transport). The amount of water transported in the Ekman layer is independent of its depth and only depends on the wind and Coriolis force [Tomczak and Godfrey, 2001].

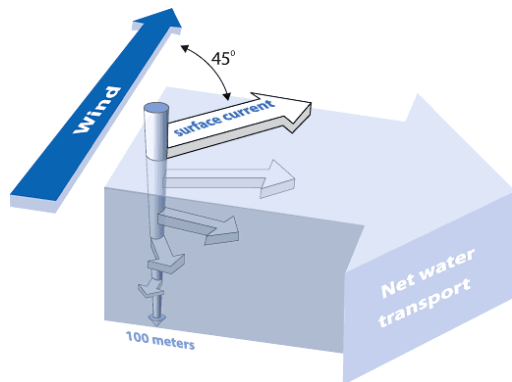


Figure 1.3 Ekman spiral occurs as consequence of the Coriolis force. The average flow over the full spiral is call Ekman transport, and is at 90° to the direction of the wind. (from NOAA, www.oceanservice.noaa.gov).

Although the major wind patterns on Earth are relatively stable (e.g. Trade winds, Westerlies and Polar Easterlies), temporal variability in wind strength and direction in these systems, thereby also the Ekman transport, is to be expected. In some regions the Ekman transport produces an accumulation (convergence) of surface waters, but in other it removes surface water (producing divergences). The accumulation or export of surface water to or from specific areas affect the upper ocean structure. For example, the typical east-west tilt of the thermocline in the equatorial Pacific is a consequence of the warm water being piled up against Australia by the Trade winds.

In the southern hemisphere between 30° and 60°, the prevailing winds blow from west towards the east (Figure 1.5). The Southern Westerly Winds (SWWs) propel the largest oceanic current, the Antarctic Circumpolar Current, and influence the global climate system at different time scales. Consequently, the SWWs are often considered as a vital factor responsible for the glacial to interglacial CO₂ increase observed in ice-cores [Anderson et al., 2009; Hodgson and Sime, 2010; Siani et al., 2013]. Toggweiler et al., [2006], in the so-called “westerly shift” hypothesis, proposed that during the deglaciations the poleward-shifted and/or strengthened SWW enhanced the Southern Ocean (SO) upwelling, amplifying the deep-ocean ventilation thereby resulting in a larger respired CO₂ outgassing into the atmosphere.

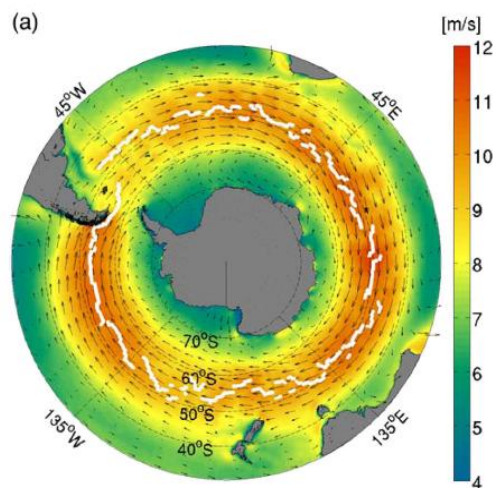


Figure 1.4 (a) Mean austral summer (DJF) winds in ms^{-1} based on 12 year of CCMP data (2000-2011). The white dotted contour indicates the mean position of the maximum westerlies ($\sim 55^\circ$ S) [from Carranza and Gille, 2015].

In spite the relevance of the SWW on Earth's climate, a general consensus on its potential displacement and/or strengthening relative to modern conditions is still lacking [Kohfeld *et al.*, 2013]. Simulations from Atmosphere General Circulation Models (AGCMs) and Atmosphere-Ocean General Circulation Models (AOGCMs) produce contrasting results regarding the position and intensity of the SWW during the LGM relative to today; from an equatorward shift [Williams and Bryan, 2006] and weakened strength [Kim *et al.*, 2002; 2003], a poleward shift and increased strength [Shin *et al.*, 2003; Sime *et al.*, 2013], to an increase in strength with no latitudinal shift [Otto-Bliesner *et al.*, 2006].

On the other hand, marine paleo-evidence mostly supports an equatorward shift of the SWW during glacials, in spite of the fact that the link between paleoceanographic data (SST reconstructions) and the wind field is not always straightforward [Kohfeld *et al.*, 2013]. Reconstructed SST from the SEP have often been interpreted as reflecting large equatorward shift of SWW and the oceanic front system (Subtropical Front (STF), Polar Front (PF) and Subantarctic Front (SAF)) during glacial stages [Feldberg and Mix, 2003; Gersonde *et al.*, 2003; 2005; Kaiser *et al.*, 2005; Verleye and Louwye, 2010; Caniupán *et al.*, 2011; Ho *et al.*, 2012; Lamy and DePol-Holz, 2013]. This is in contrast to the central south Pacific, where reconstructions based on siliceous microfossils counting have suggested a minor glacial northward displacement of the PF ($< 4^\circ$) during the LGM [Gersonde *et al.*, 2003; 2005]. Meanwhile, in the southwest Pacific, most of the reconstructions suggest no migration of the oceanic fronts during glacials [Kohfeld *et al.*, 2013 and reference therein].

1.4 Intermediate Waters in the South Pacific

The Southern Ocean Intermediate waters (SOIWs), including Subantarctic Mode Water (SAMW) and Antarctic Intermediate Water (AAIW), are relevant vehicles connecting

high-low latitudes [Liu *et al.*, 2002; Sarmiento *et al.*, 2004; Dubois *et al.*, 2011; Pena *et al.*, 2013], as well as the atmosphere and the deep ocean, by sequestering anthropogenic CO₂ and other atmospheric gasses in the ocean interior [McCartney, 1977; Russell and Dickson, 2003; Sabine *et al.*, 2004; Talley *et al.*, 2011]. Several studies have suggested a tight link between these intermediate waters formed in the SO and the atmospheric CO₂ variations in the past [Spero and Lea, 2002; Bostock *et al.*, 2004; Pahnke and Zahn, 2005; Anderson *et al.*, 2009; Basak *et al.*, 2010; Ziegler *et al.*, 2013].

The formation and physical properties of SAMW and AAIW are influenced by the interplay of numerous processes (Figure 1.5). Earliest studies related the formation of the AAIW to the Antarctic surface waters (AASW) [Deacon, 1937; 1982]. AASW is converted to AAIW through air-sea fluxes equatorward of the Polar Front (PF) and subducts at the Subantarctic front (SAF) [Sloyan and Rintoul, 2001a]. AAIW is characterized by a vertical salinity minimum at intermediate water depths (~500 – 1500 m water depth). SAMW is located equatorward of AAIW formation, at the northern side of the SAF (throughout the Southern Hemisphere) [Hartin *et al.*, 2011], where the deepening of mixed layers during wintertime convection and the subsequent mixing controls its formation [Sloyan *et al.*, 2010; Holte *et al.*, 2013] (Figure 1.5)

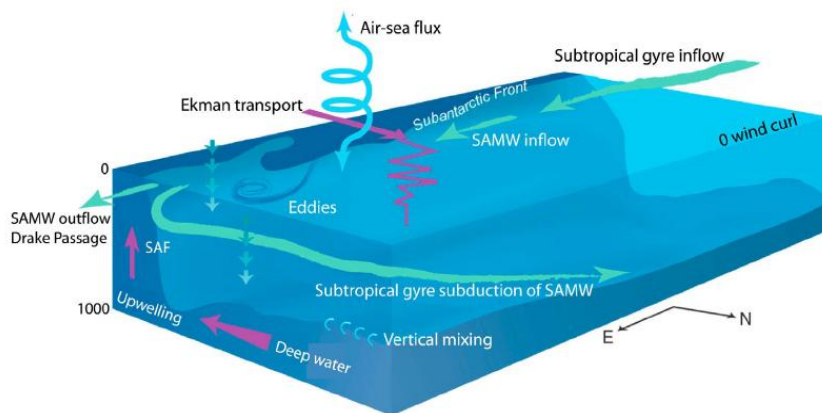


Figure 1.5 Schematic of the various processes involve in the formation of SAMW in the SE-Pacific [from Holte *et al.*, 2013].

The temperature and salinity properties of the SAMW-AAIW are controlled by the incorporation of fresh water via precipitation, ice melt and northward Ekman transport [Schneider and Bravo, 2006]. McCartney [1977] argued that the formation of AAIW is related to SAMW, as they share similar temperature and salinity properties in the southeast Pacific (SEP). In the literature, AAIW is often considered as the coldest and densest variety of SAMW [Sloyan *et al.*, 2010; Hartin *et al.*, 2011; Herraiz-Borreguero and Rintoul, 2011; Holte *et al.*, 2012]. On the other hand, Molinelli [1981] suggested that AAIW is formed by isopycnal exchange across the PF with two major hotspots of formation; one in the SEP and the other

near the Kerguelen Plateau (southern Indian Ocean). However, some studies have proposed that the presence of these two “mechanisms of formation” in different locations are necessary to explain the observed range of AAIW characteristics [Piola and Gordon, 1989; Bostock et al., 2013].

Although several formation centres of intermediate waters have been identified in the South Pacific, the main region supplying SAMW and AAIW to the Pacific Ocean is the SEP (Figure 1.6) [McCartney, 1977; Tsuchiya and Talley, 1996; Tsimplis et al., 1998; Tsuchiya and Talley, 1998; Wijffels et al., 2001; Bostock et al., 2010; Sallée et al., 2010; Sloyan et al., 2010; Hartin et al., 2011; Herraiz-Borreguero and Rintoul, 2011; Bostock et al., 2013; Zilberman et al., 2014].

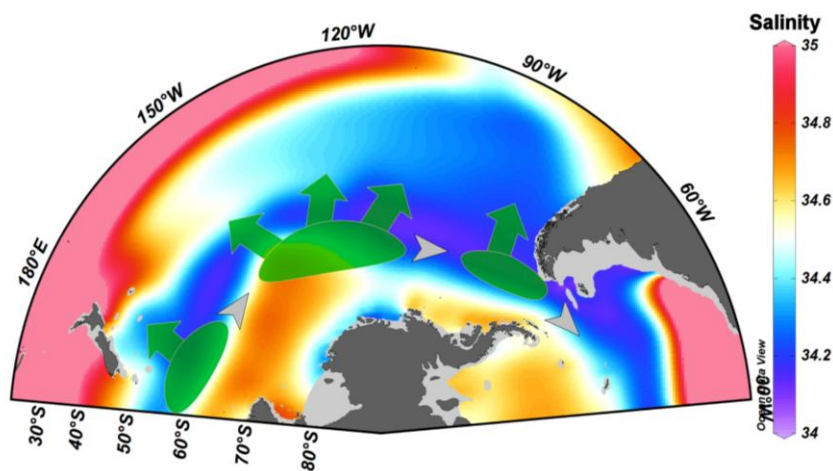


Figure 1.6 Colour chart denoting the subsurface salinity (300 water depth m), and the inferred subduction areas (shaded ellipses) with their respective maximum export path (green arrows) related to SAMW and AAIW in the Pacific sector of the Southern Ocean [Sallée et al., 2010; Hartin et al., 2011; Herraiz-Borreguero and Rintoul, 2011; Bostock et al., 2013].

The circulation of the intermediate water (SAMW and AAIW) in the South Pacific follows the wind-driven subtropical gyre surface circulation [Bostock et al., 2010; Zilberman et al., 2014] (Figure 1.7), eastward with the Antarctic Circumpolar Current (ACC), and northward into the adjacent subtropical gyres. The AAIW can be traced throughout the subtropical gyre by its distinctive salinity minimum [Tsuchiya and Talley, 1996; 1998; Schneider et al., 2005].

At 32°S the meridional circulation between 180° to ~70° W at subsurface transports cool and fresh SAMW and AAIW towards the equator (Figure 1.7) [Tsimplis et al., 1998; Wijffels et al., 2001; Schneider et al., 2003; Chaigneau, 2005; Ridgway and Dunn, 2007; Tomczak, 2007; Sloyan et al., 2010; Herraiz-Borreguero and Rintoul, 2011; Bostock et al., 2013; Zilberman et al., 2014]. The SAMW and AAIW later return poleward in the East

Australian Current region ($> 180^\circ$ W) as saltier and warmer waters [Bostock et al., 2010; 2013; Zilberman et al., 2014] (Figure 1.7).

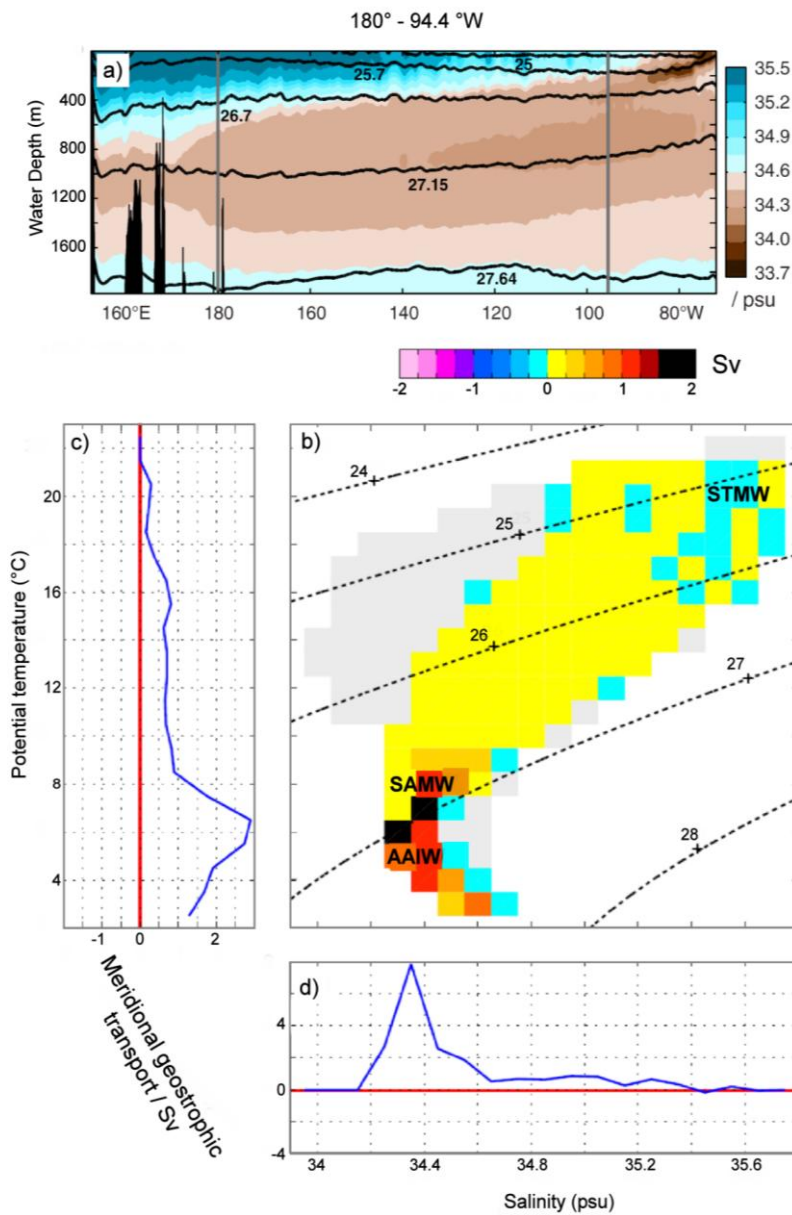


Figure 1.7 (a) Averaged salinity values between 2004 and 2012 at 32° S. Trajectory-based transport (2004 to 2012) for the section 180° to 94.4° W (b) separated into 1°C by 1 psu bins, (c) per unit of temperature ($^\circ\text{C}$) summed across all the salinities, and (d) per 1 psu of salinity summed across the temperatures [modified from Zilberman et al., 2014].

1.5 Relationship Between Intermediate Waters and Oceanic Frontal System in the Southern Ocean

The SAMW and AAIW are related to the oceanic fronts [McCartney, 1977; Molinelli, 1981; Sloyan et al., 2010; Hartin et al., 2011; Carter et al., 2014], as their physical properties are controlled by wind driven processes such as the Ekman transport, eddy fluxes, convection mixing, and mixing within the SAF [McCartney, 1977; Ribbe, 2001; Santoso and England, 2004; Lovenduski and Gruber, 2005; Schneider and Bravo, 2006; Dong et al.,

2008; Sijp and England, 2008; Sallée et al., 2010; Sloyan et al., 2010; Hartin et al., 2011; Carter et al., 2014] (see section 1.4). This relationship has been studied by numerous proxy reconstructions at mid and low latitudes (Figure 1.8). Stronger glacial SWW and latitudinal displacement of the frontal system together with its associated formation centres of intermediate water in the Southern Ocean have been recurrently invoked to explain the enhanced SOIW's signature during cold periods [Pena et al., 2008; Muratli et al., 2010; Martínez-Méndez et al., 2013; Pena et al., 2013]. However, an opposite scenario, i.e. reduced formation of SOIWs during cold periods has been suggested for the South West Pacific (SWP) off New Zealand [Pahnke and Zahn, 2005; Ronge et al., 2015]. Ronge et al. [2015] invoked a combination of lower salinities in the upper ocean and reduced wind-stress due to a northward displacement of the SWW during glacial stages in the ACC's sector.

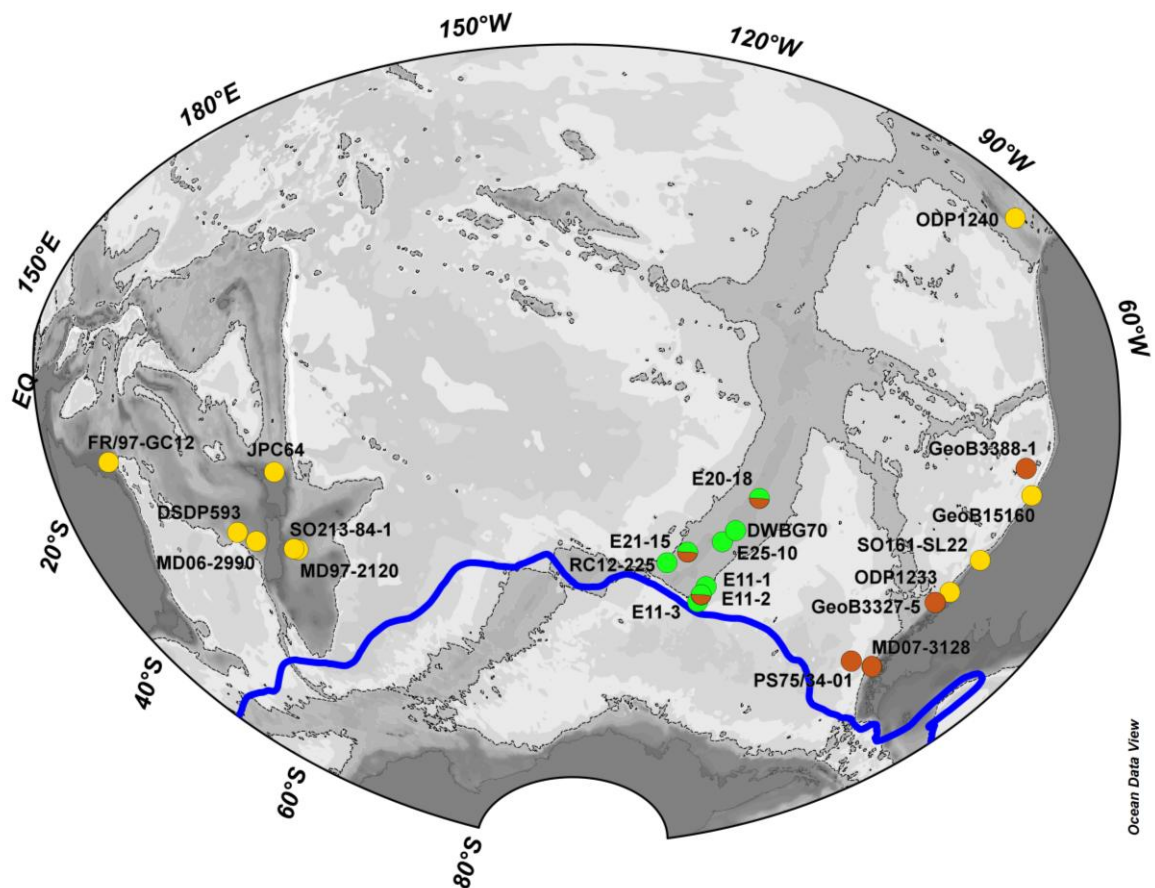


Figure 1.8 Bathymetric chart showing the location of sites relevant to this thesis. Sea surface temperature reconstructions in the south Pacific can be categorized in continuous records (in orange) and Holocene-LGM time-slices (in green). Records used to reconstruct intermediate waters (in yellow) are restricted to the continental margins [Luz, 1977; Mashiotta et al., 1999; Bostock et al., 2004; Pahnke and Zahn, 2005; Loubere and Bennett, 2008; Pena et al., 2008; De Pol-Holz et al., 2010; Muratli et al., 2010; Rose et al., 2010; Caniupán et al., 2011; Ho et al., 2012; Martínez-Méndez et al., 2013; Pena et al., 2013; Schiraldi et al., 2014; Elmore et al., 2015; Ronge et al., 2015]. The position of the SAF is denoted by blue line.

These regional differences emphasize further need of geographical constraint in the data-poor South Pacific, in order to better understand the spatio-temporal variability in SOIW's formation/distribution in the South Pacific basin.

1.6 Outstanding Research Issues

To date there is no report of past changes of the water column structure (surface to thermocline) in the SPG. Indeed most of the paleoceanographic reconstructions in the south Pacific are located at the outer rim of the SPG, i.e. equatorial Pacific, South Pacific (~ 55° S) or close to the continental margin of South America or New Zealand (Figure 1.8). These represent just a small area of the vast South Pacific. In addition, a limit in temporal coverage is evident since a large number of the reconstructions in the domain of the SPG are time slices (e.g. Holocene vs LGM) [Gersonde *et al.*, 2003; 2005] or cover no more than the last ~100 kyr (e.g. E11-2, E21-15 and E20-18) [Luz, 1977; Mashiotta *et al.*, 1999; Loubere and Bennett, 2008] (Figure 1.8). Consequently the climatic history of the surface South Pacific prior to MIS 5 is virtually unknown, as well as its response to large climatic reorganization of the glacial-interglacial cycles such as the Mid-Brunhes Event (MBE) or Mid-Pleistocene Transition (MPT).

Whereas the sea surface temperature reconstructions in the South Pacific are scarce and with limited temporal coverage, studies on the evaluation of the upper ocean structure are absent altogether, since to do so requires both surface and subsurface proxy data. This lack of information leaves a basic question such as “Has the SAMW-AAIW changed over time in the SPG?” without a proper answer.

In the South Pacific, the long term evolution of SAMW-AAIW has been largely inferred from benthic foraminifera $\delta^{13}\text{C}$ from New Zealand and Chilean margin [Pahnke and Zahn, 2005; Martínez-Méndez *et al.*, 2013; Ronge *et al.*, 2015]. Changes in the benthic foraminiferal $\delta^{13}\text{C}$ signature through time have been interpreted as the vertical movement of AAIW's lower boundary (~1500 m water depth), which interacts with the Upper Circumpolar Deep Water (UCDW) or Pacific Deep Water (PDW). This approach assumes that the presence “of a similar signature” to modern day AAIW- $\delta^{13}\text{C}$ signature across time depends on the amount of water being produced and advected to a specific site.

Interestingly two opposing scenarios regarding AAIW changes have been suggested for the South Pacific. Benthic foraminiferal $\delta^{13}\text{C}$ suggests a stronger AAIW signal during glacial stages in the eastern South Pacific [Martínez-Méndez *et al.*, 2013], but the opposite, i.e. stronger presence of AAIW during interglacial stages, in the southwest Pacific [Pahnke and Zahn, 2005; Ronge *et al.*, 2015]. At the same time, reconstructions based on deep dwelling planktic foraminifera [Pena *et al.*, 2008; 2013] and ventilation proxies [Muratli *et al.*,

2010] support the idea of an enhanced AAIW-signal during glacials. Martinez-Mendez et al. [2013] suggested that this dichotomy of SWP-SEP reflects large latitudinal disparities in the AAIWs properties as a result of different formation processes. These contrasting observations emphasize the need of better resolved geographic information in order to constraint the spatio-temporal variability of SAMW and AAIW in the South Pacific basin.

Taking into consideration the aforementioned issues, this thesis is driven by three main specific scientific questions:

- Did the SAMW-AAIW signatures change over time in the SPG?
- How do changes in SAMW-AAIW's signature at the SPG relate to previous reconstructions in the South Pacific?
- How has the upper ocean structure evolved during the Pleistocene in the SPG?

1.7 References

- Anderson, R. F., S. Ali, L. I. Bradtmiller, S. H. H. Nielsen, M. Q. Fleisher, B. E. Anderson, and L. H. Burckle (2009), Wind-driven upwelling in the Southern Ocean and the deglacial rise in atmospheric CO₂, *Science*, 323(5920), 1443–1448.
- Anderson, R. F., Z. Chase, M. Q. Fleisher, and J. Sachs (2002), The Southern Ocean's biological pump during the last glacial maximum, *Deep-Sea Research Part II*, 49(9), 1909–1938.
- Basak, C., E. E. Martin, K. Horikawa, and T. M. Marchitto (2010), Southern Ocean source of, *Nat. Geosci.*, 3(11), 770–773, doi:10.1038/ngeo987.
- Bostock, H. C., B. N. Opdyke, and M. J. M. Williams (2010), Characterising the intermediate depth waters of the Pacific Ocean using $\delta^{13}\text{C}$ and other geochemical tracers, *Deep-Sea Res. Part I*, 57(7), 847–859, doi:10.1016/j.dsr.2010.04.005.
- Bostock, H. C., B. N. Opdyke, M. K. Gagan, and L. K. Fifield (2004), Carbon isotope evidence for changes in Antarctic Intermediate Water circulation and ocean ventilation in the southwest Pacific during the last deglaciation, *Paleoceanography*, 19, PA4013, doi:10.1029/2004PA001047.
- Bostock, H. C., P. J. Sutton, M. Williams, and B. N. Opdyke (2013), Reviewing the circulation and mixing of Antarctic Intermediate Water in the South Pacific using evidence from geochemical tracers and Argo float trajectories, *Deep-Sea Res. Part I*, 73, 84–98, doi:10.1016/j.dsr.2012.11.007.
- Brown, P. J. et al. (2015), Carbon dynamics of the Weddell Gyre, Southern Ocean, *Global Biogeochem. Cycles*, doi:10.1002/2014GB005006.
- Burke, A., and L. F. Robinson (2012), The Southern Ocean's Role in Carbon Exchange During the Last Deglaciation, *Science*, 335(6068), 557–561, doi:10.1126/science.1208163.
- Caniupán, M., F. Lamy, C. B. Lange, J. Kaiser, H. Arz, R. Kilian, O. B. Urrea, C. Aracena, D. Hebbeln, and C. Kissel (2011), Millennial-scale sea surface temperature and Patagonian Ice Sheet changes off southernmost Chile (53° S) over the past~ 60 kyr, *Paleoceanography*, 26(3), PA3221, doi:10.1029/2010PA002049.
- Carter, B. R., L. D. Talley, and A. G. Dickson (2014), Mixing and remineralization in waters detrained from the surface into Subantarctic Mode Water and Antarctic Intermediate Water in the southeastern Pacific, *J. Geophys. Res. Oceans*, n/a–n/a, doi:10.1002/2013JC009355.
- Chaigneau, A., and Ó. Pizarro (2005), Surface circulation and fronts of the South Pacific Ocean, east of 120°W, *Geophys. Res. Lett.*, 32(8), doi:10.1029/2004GL022070.
- De Pol-Holz, R., L. Keigwin, J. Southon, D. Hebbeln, and M. Mohtadi (2010), No signature of abyssal carbon in intermediate waters off Chile during deglaciation, *Nat. Geosci.*, 3(3), 192–195, doi:10.1038/ngeo745.
- Deacon, G. (1937), The hydrology of the Southern Ocean, *Discovery Report*.
- Deacon, G. E. R. (1982), Physical and biological zonation in the Southern Ocean, *Deep-Sea*

Res, 29, 1–15.

- Dong, S., J. Sprintall, S. T. Gille, and L. Talley (2008), Southern Ocean mixed-layer depth from Argo float profiles, *J. Geophys. Res.*, 113(C6), doi:10.1029/2006JC004051.
- Dubois, N., M. Kienast, S. Kienast, C. Normandeau, S. E. Calvert, T. D. Herbert, and A. Mix (2011), Millennial-scale variations in hydrography and biogeochemistry in the Eastern Equatorial Pacific over the last 100 kyr, *Quat. Sci. Rev.*, 30(1-2), 210–223, doi:10.1016/j.quascirev.2010.10.012.
- Elmore, A. C., E. L. McClymont, H. Elderfield, S. Kender, M. R. Cook, M. J. Leng, M. Greaves, and S. Misra (2015), Earth and Planetary Science Letters, *Earth Plan. Sci. Lett.*, 428(C), 193–203, doi:10.1016/j.epsl.2015.07.013.
- Feldberg, M. J., and A. C. Mix (2003), Planktonic foraminifera, sea surface temperatures, and mechanisms of oceanic change in the Peru and south equatorial currents, 0–150 ka BP, *Paleoceanography*, 18(1), 1016, doi:10.1029/2001PA000740.
- Gersonde, R. et al. (2003), Last glacial sea surface temperatures and sea-ice extent in the Southern Ocean (Atlantic-Indian sector): a multiproxy approach, *Paleoceanography*, 18(3), 1061, doi:10.1029/2002PA000809.
- Gersonde, R., X. Crosta, A. Abelmann, and L. Armand (2005), Sea-surface temperature and sea ice distribution of the Southern Ocean at the EPILOG Last Glacial Maximum—a circum-Antarctic view based on siliceous microfossil records, *Quat. Sci. Rev.*, 24(7), 869–896, doi:10.1016/j.quascirev.2004.07.015.
- Gupta, Sen, A., and B. I. McNeil (2012), Variability and change in the Ocean, in *The Future of the World's Climate*, edited by A. Henderson-Sellers and K. McGuffie, pp. 141–165, Elsevier, Amsterdam.
- Hartin, C. A., R. Fine, B. M. Sloyan, L. D. Talley, T. K. Chereskin, and J. Happell (2011), Formation rates of Subantarctic mode water and Antarctic intermediate water within the South Pacific, *Deep-Sea Res. Part I*, 58, 524–534, doi:10.1016/j.dsr.2011.02.010.
- Herraiz-Borreguero, L., and S. R. Rintoul (2011), Subantarctic mode water: distribution and circulation, *Ocean Dynamics*, 61(1), 103–126, doi:10.1007/s10236-010-0352-9.
- Ho, S. L., G. Mollenhauer, F. Lamy, A. Martínez-García, M. Mohtadi, R. Gersonde, D. Hebbeln, S. Nuñez-Ricardo, A. Rosell-Melé, and R. Tiedemann (2012), Sea surface temperature variability in the Pacific sector of the Southern Ocean over the past 700 kyr, *Paleoceanography*, 27(4), PA4202, doi:10.1029/2012PA002317.
- Hodgson, D. A., and L. C. Sime (2010), Southern westerlies and CO₂, *Nat. Geosci.*, 3(10), 666–667, doi:10.1038/ngeo970.
- Holte, J. W., L. D. Talley, T. K. Chereskin, and B. M. Sloyan (2013), Subantarctic mode water in the southeast Pacific: Effect of exchange across the Subantarctic Front, *J. Geophys. Res. Oceans*, 118(4), 2052–2066, doi:10.1002/jgrc.20144.
- Holte, J. W., L. D. Talley, T. K. Chereskin, and B. M. Sloyan (2012), The role of air-sea fluxes in Subantarctic Mode Water formation, *J. Geophys. Res.*, 117, C03040, doi:10.1029/2011JC007798.

- Jones, I. S. F., and Y. Toba (Eds.) (2001), *Wind Stress Over the Ocean*, Cambridge University Press, New York.
- Kaiser, J., F. Lamy, and D. Hebbeln (2005), A 70-kyr sea surface temperature record off southern Chile (Ocean Drilling Program Site 1233), *Paleoceanography*, 20(4), doi:10.1029/2005PA001146.
- Kim, S.-J., F. G. B. G., and M. N. (2002), A coupled climate model simulation of the Last Glacial Maximum, Part 1: transient multi-decadal response, *Clim. Dyn.*, 19(5-6), 515–537, doi:10.1007/s00382-002-0243-y.
- Kim, S.-J., G. Flato, and G. Boer (2003), A coupled climate model simulation of the Last Glacial Maximum, Part 2: approach to equilibrium, *Clim. Dyn.*, 20(6), 635–661, doi:10.1007/s00382-002-0292-2.
- Kohfeld, K. E., R. M. Graham, A. M. de Boer, L. C. Sime, E. W. Wolff, C. Le Quéré, and L. Bopp (2013), Southern Hemisphere westerly wind changes during the Last Glacial Maximum: paleo-data synthesis, *Quat. Sci. Rev.*, 68, 76–95, doi:10.1016/j.quascirev.2013.01.017.
- Kucera, M. (2007), Planktonic Foraminifera as Tracers of Past Oceanic Environments, in *Proxies in Late Cenozoic Paleoceanography*, vol. 1 of Developments in Marine Geology, edited by C. Hillaire-Marcel and A. de Vernal, pp. 213–262, Elsevier.
- Labracherie, M., L. D. Labeyrie, J. Duprat, E. Bard, M. Arnold, J.-J. Pichon, and J.-C. Duplessy (2010), The last deglaciation in the Southern Ocean, *Paleoceanography*, 4(6), 629–638, doi:10.1029/PA004i006p00629.
- Lamy, F., and R. DePol-Holz (2013), Postglacial South Pacific, in *The Encyclopedia of Quaternary Science*, vol. 3, edited by S. A. Elias, pp. 77–85, Elsevier, Amsterdam.
- Liu, Z., S. I. Shin, B. Otto-Bliesner, J. E. Kutzbach, E. C. Brady, and D. E. Lee (2002), Tropical cooling at the last glacial maximum and extratropical ocean ventilation, *Geophys. Res. Lett.*, 29(10), 1409, doi:10.1029/2001GL013938.
- Loubere, P., and S. Bennett (2008), Southern Ocean biogeochemical impact on the tropical ocean: Stable isotope records from the Pacific for the past 25,000 years, *Global and Planetary Change*, 63(4), 333–340, doi:10.1016/j.gloplacha.2008.08.001.
- Lovenduski, N. S., and N. Gruber (2005), Impact of the Southern Annular Mode on Southern Ocean circulation and biology, *Geophys. Res. Lett.*, 32, L11603, doi:10.1029/2005GL022727.
- Lovenduski, N. S., N. Gruber, S. C. Doney, and I. D. Lima (2007), Enhanced CO₂ outgassing in the Southern Ocean from a positive phase of the Southern Annular Mode, *Global Biogeochem. Cycles*, 21(2).
- Luz, B. (1977), Late Pleistocene paleoclimates of the South Pacific based on statistical analysis of planktonic foraminifers, *Palaeogeogr. Palaeoclimatol. Palaeoecol.*, 22(1), 61–78.
- Martínez-Méndez, G., D. Hebbeln, M. Mohtadi, F. Lamy, R. DePol-Holz, D. Reyes-Macaya, and T. Freudenthal (2013), Changes in the advection of Antarctic Intermediate Water to the northern Chilean coast during the last 970 kyr, *Paleoceanography*, 28,

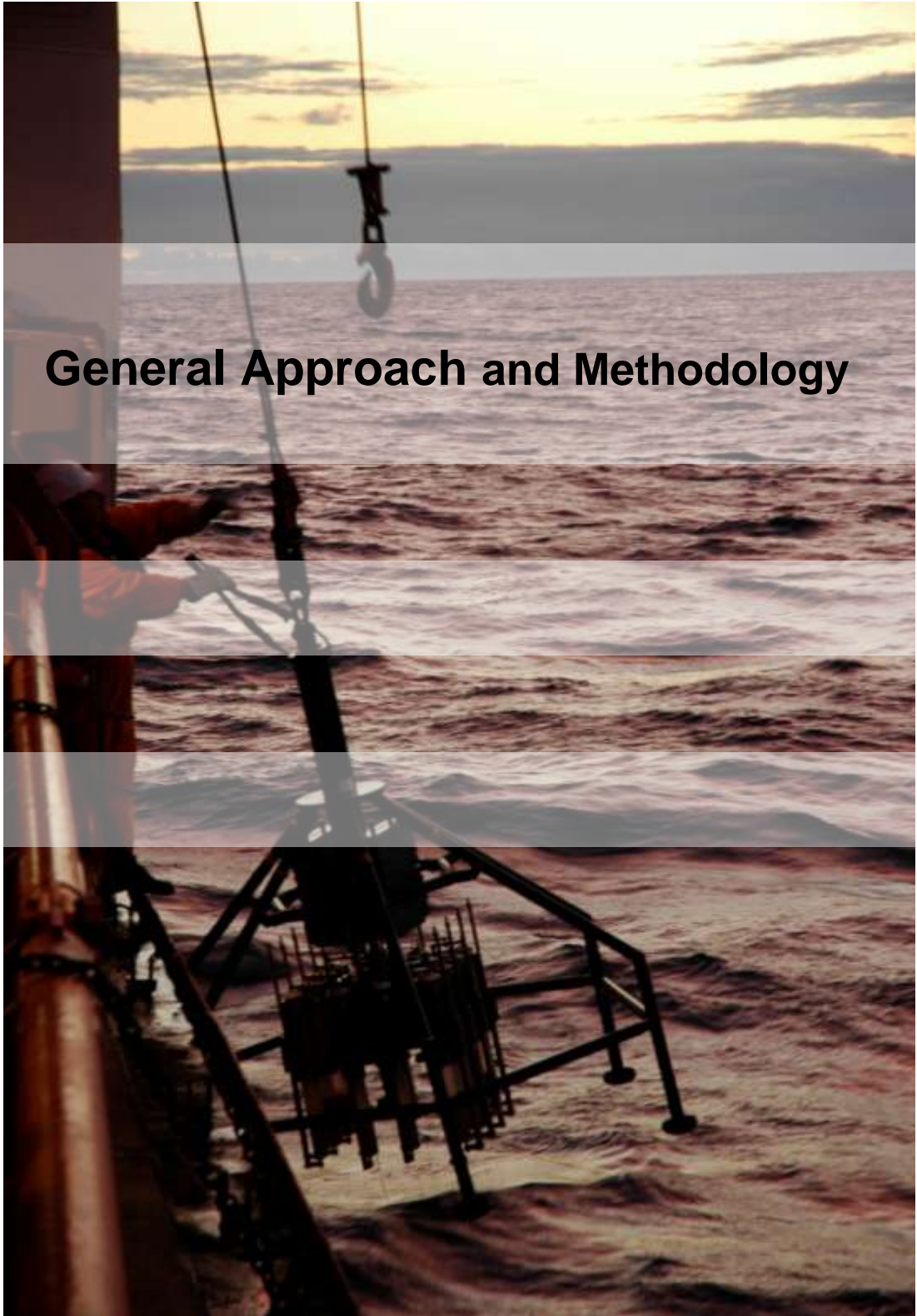
doi:10.1002/palo.20047.

- Mashiotta, T. A., D. W. Lea, and H. J. Spero (1999), Glacial–interglacial changes in Subantarctic sea surface temperature and $\delta^{18}\text{O}$ -water using foraminiferal Mg, *Earth Plan. Sci. Lett.*, 170, 417–432.
- McCartney, M. S. (1977), Subantarctic Mode Water, in *A Voyage of Discovery, George Deacon 70th Anniversary Volume*, edited by M. Angel, pp. 103–119, Pergamon, New York.
- McClymont, E. L., and A. Rosell-Melé (2005), Links between the onset of modern Walker circulation and the mid-Pleistocene climate transition, *Geol.*, 33(5), 389, doi:10.1130/G21292.1.
- McPhaden, M. J., S. E. Zebiak, and M. H. Glantz (2006), ENSO as an integrating concept in earth science, *Science*, 314, 1740, doi:10.1126/science.1132588.
- Merkel, U., M. Prange, and M. Schulz (2010), Quaternary Science Reviews, *Quat. Sci. Rev.*, 29(1-2), 86–100, doi:10.1016/j.quascirev.2009.11.006.
- Metzl, N., C. Brunet, A. Jabaud-Jan, A. Poisson, and B. Schauer (2006), Summer and winter air–sea CO₂ fluxes in the Southern Ocean, *Deep Sea Research Part I: Oceanographic Research Papers*, 53(9), 1548–1563, doi:10.1016/j.dsr.2006.07.006.
- Molinelli, E. (1981), The Antarctic influence on Antarctic Intermediate Water, *Journal Marine Research*, 267–293.
- Muratli, J. M., Z. Chase, A. C. Mix, and J. McManus (2010), Increased glacial-age ventilation of the Chilean margin by Antarctic Intermediate Water, *Nat. Geosci.*, 3, 23–26, doi:10.1038/ngeo715.
- Ninnemann, U. S., and C. D. Charles (2002), Changes in the mode of Southern Ocean circulation over the last glacial cycle revealed by foraminiferal stable isotopic variability, *Earth Plan. Sci. Lett.*, 201(2), 383–396.
- Otto-Bliesner, B. L., E. C. Brady, G. Clauzet, R. Tomas, S. Levis, and Z. Kothavala (2006), Last Glacial Maximum and Holocene Climate in CCSM3, *J. Climate*, 19(11), 2526–2544, doi:10.1175/JCLI3748.1.
- Pahnke, K., and R. Zahn (2005), Southern Hemisphere water mass conversion linked with North Atlantic climate variability, *Science*, 307, 1741–1746, doi:10.1126/science.1102163.
- Pena, L. D., I. Cacho, P. Ferretti, and M. A. Hall (2008), El Niño–Southern Oscillation–like variability during glacial terminations and interlatitudinal teleconnections, *Paleoceanography*, 23, PA3101, doi:10.1029/2008PA001620.
- Pena, L. D., S. L. Goldstein, S. R. Hemming, K. M. Jones, E. Calvo, C. Pelejero, and I. Cacho (2013), Rapid changes in meridional advection of Southern Ocean intermediate waters to the tropical Pacific during the last 30 kyr, *Earth Plan. Sci. Lett.*, 368, 20–32, doi:10.1016/j.epsl.2013.02.028.
- Piola, A. R., and A. L. Gordon (1989), Intermediate waters in the southwest South Atlantic, *Deep-Sea Res*, 36(1), 1–16.

- Ribbe, J. (2001), Intermediate water mass production controlled by southern hemisphere winds, *Geophys. Res. Lett.*, 28(3), 535–538, doi:10.1029/2000GL012242.
- Ridgway, K. R., and J. R. Dunn (2007), Observational evidence for a Southern Hemisphere oceanic supergyre, *Geophys. Res. Lett.*, 34(13), doi:10.1029/2007GL030392.
- Robinson, R. S., A. Mix, and P. Martinez (2007), Southern Ocean control on the extent of denitrification in the southeast Pacific over the last 70ka, *Quat. Sci. Rev.*, 26(1), 201–212, doi:10.1016/j.quascirev.2006.08.005.
- Ronge, T. A., S. Steph, R. Tiedemann, M. Prange, U. Merkel, D. Nürnberg, and G. Kuhn (2015), Pushing the boundaries: Glacial/Interglacial variability of intermediate- and deep-waters in the southwest Pacific over the last 350,000 years, *Paleoceanography*, 30, 23–38, doi:10.1002/2014PA002727.
- Rose, K. A., E. L. Sikes, T. P. Guilderson, P. Shane, T. M. Hill, R. Zahn, and H. J. Spero (2010), Upper-ocean-to-atmosphere radiocarbon offsets imply fast deglacial carbon dioxide release, *Nature*, 466(7310), 1093–1097, doi:10.1038/nature09288.
- Rosenthal, Y., M. Dahan, and A. Shemesh (2000), Southern ocean contributions to glacial-interglacial changes of atmospheric pCO₂: An assessment of carbon isotope records in diatoms, *Paleoceanography*, 15(1), 65–75, doi:10.1029/1999PA000369.
- Russell, J. L., and A. G. Dickson (2003), Variability in oxygen and nutrients in South Pacific Antarctic Intermediate Water, *Global Biogeochem. Cycles*, 17(2), 1033, doi:10.1029/2000GB001317.
- Sabine, C. L. et al. (2004), The oceanic sink for anthropogenic CO₂, *Science*, 305(5682), 367–371, doi:10.1126/science.1097403.
- Sallée, J. B., K. Speer, S. Rintoul, and S. Wijffels (2010), Southern Ocean Thermocline Ventilation, *J. Phys. Oceanogr.*, 40, 509–529, doi:10.1175/2009JPO4291.1.
- Sallée, J. B., R. J. Matear, S. R. Rintoul, and A. Lenton (2012), Localized subduction of anthropogenic carbon dioxide in the Southern Hemisphere oceans, *Nat. Geosci.*, 5, 579–584, doi:10.1038/ngeo1523.
- Santoso, A., and M. H. England (2004), Antarctic Intermediate Water circulation and variability in a coupled climate model, *J. Phys. Oceanogr.*, 34(10), 2160–2179.
- Sarmiento, J. L., N. Gruber, M. A. Brzezinski, and J. P. Dunne (2004), High-latitude controls of thermocline nutrients and low latitude biological productivity, *Nature*, 427, 56–60.
- Schiraldi, B., E. L. Sikes, A. C. Elmore, M. S. Cook, and K. A. Rose (2014), The Southwest Pacific subtropics responds to the last deglacial warming with changes in shallow water sources, *Paleoceanography*, doi:10.1002/2013PA002584.
- Schneider, W., and L. Bravo (2006), Argo profiling floats document Subantarctic Mode Water formation west of Drake Passage, *Geophys. Res. Lett.*, 33, doi:10.1029/2006GL026463.
- Schneider, W., M. Fukasawa, H. Uchida, T. Kawano, I. Kaneko, and R. Fuenzalida (2005), Observed property changes in eastern South Pacific Antarctic Intermediate Water, *Geophys. Res. Lett.*, 32, L14602, doi:10.1029/2005GL022801.

- Schneider, W., R. Fuenzalida, E. Rodríguez-Rubio, and J. Garcés-Vargas (2003), Characteristics and formation of Eastern South Pacific Intermediate Water, *Geophys. Res. Lett.*, 30(11), doi:10.1029/2003GL017086.
- Shin, S. I., Z. Liu, B. Otto Bliesner, E. Brady, J. Kutzbach, and S. Harrison (2003), A simulation of the Last Glacial Maximum climate using the NCAR-CCSM, *Clim. Dyn.*, 20(2-3), 127–151.
- Siani, G., E. Michel, R. De Pol-Holz, T. DeVries, F. Lamy, M. Carel, G. Isguder, F. Dewilde, and A. Lourantou (2013), Carbon isotope records reveal precise timing of enhanced Southern Ocean upwelling during the last deglaciation, *Nature Communications*, 4, doi:10.1038/ncomms3758.
- Sijp, W. P., and M. H. England (2008), The effect of a northward shift in the southern hemisphere westerlies on the global ocean, *Prog. Oceanogr.*, 79, 1–19, doi:10.1016/j.pocean.2008.07.002.
- Sime, L. C., K. E. Kohfeld, C. Le Quéré, and E. W. Wolff (2013), Southern Hemisphere westerly wind changes during the Last Glacial Maximum: model-data comparison, *Quat. Sci. Rev.*, doi:10.1016/j.quascirev.2012.12.008.
- Sloyan, B. M., and S. R. Rintoul (2001a), Circulation, Renewal, and Modification of Antarctic Mode and Intermediate Water*, *J. Phys. Oceanogr.*, 31, 1005–1030.
- Sloyan, B. M., and S. R. Rintoul (2001b), The Southern Ocean limb of the global deep overturning circulation, *J. Phys. Oceanogr.*, 31(1), 143–173.
- Sloyan, B. M., L. D. Talley, T. K. Chereskin, R. Fine, and J. Holte (2010), Antarctic Intermediate Water and Subantarctic Mode Water formation in the Southeast Pacific: the role of turbulent mixing, *J. Phys. Oceanogr.*, 40, 1558–1574, doi:10.1175/2010JPO4114.1.
- Spero, H. J., and D. W. Lea (2002), The cause of carbon isotope minimum events on glacial terminations, *Science*, 296(5567), 522–525.
- Talley, L. D., G. L. Pickard, W. J. Emery, and J. H. Swift (2011), *Descriptive physical oceanography: an introduction*, 6 ed., Academic press, New York.
- Toggweiler, J. R., J. L. Russell, and S. R. Carson (2006), Midlatitude westerlies, atmospheric CO₂, and climate change during the ice ages, *Paleoceanography*, 21(2), doi:10.1029/2005PA001154.
- Tomczak, M. (2006), Variability of Antarctic intermediate water properties in the South Pacific Ocean, *Ocean Science Discussions*, 3(3), 32021–205863–377.
- Tomczak, M., and J. S. Godfrey (2001), *Regional Oceanography*, Butler & Tanner Ltda., London.
- Tsimplis, M., S. Bacon, and H. Bryden (1998), The circulation of the subtropical South Pacific derived from hydrographic data, *J. Geophys. Res.*, 103(C10), 21443–21–468.
- Tsuchiya, M., and L. D. Talley (1996), Water-property distributions along an eastern Pacific hydrographic section at 135W, *Journal of marine research*, 54(3), 541–564.

- Tsuchiya, M., and L. D. Talley (1998), A Pacific hydrographic section at 88°W: water-property distribution, *J. Geophys. Res.*, 103(C6), 12899–12918.
- Verdy, A., S. Dutkiewicz, M. J. Follows, J. Marshall, and A. Czaja (2007), Carbon dioxide and oxygen fluxes in the Southern Ocean: Mechanisms of interannual variability, *Global Biogeochem. Cycles*, 21(2), GB2020, doi:10.1029/2006GB002916.
- Verleye, T. J., and S. Louwye (2010), Late Quaternary environmental changes and latitudinal shifts of the Antarctic Circumpolar Current as recorded by dinoflagellate cysts from offshore Chile (41° S), *Quat. Sci. Rev.*, 29, 1025–1039, doi:10.1016/j.quascirev.2010.01.009.
- Wijffels, S. E., J. M. Toole, and R. Davis (2001), Revisiting the South Pacific subtropical circulation: A synthesis of World Ocean Circulation Experiment observations along 32°S, *J. Geophys. Res.*, 106(C9), 19481–19513, doi:10.1029/1999JC000118.
- Williams, G. P., and K. Bryan (2006), Ice Age Winds: An Aquaplanet Model, *J. Climate*, 19(9), 1706–1715, doi:10.1175/JCLI3766.1.
- Xue, L., L. Gao, W. J. Cai, W. Yu, and M. Wei (2015), Response of sea surface fugacity of CO₂ to the SAM shift south of Tasmania: Regional differences, *Geophys. Res. Lett.*, 42(10), 3973–3979, doi:10.1002/2015GL063926.
- Ziegler, M., P. Diz, I. R. Hall, and R. Zahn (2013), Millennial-scale changes in atmospheric CO₂ levels linked to the Southern Ocean carbon isotope gradient and dust flux, *Nat. Geosci.*, 6(6), 457–461, doi:10.1038/ngeo1782.
- Zilberman, N. V., D. H. Roemmich, and S. T. Gille (2014), Meridional volume transport in the South Pacific: Mean and SAM-related variability, *J. Geophys. Res. Oceans*, 119(4), 2658–2678, doi:10.1002/2013JC009688.



General Approach and Methodology

CHAPTER 2

2.1 PROXY BACKGROUND

The narrow time window covered by instrumental temperature data (i.e. last two centuries) severely restricts our ability to understand how the ocean and atmosphere behave under different climatic regimes, thereby impeding a robust assessment of the natural climatic variability. Beyond the instrumental era, inferring past temperatures relies on the so-called “proxy”, which is made possible by the fact that temperature affects both metabolic and thermodynamic processes thereby leaving a distinct “signature” in fossil material. The translation of these “signature” into measurable descriptor (“proxy”) has been the backbone of paleoceanography and paleoclimatology [Lea, 1999; Lea *et al.*, 1999; Rohling and Cooke, 1999; Lynch-Stieglitz, 2003; Lea, 2006; Jorissen *et al.*, 2007; Kucera, 2009; Ravelo and Hillaire-Marcel, 2007; Naveira Garabato *et al.*, 2009; Vivier *et al.*, 2010; Lea, 2014]. Studies of continuous proxy records spanning centuries to millions of years help extend the instrumental record further into the geologic past, aiding our understanding of when, why, by how much and how fast the ocean temperatures and Earth climate have changed in the past on various time-scales.

As the mixed layer roughly corresponds to the “sunlight zone”, the habitat of phytoplankton and photosymbiotic organisms are somehow restricted to it. However, some planktic foraminifera species can live below the mixed layer, recording the temperature of greater depths i.e. thermocline [Spero and Lea, 2002; Toggweiler *et al.*, 2006; Cléroux *et al.*, 2007; Groeneveld and Chiessi, 2011; Cléroux *et al.*, 2013; Ziegler *et al.*, 2013], rather than the surface ocean (Figure 2.1). Ecological niche such as this offers us the possibility to infer past changes in the stratification of the upper ocean, usually defined by the depth of the thermocline [Tomczak and Godfrey, 2001].

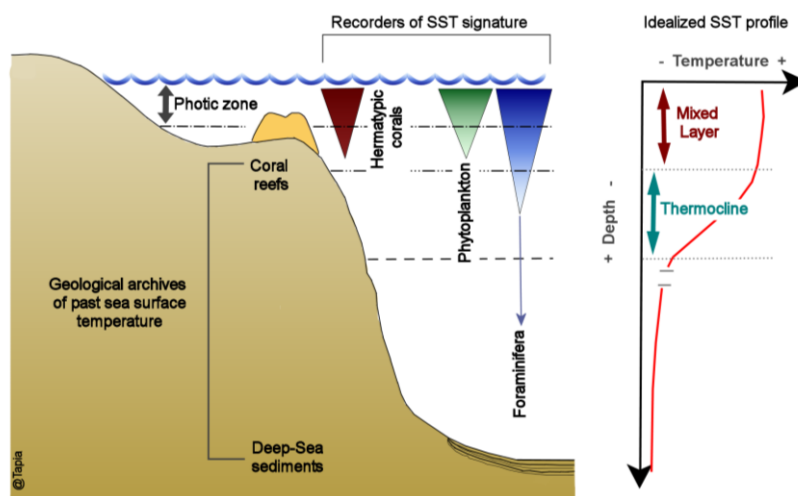


Figure 2.1 Idealized scheme of the habitat of SST signal carriers. Corals and phytoplankton grow only in the photic zone, which normally overlaps with the mixed layer, however some species of planktic foraminifera can live below the photic zone and record deeper water temperatures (i.e. thermocline) [modified from Kucera, 2009].

The following sections will be dedicated to detailed description of foraminifera-based geochemical proxies used in this thesis for reconstructing past oceanographic changes in the South Pacific.

2.1.1 Planktic Foraminiferal $\delta^{18}\text{O}$ and $\delta^{13}\text{C}$ as Paleo Proxies

Stable Oxygen Isotopes ($\delta^{18}\text{O}$)

Oxygen is present in three atomic forms: ^{16}O , ^{17}O , and ^{18}O . These stable isotopes have relative abundances of 99.76%, 0.04%, and 0.20%, respectively [Rohling and Cooke, 1999]. Due to the higher abundances of ^{16}O and the greater mass difference between ^{16}O and ^{18}O , research on oxygen isotopic ratios is normally based on $^{18}\text{O}/^{16}\text{O}$ ratios [Rohling and Cooke, 1999].

Although the absolute abundance of the minor isotopes cannot be determined accurately, it is still possible to get quantitative estimates for $^{18}\text{O}/^{16}\text{O}$ ratio by comparing measurement of an unknown sample (sample) with a known external standard (standard) [Rohling and Cooke, 1999], and is reported in “ δ ” notation calculated as follows:

$$\delta^{18}\text{O}_{\text{sample}} = 1000 \times \frac{[(^{18}\text{O}/^{16}\text{O})_{\text{sample}} - (^{18}\text{O}/^{16}\text{O})_{\text{standard}}]}{(^{18}\text{O}/^{16}\text{O})_{\text{standard}}} \quad (\text{eq. 1})$$

The oxygen isotopic composition of the foraminiferal test ($\delta^{18}\text{O}_{\text{calcite}}$) is controlled by the temperature of seawater during the calcification ($\approx -0.2\text{‰} \delta^{18}\text{O}_{\text{SW}}$ per $^{\circ}\text{C}$), the $\delta^{18}\text{O}$ of seawater ($\delta^{18}\text{O}_{\text{SW}}$), and species-dependent vital effects [Rohling and Cooke, 1999; Ravelo et al., 2007].

$$T = a + b (\delta^{18}\text{O}_{\text{calcite}} - \delta^{18}\text{O}_{\text{SW}}) + c (\delta^{18}\text{O}_{\text{calcite}} - \delta^{18}\text{O}_{\text{SW}})^2 \quad (\text{eq. 2})$$

As the $\delta^{18}\text{O}_{\text{SW}}$ correlates linearly with seawater salinity at least on regional scales [Fairbanks, 1989; LeGrande and Schmidt, 2006], this linear relationship allows the use of the $\delta^{18}\text{O}_{\text{SW}}$ as a proxy of past salinity, a key factor determining the density of the sea water [Lynch-Stieglitz et al., 1999; Hirschi and Lynch-Stieglitz, 2006], and by extension also oceanic circulation (e.g. thermohaline circulation). In combination with independent temperature proxy, past changes in $\delta^{18}\text{O}_{\text{SW}}$ can be isolated from foraminifera $\delta^{18}\text{O}_{\text{calcite}}$ (eq. 2), therefore changes in salinity can be inferred [e.g. Mix et al., 2000; Barker et al., 2005; Nürnberg and Groeneveld, 2006; Pena et al., 2008]. However, $\delta^{18}\text{O}_{\text{SW}}$ is not a

straightforward salinity proxy as it may also be influenced by other processes on local and global scale:

- *Local/regional:* river-water input and evaporation/precipitation patterns.
- *Global:* latitudinal transport of water vapor and continental ice volume influence the $\delta^{18}\text{O}_{\text{SW}}$ (i.e. Rayleigh distillation; [Figure 2.2](#)) [Rohling and Cooke, 1999].

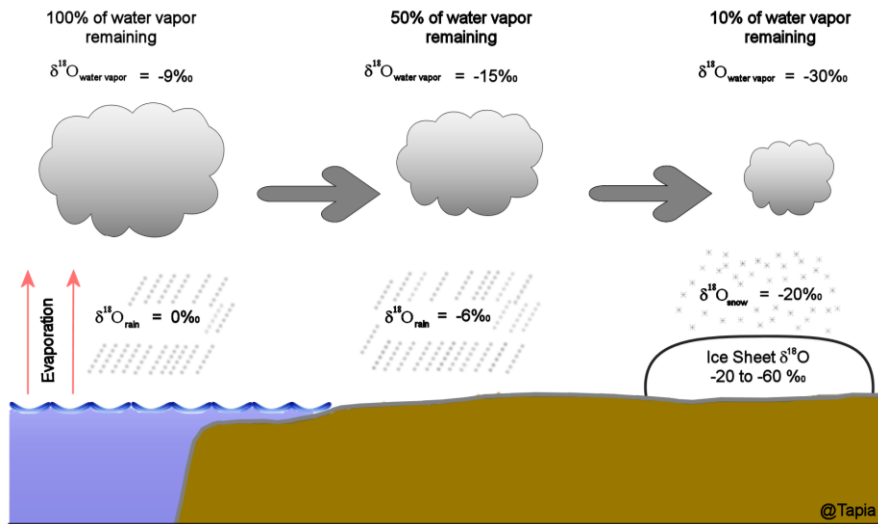


Figure 2.2 Illustration of the Rayleigh distillation process on the $\delta^{18}\text{O}$ values as clouds move over land and into the polar regions. Decreasing air temperatures cause moisture to rain/snow out of the cloud. Fractionation of the oxygen isotopes during condensation further decreases values. By the point that a cloud reaches the high latitudes, less than 10% of the original water vapor remains. Snowfall on Antarctica has values between -20 and 60‰. The average $\delta^{18}\text{O}$ for ice on Antarctica $\sim -40\text{‰}$, modified from Rohling and Cooke [1999].

Consequently, further corrections and assumptions must be considered in the calculations of salinity. It has been suggested that for long-term climate changes, such as glacial-interglacial cycles, the relationship $\delta^{18}\text{O}_{\text{SW}}$ -salinity was primarily controlled by changes in continental ice volume, by its storage of lighter $\delta^{18}\text{O}_{\text{SW}}$ on land (then the mean oceanic $\delta^{18}\text{O}$ value was relatively high) [Rohling and Bigg, 1998; Rohling and Cooke, 1999; Ravelo and Hillaire-Marcel, 2007; Rohling, 2013]. As the amount of water stored on land in the form of ice vary through time, this impacts the mean oceanic $\delta^{18}\text{O}$ values and consequently compromising the linear $\delta^{18}\text{O}_{\text{SW}}$ -salinity relationship. Studies based on different approaches have evaluated the effect of changes in sea level (or ice volume) on the oceanic $\delta^{18}\text{O}$ values at different time scales [e.g. Fairbanks, 1989; Waelbroeck et al., 2002; Bintanja et al., 2005; Sosdian and Rosenthal, 2009; Elderfield et al., 2012], and they roughly suggest that the mean oceanic $\delta^{18}\text{O}$ varied $\sim 0.09\text{‰}$ per -10 m of sea level.

Carbon Stable Isotopes ($\delta^{13}\text{C}$)

The $\delta^{13}\text{C}$ was the first geochemical proxy routinely measured in the same sample with $\delta^{18}\text{O}$. In contrast to the $\delta^{18}\text{O}$ that reflects $\delta^{18}\text{O}_{\text{SW}}$ and ambient temperature, the $\delta^{13}\text{C}$ value in foraminifera mainly reflect the $\delta^{13}\text{C}$ signature of seawater dissolved inorganic carbon (DIC) [Rohling and Cooke, 1999; Lynch-Stieglitz, 2003; Ravelo and Hillaire-Marcel, 2007]; thus the planktic foraminiferal $\delta^{13}\text{C}$ reflects the $\delta^{13}\text{C}_{\text{DIC}}$ of the upper ocean where they dwell [Katz et al., 2010]. However, factors such as foraminiferal test size, pH, light intensity, and symbionts may influence the foraminiferal $\delta^{13}\text{C}$ [Spero and Lea, 1996; Rohling and Cooke, 1999; Ravelo and Hillaire-Marcel, 2007].

The $\delta^{13}\text{C}_{\text{DIC}}$ in sea surface waters is affected by primary productivity, which results in higher $\delta^{13}\text{C}_{\text{DIC}}$ as lighter carbon isotopes (^{12}C) are preferentially taken for photosynthesis [Rohling and Cooke, 1999]. The light $\delta^{13}\text{C}$ signature in organic matters is released to the water mass as they sink, therefore subsurface water masses become more depleted in $\delta^{13}\text{C}$ because they accumulate DIC released by the remineralization of ^{12}C -enriched organic matter. Physical processes can alter the $\delta^{13}\text{C}_{\text{DIC}}$ in the upper ocean, such as 1) temperature-dependent air-sea exchange, which increase (decrease) $\delta^{13}\text{C}_{\text{DIC}}$ in cold (warm) waters and, 2) Seawater mixing and advection, both horizontally and vertically (e.g. upwelling of deep ^{12}C -enriched waters) [Lynch-Stieglitz, 2003; Ravelo and Hillaire-Marcel, 2007].

2.1.2 Planktic Foraminiferal Mg/Ca as a Paleothermometer

The Mg^{2+} is one of the numerous divalent cations which may substitute the Ca^{+2} during the formation of biogenic calcium carbonate due to their similar ionic radius and charge [Barker et al., 2005]. In planktic foraminifera, the incorporation of Mg^{2+} into their shells is determined by the temperature of the water in which the foraminifera dwell; the higher the temperature the more Mg^{2+} gets incorporated. Therefore, the Mg/Ca ratios in the foraminiferal calcite increase with temperature [Lea, 1999; Anand et al., 2003; Barker et al., 2005; Lea, 2006; 2014].

The relationship between temperature and planktic foraminiferal Mg/Ca ratio is exponential (eq. 3):

$$\text{Mg/Ca} = \text{Be}^{\text{AT}} \quad (\text{eq. 3})$$

; where B is the pre-exponential constant, A is the exponential constant (consistently found to be around 0.09–0.1 which reflects a temperature sensitivity of ~10% in Mg/Ca per 1 °C increase in temperature), and T denotes the calcification temperature [Lea, 1999; Lea et

al., 1999; *Lea*, 2006; 2014].

2.1.2.1 Mg/Ca-Temperature Conversion

There are three common approaches to determine the Mg/Ca-calcification temperature relationships in the foraminiferal calcite: a) culture experiments [e.g. *Nürnberg et al.*, 1996; *Lea et al.*, 1999; *Langen*, 2005]; b) sediment-trap and water-column studies [e.g. *Anand et al.*, 2003; *McConnell and Thunell*, 2005; *Martínez-Botí et al.*, 2011]; c) and surface sediment (core-top) studies [e.g. *Nürnberg*, 1995; *Elderfield and Ganssen*, 2000; *Regenberg et al.*, 2009; *Groeneveld and Chiessi*, 2011].

Each approach has its own strengths and weaknesses. For example, culture-based calibrations have the advantage of temperature (T) control during the experiment. But, it is impossible to reproduce realistic natural environment in laboratory cultures to ensure the foraminiferal reproduction and the natural chamber growth in foraminifera, thus juvenile specimens must be collected from their natural habitat before culturing [*Lea et al.*, 1999; *Hönisch et al.*, 2013]. Consequently, the aforementioned controlled conditions only apply to the later stages of test formation (i.e. chambers formed during culture) [*Lea et al.*, 1999; *Lea*, 2014]. It is therefore unclear if Mg/Ca-temperature calibrations derived from culture experiments is valid for paleotemperature reconstruction that is normally performed on calcites that represents the entire period of test growth [*Lea et al.*, 1999; *Barker et al.*, 2005; *Lea*, 2014].

In the case of core-top, plankton tow or trap studies the temperature is usually estimated using climatological atlas or derivation of the calcification temperature attained either from foraminiferal or sea water $\delta^{18}\text{O}$ [*Elderfield and Ganssen*, 2000; *Anand et al.*, 2003; *Barker et al.*, 2005; *McConnell and Thunell*, 2005]. In these approaches, the temperature itself becomes a dependent variable and may introduce an error into the calibration even larger than the measurement of Mg/Ca [*Anand et al.*, 2003; *Barker et al.*, 2005]. Further, core-top samples from deep ocean may have experienced post-depositional alteration [*Barker et al.*, 2005], which complicates the interpretation of Mg/Ca as a temperature proxy. However, calibrations derived from core-top samples are attractive for reconstruction purposes because they are based on foraminifera that completed its life cycle (e.g. gametogenesis and any secondary calcite formation) and eventually form part of the sedimentary record.

During the last years a large number of species-specific Mg/Ca-temperature calibrations have been proposed [e.g. *Mashiotta et al.*, 1999; *Elderfield and Ganssen*, 2000; *Anand et al.*, 2003; *Regenberg et al.*, 2009; *Groeneveld and Chiessi*, 2011; *Marr et al.*, 2011; *Mortyn et al.*, 2011; *Cléroux et al.*, 2013]. However, the use of multispecies calibrations can

yields in comparable results from those obtained from species-specific calibrations (Figure 2.3 and Table 1).

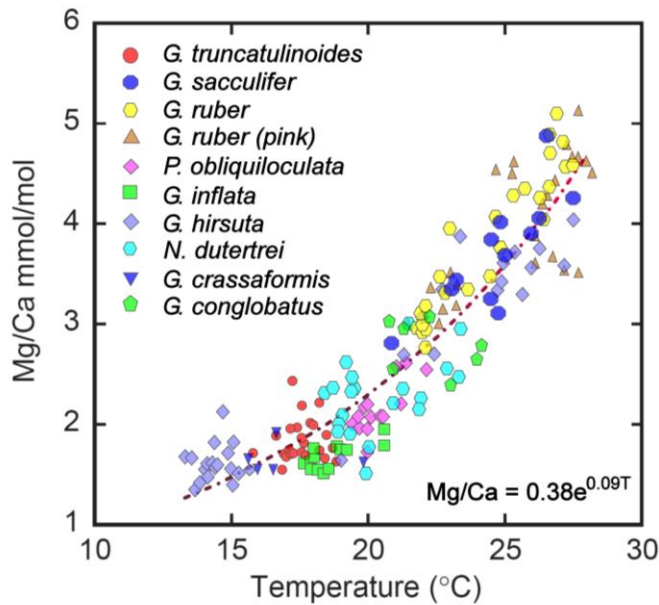


Figure 2.3 Mg/Ca calibration for several species of planktic foraminifera, temperatures were isotopically derived [Anand et al., 2003]. The data can be describe by a single equation [modified from Baker et al., 2005].

Table 2.1 Summary of published Mg/Ca-temperature calibrations for single and multiple species of planktic, a very good agreement has been achieved between all three approaches [Lea et al., 1999; Elderfield and Ganssen, 2000; Dekens et al., 2002; Anand et al., 2003; Barker et al., 2005; McConnell and Thunell, 2005; Greaves, 2008; Cléroux et al., 2013].

Species	Source	Temperature range (°C)	B	A	Reference
<i>G. ruber</i>	Coretop	21-29	0.38	0.089	Dekens et al. (2002)
	Sediment trap	22-28	0.34	0.102	Anand et al. (2003)
<i>G. bulloides</i>	Culture	16-25	0.53	0.102	Lea et al. (1999)
	Coretop/culture	10-25	0.474	0.107	Mashiotta et al. (1999)
	Coretop	8-15	0.56	0.1	Elderfield and Ganssen (2000)
	Sediment trap	16-31	0.2	0.057	McConnell (2005)
<i>G. inflata</i>	Coretop	8 - 15	0.49	0.1	Elderfield and Ganssen (2000)
	Coretop	3.1-16.5	0.72	0.076	Groeneveld and Chiessi (2011)
	Coretop	10-18	0.585	0.133	Cleroux et al. (2013)
	Sediment trap	17-21	0.299	0.090	Anand et al. (2003)
Mixed (8 spp)	Coretop	0-19	0.52	0.1	Elderfield and Ganssen (2000)
Mixed (10 spp)	Sediment trap	13-28	0.38	0.09	Anand et al. (2003)

Mg/Ca has become a routinely measured geochemical temperature proxy, in part due to its advantages over other proxies [see Barker et al., 2005 for details]:

- The long residence time of Mg^{2+} and Ca^{2+} (10^6 and 10^7 years, respectively), makes that the Mg/Ca ratios in seawater can be considered constant during the last ~2 Ma

[Medina-Elizalde et al., 2008], thus allowing temperature reconstructions throughout the Quaternary.

- Since Mg/Ca and foraminiferal oxygen isotope measurements are attained from a single medium (foraminiferal calcite) and incorporated under the exact same environmental conditions (depth habitat, season, etc.) [Mix et al., 2000; Barker et al., 2005; Lea, 2006; 2014], paired Mg/Ca and $\delta^{18}\text{O}_{\text{Calcite}}$ measurements allow reconstruction of past oxygen isotopic composition of sea water [Mashiotta et al., 1999; Elderfield and Ganssen, 2000; Pahnke et al., 2003; Nürnberg and Groeneveld, 2006].
- Each planktic species is known to dwell within a certain water depth range, therefore analyzing multiple species of foraminifera with different habitat depth preference allows reconstructions of vertical temperature gradients within the upper water column [e.g. Steinke et al., 2005; Thornalley et al., 2008; Farmer et al., 2011; Cléroux et al., 2013].

Despite the aforementioned advantages, an accurate interpretation of foraminiferal Mg/Ca data as temperature estimates requires careful consideration of factors which might confound Mg/Ca-temperature relationship, including:

1) Specimen Selection and Sample Preparation

a) Foraminiferal Species and Morphotypes

In general, foraminifera of different species are thought to have different depth habitats due to their ecological preferences, in terms of salinity, temperature, nutrient availability, and so on [Kucera, 2007]. However, the existing taxonomy of foraminifera is founded on the morphology of their shells instead of their genomics, therefore foraminifera within the same morphospecies may not necessarily share the same ecological preferences [Darling et al., 2000; 2003; 2006; Darling and Wade, 2008; Morard et al., 2011]. Reconstructing temperatures using mixed morphotypes from the same species, for instance the *sensu latus* and *sensu strictus* morphotypes from *G. ruber*, will result in an integrated temperature signal over depth range and season, reflecting neither one of the morphotypes [Cléroux et al., 2007; Regenberg et al., 2009].

b) Size Fraction

Friedrich et al. [2012] found decreasing Mg/Ca ratios with increasing test size, for both symbiont-barren and symbiont-bearing species (i.e. *G. ruber*), in contrast to earlier findings [Elderfield and Ganssen, 2000]. Although the size fraction effect on intermediate sized organisms (250 to 400 μm) is negligible, it does however imply that Mg/Ca analyses should be carried out on a narrow size fraction, usually within 100 micron, in order to

circumvent the size fraction bias.

c) Cleaning Protocol Selection (Reductive vs. Non-Reductive)

In the past decades, the analytical capability to determinate trace elements from foraminiferal calcite has largely improved [Lea, 2014]. The standard sample work-up of foraminiferal Mg/Ca analysis involves cleaning foraminiferal shells prior to the measurement, which can be achieved via either non-reductive or reductive cleaning protocols [Barker *et al.*, 2003]. The objective of an additional reductive step is to remove post-depositional coating such as Mn-Ca-Mg and/or Fe-Mn (ferromanganese) [Barker *et al.*, 2003], because these Mg-enriched coatings may increase the foraminiferal Mg/Ca ratio thereby biasing the reconstructed temperatures [Pena *et al.*, 2005], or, in some extreme case, completely overprinting the geochemical signature of the primary calcite [Boussetta *et al.*, 2011; van Raden *et al.*, 2011]. Some studies suggest that the reductive cleaning protocol may remove 10-15% of Mg from the shells, resulting in anomalously low Mg/Ca-derived temperatures values [Barker *et al.*, 2003; Rosenthal *et al.*, 2004; Pena *et al.*, 2005]. On the other hand, recent studies on the comparison of the two aforementioned cleaning protocols suggest lower offsets 4–10% [Steinke *et al.*, 2010; Marr *et al.*, 2013; Johnstone *et al.*, 2016], in same species the use of reductive cleaning didn't affect its Mg/Ca ratio [Johnstone *et al.*, 2016].

2) Other Environmental Effects on Foraminiferal Mg/Ca

a) Dissolution

During the sinking until the final settling on the sea floor, various processes can act on the foraminiferal shells and affect the Mg/Ca ratio, for instance carbonate dissolution. Dissolution preferentially removes Mg over Ca, therefore reducing the Mg/Ca ratio and its inferred temperature estimate [Brown and Elderfield, 1996; Dekens *et al.*, 2002]. The effect of dissolution on the foraminiferal Mg/Ca is known to be a problem for temperature reconstruction using planktic foraminiferal Mg/Ca [Dekens *et al.*, 2002; Regenberg *et al.*, 2006; Fehrenbacher and Martin, 2014; Regenberg *et al.*, 2014], but the factors controlling the dissolution susceptibility still remain poorly understood. This is evident since the amount of loss in Mg/Ca caused by dissolution varies between species, with some species showing larger decrease in their Mg/Ca ratios than others [Dekens *et al.*, 2002]. It has been related to preferential dissolution of high-Mg/Ca calcite [Brown and Elderfield, 1996] and more recently as a function of the surface area of each species [Regenberg *et al.*, 2013]. Some species such as *G. bulloides* seems to show a higher

resistance to selective dissolution and the ability to reliably preserve temperature signal, as demonstrated by the comparison between Mg/Ca values and dissolution proxies, as well as laboratory experiments of acid leaching [Mekik *et al.*, 2007; Marr *et al.*, 2013]. Given the potential bias caused by selective dissolution on the absolute values and temporal trends in Mg/Ca-inferred temperature records, several methods to correct for the loss of Mg have been proposed, albeit with variable degree of effectiveness [Dekens *et al.*, 2002; Regenberg *et al.*, 2006; Sadekov *et al.*, 2010; Regenberg *et al.*, 2014].

b) Salinity

Contradictory results concerning the salinity effect on foraminiferal Mg/Ca have been obtained from laboratory culture and core-top studies. Earlier laboratory culture studies found that salinity exerts a small effect on Mg/Ca, which increases by 4–8% per salinity unit [e.g. Nürnberg *et al.*, 1996; Lea *et al.*, 1999], while sediment core-top studies suggest a larger Mg/Ca sensitivity to salinity, up to 59% per salinity unit [Ferguson *et al.*, 2008; Mathien-Blard and Bassinot, 2009; Arbuszewski *et al.*, 2010]. A recent study based on both laboratory culture and core-tops found a substantially lower Mg/Ca sensitivity to salinity of 3 to 5% for *G. ruber* [Hönisch *et al.*, 2013], and hypothesized that the strong salinity effect previously reported by Arbuszewski *et al.* [2010] was driven by seasonal variability in foraminiferal habitat depth.

2.2 MATERIALS and METHODOLOGY

This thesis is build upon results obtained from analyzing sediment samples from the South Pacific (details in [Table 2](#) and [Figure 2.4](#)), retrieved during the cruises SO213–SOPATRA [*Tiedemann et al.*, 2014] and ANT-XXVII/2 [*Gersonde*, 2011] on R/V Sonne and R/V Polarstern, respectively.

Table 2.2 List of sediment samples selected for this study. Surface samples were collected with Multicore (MUC), meanwhile downcore were collected through Gravity core (GC) and Piston core (PC).

Station No.	Gear	Latitude (deg/min)	Longitude (deg/min)	Water depth (m)	
Surface samples					
SO213-59-1	MUC	45° 49.72' S	116° 52.68' W	3159	
SO213-60-2	MUC	44° 57.82' S	119° 33.06' W	3468	
PS75/34-01	MUC	54° 22.11' S	80° 05.3' W	4425	
PS75/51-02	MUC	52° 48.73' S	107° 48.33' W	3849	
PS75/76-01	MUC	55° 31.71' S	156° 08.39' W	3742	
Downcore					
					Length (m)
SO213-59-2	GC	45° 49.73' S	116° 52.76' W	3161	2.11
SO213-60-1	GC	44° 57.83' S	119° 33.07' W	3471	6.73
PS75/056-1	PC	55° 09.74' S	114° 47.31' W	3581	10.21
PS75/059-2	PC	54° 12.90' S	125° 25.53' W	3613	13.98
PS75/079-2	PC	57° 30.16' S	157° 35.18' W	3770	18.51

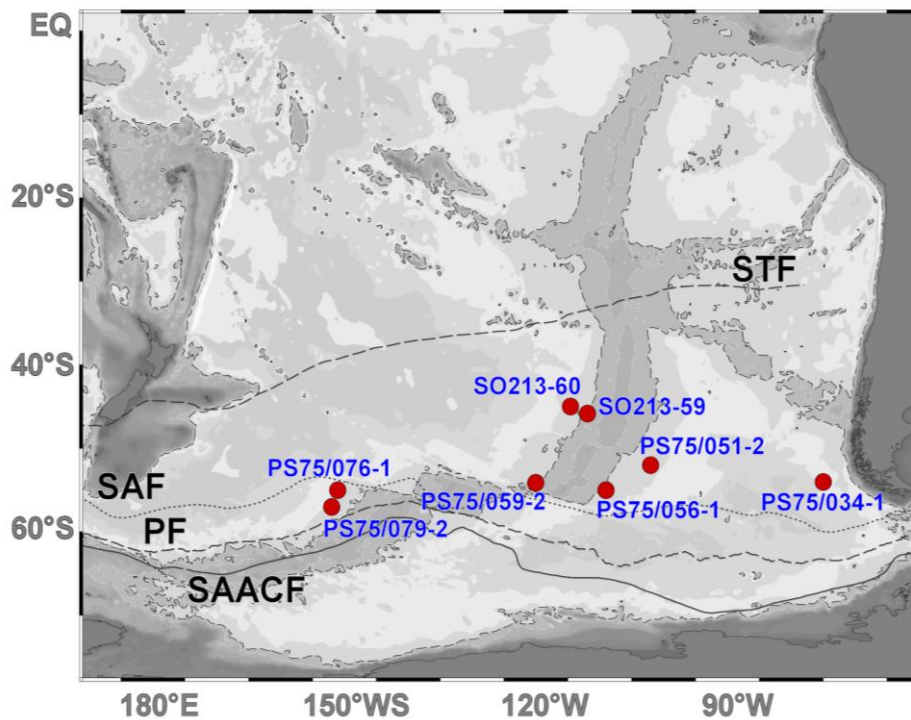


Figure 2.4 Location of the sediment samples (red) used; SO213-59 (chapters 3), PS75/059-2, (chapters 4, Appendix 1), SO213-60 (chapters 5, Appendix 2), PS75/034-1, PS75/051-2, PS75/056-2, PS75/076-1 and

PS75/079-2 (Appendix 1). Main oceanographic features in the South Pacific ACC front (SACCF), Polar front (PF), Subantarctic front (SAF) and Subtropical front (STF) are denoted by lines.

2.2.1 Planktic Foraminifera Used for Geochemical Analyses

The following sections describe the geographical distribution and ecology of the planktic foraminiferal species used in the thesis as a substrate of geochemical analyses.

2.2.1.1 *Globigerina bulloides*

Globigerina bulloides [d'Orbigny, 1826] (Figure 2.5a), is a non-symbiotic, spinose species that inhabits temperate and sub-polar waters [Bé, 1959; 1960; Bé and Hamlin, 1967; Tolderlund and Bé, 1971; Schiebel et al., 1997; Kucera, 2007]. This species is strongly associated with upwelling environments, such as the north-western Africa margin western Arabian Sea and Humboldt current system [Schiebel et al., 1997; Marchant et al., 1998; 2004; Mohtadi et al., 2005]. *G. bulloides* is known to calcify above the thermocline, and several studies proposed the upper 60 metres of the water column as its preferred water depth [Schiebel et al., 1997; Peeters et al., 2002; Mekik et al., 2007; Farmer et al., 2011]. The SST tolerance range of *G. bulloides* is between 0 and 27°C, with peak abundances found between 3 and 19°C [Schiebel et al., 1997; Niebler and Gersonde, 1998; Kucera, 2007].

2.2.1.2 *Globorotalia inflata*

Globorotalia inflata [d'Orbigny, 1839] (Figure 2.5b), has no spines or symbionts, and it can be found in transitional and sub-polar waters [Boltovskoy, 1959; Kennett, 1978; Niebler and Gersonde, 1998; Groeneveld and Chiessi, 2011; Morard et al., 2011; Cléroux et al., 2013]. Relative to *G. bulloides*, *G. inflata* is considered a deeper dweller, calcifying down to water depths of 500–800 m [Wilke et al., 2009]. In contrast, Elderfield and Ganssen [2000] proposed a narrower, intermediate depth habitat for *G. inflata* in the North Atlantic at 300–400 m water depth, which was later confirmed for other locations [Lončarić et al., 2006; Cléroux et al., 2007]. This species lives in waters between 1 and 27°C, and peak abundances are found in waters between 13 and 19 °C [Tolderlund and Bé, 1971; Niebler and Gersonde, 1998; Groeneveld and Chiessi, 2011].

2.2.1.3 *Globorotalia truncatulinoides*

Globorotalia truncatulinoides [d'Orbigny, 1839] (Figure 2.5c), is a non-symbiotic, non-spinose species inhabiting subtropical and sub-polar waters. This species reproduces at approximately 600 metres, thereafter the juveniles travel back to surface waters and subsequently sink down the water column. They add chambers to their shell during their descent [Bé and Hutson, 1977; Bé et al., 1977; Renaud and Schmidt, 2003] and may calcify

at depths down to ~800 m [Bé, 1960; Lohmann and Schweitzer, 1990; LeGrande, 2004]. *G. truncatulinoides* has been intensely studied [Kennett, 1968; Healy-Williams, 1983; Lohmann and Schweitzer, 1990; Martínez, 1997; Mulitza et al., 1997; Spencer-Cervato and Thierstein, 1997; Jian et al., 2000; Renaud and Schmidt, 2003; LeGrande, 2004; Cléroux et al., 2007; 2009; Feldmeijer et al., 2014], firstly because of its size and abundance in the sediment, and secondly because they appear to dwell, therefore record, the local hydrography around the thermocline at the density surface of 27 kgm^{-3} [Lohmann and Schweitzer, 1990; Ravelo and Fairbanks, 1992; Martínez, 1997; LeGrande, 2004; Steph et al., 2009], which roughly corresponds to the density surface of Antarctic Intermediate Water. *G. truncatulinoides* occurs in waters between 4 and 27 °C, with peak abundances occurring in waters between 17 and 22 °C [Kennett, 1968; Quillévére et al., 2011; Spear and Poore, 2011]. Although *G. truncatulinoides* and *G. inflata* have similar depth habitat, *G. truncatulinoides* always lives at greater depth than *G. inflata* when both species are present in the same area [Cleroux et al., 2007].

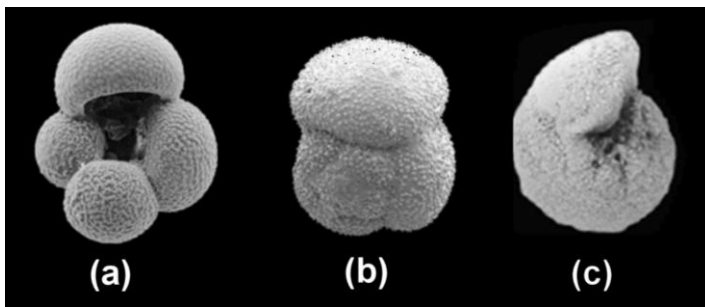


Figure 2.5 SEM from the planktic species selected in this thesis. Surface dweller *G. bulloides* (a), the deep-dwellers *G. inflata* (b) and *G. truncatulinoides* (c). (Hayward [2015]; www.marinespecies.org).

2.2.2. Stratigraphic Framework of Sediment Samples

The stratigraphic framework of the sediment records used in this thesis is based on 1) visual correlation of benthic oxygen isotope records to reference records and 2) Accelerated mass spectrometer (AMS) ^{14}C dating performed on planktic foraminifera.

The benthic oxygen isotope records based on *Cibicides wuellerstorfi* or *Cibicidoides* spp. (SO213-59-2, PS75/059-2, PS75/056-1, PS75/079-2) and *Uvigerina peregrina* (SO213-60-1) are used for stratigraphic controls. These benthic oxygen isotope records were visually correlated either to a globally averaged benthic $\delta^{18}\text{O}$ stacks, i.e. the LR04 [Lisiecki and Raymo, 2005] (SO213-59-2, PS75/059-2, PS75/056-1, PS75/079-2) or to geographically representative stack, i.e. the ODP1123 [Elderfield et al., 2012] (SO213-60-1) (for details see respective chapter).

The AMS ^{14}C radiocarbon analysis was performed on samples either composed exclusively of *Globobulimina bulloides* or a mix of planktic foraminifera species when a single

species does not occur in sufficient amount. The dating was performed at the Leibniz–Laboratory for Radiometric Dating and Isotope Research of the University of Kiel (see [Table 4](#)). AMS¹⁴C ages were converted to calendar age using the software CALIB 7.0 [Stuiver and Reimer, 1993] with the Marine13 database [Reimer et al., 2009], and ΔR correction of 560 years [Bremen reservoir age database; Franke et al., 2008]. The reservoir age is within the range of ~400 and ~600 years suggested for the latitudinal band of 30°S and 60°S [Bard, 1988; Bard et al., 1989]. The purposes of this analysis are 1) to confirm the Holocene age of the surface sediments to validate the comparison with modern climatological data and, 2) to refine the age model generated via visual correlation of benthic oxygen isotope.

Table 2.3 AMS¹⁴C ages analyzed on planktic foraminifera and calibrated ages.

Core	Depth (cm)	Species	Conventional age (yr BP)	Standard deviation (\pm yr)	Reservoir Age (yr)	Laboratory code
SO213-60-2 (Multicore)	0–1	Planktic mix	11169	246	560	KIA45889
SO213-59-1 (Multicore)	0–1	Planktic mix	8001	210	560	KIA 45888
SO213-59-2 (Gravity Core)	9–10	<i>G. bulloides</i>	10669	122	560	KIA 47137
	45–46	<i>G. bulloides</i>	33487	366	560	KIA 47139

2.2.3. Measuring Trace Elements and Stable Isotopes in Foraminifera

All the samples analyzed to generate the Mg/Ca and stable isotope ($\delta^{18}\text{O}$ and $\delta^{13}\text{C}$) data discussed in the next chapters underwent the same analytical and cleaning procedures described in this section.

2.2.3.1. Foraminiferal Species Selection, Picking and Homogenization

The planktic foraminiferal species *Globigerina bulloides*, *Globorotalia inflata*, and *Globorotalia truncatulinoides* were used to reconstruct surface conditions or surface to thermocline conditions for each study. The selection of these species is centered on their ecological/habitat preferences, i.e. surface-dwelling (*Globigerina bulloides*) or subsurface-dwelling (*Globorotalia inflata* and *Globorotalia truncatulinoides*) and their affinity to a specific hydrographic feature along the water column at the study sites, such as the mixed layer, the thermocline, the deep thermocline and density surfaces (see [section 2.2.1](#)). These species were also chosen for their high abundance in the sediment samples.

Mg/Ca and stable isotope ($\delta^{18}\text{O}$ and $\delta^{13}\text{C}$) analyses were performed on the same sample, composed of 30 to 40 tests of each species. In most cases, the planktic foraminifera

were picked from the fraction 355–400 μm . The size fraction was occasionally extended (315–400 μm) in order to recover enough carbonate for the combined analysis of Mg/Ca and stable isotopes.

Prior to geochemical analyses, the shells were gently crushed between two methanol-cleaned microscope glass plates to open the chambers, mixed with a brush to homogenize the sample to minimize error arising from sample heterogeneity, and then split into subsamples for stable isotope analyses and Mg/Ca measurements [Anand *et al.*, 2003].

2.2.3.2. Sample Cleaning and Geochemical Analyses

Prior to stable isotope analyses, the subsamples were ultrasonically cleaned with deionized water and methanol. The analyses were performed at GEOMAR using a MAT253 spectrometer coupled with a Kiel IV Carbonate device (Thermo Fisher Scientific, Germany). The mass spectrometer is calibrated to NBS 19, and the isotope values are reported on the VPDB (Vienna PDB) scale. The analytical error was < 0.06 ‰ for $\delta^{18}\text{O}$ and < 0.04 ‰ for $\delta^{13}\text{C}$.

The Mg/Ca subsamples were cleaned according to Barker *et al.* [2003], adding a reductive step. The samples were rinsed 5 times with ultrapure water and twice with methanol (suprapure), including ultrasonic treatment after each rinse. Subsequently, samples were treated twice with 250 mL of a hot (97 °C) oxidizing 1% NaOH/H₂O₂ reagent (10 mL 0.1 N NaOH (analytical grade); 100 mL 30% H₂O₂ (suprapure) for 10 minutes. Every 2.5 minutes, the solution was cautiously agitated in order to release any gaseous build-up. After 5 minutes, the samples were placed in an ultrasonic bath for a few seconds in order to maintain the chemical reaction. The remaining oxidizing solution was removed through three rinsing steps with ultrapure water. After transferring the samples into clean vials, a weak acid leach with 250 mL 0.001 M nitric acid (HNO₃, subboiled distilled) was applied with 30 seconds ultrasonic treatment, followed by two rinses with ultrapure water. After removal of any remaining solution, the samples were dissolved in 500 mL 0.075 M HNO₃ (sub-boiling distilled), and diluted with ultrapure water to achieve Ca concentrations of 30–70 ppm.

Analyses were performed on an ICP OES (VARIAN 720–ES, GEOMAR) with a long-term analytical precision of ± 0.1 mmolmol⁻¹ for Mg/Ca of ECRM752–1 standard. Because clay contamination and post-depositional Mn-rich carbonate coatings can exert a significant control on Mg/Ca ratios, the efficiency of the cleaning was evaluated by monitoring the elements Fe, Al and Mn, which were measured alongside Mg (see corresponding chapter).

2.2.3.3. Mg/Ca-Temperature Conversion

The choice of the calibrations used in each study (Table 5) is based on 1) the availability of species-specific calibrations, 2) agreement between climatological data and

proxy signal in surface samples and/or the upper most samples of each core, and 3) comparison between the reconstructed record at each water depth assuming that surface temperature records should be warmer than those at greater depths.

Table 2.4 List of species and calibration used in the different chapters of this thesis.

Core site	Species	Calibration	Reference
SO213-59-1	<i>G. bulloides</i>	$Mg/Ca = 0.474e^{0.107T}$	Mashiotta et al. [1999]
SO213-59-2	<i>G. inflata</i>	$Mg/Ca = 0.72e^{0.076T}$	Groeneveld and Chiessi [2011]
	<i>G. truncatulinoides</i>	$Mg/Ca = 0.84e^{0.083T}$	Regenberg et al. [2009]
SO213-60-1	<i>G. bulloides</i>	$Mg/Ca = 0.474e^{0.107T}$	Mashiotta et al. [1999]
SO213-60-2	<i>G. inflata</i>	$Mg/Ca = 0.72e^{0.076T}$	Groeneveld and Chiessi [2011]
PS75/059-2	<i>G. bulloides</i>	$Mg/Ca = 0.474e^{0.107T}$	Mashiotta et al. [1999]
	<i>G. inflata</i>	$Mg/Ca = 0.52e^{0.1T}$	Elderfield and Ganssen [2000]

2.2.3.4. Reconstructing Salinity

As the local $\delta^{18}O_{SW}$ correlates linearly with seawater salinity on regional scales [LeGrande and Schmidt, 2006], we used the seawater $\delta^{18}O$ as a qualitative proxy for local salinity changes. However, we refrained from converting the $\delta^{18}O_{SW}$ signal into salinity unit because the $\delta^{18}O$ in the ocean is also determined by other factors in addition to salinity [LeGrande and Schmidt, 2011].

The $\delta^{18}O_{SW-IVC}$ calculation involves the subtraction of the temperature effect from the planktic $\delta^{18}O$ data ($\delta^{18}O_{SW} (VSMOW) = \delta^{18}O + 0.27 - (4.38 - (4.38^2 - 4 \times 0.1 (16.9 - T))^{1/2}) / (0.1 \times 2)$) [Shackleton, 1974], followed by the removal of the ice volume component (IVC) of the seawater $\delta^{18}O$ composition [Waelbroeck et al., 2002; Elderfield et al., 2010]. We linearly interpolated the [Waelbroeck et al., 2002; Elderfield et al., 2010] record at the time step of the respective core profile and subtracted the mean ocean $\delta^{18}O_{SW}$ from the reconstructed $\delta^{18}O_{SW}$ values.

2.3 Thesis Objective and Outline

The over-arching objective of this thesis is to reconstruct the evolution of the physical properties, i.e. temperature and salinity, of the upper South Pacific Ocean on different time-scales. In order to generate a representative picture of the upper ocean, different species of planktic foraminifera with well-known water depth preferences and various geochemical proxies were used. Comparing the environmental signal recorded by surface/mixed layer-

dwelling and deep/thermocline-dwelling foraminifera allows us to infer past changes at various water depths, from the sea surface to the thermocline (see section 1.6).

The manuscripts “*Evolution of the sea surface temperature and salinity in the central South Pacific during the past 500 ka: implications on ocean circulation*” (in preparation, Appendix 1) and “*Reduced admixture of North Atlantic Deep Water to the deep central South Pacific during the last two glacial periods*” (submitted, Appendix 2) are also associated to this thesis.

2.4. Thesis Outline

Chapter N°3 The Intermediate Waters formed in the Southern Ocean are critical for ventilating the thermocline in the Southern Hemisphere Gyres. However the impact of the Southern Ocean Intermediate Waters on the South Pacific Gyre’s thermocline is largely unknown. This manuscript entitled “*Disparities in glacial advection of Southern Ocean Intermediate Water to the South Pacific Gyre*” offers the first upper ocean reconstruction in the SPG. The $\text{Mg/Ca}_{\text{Temperature}}$ and stable oxygen isotope ($\delta^{18}\text{O}$) records were combined to reconstruct salinity variations during the last ~200 kyr at tree water depths i.e. surface, thermocline and deep-thermocline.

Chapter N°4 Antarctic Intermediate Water and Subantarctic Mode Water are considered as key players in the modulation of global climate system during glacial-interglacial time scales. They transfer climatic signals (e.g. heat, fresh water, salt and chemicals species) from the Southern Ocean to low latitudes through mechanisms such as “oceanic tunneling”. The manuscript entitled “*Glacial signature of Southern Ocean Intermediate Water at the Central South Pacific: implications for subsurface transfer of climatic signals*” focuses on the subsurface variability controlled by Antarctic Intermediate Water, which subducts at the Subantarctic Front (~54°S), and explore the differences and similarities of the subsurface signal between 54°S and the SPG (~45°S)(chapter 3).

Chapter N°5 entitled “*Evolution of the South Pacific Gyre’s thermocline in the past 600 kyr*” reconstructs the upper ocean reconstruction at the SPG (~44°S) at two water depths i.e. surface and thermocline. The $\text{Mg/Ca}_{\text{Temperature}}$ and stable oxygen isotope ($\delta^{18}\text{O}$) records were combined to reconstruct the SAMW-AAIW variability across the Mid-Bruhnes Event (MBE) and late Mid Pleistocene Transition.

2.5 References

- Anand, P., H. Elderfield, and M. H. Conte (2003), Calibration of Mg/Ca thermometry in planktonic foraminifera from a sediment trap time series, *Paleoceanography*, 18(2), 1050, doi:10.1029/2002PA000846.
- Arbuszewski, J., P. deMenocal, A. Kaplan, and E. C. Farmer (2010), On the fidelity of shell-derived $\delta^{18}\text{O}_{\text{seawater}}$ estimates, *Earth Plan. Sci. Lett.*, 300(3-4), 185–196, doi:10.1016/j.epsl.2010.10.035.
- Bard, E. (1988), Correction of accelerator mass spectrometry ^{14}C ages measured in planktonic foraminifera: paleoceanographic implications, *Paleoceanography*, 3(6), 635–645, doi:10.1029/PA003i006p00635.
- Bard, E., L. Labeyrie, M. Arnold, M. Labracherie, J.-J. Pichon, J. Duprat, and J.-C. Duplessy (1989), AMS- ^{14}C ages measured in deep sea cores from the Southern Ocean: implications for sedimentation rates during isotope stage 2, *Quat. Res.*, 31(2), 309–317.
- Barker, S., I. Cacho, H. Benway, and K. Tachikawa (2005), Planktonic foraminiferal Mg/Ca as a proxy for past oceanic temperatures: a methodological overview and data compilation for the Last Glacial Maximum, *Quat. Sci. Rev.*, 24(7-9), 821–834, doi:10.1016/j.quascirev.2004.07.016.
- Barker, S., M. Greaves, and H. Elderfield (2003), A study of cleaning procedures used for foraminiferal Mg/Ca paleothermometry, *Geochem. Geophys. Geosyst.*, 4, doi:10.1029/2003GC000559.
- Bé, A. (1959), Ecology of recent planktonic foraminifera - Part I: Areal Distribution in the Western North Atlantic, *Micropaleontology*, 5(1), 77–100.
- Bé, A. (1960), Ecology of recent planktonic foraminifera - Part 2: Bathymetric and seasonal distributions in the Sargasso Sea off Bermuda, *Micropaleontology*, 6(4), 373–392.
- Bé, A., and W. H. Hamlin (1967), Ecology of recent planktonic foraminifera - Part 3: distribution in the North Atlantic during the summer of 1962, *Micropaleontology*, 13(1), 87–106.
- Bé, A., and W. H. Hutson (1977), Ecology of planktonic foraminifera and biogeographic patterns of life and fossil assemblages in the Indian Ocean, *Micropaleontology*, 23(4), 369–414.
- Bé, A., C. Hemleben, O. R. Anderson, and M. Spindler (1977), Laboratory and field observations of living planktonic foraminifera, *Micropaleontology*, 23(2), 155–179.
- Bintanja, R., R. S. W. van de Wal, and J. Oerlemans (2005), Modelled atmospheric temperatures and global sea levels over the past million years, *Nature*, 437(7055), 125–128, doi:10.1038/nature03975.
- Boltovskoy, E. (1959), Foraminifera as biological indicators in the study of ocean currents, *Micropaleontology*, 5(4), 473–481.
- Boussetta, S., F. Bassinot, A. Sabbatini, N. Caillon, J. Nouet, N. Kallel, H. Rebaubier, G. Klinkhammer, and L. Labeyrie (2011), Diagenetic Mg-rich calcite in Mediterranean sediments: Quantification and impact on foraminiferal Mg/Ca thermometry, *Mar. Geol.*,

doi:10.1016/j.margeo.2010.12.011.

- Brown, S. J., and H. Elderfield (1996), Variations in Mg/Ca and Sr/Ca ratios of planktonic foraminifera caused by postdepositional dissolution: Evidence of shallow Mg-dependent dissolution, *Paleoceanography*, 11(5), 543–551.
- Cléroux, C., E. Cortijo, J.-C. Duplessy, and R. Zahn (2007), Deep-dwelling foraminifera as thermocline temperature recorders, *Geochem. Geophys. Geosyst.*, 8(4), doi:10.1029/2006GC001474.
- Cléroux, C., J. Lynch-Stieglitz, M. W. Schmidt, E. Cortijo, and J.-C. Duplessy (2009), Evidence for calcification depth change of *Globorotalia truncatulinoides* between deglaciation and Holocene in the Western Atlantic Ocean, *Marine Micropaleontology*, 73(1-2), 57–61, doi:10.1016/j.marmicro.2009.07.001.
- Cléroux, C., P. deMenocal, J. Arbuszewski, and B. Linsley (2013), Reconstructing the upper water column thermal structure in the Atlantic Ocean, *Paleoceanography*, doi:10.1002/palo.20050.
- d'Orbigny, A. D. (1826), Tableau méthodique de la classe des Céphalopodes, *Ann. Sci. Nat., sér 1*(tome 7), 277.
- d'Orbigny, A. D. (1839), Foraminifères des Iles Canaries, in *Histoire naturelles des Iles Canaries*, vol. 2(2), edited by W. Barker and P. Berthelot, pp. 1–1, Paris.
- Darling, K. F., and C. M. Wade (2008), The genetic diversity of planktic foraminifera and the global distribution of ribosomal RNA genotypes, *Marine Micropaleontology*, 67(3-4), 216–238, doi:10.1016/j.marmicro.2008.01.009.
- Darling, K. F., C. M. Wade, I. A. Stewart, D. Kroon, and R. Dingle (2000), Molecular evidence for genetic mixing of Arctic and Antarctic subpolar populations of planktonic foraminifers, *Nature*, 405, 43–47.
- Darling, K. F., M. Kucera, C. M. Wade, P. von Langen, and D. Pak (2003), Seasonal distribution of genetic types of planktonic foraminifer morphospecies in the Santa Barbara Channel and its paleoceanographic implications, *Paleoceanography*, 18(2), 1032, doi:10.1029/2001PA000723.
- Darling, K. F., M. Kucera, D. Kroon, and C. M. Wade (2006), A resolution for the coiling direction paradox in *Neogloboquadrina pachyderma*, *Paleoceanography*, 21(PA2011), doi:10.1029/2005PA001189.
- Dekens, P. S., D. W. Lea, D. K. Pak, and H. J. Spero (2002), Core top calibration of Mg/Ca in tropical foraminifera: Refining paleotemperature estimation, *Geochem. Geophys. Geosyst.*, 3(4), doi:10.1029/2001GC000200.
- Elderfield, H., and G. Ganssen (2000), Past temperature and $\delta^{18}\text{O}$ of surface ocean waters inferred from foraminiferal Mg/Ca ratios, *Nature*, 405, 442–445, doi:10.1038/35013033.
- Elderfield, H., M. Greaves, S. Barker, I. R. Hall, A. Tripathi, P. Ferretti, S. Crowhurst, L. Booth, and C. Daunt (2010), A record of bottom water temperature and seawater $d^{18}\text{O}$ for the Southern Ocean over the past 440 kyr based on Mg/Ca of benthic foraminiferal *Uvigerina* spp, *Quat. Sci. Rev.*, 29(1-2), 160–169, doi:10.1016/j.quascirev.2009.07.013.

- Elderfield, H., P. Ferretti, M. Greaves, and S. Crowhurst (2012), Evolution of Ocean Temperature and Ice Volume Through the Mid-Pleistocene Climate Transition, *Science*, doi:10.1126/science.1221294.
- Fairbanks, R. G. (1989), A 17, 000-year glacio-eustatic sea level record: influence of glacial melting rates on the Younger Dryas event and deep-ocean circulation, *Nature*, 342(6250), 637–642.
- Fairbanks, R. G., and P. H. Wiebe (1980), Foraminifera and chlorophyll maximum: vertical distribution, seasonal succession, and paleoceanographic significance, *Science*, 209(4464), 1524–1526.
- Farmer, E. J., M. R. Chapman, and J. E. Andrews (2011), Holocene temperature evolution of the subpolar North Atlantic recorded in the Mg/Ca ratios of surface and thermocline dwelling planktonic foraminifers, *Global and Planetary Change*, 79(3-4), 234–243, doi:10.1016/j.gloplacha.2011.02.003.
- Feldmeijer, W., B. Metcalfe, G.-J. A. Brummer, and G. M. Ganssen (2014), Reconstructing the depth of the permanent thermocline through the morphology and geochemistry of the deep dwelling planktonic foraminifer *Globorotalia truncatulinoides*, *Paleoceanography*, 30, 1–22, doi:10.1002/2014PA002687.
- Ferguson, J., G. Henderson, M. Kucera, and R. Rickaby (2008), Systematic change of foraminiferal Mg/Ca ratios across a strong salinity gradient, *Earth Plan. Sci. Lett.*, 265(1-2), 153–166, doi:doi:10.1016/j.epsl.2007.10.011.
- Franke, J., A. Paul, and M. Schulz (2008), Modeling variations of marine reservoir ages during the last 45 000 years, *Clim. Past*, 4(1), 81–110.
- Friedrich, O., R. Schiebel, and P. Wilson (2012), Influence of test size, water depth, and ecology on Mg/Ca, Sr/Ca, $\delta^{18}\text{O}$ and $\delta^{13}\text{C}$ in nine modern species of planktic foraminifers, *Earth Plan. Sci. Lett.*, doi:10.1016/j.epsl.2011.12.002.
- Greaves, M. J. (2008), Trace Elements in Marine Biogenic Carbonates: Analysis and Application to Past Ocean Chemistry, 1–212 pp. University of Southampton, 4 March.
- Groeneveld, J., and C. M. Chiessi (2011), Mg/Ca of *Globorotalia inflata* as a recorder of permanent thermocline temperatures in the South Atlantic, *Paleoceanography*, 26(2), doi:10.1029/2010PA001940.
- Hayward, B. W. et al. (2008), The effect of submerged plateaux on Pleistocene gyral circulation and sea-surface temperatures in the Southwest Pacific, *Global and Planetary Change*, 63(4), 309–316, doi:10.1016/j.gloplacha.2008.07.003.
- Healy-Williams, N. (1983), Fourier shape analysis of *Globorotalia truncatulinoides* from late Quaternary sediments in the southern Indian Ocean, *Marine Micropaleontology*, 8(1), 1–15.
- Hirschi, J. J. M., and J. Lynch-Stieglitz (2006), Ocean margin densities and paleoestimates of the Atlantic meridional overturning circulation: A model study, *Geochem. Geophys. Geosyst.*, 7(10), doi:10.1029/2006GC001301.
- Hönisch, B., K. A. Allen, D. W. Lea, and H. J. Spero (2013), The influence of salinity on Mg/Ca in planktic foraminifers – Evidence from cultures, core-top sediments and

- complementary $\delta^{18}\text{O}$, *Geochim. Cosmochim. Acta*, 121, 196–213, doi:dx.doi.org/10.1016/j.gca.2013.07.028.
- Jian, Z., B. Li, B. Huang, and J. Wang (2000), Globorotalia truncatulinoides as indicator of upper-ocean thermal structure during the Quaternary: evidence from the South China Sea and Okinawa Trough, *Palaeogeogr. Palaeoclimatol. Palaeoecol.*, 162(3-4), 287–298, doi:10.1016/S0031-0182(00)00132-2.
- Katz, M. E., B. S. Cramer, A. Franzese, B. Hönisch, K. Miller, Y. Rosenthal, and J. D. Wright (2010), Traditional and emerging geochemical proxies in foraminifera, *The Journal of Foraminiferal Research*, 40(2), 165–192.
- Kennett, J. P. (1968), Globorotalia truncatulinoides as a paleo-oceanographic index, *Science*, 159(3822), 1461–1463.
- Kennett, J. P. (1978), The development of planktonic biogeography in the Southern Ocean during the Cenozoic.
- Kucera, M. (2009), Determination of past sea surface temperatures, in *Climate and Oceans*, edited by J. H. Steele, S. A. Thorpe, and K. K. Turekian, pp. 328–343, Elsevier, Amsterdam.
- Kucera, M. (2007), Chapter Six Planktonic Foraminifera as Tracers of Past Oceanic Environments, vol. 1, pp. 213–262, Elsevier.
- Langen, von, P. J. (2005), Effects of temperature on Mg/Ca in neogloboquadrinid shells determined by live culturing, *Geochem. Geophys. Geosyst.*, 6(10), doi:10.1029/2005GC000989.
- Lea, D. W. (1999), Trace Elements in Foraminiferal Calcite, in *Modern Foraminifera*, edited by B. K. Sen Gupta, pp. 259–277, Kluwer Academic Publishers.
- Lea, D. W. (2006), Elemental and Isotopic Proxies of Past Ocean Temperatures, in *Treatise on Geochemistry*, vol. 6, edited by H. D. Holland and K. K. Turekian, pp. 365–390, Elsevier, Oxford.
- Lea, D. W. (2014), Elemental and Isotopic Proxies of Past Ocean Temperatures, in *Treatise on Geochemistry*, vol. 8, edited by H. D. Holland and K. K. Turekian, pp. 373–397, Elsevier, Oxford.
- Lea, D. W., T. A. Mashiotta, and H. J. Spero (1999), Controls on magnesium and strontium uptake in planktonic foraminifera determined by live culturing, *Geochim. Cosmochim. Acta*, 63(16), 2369–2379, doi:10.1016/S0016-7037(99)00197-0.
- LeGrande, A. N., and G. A. Schmidt (2006), Global gridded data set of the oxygen isotopic composition in seawater, *Geophys. Res. Lett.*, 33(12), L12604, doi:10.1029/2006GL026011.
- LeGrande, A. N., and G. A. Schmidt (2011), Water isotopologues as a quantitative paleosalinity proxy, *Paleoceanography*, 26(3), PA3225, doi:10.1029/2010PA002043.
- LeGrande, A. N., J. Lynch-Stieglitz, and E. C. Farmer (2004), Oxygen isotopic composition of Globorotalia truncatulinoides as a proxy for intermediate depth density, *Paleoceanography*, 19(4), doi:10.1029/2004PA001045.

- Lisiecki, L. E., and M. E. Raymo (2005), A Pliocene-Pleistocene stack of 57 globally distributed benthic $\delta^{18}\text{O}$ records, *Paleoceanography*, 20(1), doi:10.1029/2004PA001071.
- Lohmann, G. P., and N. Schweitzer (1990), *Globorotalia truncatulinoides* Growth and Chemistry as Probe of the Past Thermocline: 1. Shell Size, *Paleoceanography*, 5(1), 55–75.
- Lončarić, N., F. J. Peeters, D. Kroon, and G.-J. A. Brummer (2006), Oxygen isotope ecology of recent planktic foraminifera at the central Walvis Ridge (SE Atlantic), *Paleoceanography*, 21(3), doi:10.1029/2005PA001207.
- Lynch-Stieglitz, J. (2003), Tracers of Past Ocean Circulation, in *Treatise on Geochemistry*, vol. 6, edited by H. D. Holland and K. K. Turekian, pp. 433–451, Elsevier, Oxford.
- Lynch-Stieglitz, J., W. B. Curry, and N. Slowey (1999), A geostrophic transport estimate for the Florida Current from the oxygen isotope composition of benthic foraminifera, *Paleoceanography*, 14(3), 360–373.
- Marchant, M., D. Hebbeln, and G. Wefer (1998), Seasonal flux patterns of planktic foraminifera in the Peru–Chile Current, *Deep-Sea Res. Part I*, 45(7), 1161–1185.
- Marchant, M., D. Hebbeln, S. Giglio, C. Coloma, and H. E. González (2004), Seasonal and interannual variability in the flux of planktic foraminifera in the Humboldt Current System off central Chile (30°S), *Deep Sea Research Part II: Topical Studies in Oceanography*, 51(20-21), 2441–2455, doi:10.1016/j.dsr2.2004.08.013.
- Marr, J. P., H. C. Bostock, L. Carter, A. Bolton, and E. Smith (2013), Differential effects of cleaning procedures on the trace element chemistry of planktonic foraminifera, *Chemical Geology*, 351, 310–323, doi:10.1016/j.chemgeo.2013.05.019.
- Marr, J. P., J. A. Baker, L. Carter, A. S. R. Allan, G. B. Dunbar, and H. C. Bostock (2011), Ecological and temperature controls on Mg/Ca ratios of *Globigerina bulloides* from the southwest Pacific Ocean, *Paleoceanography*, 26(2), doi:10.1029/2010PA002059.
- Martínez, R. (1997), Decreasing influence of Subantarctic Mode Water north of the Tasman Front over the past 150 kyr, *Palaeogeogr. Palaeoclimatol. Palaeoecol.*, 131(3), 355–364.
- Martínez-Botí, M., P. Mortyn, D. Schmidt, D. Vance, and D. Field (2011), Mg/Ca in foraminifera from plankton tows: Evaluation of proxy controls and comparison with core tops, *Earth Plan. Sci. Lett.*, 307, 113–125, doi:doi:10.1016/j.epsl.2011.04.019.
- Mashiotta, T. A., D. W. Lea, and H. J. Spero (1999), Glacial–interglacial changes in Subantarctic sea surface temperature and $\delta^{18}\text{O}$ -water using foraminiferal Mg, *Earth Plan. Sci. Lett.*, 170, 417–432.
- Mathien-Blard, E., and F. Bassinot (2009), Salinity bias on the foraminifera Mg/Ca thermometry: Correction procedure and implications for past ocean hydrographic reconstructions, *Geochem. Geophys. Geosyst.*, 10(12), doi:10.1029/2008GC002353.
- McConnell, M. C., and R. C. Thunell (2005), Calibration of the planktonic foraminiferal Mg/Ca paleothermometer: Sediment trap results from the Guaymas Basin, Gulf of California, *Paleoceanography*, 20(2), doi:10.1029/2004PA001077.
- Medina-Elizalde, M., D. W. Lea, and M. S. Fantle (2008), Implications of seawater Mg/Ca

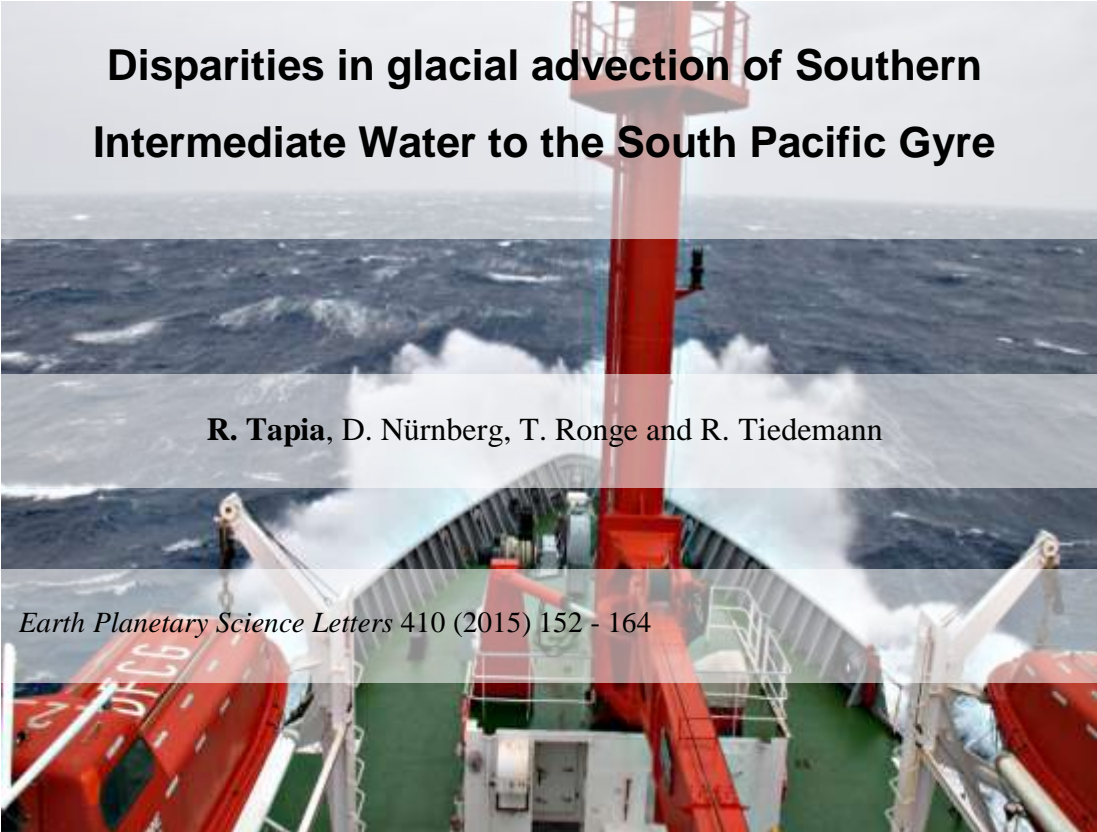
- variability for Plio-Pleistocene tropical climate reconstruction, *Earth Plan. Sci. Lett.*, 269(3), 585–595, doi:doi:10.1016/j.epsl.2008.03.014.
- Mekik, F., R. François, and M. Soon (2007), A novel approach to dissolution correction of Mg/Ca–based paleothermometry in the tropical Pacific, *Paleoceanography*, 22(3), doi:10.1029/2007PA001504.
- Mix, A. C., E. Bard, G. Eglinton, L. D. Keigwin, A. C. Ravelo, and Y. Rosenthal (2000), Alkenones and multiproxy strategies in paleoceanographic studies, *Geochem. Geophys. Geosyst.*, 1.
- Mohtadi, M., D. Hebbeln, and M. Marchant (2005), Upwelling and productivity along the Peru–Chile Current derived from faunal and isotopic compositions of planktic foraminifera in surface sediments, *Mar. Geol.*, 216(3), 107–126, doi:10.1016/j.margeo.2005.01.008.
- Morard, R., F. Quillévéré, C. J. Douady, C. de Vargas, T. de Garidel-Thoron, and G. Escarguel (2011), Worldwide Genotyping in the Planktonic Foraminifer *Globoconella inflata*: Implications for Life History and Paleoceanography, edited by A. Stepanova, *PLoS ONE*, 6(10), e26665, doi:10.1371/journal.pone.0026665.t003.
- Mortyn, P. G., J. C. Herguera, and M. A. Martínez-Botí (2011), Instrumental validation of *Globigerinoides ruber* Mg/Ca as a proxy for NE Pacific summer SST, *Geophys. Res. Lett.*, 38(16), doi:10.1029/2011GL047803.
- Mulitza, S., A. Dürkoop, W. Hale, G. Wefer, and H. S. Niebler (1997), Planktonic foraminifera as recorders of past surface-water stratification, *Geol.*, 25(4), 335–338, doi:10.1130/0091-7613(1997)025<0335:PFAROP>2.3.CO;2.
- Niebler, H. S., and R. Gersonde (1998), A planktic foraminiferal transfer function for the southern South Atlantic Ocean, *Marine Micropaleontology*, 34(3), 213–234.
- Nürnberg, D. (1995), Magnesium in Tests of *Neogloboquadrina*-*Pachyderma* Sinistral From High Northern and Southern Latitudes, *The Journal of Foraminiferal Research*, 25(4), 350–368.
- Nürnberg, D., and J. Groeneveld (2006), Pleistocene variability of the Subtropical Convergence at East Tasman Plateau: evidence from planktonic foraminiferal Mg/Ca (ODP Site 1172A), *Geochem. Geophys. Geosyst.*, 7, Q04P11, doi:10.1029/2005GC000984.
- Nürnberg, D., J. Bijma, and C. Hemleben (1996), Assessing the reliability of magnesium in foraminiferal calcite as a proxy for water mass temperatures, *Geochim. Cosmochim. Acta*, 60(5), 803–814.
- Pahnke, K., R. Zahn, H. Elderfield, and M. Schulz (2003), 340,000-year centennial-scale marine record of Southern Hemisphere climatic oscillation, *Science*, 301(5635), 948–952, doi:10.1126/science.1084451.
- Peeters, F. J. C., G.-J. A. Brummer, and G. Ganssen (2002), The effect of upwelling on the distribution and stable isotope composition of *Globigerina bulloides* and *Globigerinoides ruber* (planktic foraminifera) in modern surface waters of the NW Arabian Sea, *Global and Planetary Change*, 34(3), 269–291.

- Pena, L. D., E. Calvo, I. Cacho, S. Eggins, and C. Pelejero (2005), Identification and removal of Mn-Mg-rich contaminant phases on foraminiferal tests: Implications for Mg/Ca past temperature reconstructions, *Geochem. Geophys. Geosyst.*, 6, doi:10.1029/2005GC000930.
- Pena, L. D., I. Cacho, P. Ferretti, and M. A. Hall (2008), El Niño–Southern Oscillation–like variability during glacial terminations and interlatitudinal teleconnections, *Paleoceanography*, 23, PA3101, doi:10.1029/2008PA001620.
- Quillévéré, F., R. Morard, G. Escarguel, C. J. Douady, Y. Ujiie, T. de Garidel-Thoron, and C. de Vargas (2011), Global scale same-specimen morpho-genetic analysis of *Truncorotalia truncatulinoides*: A perspective on the morphological species concept in planktonic foraminifera, *Palaeogeogr. Palaeoclimatol. Palaeoecol.*, doi:doi:10.1016/j.palaeo.2011.03.013.
- Ravelo, A. C., and C. Hillaire-Marcel (2007), The Use of Oxygen and Carbon Isotopes of Foraminifera in Paleoceanography, in *Proxies in Late Cenozoic Paleoceanography*, vol. 1 of Developments in Marine Geology, edited by C. Hillaire-Marcel and A. De Vernal, pp. 735–764, Elsevier.
- Ravelo, A. C., K. Billups, P. S. Dekens, T. D. Herbert, and K. T. Lawrence (2007), Deep-Time Perspectives on Climate Change: Marrying the Signal from Computer Models and Biological Proxies, in *Deep-Time Perspectives on Climate Change: Marrying the Signal from Computer Models and Biological Proxies.*, edited by M. Williams, A. M. Haywood, F. J. Gregory, and D. N. Schmidt, pp. 563–573, The Micropaleontology Society, Special Publication, London.
- Ravelo, A., and R. Fairbanks (1992), Oxygen isotopic composition of multiple species of planktonic foraminifera: Recorders of the modern photic zone temperature gradient, *Paleoceanography*, 7(6), 815–831.
- Regenberg, M., A. Regenberg, D. Garbe-Schönberg, and D. W. Lea (2014), Global dissolution effects on planktonic foraminiferal Mg/Ca ratios controlled by the calcite-saturation state of bottom waters, *Paleoceanography*, doi:10.1002/2013PA002492.
- Regenberg, M., D. Nürnberg, S. Steph, J. Groeneveld, D. Garbe-Schönberg, R. Tiedemann, and W.-C. Dullo (2006), Assessing the effect of dissolution on planktonic foraminiferal Mg/Ca ratios: Evidence from Caribbean core tops, *Geochem. Geophys. Geosyst.*, 7, doi:10.1029/2005GC001019.
- Regenberg, M., S. Steph, D. Nürnberg, R. Tiedemann, and D. Garbe-Schönberg (2009), Calibrating Mg/Ca ratios of multiple planktonic foraminiferal species with $\delta^{18}\text{O}$ -calcification temperatures: paleothermometry for the upper water column, *Earth Plan. Sci. Lett.*, 278, 324–336, doi:10.1016/j.epsl.2008.12.019.
- Reimer, P. J., M. G. Baillie, E. Bard, A. Bayliss, J. W. Beck, P. G. Blackwell, C. B. Ramsey, C. E. Buck, G. S. Burr, and R. L. Edwards (2009), IntCal09 and Marine09 radiocarbon age calibration curves, 0-50,000 years cal BP, *Radiocarbon*, 51(3), 1111–1150.
- Renaud, S., and D. N. Schmidt (2003), Habitat tracking as a response of the planktic foraminifer *Globorotalia truncatulinoides* to environmental fluctuations during the last 140 kyr, *Marine Micropaleontology*, 49(1-2), 97–122, doi:10.1016/S0377-8398(03)00031-8.
- Rohling, E. J. (2013), Oxygen isotope composition of seawater, edited by S. A. Elias,

Encyclopedia of Quaternary Science, 2, 915–922.

- Rohling, E. J., and G. R. Bigg (1998), Paleosalinity and $\delta^{18}\text{O}$: A critical assessment, *J. Geophys. Res.*, 103(C1), 1307, doi:10.1029/97JC01047.
- Rohling, E. J., and S. Cooke (1999), Stable oxygen and carbon isotopes in foraminiferal carbonate shells, in *Modern Foraminifera*, edited by B. K. Sen Gupta, pp. 239–258, Kluwer Academic Publishers, Dordrecht.
- Sadekov, A. Y., S. M. Eggins, G. P. Klinkhammer, and Y. Rosenthal (2010), Effects of seafloor and laboratory dissolution on the Mg/Ca composition of Globigerinoides sacculifer and Orbulina universa tests--A laser ablation ICPMS microanalysis perspective, *Earth Plan. Sci. Lett.*, 292(3-4), 312–324, doi:doi:10.1016/j.epsl.2010.01.039.
- Schiebel, R., J. Bijma, and C. Hemleben (1997), Population dynamics of the planktic foraminifer Globigerina bulloides from the eastern North Atlantic, *Deep Sea Research Part I: Oceanographic Research Papers*, 44(9-10), 1701–1713, doi:10.1016/S0967-0637(97)00036-8.
- Shackleton, N. J. (1974), Attainment of isotopic equilibrium between ocean water and the benthonic foraminifera genus *Uvigerina*: isotopic changes in the ocean during the last glacial, *Cent. Nat. Rech. Sci. Colloq. Int.* (219), 203–209.
- Sosdian, S., and Y. Rosenthal (2009), Deep-Sea Temperature and Ice Volume Changes Across the Pliocene-Pleistocene Climate Transitions, *Science*, 325(5938), 306–310, doi:10.1126/science.1169938.
- Spear, J., and R. Poore (2011), Globorotalia truncatulinoides (dextral) Mg/Ca as a proxy for Gulf of Mexico winter mixed-layer temperature: Evidence from a sediment trap in the northern ..., doi:doi:10.1016/j.marmicro.2011.05.001.
- Spencer-Cervato, C., and H. R. Thierstein (1997), First appearance of Globorotalia truncatulinoides: cladogenesis and immigration, *Marine Micropaleontology*, 30(4), 267–291.
- Spero, H. J., and D. W. Lea (1996), Experimental determination of stable isotope variability in Globigerina bulloides: implications for paleoceanographic reconstructions, *Marine Micropaleontology*, 28(3), 231–246.
- Steinke, S., H.-Y. Chiu, P.-S. Yu, C.-C. Shen, L. Löwemark, H.-S. Mii, and M.-T. Chen (2005), Mg/Ca ratios of two Globigerinoides ruber(white) morphotypes: Implications for reconstructing past tropical/subtropical surface water conditions, *Geochem. Geophys. Geosyst.*, 6(11), doi:10.1029/2005GC000926.
- Steinke, S., J. Groeneveld, H. Johnstone, and R. Rendle-Bühning (2010), East Asian summer monsoon weakening after 7.5 Ma: Evidence from combined planktonic foraminifera Mg/Ca and $\delta^{18}\text{O}$ (ODP Site 1146; northern South China Sea), *Palaeogeogr. Palaeoclimatol. Palaeoecol.*, 289(1), 33–43, doi:10.1016/j.palaeo.2010.02.007.
- Steph, S., M. Regenberg, R. Tiedemann, S. Mulitza, and D. Nürnberg (2009), Stable isotopes of planktonic foraminifera from tropical Atlantic/Caribbean core-tops: Implications for reconstructing upper ocean stratification, *Marine Micropaleontology*, 71(1-2), 1–19, doi:10.1016/j.marmicro.2008.12.004.

- Stuiver, M., and P. J. Reimer (1993), Extended C-14 Data-Base and Revised Calib 3.0 C-14 Age Calibration Program, *Radiocarbon*, 35(1), 215–230.
- Thornalley, D. J. R., H. Elderfield, and I. N. McCave (2008), Holocene oscillations in temperature and salinity of the surface subpolar North Atlantic, *Nature*, 457(7230), 711–714, doi:10.1038/nature07717.
- Tolderlund, D. S., and A. Bé (1971), Seasonal distribution of planktonic foraminifera in the western North Atlantic, *Micropaleontology*, 17(3), 297–329.
- van Raden, U. J., J. Groeneveld, M. Raitzsch, and M. Kucera (2011), Mg/Ca in the planktonic foraminifera *Globorotalia inflata* and *Globigerinoides bulloides* from Western Mediterranean plankton tow and core top samples, *Marine Micropaleontology*, 78(3-4), 101–112, doi:10.1016/j.marmicro.2010.11.002.
- Waelbroeck, C., L. Labeyrie, E. Michel, J. C. Duplessy, J. McManus, K. Lambeck, E. Balbon, and M. Labracherie (2002), Sea-level and deep water temperature changes derived from benthic foraminifera isotopic records, *Quat. Sci. Rev.*, 21, 295–305.
- Wilke, I., H. Meggers, and T. Bickert (2009), Depth habitats and seasonal distributions of recent planktic foraminifers in the Canary Islands region (29° N) based on oxygen isotopes, *Deep-Sea Res. Part I*, 56(1), 89–106, doi:doi:10.1016/j.dsr.2008.08.001.



Disparities in glacial advection of Southern Intermediate Water to the South Pacific Gyre

R. Tapia, D. Nürnberg, T. Ronge and R. Tiedemann

Earth Planetary Science Letters 410 (2015) 152 - 164

Abstract

The Intermediate Waters formed in the Southern Ocean are critical for ventilating the thermocline in the Southern Hemisphere Gyres and transporting climatic signals from high to low latitudes on glacial–interglacial time-scales. Despite the importance of the Southern Ocean Intermediate Waters (SOIWs), information on past changes in SOIWs formation is fragmentary, and its impact on the South Pacific Gyre (SPG)′s thermocline largely unknown. Here, we present a 200 kyr record of paired Mg/Ca ratios and stable oxygen isotope from surface and deep dwelling planktic foraminifera, from the SPG. On average, the *Globigerina bulloides* Mg/Ca-derived sea surface temperatures show similar conditions during the LGM and Marine Isotope Stage (MIS) 6 (9.4 °C versus 9.8 °C). In contrast, the subsurface temperatures derived from the Mg/Ca values of *Globorotalia inflata* and *Globorotalia truncatulinoides* suggest that LGM is ~3 to ~2 °C colder than MIS 6. Furthermore, at subsurface depths the reconstructed $\delta^{18}\text{O}_{\text{SW-IVC}}$ record (proxy for relative local salinity changes) suggests opposite glacial conditions, with slightly saltier–than–Holocene waters during MIS 6, and fresher–than–Holocene waters during LGM. Contrasting glacial scenarios, plausibly due to changes in the presence of SOIWs at the study site, suggest variable formation and/or advection of SOIWs to the SPG during different glacial stages. The variability in SOIWs is probably driven by the changes in the intensity of the Southern Westerly Winds.

CHAPTER 3

3.1 Introduction

The Southern Ocean Intermediate Waters (SOIWs), such as Antarctic Intermediate Water (AAIW) and Subantarctic Mode Water (SAMW), are critical pathways for atmospheric gases and upwelled nutrients [Russell and Dickson, 2003; Sabine *et al.*, 2004; Sarmiento *et al.*, 2004] to be transported to the ocean interior. Various studies suggest that these water masses, which are located at intermediate water depths, have played an important role in climate modulation and oceanic reorganization on glacial-interglacial time-scales [Spero and Lea, 2002; Bostock *et al.*, 2004; Pahnke and Zahn, 2005; Pahnke *et al.*, 2008; Pena *et al.*, 2008; 2013].

The South East Pacific (SEP, a list of acronyms is given in Table 3.1) is the principal formation area of SAMW and AAIW (Figure 3.1) [Tsuchiya and Talley, 1998; Hanawa and Talley, 2001; Sallée *et al.*, 2006; Bostock *et al.*, 2010; Hartin *et al.*, 2011; Hasson *et al.*, 2011; Bostock *et al.*, 2013; Holte *et al.*, 2013]. The SAMW is formed just north of the Subantarctic Front (SAF) via the deepening of mixed layers during wintertime convection [Sloyan *et al.*, 2010]. The temperature and salinity properties of the SAMW are controlled by the incorporation of fresh water (i.e. via precipitation, ice melt and northward Ekman transport of the Subantarctic Surface Water (SASW)) during its formation in the SEP [Schneider and Bravo, 2006].

The SAMW becomes progressively colder, fresher, and denser as it approaches the Drake Passage [~ 4 °C; McCartney, 1977], forming the coldest and densest variety of SAMW known as AAIW [McCartney, 1977; Lisiecki and Raymo, 2005]. The AAIW is characterized by a vertical salinity minimum and high gas content [Hartin *et al.*, 2011]. SAMW and AAIW are exported to the lower thermocline in the Subtropical Gyres of Southern Hemisphere oceans [McCartney, 1977; Hanawa and Talley, 2001]. These water masses play a fundamental role in ventilating the modern thermocline of the subtropical South Pacific Gyre (SPG) [Hartin *et al.*, 2011; Herraiz-Borreguero and Rintoul, 2011a; Holte *et al.*, 2012] as well as transporting heat, salt and nutrient from the Southern Ocean to lower latitudes, via processes such as “oceanic tunneling” on glacial-interglacial time-scales [Liu *et al.*, 2002; Pena *et al.*, 2008; 2013].

To date, the enhanced SOIWs presence during cold periods in mid and low latitudes of the East Pacific has been explained by invoking either latitudinal displacement and/or stronger Southern Westerly Wind (SWW) [Pena *et al.*, 2008; Muratli *et al.*, 2010; Martínez-Méndez *et al.*, 2013; Pena *et al.*, 2013]. An opposite situation, i.e. increased formation of SOIWs during warm periods, has been proposed in the South West Pacific (SWP) off New Zealand [Pahnke and Zahn, 2005]. These regional differences emphasize further need of

geographical constraint in the data-poor South Pacific, in order to better understand the spatial pattern of SOIWs formation and distribution in the South Pacific.

Here we present paired Mg/Ca and $\delta^{18}\text{O}$ records of three species of planktic foraminifera (*Globigerina bulloides*, *Globorotalia inflata* and *Globorotalia truncatulinoides*) from core SO213-59-2 in the central South Pacific covering the last 200 kyr. The aim of this study is to reconstruct the water column structure in the subtropical SPG during the late Quaternary, and to evaluate the subsurface variability (thermocline water depth) potentially influenced by the “enhanced injection” of SOIWs (SAMW/AAIW) formed in the SEP during glacial stages.

Table 3.1 Acronyms and abbreviations.

ACC	Antarctic Circumpolar Current	SEP	South East Pacific
AAIW	Antarctic Intermediate Water	SOIW	Southern Ocean Intermediate Waters
DT	Deep–Thermocline Temperature	SPG	South Pacific Gyre
PF	Polar Front	STF	Subtropical Front
PDW	Pacific Deep Water	SST	Sea Surface Temperature
SAF	Subantarctic Front	SWP	South West Pacific
SAM	Southern Annular Mode	SWW	Southern Westerly Winds
SAMW	Sub Antarctic Mode Water	TT	Thermocline Temperature
SASW	Subantarctic Surface Water		

3.2 Material and Methods

The age model of the gravity core SO213-59-2 (45°49' S, 116°52' W; 3161 m water depth; [Figure 1a](#)), retrieved from the East Pacific Rise during R/V Sonne cruise SOPATRA, is based on the correlation of benthic foraminiferal $\delta^{18}\text{O}$ record (*Cibicidoides wuellerstorfi*, 250–315 μm) to the global benthic $\delta^{18}\text{O}$ stack LR04 [Lisiecki and Raymo, 2005] using the software package AnalySeries 2.0 [Paillard et al., 1996]. The age model is further supported by two ^{14}C accelerator mass spectrometer (AMS) dates of *G. bulloides* measured at the Leibniz-Laboratory for Radiometric Dating and Isotope Research of the University of Kiel. AMS ^{14}C ages were converted to calendar age using the software CALIB 7.0 [Stuiver and Reimer, 1993] with the Marine13 database [Reimer et al., 2009], and ΔR correction of 560 years [Bremen reservoir age database; Franke et al., 2008]. The reservoir age is within the range of ~400 and ~600 years suggested for the latitudinal band of 30° S and 60° S [Bard, 1988;

Bard et al., 1989]. The uppermost sediment (0–1 cm) from multicore SO213-59-1 (same location as the gravity core) was also radiocarbon dated (Table 3.2).

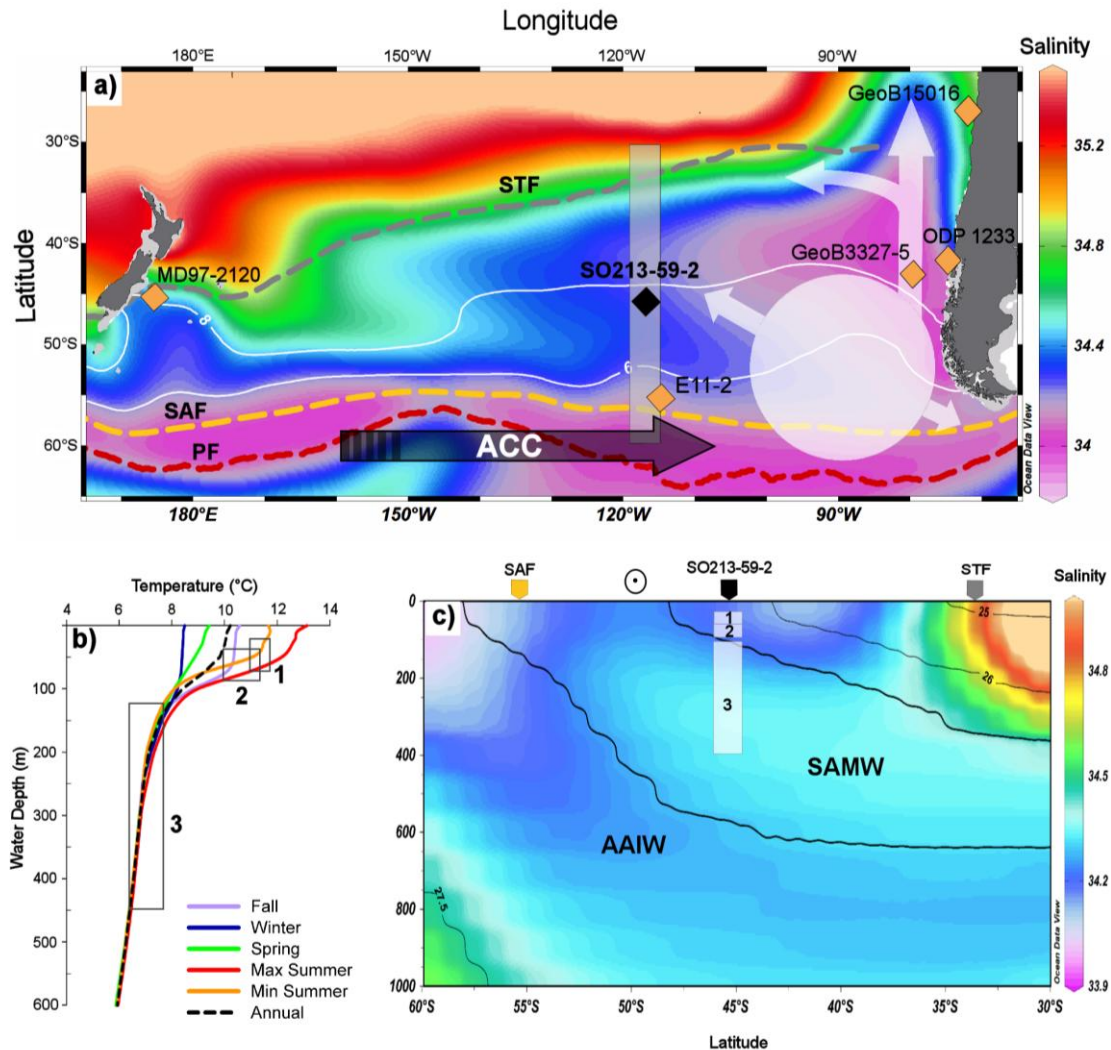


Figure 3.1 (a) Chart showing salinity (colours) and temperature (white contour lines; WOA09) at 150 m water. The location of the core SO213-59-2 and reference sites MD97-2120 [Pahnke et al., 2003], EC11-2 [Mashiotta et al., 1999], GeoB3327-5 [Ho et al., 2012], ODP 1233 [Muratli et al., 2010] and GeoB15016 [Martínez-Méndez et al., 2013] are indicated by diamonds. The main SOIW formation area and dispersal path are marked by white area and arrows [after Hartin et al., 2011; Herraiz-Borreguero and Rintoul, 2011b]. Dashed lines denote the oceanographic frontal boundaries: the Subtropical Front (STF, grey), the Subantarctic Front (SAF, yellow), and the Polar Front (PF, red) [Orsi et al., 1995]. (b) Vertical profile of the annual mean, the seasonal mean, the minimum and the maximum summer temperature of the upper 600 m of the water column at the core location (WOA09). The average Holocene Mg/Ca–temperature for *G. bulloides* (1), *G. inflata* (2) and *G. truncatulinoides* (3) are plotted against the estimated habitat water depth of each species. The depth ranges of *G. bulloides* (< 50 m), *G. inflata* (~50 – 100 m) and *G. truncatulinoides* (> 150 m) are used to define “surface water”, “thermocline water” and “deep-thermocline water”. Boxes mark ranges of Mg/Ca–temperatures from surface sediments + Holocene sediments. (c) Detail of the S-N transect denoted in (a; vertical bar), indicating the vertical distribution of SAMW (26.6 – 27 kgm⁻³; ~100 – 600 m) and AAIW (> 27 kgm⁻³; > 600 m) [Tsuchiya and Talley, 1998; Hanawa and Talley, 2001]. Numbers in the white boxes correspond to the assumed habitat depth range of the planktic foraminifera species analyzed as in (b). Open circle with dot denotes eastward directed flow of the maximum SWW. Colour-coded arrows mark oceanic fronts depicted in (a).

Table 3.2 AMS¹⁴C ages analyzed on planktic foraminifera and calibrated ages at the site SO213-59 (45°49' S, 116°52' W).

Core	Depth (cm)	Species	Conventional age (yr BP)	Standard deviation (\pm yr)	Reservoir Age (yr)	Laboratory code
SO213-59-1 (Multicore)	0–1	Planktic mix	8001	210	560	KIA 45888
SO213-59-2 (Gravity Core)	9–10	<i>G. bulloides</i>	10669	122	560	KIA 47137
	45–46	<i>G. bulloides</i>	33487	366	560	KIA 47139

Three planktic foraminiferal species, a mixed layer dweller i.e. *G. bulloides* and two deep dwellers i.e. *G. inflata*, and *G. truncatulinoides* (dextral), were picked from surface sediments (top 1 cm of multicore) and SO213-59-2 at 2 cm intervals. The Mg/Ca and stable isotope ($\delta^{18}\text{O}$) measurements were performed on the same sample composing 30 to 40 shells from the size fraction 355–400 μm . Occasionally, we extended the size fraction to 315–400 μm to recover enough calcite material from *G. inflata* and *G. truncatulinoides*.

The $\delta^{18}\text{O}$ measurements were performed at GEOMAR, Kiel, using a MAT 253 mass spectrometer (Thermo Fisher Scientific, Germany) coupled with a Kiel IV Carbonate device (Thermo Scientific, Germany). Results were referenced to the NBS19 standard and calibrated to the PDB scale. Analytical errors were $\pm 0.06\text{‰}$ for $\delta^{18}\text{O}$. Numerous biological processes (e.g. symbiont activity, ontogeny) may affect the $\delta^{18}\text{O}$ fractionation processes in planktic foraminifera [Rohling and Cooke, 1999], known as vital effect, varies between species and is particularly difficult to estimate for species with a large habitat depth range, and for species for which no culture data are available [Spero and Lea, 1996]. Previous work [e.g. Deuser et al., 1981; Mortyn and Charles, 2003; Spero et al., 2003; Lončarić et al., 2006; Steph et al., 2009; Wilke et al., 2009] suggests that the species considered here (*G. inflata* and *G. truncatulinoides*) have a large a spread of disequilibria frequently centered about a zero offset (Table 3.3). Consequently there is no consensus on possible oxygen isotopic disequilibrium. For this reason, and because nonsymbiotic *G. inflata* and *G. truncatulinoides* are believed to calcify at or close to equilibrium [Fairbanks et al., 1980], in this study we assume no vital effect on the fractionation between foraminiferal $\delta^{18}\text{O}$ and seawater $\delta^{18}\text{O}$.

Pretreatment and analytical procedures for Mg/Ca analyses followed the method described by Nürnberg and Groeneveld [2006], the cleaning protocol proposed by Barker et al. [2003], and an additional reductive cleaning step. Analyses were performed on an ICP

OES (VARIAN 720–ES) which has a long-term analytical precision of $\pm 0.1 \text{ mmolmol}^{-1}$ for Mg/Ca of ECRM752–1 standard. Fe/Ca and Mn/Ca ratios were determined in conjunction with Mg/Ca as clay contamination and postdepositional Mn-rich carbonate coatings can exert a significant control on Mg/Ca ratios [Barker *et al.*, 2003]. We exclude this possibility as these ratios were negligibly in all the samples ($< 0.2 \text{ mmolmol}^{-1}$ for Mn/Ca, $< 0.1 \text{ mmolmol}^{-1}$ for Fe/Ca, Figure 3.2).

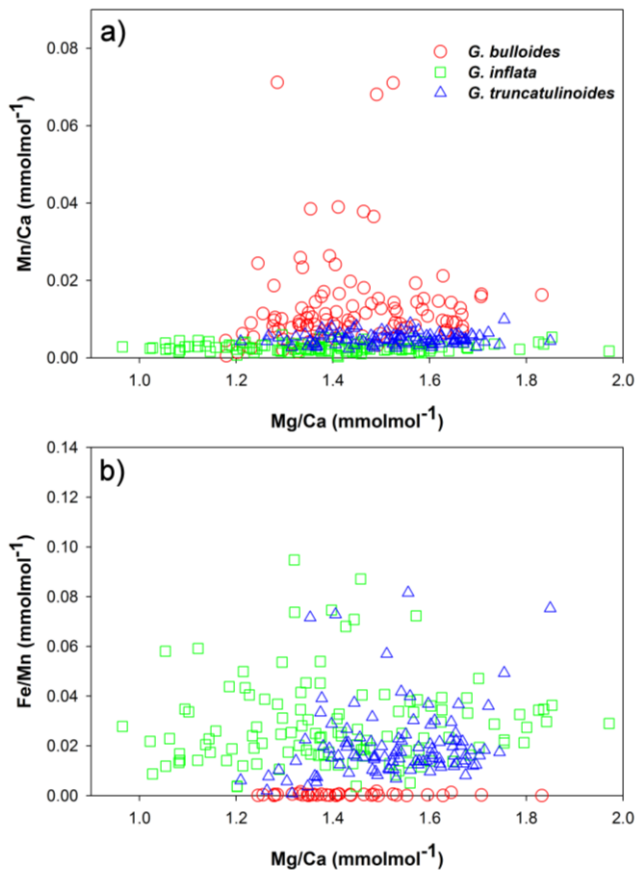


Figure 3.2 Mg/Ca plotted against (a) Mn/Ca and (b) Fe/Ca, low values and lack of covariance indicate that contamination has not controlled Mg/Ca variability

The conversion of Mg/Ca values to temperatures was conducted according to the calibrations of Mashiotta *et al.* [1999] ($\text{Mg/Ca} = 0.474 \exp(0.107 \times T)$), Groeneveld and Chiessi [2011] ($\text{Mg/Ca} = 0.72 \exp(0.076 \times T)$) and Regenberg *et al.* [2009] ($\text{Mg/Ca} = 0.84 \exp(0.083 \times T)$) for *G. bulloides*, *G. inflata*, and *G. truncatulinoides*, respectively. To estimate the habitat depth range of each species, we averaged the Mg/Ca-temperatures from surface sediments (top 1 cm of multicore) and Holocene sediments (0 – 10 ka) from core SO213-59-2, and compared them with modern climatological data from World Ocean Atlas 2009 [Antonov *et al.*, 2010; Locarnini *et al.*, 2010; Regenberg *et al.*, 2014]. To estimate the amplitude of temperature changes across each Marine Isotope Stage (MIS), we averaged the temperature estimates within each of the glacial (MIS 2 and MIS 6) and interglacial (MIS

1 and MIS 5) intervals. The intervals were defined according to the boundaries proposed by Lisiecki and Raymo [2005].

Foraminiferal $\delta^{18}\text{O}$ is driven mainly by changes in global ice volume, but in particular the planktic $\delta^{18}\text{O}$ signal may be strongly affected by sometimes rather large upper ocean temperature and salinity variations [Rohling and Cooke, 1999; Ravelo and Hillaire-Marcel, 2007]. Insofar, the planktic foraminiferal $\delta^{18}\text{O}$ by itself cannot be applied as a temperature proxy as initially suggested. Instead, our discussion on thermal gradients in the upper ocean is based on foraminiferal Mg/Ca, which is reliably recording water temperature [Nürnberg *et al.*, 1996]. By taking into account both the global ice volume effect deduced from benthic $\delta^{18}\text{O}$ and the temperature effect reconstructed from Mg/Ca measured on the same foraminiferal sample, we are able to extract the pure $\delta^{18}\text{O}$ of seawater ($\delta^{18}\text{O}_{\text{SW}}$) signal.

Table 3.3 Values of “Vital Effects” reported in the literature.

	Disequilibrium (‰)	Size Fraction (μm)	Reference
<i>G. inflata</i>	-0.4 to +0.4	> 200	Niebler <i>et al.</i> , 1999
	+0.01 to +0.25	350 – 450	Loncaric <i>et al.</i> , 2006
	0.94	150 – 250	Mortyn and Charles, 2003
	-0.2	NA	Deuser <i>et al.</i> , 1981
<i>G. truncatulinoides</i>	0	NA	Deuser <i>et al.</i> , 1981
	+0.2	>250	Niebler <i>et al.</i> , 1999
	-0.3 to +0.2	NA	Steph <i>et al.</i> , 2009
	-0.10 to +0.16	350 – 450	Loncaric <i>et al.</i> , 2006
	1.1	150 – 250	Mortyn and Charles, 2003
	-0.11	280 – 440	Wilke <i>et al.</i> , 2009

As the local $\delta^{18}\text{O}_{\text{SW}}$ correlates linearly with seawater salinity on regional scales [LeGrande and Schmidt, 2006], we used the seawater $\delta^{18}\text{O}$ as a semi-quantitative proxy for local salinity changes. However, we refrained from converting the $\delta^{18}\text{O}_{\text{SW}}$ signal into salinity because the variation of $\delta^{18}\text{O}$ in the ocean is more complicated than salinity. Processes such as sea ice formation may affect $\delta^{18}\text{O}_{\text{SW}}$ and salinity differently. These additional complications result in only regionally-coherent $\delta^{18}\text{O}_{\text{SW}}$ to salinity relationships [LeGrande and Schmidt, 2011].

The ice volume corrected (ivc) $\delta^{18}\text{O}_{\text{SW-IVC}}$ calculation involves the subtraction of the temperature effect from the planktic $\delta^{18}\text{O}$ data ($\delta^{18}\text{O}_{\text{SW}} (\text{VSMOW}) = \delta^{18}\text{O} + 0.27 - (4.38 - (4.38^2 - 4 \times 0.1 (16.9 - T_{\text{Mg/Ca}})^{1/2}) / (0.1 \times 2))$) [Shackleton, 1974] followed by the removal of the ice volume component [Waelbroeck *et al.*, 2002]. We linearly interpolated the Waelbroeck *et al.* [2002] record at the time step of the core SO213-59-2 profile and subtracted the mean ocean $\delta^{18}\text{O}_{\text{SW}}$ from the reconstructed $\delta^{18}\text{O}_{\text{SW}}$ values. The absolute error in calculating $\delta^{18}\text{O}_{\text{SW}}$ is $\sim \pm 0.3\text{‰}$ [Rohling, 2007].

3.3 Results

3.3.1 Planktic Foraminiferal Mg/Ca-Temperatures

The Mg/Ca (temperature) values of *G. bulloides*, *G. inflata* and *G. truncatulinoides* in surface sediments (top 1 cm of multicore) are 1.66 mmolmol⁻¹ (~11.7 °C), 1.59 mmolmol⁻¹ (~10.4 °C) and 1.52 mmolmol⁻¹ (~7.1 °C), respectively (Figure 3.2). The averaged reconstructed temperatures (surface sediments + Holocene) range between 11.3 (±0.4) °C for *G. bulloides*, 10.6 (±0.8) °C for *G. inflata* and 7.1 (±0.6) °C for *G. truncatulinoides* (Figure 3.3), consistent with climatological temperatures [Pahnke et al., 2003; Locarnini et al., 2010] typical for water depths < 50 m, ~50 – ~100 m and 150 – ~400 m, respectively, during the austral summer (Figure 3.1b). The inferred seasonality of the Mg/Ca signals is in agreement with sediment trap data east of New Zealand, which suggest that the maximum fluxes of *G. bulloides* and *G. inflata* are mainly bound to Southern Hemisphere's late spring to summer in subantarctic waters [King and Howard, 2003; Northcote and Neil, 2005; Bostock et al., 2011]. Based on the correlation with the WOA09 temperature, we interpret these species as reflecting the austral summer water temperature at the surface (*G. bulloides*- SST_{Mg/Ca}), the thermocline (*G. inflata* – TT_{Mg/Ca}) and the deep-thermocline (*G. truncatulinoides* – DTT_{Mg/Ca}).

Downcore SO213-59-2, Mg/Ca ranges between 1.17 – 1.83 mmolmol⁻¹ in *G. bulloides*, 0.96 – 1.97 mmolmol⁻¹ in *G. inflata* and 1.21 – 1.85 mmolmol⁻¹ in *G. truncatulinoides* over the past 220 kyr, with higher ratios during interglacials. Large TT_{Mg/Ca} amplitude variations of ~8 °C (from ~5 to ~13 °C) are observed at the thermocline level (Figure 3.3). Smaller temperature variabilities are observed at the surface (*G. bulloides*) and the deep-thermocline (*G. truncatulinoides*), with SST_{Mg/Ca} ranges of ~4 °C (~9 to ~13 °C) and DTT_{Mg/Ca} of ~6 °C (~4 to ~10 °C), respectively (Figure 3.3). The inferred SST_{Mg/Ca}, TT_{Mg/Ca}, and DTT_{Mg/Ca} show glacial-interglacial amplitudes of ~2, ~4 and ~2 °C, respectively (Figure 3.3). Our results suggest, on average, similar interglacial surface conditions (MIS 1 vs. MIS 5) in the subtropical SPG, with no differences in SST_{Mg/Ca} during both interglacials (~11.2 °C). Similar condition is observed at thermocline level, with TT_{Mg/Ca} of ~10.1 °C (MIS 1) vs. ~10.8 °C (MIS 5) (Figure 3b, c). On the other hand, slightly larger temperature differences between interglacials can be observed at the deep thermocline level with DTT_{Mg/Ca} of ~6.7 °C (MIS 1) vs. ~7.9 °C (MIS 5) (Figure 3d).

The average glacial SST_{Mg/Ca} is similar during MIS 2 and MIS 6 (9.4 °C versus 9.8 °C, respectively). In contrast, marked glacial differences are observed at the thermocline, where TT_{Mg/Ca} suggests a glacial difference of ~3 °C between MIS 2 and MIS 6 (~6.7 °C versus ~9.3 °C, respectively). The minimum temperature of ~4.6 °C centered at ~20 ka, is ~3 °C colder than the lowest temperature observed in MIS 6 (~8.1 °C). At the deep-thermocline, a similar

trend can be observed, i.e. the $\text{DTT}_{\text{Mg/Ca}}$ show on average $\sim 2^\circ\text{C}$ colder conditions during MIS 2 than MIS 6 ($\sim 5.7^\circ\text{C}$ versus $\sim 7.6^\circ\text{C}$, respectively), with minimum temperatures of $\sim 4.4^\circ\text{C}$ and $\sim 6.4^\circ\text{C}$ at $\sim 20\text{ ka}$ and $\sim 148\text{ ka}$, respectively.

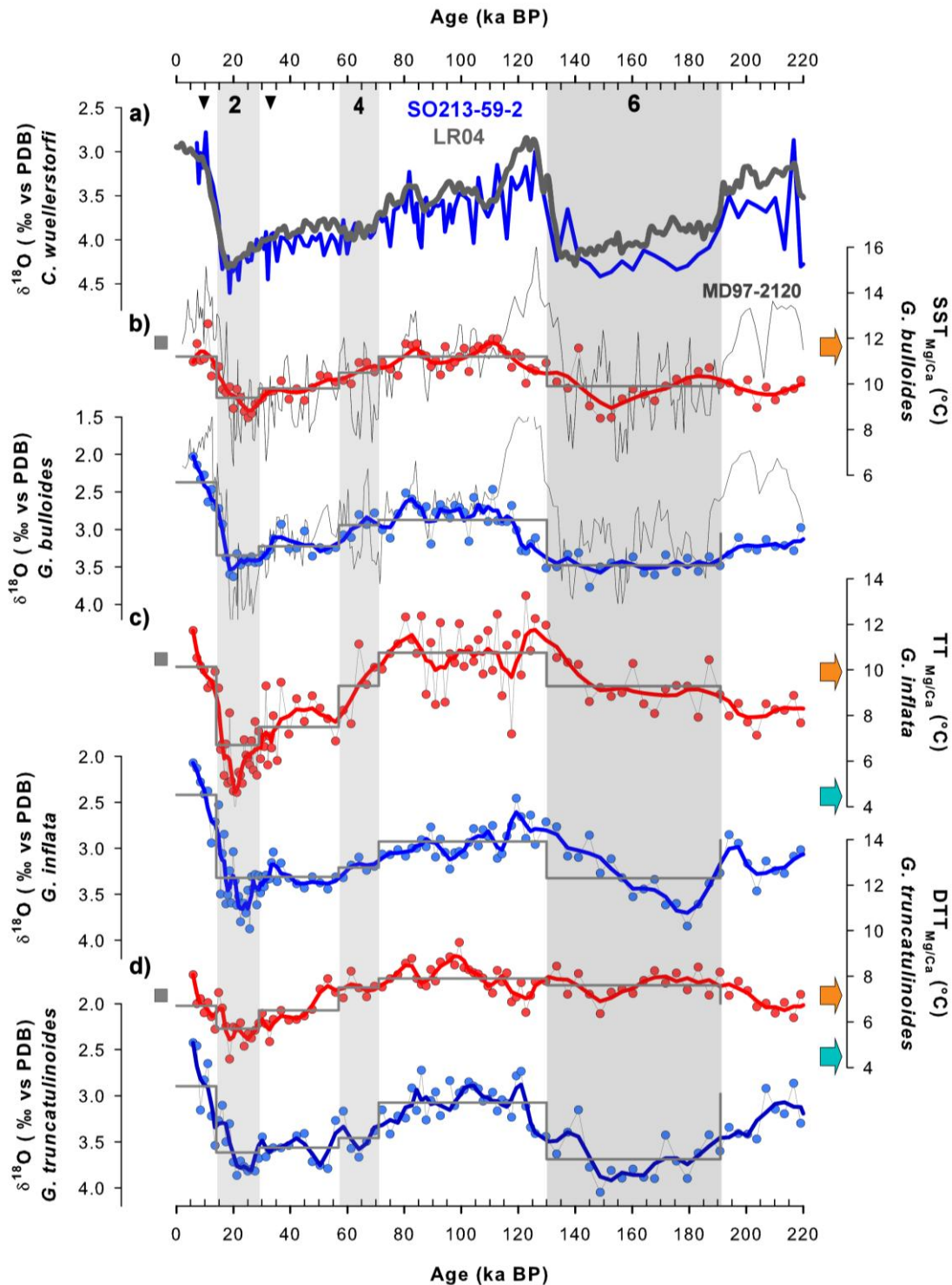


Figure 3.3 Foraminiferal (isotope) geochemical data of core SO213-59-2. (a) Age model for core SO213-59-2 based on the correlation of the benthic foraminiferal $\delta^{18}\text{O}$ record (blue curve) to the benthic $\delta^{18}\text{O}$ stack LR04 [Lisiecki and Raymo, 2005]. Auxiliary AMS^{14}C age control points are indicated by black triangles (Table 2). Shaded

bars indicate glacial intervals; black numbers in the bars represent the Marine Isotope Stages (MIS). Calculated seawater Mg/Ca-temperatures (red circles, red curve illustrates 3-points running average) and $\delta^{18}\text{O}$ (blue circles, blue curve illustrates 3-points running average) derived from (b) *G. bulloides*, (c) *G. inflata* and (d) *G. truncatulinoides*. $SST_{\text{Mg/Ca}}$ = seasurface temperature, $TT_{\text{Mg/Ca}}$ = thermocline temperature, $DTT_{\text{Mg/Ca}}$ = deep-thermocline temperature. Surface sediment data from MUC SO213-59-1 are indicated by grey squares. Continuous grey lines denote average temperatures computed per each isotopic stage (MIS 1 to MIS 6). Orange arrows indicate the summer ocean temperature at 50 m (b, assumed mean living depth of *G. bulloides*), 75 m (c, assumed mean living depth of *G. inflata*) and 300 m (d, assumed mean living depth of *G. truncatulinoides*) water depth (WOA09); cyan arrows denote the modern temperature of SOIW in the SEP (4-5 °C)[Hartin et al., 2011]. The downcore $SST_{\text{Mg/Ca}}$ and $\delta^{18}\text{O}$ record of core SO213-59-2 shows smaller variability than the high resolution $SST_{\text{Mg/Ca}}$ and $\delta^{18}\text{O}$ record (*G. bulloides*) reconstruction from the MD97-2120 (thin grey line) at 45° S [Pahnke et al., 2003; Cléroux et al., 2007].

3.3.2 Planktic Foraminifera Stable Oxygen Isotopes and Relative Salinity Reconstruction

The $\delta^{18}\text{O}$ values of *G. bulloides*, *G. inflata* and *G. truncatulinoides* from the surface sediments (top 1 cm of multicore) are 1.87, 2.27 and 2.37‰, respectively. Along the analyzed time interval, the $\delta^{18}\text{O}$ values show glacial-interglacial fluctuations ranging between 3.8 and 2.02‰ at the sea surface, between 3.8 and 2.07‰ at the thermocline, and between 4.05 and 2.12‰ at the deep-thermocline (Figure 3.3). Although the isotopic values at all three water depths increase synchronously at ~30 ka, the heaviest $\delta^{18}\text{O}$ values are reached at different time intervals. At the thermocline level, the maximum is reached at ~25 ka, while at the surface the values continue increasing until the heaviest value is reached at ~20 ka.

Along the water column, the mean planktic $\delta^{18}\text{O}$ values of *G. bulloides*, *G. inflata* and *G. truncatulinoides* range from 2.4 to 2.9‰ during MIS 1 and from 2.9 to 3.1‰ during MIS 5, with *G. bulloides* and *G. inflata* showing lighter $\delta^{18}\text{O}$ values than *G. truncatulinoides* (Figure 3.3). During MIS 2 and MIS 6, the $\delta^{18}\text{O}$ values of these species oscillate between 3.3 and 3.7‰.

The calculated $\delta^{18}\text{O}_{\text{SW-IVC}}$ values are in the range of 0.35 – 2.23‰ at the sea surface (*G. bulloides*), -0.73 – 2.35‰ at the thermocline (*G. inflata*), and -0.51 – 1.59‰ at the deep-thermocline (*G. truncatulinoides*), respectively. These results suggest fresher conditions during the glacial and saltier conditions during the interglacial. The species-specific $\delta^{18}\text{O}_{\text{SW-IVC}}$ deviations from the averaged Holocene (0 – 10 ka) and surface sediment ($\Delta\delta^{18}\text{O}_{\text{SW-IVC}}$) range between -0.39 to 1.25‰ at the surface, -1.40 to 1.68‰ at the thermocline and -0.89 to 1.21‰ at the deep-thermocline (Figure 3.4). The $\Delta\delta^{18}\text{O}_{\text{SW-IVC}}$ values at all three water depths are highest during MIS 5 (Figure 3.4c, d, e). Moreover, our results suggest differences in glacial $\delta^{18}\text{O}_{\text{SW-IVC}}$ at all water depths, where slightly saltier-than-Holocene conditions prevailed during MIS 6, in contrast to the fresher-than-Holocene conditions during MIS 2 (Figure 3.4c, d, e).

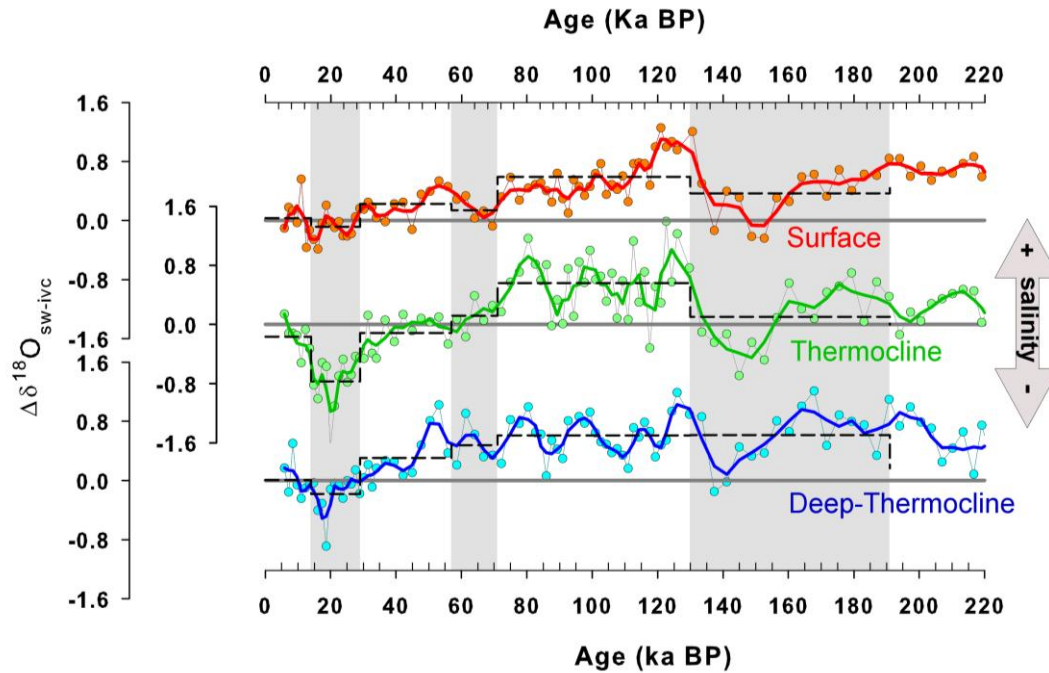


Figure 3.4 Comparison of (a) mean ocean $\delta^{18}\text{O}_{\text{SW-IVC}}$ and the reconstructed local salinity anomalies for (b) Chatham Rise core MD97-2120 [Pahnke et al., 2003] and our study site SO213-59-2 in the SPG at (c) surface, (d) thermocline and (e) deep-thermocline level. Grey continuous lines denote species-specific mean Holocene values (surface sediments plus 0 – 10 ka). Continuous lines are the 3 points running average of the raw data (circles). Black dashed lines denote average values computed per each isotopic stage (MIS 1 to MIS 6).

3.4 Discussion

3.4.1 Assessing the Impact of Dissolution on Mg/Ca-Derived Temperatures in the South Pacific

Dissolution is known to affect the preservation of the Mg/Ca signal in planktic foraminifera [Brown and Elderfield, 1996; Dekens et al., 2002; Regenberg et al., 2006; 2014], in particular in bottom waters which are undersaturated with respect to calcite, that is, when $\Delta[\text{CO}_3^{2-}] < 0 \text{ mol kg}^{-1}$ and $\Omega_{\text{calcite}} < 1$ [Brown and Elderfield, 1996; Regenberg et al., 2014]. Dissolution reduces the Mg/Ca and the test-weight of foraminifera [Brown and Elderfield, 1996; Dekens et al., 2002; Regenberg et al., 2006; 2014]. As we do not observe any correlation between the shell weight and Mg/Ca ratios of the *G. bulloides* in our core (Figure 3.5a), we concluded that our Mg/Ca record is not biased by dissolution effect. Moreover, high fidelity of temperature estimates have been suggested for *G. bulloides* based on the comparison of Mg/Ca-derived temperatures against dissolution proxies [Mekik et al., 2007] and results from laboratory experiments [Marr et al., 2013].

Site SO213-59-2 is situated close to the modern calcite saturation horizon (CSH, defined as $\Omega_{\text{calcite}} = 1$) at ~3100 m water depth in the SWP [Bostock et al., 2011], with $\Delta[\text{CO}_3^{2-}]$

] value of approximately $0 \mu\text{molkg}^{-1}$ [Regenberg *et al.*, 2014](Figure 5b and c). However, applying the Mg/Ca correction of $0.1 - 0.2 \text{ }^\circ\text{C}$ per μmolkg^{-1} for surface and $0.4 - 0.6 \text{ }^\circ\text{C}$ per μmolkg^{-1} for subsurface dwellers [Regenberg *et al.*, 2014], lead to unrealistic subsurface temperatures ~ 8 to $12 \text{ }^\circ\text{C}$ warmer than the modern values.

In the deep Pacific ($>3000 \text{ m}$ water depth), the calcite preservation was enhanced during glacials in comparison to interglacial [Anderson *et al.*, 2008] caused by a better ventilated deep Pacific, thus less corrosive bottom waters [Hall *et al.*, 2001; McCave *et al.*, 2008]. This is further supported by $\delta^{18}\text{O}$ and $\delta^{13}\text{C}$ data from the South West, Western Equatorial and North West deep Pacific, which suggest the dominance of a relatively well-ventilated deep water mass during glacials, most likely originated from the Pacific sector of the Southern Ocean, during the LGM [details in McCave *et al.*, 2008].

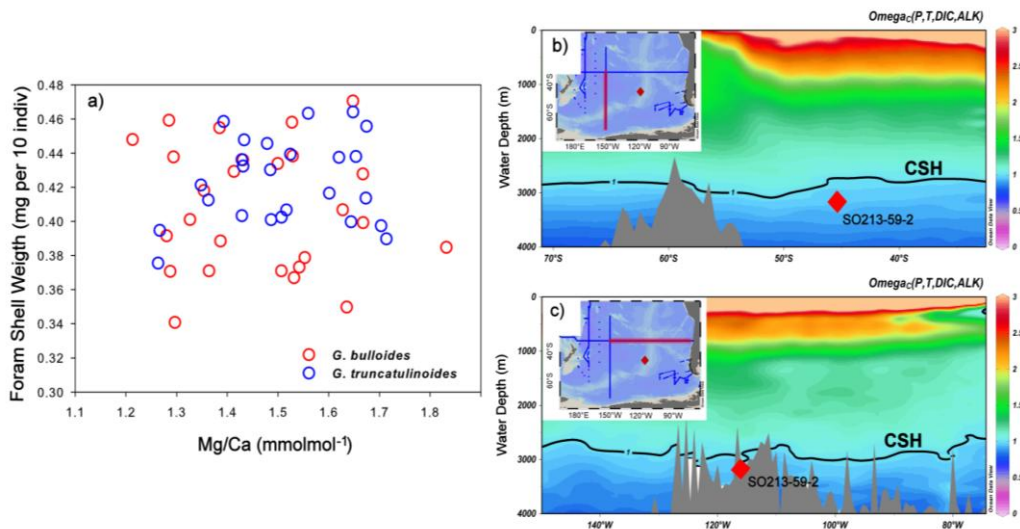


Figure 3.5 (a) Random selection of shell weights plotted against Mg/Ca in *G. bulloides* and *G. truncatulinoides*, in both cases the coefficient of correlation (R^2) is < 0.1 , discarding dissolution as the main factor controlling Mg/Ca variability. Calcite saturation horizon (CSH, $\Omega_{\text{CALCITE}} = 1$ for transects P16S 2005 (b) and P06 2003 (c), calculated from the DIC and alkalinity in the CARINA database [Brown and Elderfield, 1996; Key *et al.*, 2010]. Location of the transects and the core SO213-59-2 (red diamond) is shown on the maps.

A better ventilate deep Pacific can also be inferred from the gradient of increasing $[\text{CO}_3^{2-}]$ below $\sim 3 \text{ km}$ water depth [Broecker, 2001; Anderson and Archer, 2002]. Furthermore, $\delta^{13}\text{C}$ records from the deepest Pacific ($> 4000 \text{ m}$ water depth) show glacial values which are consistently higher than those from shallower sites [Lisiecki, 2010], suggesting that the well-ventilated conditions observed during the last glacial [McCave *et al.*, 2008] also dominated the basin during earlier glacials [Sexton and Barker, 2010]. This scenario is further supported by sedimentological and $\delta^{13}\text{C}$ data from the deep South Pacific showing faster flow and stronger ventilation in the bottom waters during glacials [Hall *et al.*, 2001]. This could cause a

deepening of the critical $\Delta[\text{CO}_3^{2-}]$ threshold of dissolution on planktic foraminifera by several hundreds of metres, leading to a better preservation of the Mg/Ca signal during glacials. Overall, *G. bulloides*-Mg/Ca values along core SO213-59-2 (1.1 – 1.8 mmolmol⁻¹) are within the range of a Mg/Ca record (0.9 – 2.4 mmolmol⁻¹ for the last 220 kyr) from a shallower site (1200 m water depth) in the SWP (MD97-2120, [Figure 3.3](#)) [*Pahnke et al.*, 2003], well above the CSH, calcium carbonate compensation and lysocline [*Bostock et al.*, 2011], and less likely affected by dissolution [*Pahnke et al.*, 2003]. Taken together, these observations suggest that the downcore Mg/Ca-derived temperature variations reconstructed at our site are unlikely to be biased by dissolution.

3.4.2 Evolution of Water Column Structure in the South Pacific

Although the habitat depth of some planktic foraminifera species can potentially vary through time [*Cl  roux et al.*, 2007], we here assume that the mean calcification depths of the different species at no time changed to such an extent that the depth-succession of species deviated from the modern conditions. In order to exclude potential temporal changes in calcification depths and/or in seasonal bias of foraminiferal abundances, we here limit our interpretation to mean glacial and interglacial ocean temperature and salinity estimations.

The ~4 °C of glacial sea surface cooling observed at our study site is comparable to the finding of previous foraminifera-based studies in the region [*Luz*, 1977; *Mashiotta et al.*, 1999]. However, it is weaker than that suggested by other studies from similar latitudes between the Subtropical Front (STF) and the SAF in the South Pacific, such as site GeoB3327-5 in the SEP (43°S) [*Ho et al.*, 2012] and site MD97-2120 in the SWP (45°S) [*Pahnke et al.*, 2003], which show a larger glacial sea surface cooling ~8 °C ([Figure 3.3b](#)).

At our study site the SST_{Mg/Ca} and surface $\Delta\delta^{18}\text{O}_{\text{SW-IVC}}$ fluctuations commonly suggest fresh-and-cool glacial and salty-and-warm interglacial conditions, as previously described by *Pahnke et al.* [2003] for the SWP (MD97-2120, [Figure 3.4b](#)). The co-variation of sea surface temperature and salinity at similar latitudes has been attributed to the northward migration of the SAF and/or larger influence of SASW during glacial stages that results in lower surface temperature and salinity [*Pahnke et al.*, 2003; *N  rnberg and Groeneveld*, 2006]. However, this mechanism is unlikely to be in play at our core location because the study site is located 10° north from the modern SAF, and siliceous microfossil transfer functions suggest no large glacial-northward displacement (< 4°) of the frontal system in the central South Pacific [*Gersonde et al.*, 2003; 2005]. Furthermore, unlike the comparable glacial surface $\delta^{18}\text{O}_{\text{SW}}$ and Mg/Ca-temperatures (9.4 °C (LGM) versus 9.8 °C (MIS 6)), our subsurface Mg/Ca-temperatures and $\Delta\delta^{18}\text{O}_{\text{SW-IVC}}$ records at thermocline and deep-thermocline water depth are characterized by large differences between the LGM and MIS 6, of ~3 °C and ~1 ‰ ($\delta^{18}\text{O}_{\text{SW}}$)

as recorded by *G. inflata* and *G. truncatulinoides* (Figure 3.3c, d and 3.4c, e). Relative to the Holocene conditions, the LGM is characterized by substantially colder and fresher subsurface waters, whereas MIS 6 is characterized by slightly colder but saltier subsurface waters (Figure 3.6a). These contrasting conditions imply a high variability in the formation process and/or the advection of the SOIWs to the SPG thermocline during glacials.

Diverging surface and subsurface conditions argue against glacial frontal migration as the controlling factor of the hydrographic changes at the core site, as a latitudinal shift in the SAF would have affected the entire upper water column. Our data show that in the subtropical SPG, substantial changes occurred at thermocline level despite a lack of variability at the sea surface. Considering the importance of the SOIWs in ventilating the thermocline in this region [Sloyan *et al.*, 2010; Martin *et al.*, 2011], we therefore interpret the subsurface Mg/Ca-temperatures and the according $\Delta\delta^{18}\text{O}_{\text{sw-ivc}}$ variations as driven by the changes in the supply of SOIWs formed in the SEP. Various proxy reconstructions suggest an enhanced SOIWs formation and/or advection to lower latitudes during cold/glacial periods [Muratli *et al.*, 2010; Martínez-Méndez *et al.*, 2013; Pena *et al.*, 2013]. In general, our subsurface reconstructions are in accordance with these observations, showing colder and fresher subsurface conditions during glacial times in comparison with the preceding interglacial (Figure 3.3 and 3.4).

Assuming no change over time in the habitat depth range of the planktic foraminifera as shown in Figure 1b and 1c, we calculate the thermal gradient between $\text{SST}_{\text{Mg/Ca}}$ and $\text{DTT}_{\text{Mg/Ca}}$ ($\Delta T_{\text{SST-DTT}}$), $\text{SST}_{\text{Mg/Ca}}$ and $\text{TT}_{\text{Mg/Ca}}$ ($\Delta T_{\text{SST-TT}}$) and $\text{TT}_{\text{Mg/Ca}}$ and $\text{DTT}_{\text{Mg/Ca}}$ ($\Delta T_{\text{TT-DTT}}$) to reconstruct the upper ocean structure. The $\Delta T_{\text{SST-DTT}}$ values range on average from ~ 5 to ~ 2 °C, and increased continuously from MIS 6 to the Holocene, i.e. from on average ~ 2.2 °C (MIS 6), ~ 3.2 °C (MIS 5), ~ 3.7 °C (MIS 2), to ~ 4.5 °C (MIS 1) (Figure 3.7a). The increasing $\Delta T_{\text{SST-DTT}}$ suggests a continuous shoaling of the thermocline since MIS 6, resulting in a thinner mixed layer towards present. Similarly, the $\Delta T_{\text{SST-TT}}$ suggests a weak stratification and deep mixed layer during MIS 6 (~ 0.5 °C), and a stronger stratification during LGM (~ 2.7 °C). Since $\text{SST}_{\text{Mg/Ca}}$ is similar for both glacial stages, the ΔT is mostly determined by the changes in subsurface temperature (see Section 3.1, Figure 3.3). At thermocline water depths, $\Delta T_{\text{TT-DTT}}$ shows on average larger thermal gradients between upper and deeper thermocline depths during interglacial MIS 1 (~ 3.4 °C) and MIS 5 (~ 2.9 °C) compared to glacials MIS 2 (~ 1 °C) and MIS 6 (~ 1.6 °C), suggesting a stronger glacial subsurface mixing (Figure 3.7b).

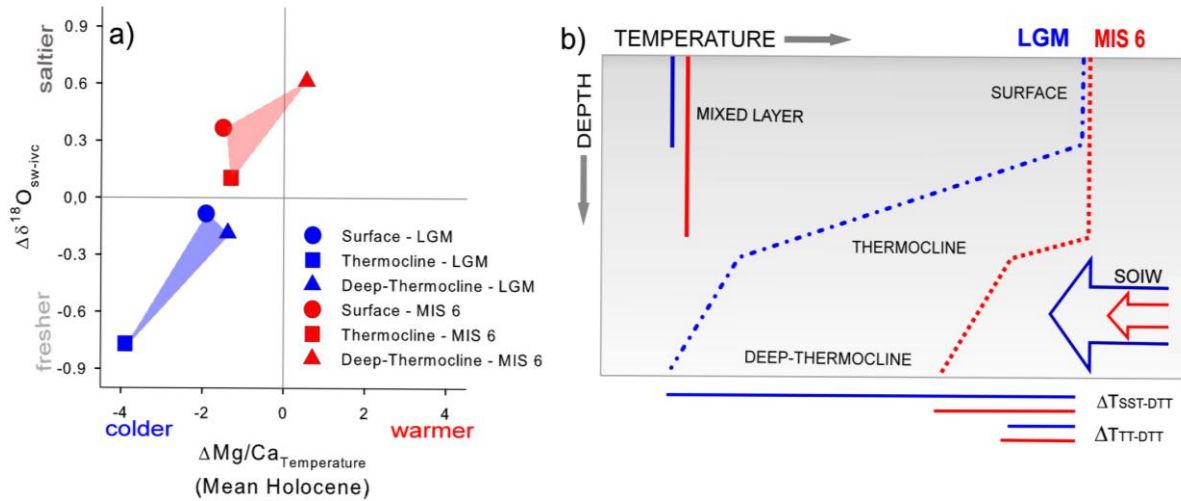


Figure 3.6 (a) Salinity and temperature differences ($\Delta\delta^{18}\text{O}_{\text{sw-ivc}}$ and ΔT) during LGM (blue) and MIS 6 (red) in comparison with mean Holocene values at surface (circle), thermocline (square) and deep-thermocline (triangle). Colder- and fresher-than-Holocene subsurface waters characterize LGM. MIS 6 conditions are saltier-than-Holocene and warmer-than-LGM subsurface waters. (b) Scheme illustrating the water column conditions during MIS 6 (red) and LGM (blue) with different positions of the thermocline and different strengths of SOIW advection. $\Delta T_{\text{SST-DTT}}$ marks the temperature gradient between $\text{SST}_{\text{Mg/Ca}}$ of *G. bulloides* and $\text{DTT}_{\text{Mg/Ca}}$ of *G. truncatulinoides*, and $\Delta T_{\text{TT-DTT}}$ marks the temperature gradient between $\text{TT}_{\text{Mg/Ca}}$ of *G. inflata* and $\text{DTT}_{\text{Mg/Ca}}$ of *G. truncatulinoides*.

The mixing of water masses can also be inferred from the isotopic composition of the seawater at different water depths as proxy [Rohling and Cooke, 1999]. Adopting this approach, we take the $\delta^{18}\text{O}_{\text{SW}}$ difference between *G. bulloides* (mixed layer) and *G. truncatulinoides* (deep thermocline) ($\Delta\delta^{18}\text{O}_{\text{SW Gb-Gt}}$), and between *G. inflata* (upper thermocline) and *G. truncatulinoides* (deep-thermocline) ($\Delta\delta^{18}\text{O}_{\text{SW Gi-Gt}}$), as a qualitative indicator of the subsurface mixing (Figure 3.7b).

The $\Delta\delta^{18}\text{O}_{\text{SW Gb-Gt}}$ and $\Delta\delta^{18}\text{O}_{\text{SW Gi-Gt}}$ values are the smallest during MIS 6 suggesting a well-mixed water column from the sea surface to the deep-thermocline (Figure 3.7b). The water column during LGM is different from that during MIS 6 (Figure 3.7b), with well-mixed subsurface waters (upper thermocline to deep-thermocline, indicated by $\Delta\delta^{18}\text{O}_{\text{SW Gi-Gt}}$) and a more stratified upper water column from the sea surface to the thermocline (indicated by $\Delta\delta^{18}\text{O}_{\text{SW Gb-Gt}}$), in agreement with the inference from the thermal gradient (Figure 3.7a).

Taken together, two general glacial scenarios, with an emphasis on the water column structure, emerge. Firstly, during MIS 6 there was a highly homogenized water column (deep mixed layer, with low values of $\Delta T_{\text{SST-TT}}$, $\Delta T_{\text{SST-DTT}}$, $\Delta\delta^{18}\text{O}_{\text{SW Gb-Gt}}$ and $\Delta\delta^{18}\text{O}_{\text{SW Gi-Gt}}$) with slightly saltier-than-Holocene waters, and it was warmer than the LGM (Figure 3.6a). Secondly, during the LGM, the water column was more stratified (thinner mixed layer, higher $\Delta T_{\text{SST-TT}}$, $\Delta T_{\text{SST-DTT}}$, $\Delta\delta^{18}\text{O}_{\text{SW Gb-Gt}}$), with fresher- and colder-than-Holocene subsurface waters (Figure 3.6a), which have temperatures similar to the modern coldest variety of SOIWs

formed in the SEP (4 – 5 °C, McCartney, 1977; Hartin et al., 2011) (Figure 3.3). These contrasting glacial scenarios are probably due to the differences in the formation and/or advection of the SOIWs to the study site (section 3.4.3, Figure 3.6b).

3.4.3 Enhanced Pacific Intermediate Mode Water Formation

Different glacial scenarios for the thermocline (discussed in section 3.4.2) suggest glacial differences in the lateral flux (advection) of the SOIWs to the SPG. Both northward displacement and stronger SWW have been invoked to explain enhanced SOIWs signals in the tropical and subtropical SEP during cold periods [Muratli et al., 2010; Martínez-Méndez et al., 2013; Pena et al., 2013]. However, a general consensus on the displacement or strengthening of the SWW during glacial stages is still lacking, with proxy reconstructions and model simulations suggesting either equatorward, or poleward displacement or increase in strength with no latitudinal shift in comparison to today [Markgraf et al., 1992; Shin et al., 2003; Lamy et al., 2004; Otto-Bliesner et al., 2006; Sime et al., 2013].

Although the relationship between sea surface temperature (SST) and wind displacements is not straightforward [Kohfeld et al., 2013], previous SST reconstructions from the SEP have often been interpreted as reflecting a northward displacement of SWW and the SO frontal system during the LGM [Lamy et al., 2004; Kaiser et al., 2005]. Latitudinal glacial displacements of 7° and ~9° for the SAF and the Polar Front (PF) have been suggested to be a recurrent feature in the region during the last 700 kyr [Ho et al., 2012], with similar magnitudes during the LGM and MIS 6. It seems unlikely that similar extent of glacial northward SWW displacement could generate different SOIWs and result in contrasting subsurface waters in the SPG, i.e. fresher-than-Holocene waters during the LGM and saltier-than-Holocene waters during MIS 6 (Figure 3.6a).

On the other hand, numerical experiments [Ribbe, 2001] and reconstructions for the LGM in the SEP [Muratli et al., 2010] have suggested a close link between the strength of the SWW and the SOIWs formation. An intensified SWW has been invoked as one of the factors controlling the increased glacial dust fluxes in East Antarctica [Lambert et al., 2008], the South Pacific [Lamy et al., 2014] and as far north as 42°S in the South Atlantic (n-alkanes and Fe) [Martínez-García et al., 2009]. The comparison of Holocene and LGM proxy data suggest an intensification of the Antarctic Circumpolar Current (ACC) [Noble et al., 2012], with no significant change of its mean location [Matsumoto et al., 2001]. Since the ACC is partially driven by the SWW, this has been interpreted as evidence for stronger winds with no change of its mean location during the LGM [Matsumoto et al., 2001].

Another analogy to evaluate the response of the ocean to changes in wind intensity is the Southern Annular Mode (SAM). SAM is the main climatic mode controlling the winds in

the Southern Hemisphere [Thompson and Solomon, 2002], defined as the alternating pattern of strengthening and weakening of westerly winds between the mid and high latitudes in the Southern Hemisphere. The SAM alters 1) the strength of northward Ekman Flow, 2) the upwelling along the Antarctic Continent, 3) the vertical tilt of the isopycnals, and 4) producing downwelling at $\sim 45^\circ\text{S}$ [Hall and Visbeck, 2002; Oke and England, 2004; Lovenduski and Gruber, 2005; Lenton and Matear, 2007]. The tight coupling between SAM and the water properties of SAMW formed in the Pacific Basin (160°E to 80°W) has been suggested by field studies [Lovenduski and Gruber, 2005; Ayers and Strutton, 2013]. During positive SAM events, the belt of strong SWW contracts, therefore intensifying SWW over the ACC and weakening the SWW north of 45°S . Conversely, a negative SAM event reflects the expansion of the belt of strong SWW towards the equator. In the Pacific Basin these wind anomalies are significantly correlated with nutrient and temperature properties of the SAMW [Ayers and Strutton, 2013]. The intensified SWW during positive SAM events produce negative (positive) wind stress curl anomalies south (north) of the maximum wind stress, and a higher northward Ekman transport throughout the region of the SWW. These conditions result in anomalous surface divergences and convergences [Hall and Visbeck, 2002; Saenko *et al.*, 2005], which drive increased upwelling south of and in the ACC area, and cause the transport of colder water northward toward the regions where SAMW and AAIW are formed [Oke and England, 2004]. The increased downwelling in the Subantarctic Zone therefore results in a rapid formation of SAMW [Lovenduski and Gruber, 2005; Ayers and Strutton, 2013].

Although a decadal oscillation as SAM cannot be resolved by the resolution of our proxy record, we assume that SAM-like changes operated over longer time-scales. Hence, we speculate that the subsurface temperature and salinity conditions at our study site are mainly controlled by the strength of the SWW, modulating the vigor of the Ekman transport toward the regions where SAMW and AAIW are formed [Oke and England, 2004] and then transported eastward within the ACC and northward into the SPG [Hanawa and Talley, 2001]. Furthermore, stronger winds in the Southern Ocean generally imply deeper mixing, and hence deeper mixed layers, which are a pre-requisite for the formation of AAIW and SAMW [McCartney, 1977; Hanawa and Talley, 2001].

3.4.4 Glacial Variability of SOIW

Proxy reconstructions from the western side of South America suggest a constant formation and northward advection of colder modes of SOIWs (namely AAIW) during glacial stages from the SEP, as suggested by the $\Delta\delta^{13}\text{C}_{\text{DIC}}$ gradient ($\Delta\delta^{13}\text{C}_{\text{DIC}}$) between the SEP Site GeoB15016 and the Pacific Deep Water (PDW) stack. The $\Delta\delta^{13}\text{C}_{\text{DIC}}$ record isolates the site-

specific $\delta^{13}\text{C}$ signal, which is driven by changing contributions from PDW and AAIW (Figure 3.6c) [Martínez-Méndez et al., 2013].

Notably, the advection process during the LGM exceeded in comparison with other glacial stages [Martínez-Méndez et al., 2013] and the Holocene [Muratli et al., 2010]. This observation is in agreement with our subsurface temperature and relative salinity reconstructions, which show a pronounced cooling and freshening during LGM in comparison with the Holocene (Figure 3.7a). In spite of the differences in proxies used, the enhanced presence of colder modes of SOIW (AAIW) during the LGM seems ubiquitous in different settings along the Chilean slope (ODP1233 and GeoB15016) [Muratli et al., 2010; Martínez-Méndez et al., 2013] and the subsurface SPG (this study).

Reconstructed LGM subsurface temperatures in the SPG resemble that of modern SEP-SOIW (4 – 5 °C) [McCartney, 1977; Hartin et al., 2011], suggesting the enhanced advection and/or a larger contribution of this water mass to the subsurface SPG. Moreover, the active advection of SOIW during LGM has been suggested by different proxy reconstructions in the Pacific Basin, i.e. the SEP [Muratli et al., 2010; Martínez-Méndez et al., 2013], the North East Pacific [Herguera et al., 2010], the Equatorial Pacific [Pena et al., 2008], the Tasman Sea [Bostock et al., 2004] and the SPG (this study), contrasting with the AAIW-glacial reduction scenario inferred in the SWP [Pahnke and Zahn, 2005]. Shallower convection depth of AAIW and/or the northward displacement of its formation areas during LGM, have been invoked to explain this dichotomy [Martínez-Méndez et al., 2013; Pena et al., 2013].

During MIS 6, the homogenous water column with warmer and saltier subsurface conditions (relative to the LGM), is probably due to a reduction and/or ceasing SOIWs advection to the SPG's thermocline from the SEP. These conditions are in contrast with the SOIWs signal observed at 27°S, where the signal during MIS 6 is on average weaker than that during the LGM, but still stronger than that during the Holocene (GeoB150106) [Martínez-Méndez et al., 2013] (Figure 3.7c). Divergent observations at the Chilean slope and offshore suggest differential variations in the advection of SOIWs during glacial stages, with a relatively stable northward advection of the denser modes of SOIWs along the South American continent and a more fluctuating advection of SOIWs that feed the SPG's thermocline.

The variation in dust flux corresponding to the decrease in the salinity during LGM and the youngest part of MIS 6 (since ~160 ka) (Figure 3.4d, e), underlines the role of SWW intensity for driving the SOIWs injection to the SPG (Figure 3.7d). Strong winds could break down the ocean stratification, thereby allowing a rapid development of a deep mixed layer,

which in turn might have led to the formation of AAIW and SAMW, and the subduction of these waters to the SPG.

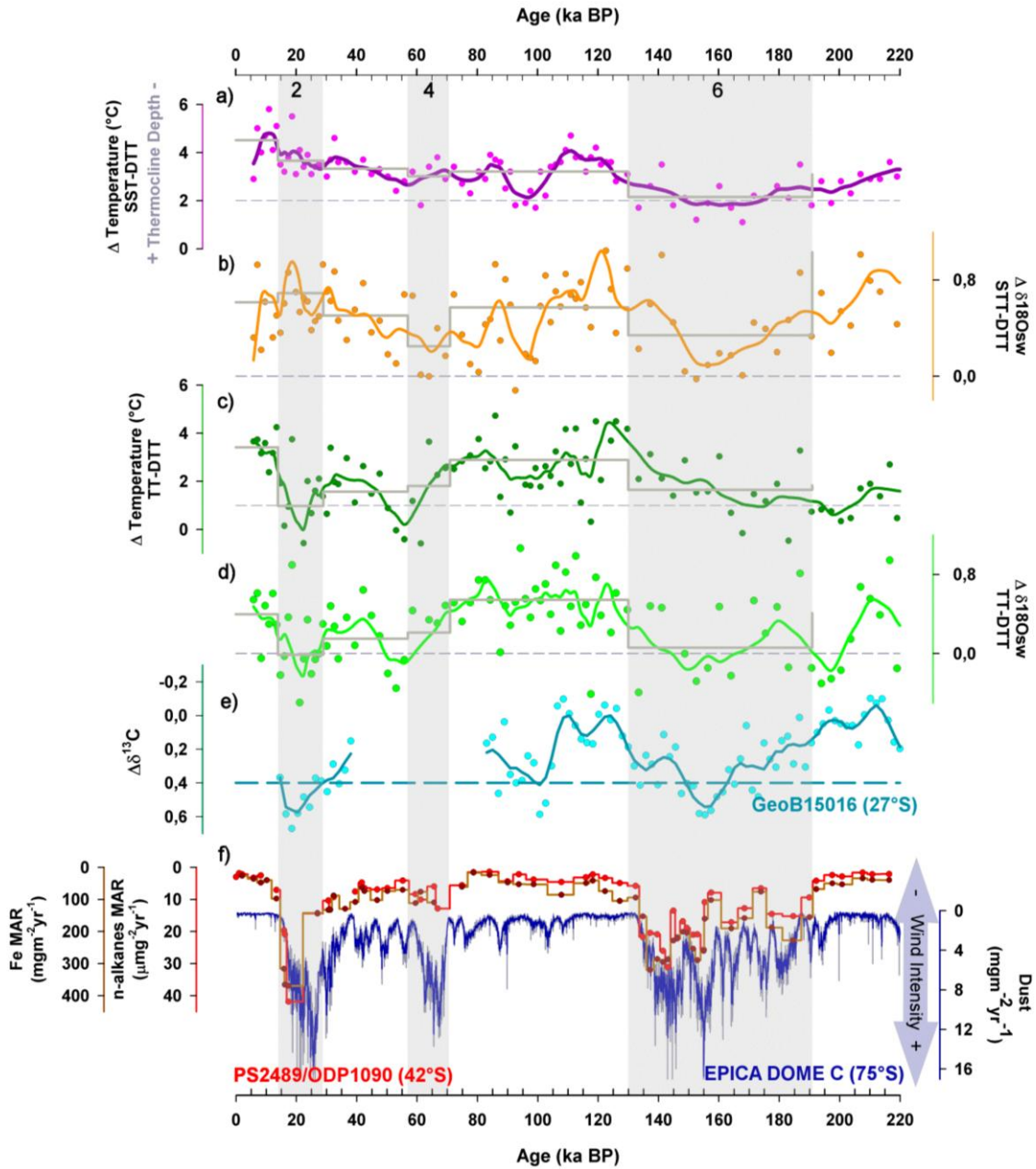


Figure 3.7 (a) Vertical temperature gradient in the water column. Orange line indicates the temperature gradient between sea surface ($SST_{Mg/Ca}$) and the deep-thermocline ($DTT_{Mg/Ca}$). Blue line denotes the temperature gradient between thermocline ($TT_{Mg/Ca}$) and deep-thermocline ($DTT_{Mg/Ca}$). (b) Calculated seawater isotopic differences ($\Delta\delta^{18}\text{O}_{sw}$). Purple colour lines indicate the $\Delta\delta^{18}\text{O}_{sw}$ between *G. bulloides* and *G. truncatulinoides* (Gb–Gt). Green colour lines denote $\Delta\delta^{18}\text{O}_{sw}$ between *G. inflata* and *G. truncatulinoides* (Gi–Gt). Thicker continuous lines denote average values computed per each isotopic stage (MIS 1 to MIS 6). (c) The $\delta^{13}\text{C}$ gradient between GeoB15016 and the Pacific Deep Water (PDW) stack ($\Delta\delta^{13}\text{C}_{DIC}$). Positive $\Delta\delta^{13}\text{C}_{DIC}$ values indicate measurable presence of AAIW, dashed cyan line denotes the modern $\Delta\delta^{13}\text{C}_{DIC}$ (0.4‰) for site GeoB15016 [Martínez-Méndez et al., 2013]. (d) Insoluble dust flux in EPICA Dome C ice core (blue) [Lambert et al., 2008] and the long-chain odd carbon-numbered n-alkanes (brown) and Fe flux (red) at core location PS2489–2/ODP1090 [Martínez-García et al., 2009]

3.5 Conclusions

In summary, our sea surface temperature and salinity reconstructions agree with previous findings of a low sensitivity ($< 4\text{ }^{\circ}\text{C}$) of the surface hydrography in the central South Pacific to glacial-interglacial changes (e.g. Luz, 1977). In contrast to the sea surface, we found large amplitude of glacial-interglacial variations in temperature and $\Delta\delta^{18}\text{O}_{\text{SW-IVC}}$ at subsurface water depth in the SPG. Considering the role of SOIWs in ventilating the subtropical thermocline, we interpret the high subsurface variability (salinity and temperature) at our study site as a consequence of the changes in formation and/or advection of the SOIWs formed in the SEP. The advection/formation of the SOIWs is plausibly driven mainly by the intensity of the SWW, rather than its glacial latitudinal migration. Our results suggest that the SOIWs advection to the SPG's thermocline during different glacials could be highly variable, resulting in colder- and fresher-than-Holocene subsurface waters during LGM, versus warmer- and saltier-than-Holocene subsurface waters during MIS 6. These findings provide a competing hypothesis to previous studies that posit a stable and continuous influence of the SOIWs in the SEP during glacials. Various scenarios of SOIWs formation/advection, inferred from our data in the SPG in combination with published data from the SEP and SWP, suggest spatial heterogeneity in the glacial northward transport of SOIWs signal in the Pacific basin.

3.6 Acknowledgments

This study is part of the project SOPATRA (SOuth PACific paleoceanographic TRAnsect) funded by the German Ministry of Education and Research (BMBF) through grant No. 03G0213B. Technical support and laboratory assistance from N. Gehre, L. Haxhijaj (GEOMAR) and L. Schönborn (AWI) are highly appreciated. We are grateful to S.L. Ho, S. Contreras and J. Groeneveld for their comments and suggestions during the preparation of this manuscript, and two anonymous reviewers for their critical comments that substantially improved the final version of this article. Data presented in this study is available in PANGAEA database (www.pangaea.de).

3.7 References

- Anderson, D. M., and D. Archer (2002), Glacial-interglacial stability of ocean pH inferred from foraminifer dissolution rates, *Nature*, *416*, doi:10.1038/416070a.
- Anderson, R. F., M. Q. Fleischer, Y. Lao, and G. Winckler (2008), Modern CaCO_3 preservation in equatorial Pacific sediments in the context of late-Pleistocene glacial cycles, *Marine Chemistry*, *111*(1), 30–46, doi:10.1016/j.marchem.2007.11.011.
- Antonov, J. I., D. Seidov, T. P. Boyer, R. A. Locarnini, A. V. Mishonov, H. E. Garcia, O. K.

- Baranova, M. M. Zweng, and D. R. Johnson (2010), World Ocean Atlas 2009, Volume 2: Salinity. S. Levitus, Ed, *NOAA Atlas NESDIS*, 69.
- Ayers, J. M., and P. G. Strutton (2013), Nutrient variability in Subantarctic Mode Waters forced by the Southern Annular Mode and ENSO, *Geophys. Res. Lett.*, 40, doi:10.1002/grl.50638.
- Bard, E. (1988), Correction of accelerator mass spectrometry ^{14}C ages measured in planktonic foraminifera: paleoceanographic implications, *Paleoceanography*, 3(6), 635–645, doi:10.1029/PA003i006p00635.
- Bard, E., L. Labeyrie, M. Arnold, M. Labracherie, J.-J. Pichon, J. Duprat, and J.-C. Duplessy (1989), AMS- ^{14}C ages measured in deep sea cores from the Southern Ocean: implications for sedimentation rates during isotope stage 2, *Quat. Res.*, 31(2), 309–317.
- Barker, S., M. Greaves, and H. Elderfield (2003), A study of cleaning procedures used for foraminiferal Mg/Ca paleothermometry, *Geochem. Geophys. Geosyst.*, 4, doi:10.1029/2003GC000559.
- Bostock, H. C., B. N. Opdyke, and M. J. M. Williams (2010), Characterising the intermediate depth waters of the Pacific Ocean using $\delta^{13}\text{C}$ and other geochemical tracers, *Deep-Sea Res. Part I*, 57(7), 847–859, doi:10.1016/j.dsr.2010.04.005.
- Bostock, H. C., B. N. Opdyke, M. K. Gagan, and L. K. Fifield (2004), Carbon isotope evidence for changes in Antarctic Intermediate Water circulation and ocean ventilation in the southwest Pacific during the last deglaciation, *Paleoceanography*, 19, PA4013, doi:10.1029/2004PA001047.
- Bostock, H. C., B. W. Hayward, H. L. Neil, K. I. Currie, and G. B. Dunbar (2011), Deep-water carbonate concentrations in the southwest Pacific, *Deep-Sea Res. Part I*, 58(1), 72–85, doi:10.1016/j.dsr.2010.11.010.
- Bostock, H. C., P. J. Sutton, M. Williams, and B. N. Opdyke (2013), Reviewing the circulation and mixing of Antarctic Intermediate Water in the South Pacific using evidence from geochemical tracers and Argo float trajectories, *Deep-Sea Res. Part I*, 73, 84–98, doi:10.1016/j.dsr.2012.11.007.
- Broecker, W. S. (2001), Glacial-to-Holocene Redistribution of Carbonate Ion in the Deep Sea, *Science*, 294(5549), 2152–2155, doi:10.1126/science.1064171.
- Brown, S. J., and H. Elderfield (1996), Variations in Mg/Ca and Sr/Ca ratios of planktonic foraminifera caused by postdepositional dissolution: Evidence of shallow Mg-dependent dissolution, *Paleoceanography*, 11(5), 543–551.
- Cléroux, C., E. Cortijo, J.-C. Duplessy, and R. Zahn (2007), Deep-dwelling foraminifera as thermocline temperature recorders, *Geochem. Geophys. Geosyst.*, 8(4), doi:10.1029/2006GC001474.
- Dekens, P. S., D. W. Lea, D. K. Pak, and H. J. Spero (2002), Core top calibration of Mg/Ca in tropical foraminifera: Refining paleotemperature estimation, *Geochem. Geophys. Geosyst.*, 3(4), doi:10.1029/2001GC000200.
- Deuser, W. G., E. H. Ross, C. Hemleben, and M. Spindler (1981), Seasonal changes in species composition, numbers, mass, size, and isotopic composition of planktonic

- foraminifera settling into the deep Sargasso Sea, *Paleogeography, Paleoclimatology, Paleogeography*, 33(1), 103–127.
- Fairbanks, R. G., P. H. Wiebe, and A. W. Be (1980), Vertical distribution and isotopic composition of living planktonic foraminifera in the western North Atlantic, *Science*, 207(4426), 61–63.
- Franke, J., A. Paul, and M. Schulz (2008), Modeling variations of marine reservoir ages during the last 45 000 years, *Clim. Past*, 4(1), 81–110.
- Gersonde, R. et al. (2003), Last glacial sea surface temperatures and sea-ice extent in the Southern Ocean (Atlantic-Indian sector): a multiproxy approach, *Paleoceanography*, 18(3), 1061, doi:10.1029/2002PA000809.
- Gersonde, R., X. Crosta, A. Abelmann, and L. Armand (2005), Sea-surface temperature and sea ice distribution of the Southern Ocean at the EPILOG Last Glacial Maximum—a circum-Antarctic view based on siliceous microfossil records, *Quat. Sci. Rev.*, 24(7), 869–896, doi:10.1016/j.quascirev.2004.07.015.
- Groeneveld, J., and C. M. Chiessi (2011), Mg/Ca of *Globorotalia inflata* as a recorder of permanent thermocline temperatures in the South Atlantic, *Paleoceanography*, 26(2), doi:10.1029/2010PA001940.
- Hall, A., and M. Visbeck (2002), Synchronous variability in the Southern Hemisphere atmosphere, sea ice, and ocean resulting from the Annular Mode, *J. Phys. Oceanogr.*, 15, 3043–3056.
- Hall, I. R., I. N. McCave, N. J. Shackleton, G. P. Weedon, and S. E. Harris (2001), Intensified deep Pacific inflow and ventilation in Pleistocene glacial times, *Nature*, 412, 809–811.
- Hanawa, K., and L. D. Talley (2001), Mode Waters, in *Ocean Circulation and Climate*, vol. 77, edited by G. Siedler, J. Church, Gould, pp. 373–386, Academic Press.
- Hartin, C. A., R. Fine, B. M. Sloyan, L. D. Talley, T. K. Chereskin, and J. Happell (2011), Formation rates of Subantarctic mode water and Antarctic intermediate water within the South Pacific, *Deep-Sea Res. Part I*, 58, 524–534, doi:10.1016/j.dsr.2011.02.010.
- Hasson, A., A. Koch-Larrouy, R. Morrow, M. Juza, and T. Penduff (2011), The origin and fate of mode water in the southern Pacific Ocean, *Ocean Dynamics*, 62(3), 335–354, doi:10.1007/s10236-011-0507-3.
- Herguera, J. C., T. Herbert, M. Kashgarian, and C. Charles (2010), Intermediate and deep water mass distribution in the Pacific during the Last Glacial Maximum inferred from oxygen and carbon stable isotopes, *Quat. Sci. Rev.*, 29(9), 1228–1245, doi:doi:10.1016/j.quascirev.2010.02.009.
- Herraiz-Borreguero, L., and S. R. Rintoul (2011a), Regional circulation and its impact on upper ocean variability south of Tasmania, *Deep Sea Research Part II: Topical Studies in Oceanography*, 58, 2071–2081, doi:10.1016/j.dsr2.2011.05.022.
- Herraiz-Borreguero, L., and S. R. Rintoul (2011b), Subantarctic mode water: distribution and circulation, *Ocean Dynamics*, 61(1), 103–126, doi:10.1007/s10236-010-0352-9.
- Ho, S. L., G. Mollenhauer, F. Lamy, A. Martínez-García, M. Mohtadi, R. Gersonde, D.

- Hebbeln, S. Nuñez-Ricardo, A. Rosell-Melé, and R. Tiedemann (2012), Sea surface temperature variability in the Pacific sector of the Southern Ocean over the past 700 kyr, *Paleoceanography*, 27(4), PA4202, doi:10.1029/2012PA002317.
- Holte, J. W., L. D. Talley, T. K. Chereskin, and B. M. Sloyan (2013), Subantarctic mode water in the southeast Pacific: Effect of exchange across the Subantarctic Front, *J. Geophys. Res. Oceans*, 118(4), 2052–2066, doi:10.1002/jgrc.20144.
- Holte, J. W., L. D. Talley, T. K. Chereskin, and B. M. Sloyan (2012), The role of air-sea fluxes in Subantarctic Mode Water formation, *J. Geophys. Res.*, 117, C03040, doi:10.1029/2011JC007798.
- Kaiser, J., F. Lamy, and D. Hebbeln (2005), A 70-kyr sea surface temperature record off southern Chile (Ocean Drilling Program Site 1233), *Paleoceanography*, 20(4), doi:10.1029/2005PA001146.
- Key, R. M., T. Tanhua, A. Olsen, M. Hoppema, S. Jutterström, C. Schirnack, S. Van Heuven, A. Kozyr, X. Lin, and A. Velo (2010), The CARINA data synthesis project: introduction and overview, *Earth System Science Data*, 2, 105–121.
- King, A. L., and W. R. Howard (2003), Planktonic foraminiferal flux seasonality in Subantarctic sediment traps: a test for paleoclimate reconstructions, *Paleoceanography*, 18(1), 1019, doi:10.1029/2002PA000839.
- Kohfeld, K. E., R. M. Graham, A. M. de Boer, L. C. Sime, E. W. Wolff, C. Le Quéré, and L. Bopp (2013), Southern Hemisphere westerly wind changes during the Last Glacial Maximum: paleo-data synthesis, *Quat. Sci. Rev.*, 68, 76–95, doi:10.1016/j.quascirev.2013.01.017.
- Lambert, F., B. Delmonte, J. R. Petit, M. Bigler, P. R. Kaufmann, M. A. Hutterli, T. F. Stocker, U. Ruth, J. P. Steffensen, and V. Maggi (2008), Dust-climate couplings over the past 800,000 years from the EPICA Dome C ice core, *Nature*, 452(7187), 616–619, doi:10.1038/nature06763.
- Lamy, F., J. Kaiser, U. S. Ninneman, D. Hebbeln, H. W. Arz, and J. Stoner (2004), Antarctic timing of surface water changes off Chile and Patagonian ice sheet response, *Science*, 304, 1959–1962, doi:10.1126/science.1097863.
- Lamy, F., R. Gersonde, G. Winckler, O. Esper, A. Jaeschke, G. Kuhn, J. Ullermann, A. Martínez-García, F. Lambert, and R. Kilian (2014), Increased dust deposition in the Pacific Southern Ocean during glacial periods, *Science*, 343(6169), 403–407.
- LeGrande, A. N., and G. A. Schmidt (2006), Global gridded data set of the oxygen isotopic composition in seawater, *Geophys. Res. Lett.*, 33(12), L12604, doi:10.1029/2006GL026011.
- LeGrande, A. N., and G. A. Schmidt (2011), Water isotopologues as a quantitative paleosalinity proxy, *Paleoceanography*, 26(3), PA3225, doi:10.1029/2010PA002043.
- Lenton, A., and R. J. Matear (2007), Role of the Southern Annular Mode (SAM) in Southern Ocean CO₂ uptake, *Global Biogeochem. Cycles*, 21(2), doi:10.1029/2006GB002714.
- Lisiecki, L. E. (2010), A benthic $\delta^{13}\text{C}$ -based proxy for atmospheric pCO₂ over the last 1.5 Myr, *Geophys. Res. Lett.*, 37(21), doi:10.1029/2010GL045109.

- Lisiecki, L. E., and M. E. Raymo (2005), A Pliocene-Pleistocene stack of 57 globally distributed benthic $\delta^{18}\text{O}$ records, *Paleoceanography*, 20(1), doi:10.1029/2004PA001071.
- Liu, Z., S. I. Shin, B. Otto-Bliesner, J. E. Kutzbach, E. C. Brady, and D. E. Lee (2002), Tropical cooling at the last glacial maximum and extratropical ocean ventilation, *Geophys. Res. Lett.*, 29(10), 1409, doi:10.1029/2001GL013938.
- Locarnini, R. A., A. V. Mishonov, J. I. Antonov, T. P. Boyer, H. E. Garcia, O. K. Baranova, M. M. Zweng, and D. R. Johnson (2010), World Ocean Atlas 2009, vol. 1, *Temperature*, NOAA Atlas NESDIS, 68.
- Lončarić, N., F. J. Peeters, D. Kroon, and G.-J. A. Brummer (2006), Oxygen isotope ecology of recent planktic foraminifera at the central Walvis Ridge (SE Atlantic), *Paleoceanography*, 21(3), doi:10.1029/2005PA001207.
- Lovenduski, N. S., and N. Gruber (2005), Impact of the Southern Annular Mode on Southern Ocean circulation and biology, *Geophys. Res. Lett.*, 32, L11603, doi:10.1029/2005GL022727.
- Luz, B. (1977), Late Pleistocene paleoclimates of the South Pacific based on statistical analysis of planktonic foraminifers, *Paleogeography, Paleoclimatology, Paleogeography*, 22(1), 61–78.
- Markgraf, V., J. R. Dodson, A. P. Kershaw, M. S. McGlone, and N. Nicholls (1992), Evolution of late Pleistocene and Holocene climates in the circum-South Pacific land areas, *Clim. Dyn.*, 6(3-4), 193–211.
- Marr, J. P., H. C. Bostock, L. Carter, A. Bolton, and E. Smith (2013), Differential effects of cleaning procedures on the trace element chemistry of planktonic foraminifera, *Chemical Geology*, 351, 310–323, doi:10.1016/j.chemgeo.2013.05.019.
- Martínez-García, A., A. Rosell-Melé, W. Geibert, R. Gersonde, P. Masqué, V. Gaspari, and C. Barbante (2009), Links between iron supply, marine productivity, sea surface temperature, and CO_2 over the last 1.1 Ma, *Paleoceanography*, 24(1), doi:10.1029/2008PA001657.
- Martínez-Méndez, G., D. Hebbeln, M. Mohtadi, F. Lamy, R. DePol-Holz, D. Reyes-Macaya, and T. Freudenthal (2013), Changes in the advection of Antarctic Intermediate Water to the northern Chilean coast during the last 970 kyr, *Paleoceanography*, 28, doi:10.1002/palo.20047.
- Mashiotta, T. A., D. W. Lea, and H. J. Spero (1999), Glacial–interglacial changes in Subantarctic sea surface temperature and $\delta^{18}\text{O}$ -water using foraminiferal Mg, *Earth Plan. Sci. Lett.*, 170, 417–432.
- Matsumoto, K., J. Lynch-Stieglitz, and R. F. Anderson (2001), Similar glacial and Holocene Southern Ocean hydrography, *Paleoceanography*, 16(5), 445–454.
- McCartney, M. S. (1977), Subantarctic Mode Water, in *A Voyage of Discovery, George Deacon 70th Anniversary Volume*, edited by M. Angel, pp. 103–119, Pergamon, New York.
- McCave, I. N., L. Carter, and I. R. Hall (2008), Glacial–interglacial changes in water mass structure and flow in the SW Pacific Ocean, *Quat. Sci. Rev.*, 27(19-20), 1886–1908,

doi:10.1016/j.quascirev.2008.07.010.

- Mekik, F., R. François, and M. Soon (2007), A novel approach to dissolution correction of Mg/Ca-based paleothermometry in the tropical Pacific, *Paleoceanography*, 22(3), doi:10.1029/2007PA001504.
- Mortyn, P. G., and C. D. Charles (2003), Planktonic foraminiferal depth habitat and $\delta^{18}\text{O}$ calibrations: Plankton tow results from the Atlantic sector of the Southern Ocean, *Paleoceanography*, 18(2), doi:10.1029/2001PA000637.
- Muratli, J. M., Z. Chase, A. C. Mix, and J. McManus (2010), Increased glacial-age ventilation of the Chilean margin by Antarctic Intermediate Water, *Nat. Geosci.*, 3, 23–26, doi:10.1038/ngeo715.
- Noble, T. L., A. M. Piotrowski, L. F. Robinson, J. F. McManus, C.-D. Hillenbrand, and A. J. M. Bory (2012), Greater supply of Patagonian-sourced detritus and transport by the ACC to the Atlantic sector of the Southern Ocean during the last glacial period, *Earth Plan. Sci. Lett.*, 317, 374–385, doi:10.1016/j.epsl.2011.10.007.
- Northcote, L. C., and H. L. Neil (2005), Seasonal variations in foraminiferal flux in the Southern Ocean, Campbell Plateau, New Zealand, *Mar. Micropaleontol.*, 56(3), 122–137, doi:10.1016/j.marmicro.2005.05.001.
- Nürnberg, D., and J. Groeneveld (2006), Pleistocene variability of the Subtropical Convergence at East Tasman Plateau: evidence from planktonic foraminiferal Mg/Ca (ODP Site 1172A), *Geochem. Geophys. Geosyst.*, 7, Q04P11, doi:10.1029/2005GC000984.
- Nürnberg, D., J. Bijma, and C. Hemleben (1996), Assessing the reliability of magnesium in foraminiferal calcite as a proxy for water mass temperatures, *Geochim. Cosmochim. Acta*, 60(5), 803–814.
- Oke, P. R., and M. H. England (2004), Oceanic response to changes in the latitude of the Southern Hemisphere subpolar westerly winds, *J. Climate*, 17(5), 1040–1054.
- Orsi, A. H., T. Whitworth, and W. D. Nowlin (1995), On the meridional extent and fronts of the Antarctic Circumpolar Current, *Deep-Sea Res. Part I*, 42(5), 641–673.
- Otto-Bliesner, B. L., E. C. Brady, G. Clauzet, R. Tomas, S. Levis, and Z. Kothavala (2006), Last Glacial Maximum and Holocene Climate in CCSM3, *J. Climate*, 19(11), 2526–2544, doi:10.1175/JCLI3748.1.
- Pahnke, K., and R. Zahn (2005), Southern Hemisphere water mass conversion linked with North Atlantic climate variability, *Science*, 307, 1741–1746, doi:10.1126/science.1102163.
- Pahnke, K., R. Zahn, H. Elderfield, and M. Schulz (2003), 340,000-year centennial-scale marine record of Southern Hemisphere climatic oscillation, *Science*, 301(5635), 948–952, doi:10.1126/science.1084451.
- Pahnke, K., S. L. Goldstein, and S. R. Hemming (2008), Abrupt changes in Antarctic Intermediate Water circulation over the past 25,000 years, *Nat. Geosci.*, 1, 870–874, doi:10.1038/ngeo360.

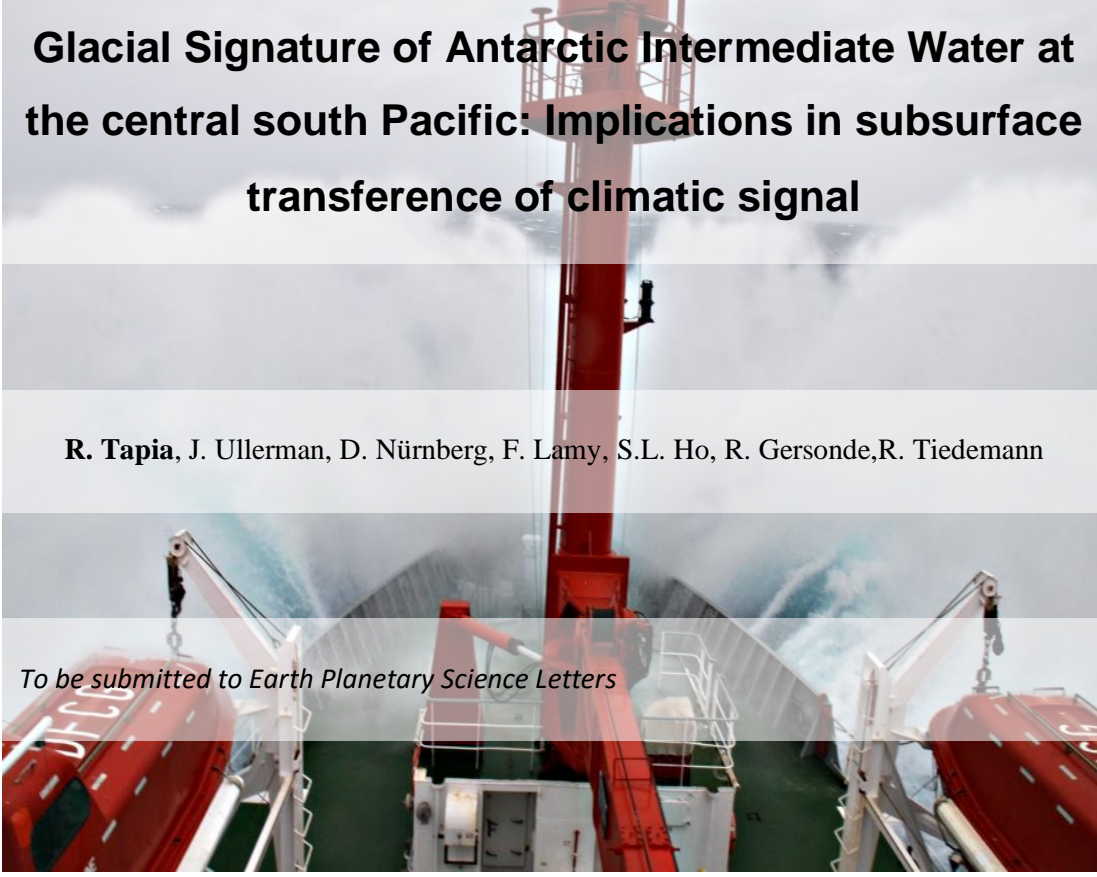
- Paillard, D., L. Labeyrie, and P. Yiou (1996), Macintosh Program performs time-series analysis, *EOS, Transactions American Geophysical Union*, 77(39), 379–379, doi:10.1029/96EO00259.
- Pena, L. D., I. Cacho, P. Ferretti, and M. A. Hall (2008), El Niño–Southern Oscillation–like variability during glacial terminations and interlatitudinal teleconnections, *Paleoceanography*, 23, PA3101, doi:10.1029/2008PA001620.
- Pena, L. D., S. L. Goldstein, S. R. Hemming, K. M. Jones, E. Calvo, C. Pelejero, and I. Cacho (2013), Rapid changes in meridional advection of Southern Ocean intermediate waters to the tropical Pacific during the last 30 kyr, *Earth Plan. Sci. Lett.*, 368, 20–32, doi:10.1016/j.epsl.2013.02.028.
- Ravelo, A. C., and C. Hillaire-Marcel (2007), The Use of Oxygen and Carbon Isotopes of Foraminifera in Paleoceanography, *Developments in Marine Geology*, 1, 735–764.
- Regenberg, M., A. Regenberg, D. Garbe-Schönberg, and D. W. Lea (2014), Global dissolution effects on planktonic foraminiferal Mg/Ca ratios controlled by the calcite-saturation state of bottom waters, *Paleoceanography*, doi:10.1002/2013PA002492.
- Regenberg, M., D. Nürnberg, S. Steph, J. Groeneveld, D. Garbe-Schönberg, R. Tiedemann, and W.-C. Dullo (2006), Assessing the effect of dissolution on planktonic foraminiferal Mg/Ca ratios: Evidence from Caribbean core tops, *Geochem. Geophys. Geosyst.*, 7, doi:10.1029/2005GC001019.
- Regenberg, M., S. Steph, D. Nürnberg, R. Tiedemann, and D. Garbe-Schönberg (2009), Calibrating Mg/Ca ratios of multiple planktonic foraminiferal species with $\delta^{18}\text{O}$ -calcification temperatures: paleothermometry for the upper water column, *Earth Plan. Sci. Lett.*, 278, 324–336, doi:10.1016/j.epsl.2008.12.019.
- Reimer, P. J., M. G. Baillie, E. Bard, A. Bayliss, J. W. Beck, P. G. Blackwell, C. B. Ramsey, C. E. Buck, G. S. Burr, and R. L. Edwards (2009), IntCal09 and Marine09 radiocarbon age calibration curves, 0-50,000 years cal BP, *Radiocarbon*, 51(3), 1111–1150.
- Ribbe, J. (2001), Intermediate water mass production controlled by southern hemisphere winds, *Geophys. Res. Lett.*, 28(3), 535–538, doi:10.1029/2000GL012242.
- Rohling, E. J. (2007), Progress in paleosalinity: Overview and presentation of a new approach, *Paleoceanography*, 22(3), doi:10.1029/2007PA001437.
- Rohling, E. J., and S. Cooke (1999), Stable oxygen and carbon isotopes in foraminiferal carbonate shells, in *Modern Foraminifera*, edited by B. K. Sen Gupta, pp. 239–258, Kluwer Academic Publishers, Dordrecht.
- Russell, J. L., and A. G. Dickson (2003), Variability in oxygen and nutrients in South Pacific Antarctic Intermediate Water, *Global Biogeochem. Cycles*, 17(2), 1033, doi:10.1029/2000GB001317.
- Sabine, C. L. et al. (2004), The oceanic sink for anthropogenic CO₂, *Science*, 305(5682), 367–371, doi:10.1126/science.1097403.
- Saenko, O. A., J. C. Fyfe, and M. H. England (2005), On the response of the oceanic wind-driven circulation to atmospheric CO₂ increase, *Clim. Dyn.*, 25, 415–426, doi:10.1007/s00382-005-0032-5.

- Sallée, J. B., N. Wienders, K. Speer, and R. Morrow (2006), Formation of subantarctic mode water in the southeastern Indian Ocean, *Ocean Dynamics*, 56, 525–542, doi:10.1007/s10236-005-0054-x.
- Sarmiento, J. L., N. Gruber, M. A. Brzezinski, and J. P. Dunne (2004), High-latitude controls of thermocline nutrients and low latitude biological productivity, *Nature*, 427, 56–60.
- Schneider, W., and L. Bravo (2006), Argo profiling floats document Subantarctic Mode Water formation west of Drake Passage, *Geophys. Res. Lett.*, 33, doi:10.1029/2006GL026463.
- Sexton, P. F., and S. Barker (2010), Onset of “Pacific-style” deep-sea sedimentary carbonate cycles at the mid-Pleistocene transition, *Earth Plan. Sci. Lett.*, 321-322, 81–94, doi:10.1016/j.epsl.2011.12.043.
- Shackleton, N. J. (1974), Attainment of isotopic equilibrium between ocean water and the benthonic foraminifera genus *Uvigerina*: isotopic changes in the ocean during the last glacial, *Cent. Nat. Rech. Sci. Colloq. Int.*, (219), 203–209.
- Shin, S. I., Z. Liu, B. Otto Bliesner, E. Brady, J. Kutzbach, and S. Harrison (2003), A simulation of the Last Glacial Maximum climate using the NCAR-CCSM, *Clim. Dyn.*, 20(2-3), 127–151.
- Sime, L. C., K. E. Kohfeld, C. Le Quéré, and E. W. Wolff (2013), Southern Hemisphere westerly wind changes during the Last Glacial Maximum: model-data comparison, *Quat. Sci. Rev.*, doi:10.1016/j.quascirev.2012.12.008.
- Sloyan, B. M., L. D. Talley, T. K. Chereskin, R. Fine, and J. Holte (2010), Antarctic Intermediate Water and Subantarctic Mode Water formation in the Southeast Pacific: the role of turbulent mixing, *J. Phys. Oceanogr.*, 40, 1558–1574, doi:10.1175/2010JPO4114.1.
- Spero, H. J., and D. W. Lea (2002), The cause of carbon isotope minimum events on glacial terminations, *Science*, 296(5567), 522–525.
- Spero, H. J., and D. W. Lea (1996), Experimental determination of stable isotope variability in *Globigerina bulloides*: implications for paleoceanographic reconstructions, *Mar. Micropaleontol.*, 28(3), 231–246.
- Spero, H. J., K. M. Mielke, E. M. Kalve, D. W. Lea, and D. K. Pak (2003), Multispecies approach to reconstructing eastern equatorial Pacific thermocline hydrography during the past 360 kyr, *Paleoceanography*, 18(1), n/a–n/a, doi:10.1029/2002PA000814.
- Steph, S., M. Regenberg, R. Tiedemann, S. Mulitza, and D. Nürnberg (2009), Stable isotopes of planktonic foraminifera from tropical Atlantic/Caribbean core-tops: Implications for reconstructing upper ocean stratification, *Mar. Micropaleontol.*, 71(1-2), 1–19, doi:10.1016/j.marmicro.2008.12.004.
- Stuiver, M., and J. Reimer (1993), Extended ^{14}C data base and revised CALIB 3.014 C age calibration program, *EDITORIAL COMMENT*, 35(1), 215–230.
- Thompson, D. W. J., and S. Solomon (2002), Interpretation of recent Southern Hemisphere climate change, *Science*, 296, 895–899, doi:10.1126/science.1069270.
- Tsuchiya, M., and L. D. Talley (1998), A Pacific hydrographic section at 88°W: water-property

distribution, *J. Geophys. Res.*, 103(C6), 12899–12918.

Waelbroeck, C., L. Labeyrie, E. Michel, J. C. Duplessy, J. McManus, K. Lambeck, E. Balbon, and M. Labracherie (2002), Sea-level and deep water temperature changes derived from benthic foraminifera isotopic records, *Quat. Sci. Rev.*, 21, 295–305.

Wilke, I., H. Meggers, and T. Bickert (2009), Depth habitats and seasonal distributions of recent planktic foraminifers in the Canary Islands region (29° N) based on oxygen isotopes, *Deep-Sea Res. Part I*, 56(1), 89–106, doi:doi:10.1016/j.dsr.2008.08.001.



Glacial Signature of Antarctic Intermediate Water at the central south Pacific: Implications in subsurface transference of climatic signal

R. Tapia, J. Ullerman, D. Nürnberg, F. Lamy, S.L. Ho, R. Gersonde, R. Tiedemann

To be submitted to Earth Planetary Science Letters

Abstract

Southern Ocean Intermediate Waters (SOIWs), such as Antarctic Intermediate Water and Subantarctic Mode Water, are considered as key player in the modulation of global climate system during glacial–interglacial time scales. They are the main paths to transfer climatic signals (e.g. heat, fresh water, salt and chemicals species) from the Southern Ocean to low latitudes through mechanisms as “oceanic tunneling”. Despite their relevance, the past evolution of the SOIWs in the central south Pacific is largely unknown. Here we compared paired Mg/Ca–temperature, stable carbon and oxygen isotope records from surface dwelling and deep dwelling planktic foraminifera at central south Pacific (54°S) to monitor changes in water column structure for the last 260 kyr. Our study focused on the subsurface variability controlled by Antarctic Intermediate Water subducted at the Subantarctic front during Last Glacial Maximum (LGM; ~29–17 ka) and Penultimate Glacial Maximum (PGM; ~180–150 ka). Relative to the Holocene colder and fresher conditions at subsurface suggests enhanced presence of Antarctic Intermediate Water. In contrast at surface, our data suggest similar glacial cooling with saltier conditions during PGM in comparison to LGM or Holocene. The $\delta^{13}\text{C}$ depletion of 0.35‰ at subsurface during PGM in comparison to LGM suggest glacial differences in the contribution of “old” low $\delta^{13}\text{C}$ deep waters. Multiple proxy records during glacial stages indicates changes in the convection depth of Antarctic Intermediate Water in the central south Pacific, overall a latitudinal comparison of water column structure resemble the effects on the ocean caused by climatic modes controlling the intensity of the Southern Westerly such as Southern Annular Mode.

CHAPTER 4

4.1 Introduction

The Southern Ocean (SO) is characterized by extensive water mass formation and transformation. Specifically, “old”, cold, and nutrient-rich deep water masses upwell and enhance the biological productivity in particular along the main oceanic fronts. It has been suggested that in the past heat, salt, and chemical signatures were transported from the Southern Ocean to other ocean basins via Southern Ocean Intermediate waters (SOIWs), such as the Subantarctic Mode Water (SAMW) and the Antarctic Intermediate Water (AAIW) [Ninnemann and Charles, 1997; Spero and Lea, 2002; Anderson *et al.*, 2009] (Figure 4.1). Thereby, the modern SOIWs link atmosphere and deep ocean, sequestering significant quantities of anthropogenic CO₂ and other atmospheric gasses in the ocean interior [Hartin *et al.*, 2011]. These processes have been suggested to play an important role in modulating climatic variability at glacial-interglacial time scales [Ninnemann and Charles, 1997; Spero and Lea, 2002; Bostock *et al.*, 2004; Anderson *et al.*, 2009].

The modern AAIW flows eastward with the Antarctic Circumpolar Current (ACC) and then northward into the adjacent subtropical gyres [Bostock *et al.*, 2013]. Circumpolar Deep Water (CDW) upwells around Antarctica and is carried northward as Antarctic Surface Waters (AASW). AASW is converted to AAIW through air-sea fluxes equatorward of the Antarctic Polar Front (APF) and subducts at the Subantarctic Front (SAF) [Hartin *et al.*, 2011; Bostock *et al.*, 2013] (Figure 4.1). AAIW can be traced by its distinctive salinity minimum at intermediate water depths [Hartin *et al.*, 2011; Bostock *et al.*, 2013]. SAMW is located equatorward of AAIW formation, north of the SAF [Hartin *et al.*, 2011; Bostock *et al.*, 2013; Holte *et al.*, 2013], where the deepening of mixed layers during wintertime convection and subsequent mixing control SAMW formation [Hartin *et al.*, 2011; Holte *et al.*, 2013]. Physical properties of SAMW, including temperature and salinity, are controlled by the incorporation of fresh water (e.g. northward Ekman transport) [Schneider and Bravo, 2006]. McCartney [1977] suggested that the formation of AAIW is closely related to SAMW, as they share similar physical properties (temperature and salinity) in the southeast Pacific (SEP), i.e. the main region supplying SAMW and AAIW to the Pacific Ocean [McCartney, 1977; Hartin *et al.*, 2011].

Previous proxy studies have underlined the spatio-temporal complexities in the formation and transport of the SOIWs in the Pacific Ocean [Muratli *et al.*, 2010; Martínez-Méndez *et al.*, 2013; Pena *et al.*, 2013; Ronge *et al.*, 2015; Tapia *et al.*, 2015], pointing to considerable regional differences. In general, the cooling and freshening at thermocline depths suggested by paired foraminiferal Mg/Ca-stable oxygen isotopes ($\delta^{18}\text{O}$) reconstructions have been interpreted as enhanced SOIWs presence during climatically cold

periods (e.g. LGM) at low and mid latitudes, as well as a varying extent of the glacial AAIW-signal [Pena et al., 2013; Tapia et al., 2015]. An opposite situation, i.e. decreased glacial formation of SOIWs has been proposed in the southwest Pacific (SWP) off New Zealand [see Ronge et al., 2015 and references therein]. Martinez-Méndez et al. [2013] suggested that this dichotomy reflects large latitudinal disparities in the SOIWs properties as result of different formation processes.

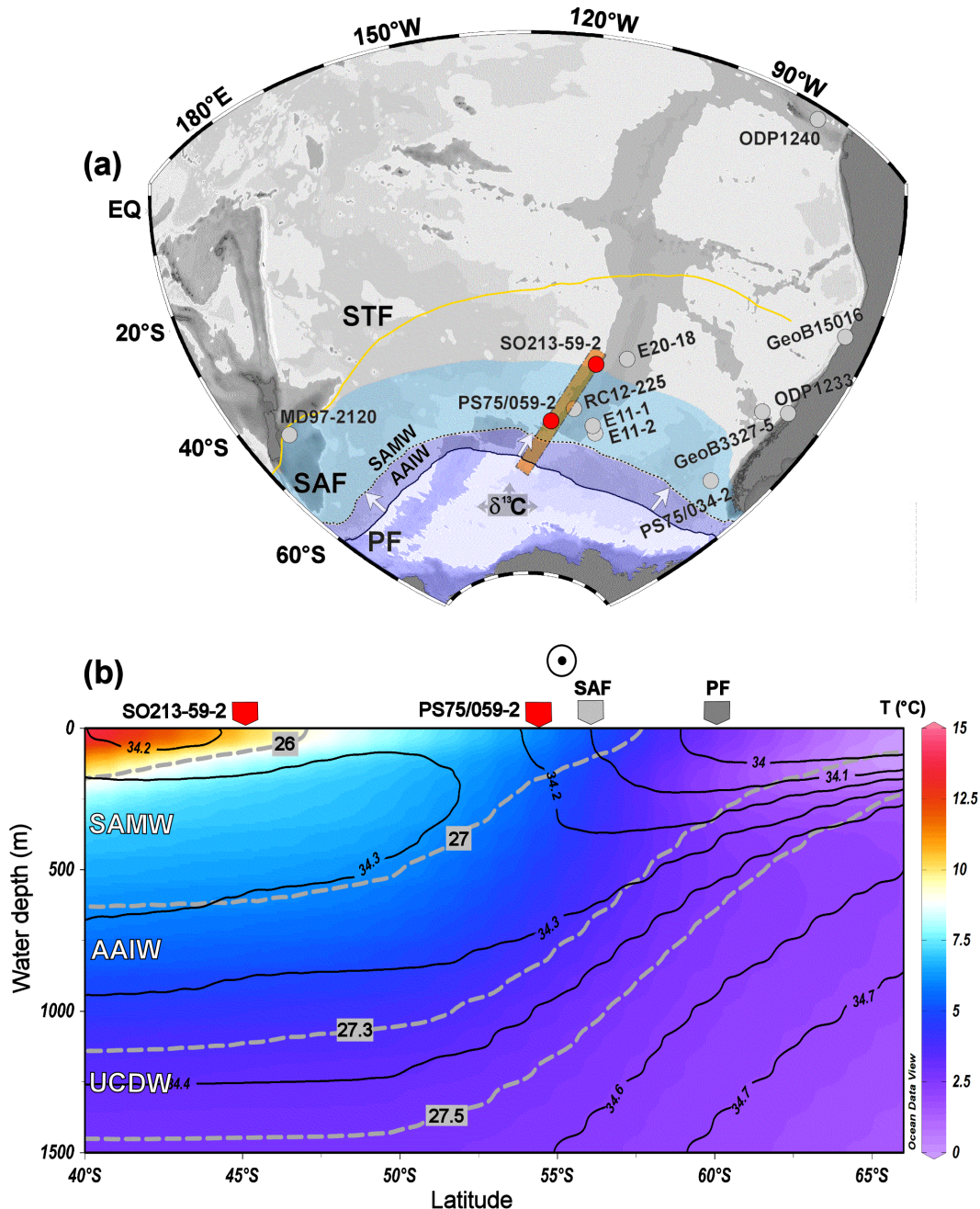


Figure 4.1 (a) Bathymetric chart of the South Pacific showing the studied sediment core PS75/059-2 and reference sites discussed in the text: MD97-2120 [Pahnke et al., 2003], SO213-59-2 [Tapia et al., 2015], E20-18, RC12-225, E11-1 [Luz, 1977], E11-2 [Mashiotta et al., 1999], GeoB15016 [Martínez-Méndez et al., 2013], ODP1233 [Muratli et al., 2010], GeoB3327-5 and PS75/034-1 [Ho et al., 2012]. Major currents and oceanographic fronts [Orsi et al.,

1995] are indicated: Subtropical Front (STF, yellow), Polar Front (PF, black) and Subantarctic Front (SAF, dotted), which separates cold and fresher polar surface waters from the warmer and saltier surface waters to the north. Subantarctic Mode Water (SAMW) forms north of the SAF (shaded area denotes the surface density of $\sigma_\theta = 26.6 \text{ kgm}^{-3}$ at 75 m); denser Antarctic Intermediate Water (AAIW) forms south of the SAF and north of the PF, and flows northwards below SAMW (arrows). (b) Temperature ($^{\circ}\text{C}$), density (σ_θ in kgm^{-3} ; dashed grey contours) and salinity (black contours) profile along the transect denoted in (a), clarifying the vertical distribution of SAMW, AAIW, and Upper Circumpolar Deep Water (UCDW). UCDW brings low $\delta^{13}\text{C}$ to the surface south of the PF. Open circle with dot denotes eastward-directed flow of the maximum SWW [Carranza and Gille, 2015]. Coloured arrows mark core positions and oceanic fronts (SAF and PF).

The planktic foraminiferal stable carbon isotope signal ($\delta^{13}\text{C}$) have been routinely applied for reconstructing water mass circulation patterns as they incorporate the $\delta^{13}\text{C}$ signature of seawater dissolved inorganic matter (DIC) into their shells [Lynch-Stieglitz, 2003; Ravelo and Hillaire-Marcel, 2007], with possible additional impacts of temperature, carbonate ion (CO_3^{2-}) concentration. The $\delta^{13}\text{C}$ of DIC in sea surface waters is influenced by primary productivity, which results in higher DIC- $\delta^{13}\text{C}$ as lighter carbon isotopes are preferentially taken for photosynthesis [Rohling and Cooke, 1999]. The light $\delta^{13}\text{C}$ signature in organic matters is released to the water mass as they sink, therefore subsurface water masses become more depleted in $\delta^{13}\text{C}$ because they accumulate DIC released from the remineralization of ^{12}C -enriched organic matter. Another factor affecting DIC- $\delta^{13}\text{C}$ in the upper ocean is the temperature-dependent air-sea exchange, which increases (decreases) DIC- $\delta^{13}\text{C}$ in cold (warm) waters ($\sim 0.1 \text{ ‰}$ per degree of cooling) [Lynch-Stieglitz, 2003]. Physical processes such as mixing and advection, both horizontally and vertically, of waters with different $\delta^{13}\text{C}$ values (e.g. upwelling of deeper ^{12}C -enriched waters) further influence $\delta^{13}\text{C}$ of seawater. As the temporal changes in $\delta^{13}\text{C}$ of organic matters at subsurface ocean is expected to track that at the sea surface where the organic matters are formed, the $\delta^{13}\text{C}$ signal of planktic foraminifera with different habitat depth preferences from a single site can therefore be used to cancel out the biological effects, highlighting the vertical differences in water properties [e.g. Schiraldi et al., 2014].

Here, we present Mg/Ca and stable isotopes ($\delta^{18}\text{O}$ and $\delta^{13}\text{C}$) records from the central SO covering the last 260 kyr, analysed on subsurface-dwelling planktic foraminifera *Globorotalia inflata*. Based on the comparison of our records with the geochemical data analysed on the near surface-dwelling planktic foraminifera *Globigerina bulloides* [Ullermann, 2015] and published datasets [Tapia et al., 2015], we reconstruct the upper ocean structure during full glacial conditions in the central Pacific sector of the Southern Ocean. Emphasis is on the subsurface variability controlled by AAIW, which is subducted at the SAF.

4.2 Material and Methods

The sediment core PS75/059-2 (54°12.9' S, 125°25.53' W; recovery 13.98 m; 3.613 m water depth) is located north of the main position of the modern SAF at the western flank of the East Pacific Rise (Figure 4.1). Sediments are carbonate-rich, with CaCO_3 contents of >90 wt-% during interglacials that decrease to 30-60 wt-% during glacials, opal and lithogenic contents reach 10–20 wt-% and 30-50 wt-%, respectively [Lamy *et al.*, 2014]. The chronostratigraphy of core PS75/059-2 has been updated from Lamy *et al.* [2014] by Ullermann *et al.* (*submitted*) (Figure 4.2a). It is based on the visual correlation of the $\delta^{18}\text{O}$ record of the benthic foraminiferal species *Cibicidoides spp.* and the global LR04 $\delta^{18}\text{O}$ reference stack [Lisiecki and Raymo, 2005] using the software “Match” [Lisiecki and Lisiecki, 2002].

For geochemical studies, the foraminiferal sampling was conducted at 5 cm intervals. We selected two planktic foraminiferal species from the 355–400 μm fraction. *Globorotalia inflata* is a deep-dwelling foraminiferal species that calcifies at water depths of 300–800 m water depth [Elderfield and Ganssen, 2000; Groeneveld and Chiessi, 2011], and used to reconstruct subsurface conditions at the thermocline [Groeneveld and Chiessi, 2011]. In combination with the near-surface dweller *Globigerina bulloides* (< 30 m water depth) [Mekik *et al.*, 2007] we intend to reconstruct the upper ocean structure of the central south Pacific over time. In the south Pacific both species show similar seasonality in their abundance with maximum fluxes occurring mainly during the austral late spring to summer [King and Howard, 2003]. Although it has been suggested that certain planktic foraminifera species can potentially vary their habitat depth through time, we here assume no change in the mean calcification depths over time.

4.2.1 Stable Isotopes and Mg/Ca paleothermometry

For each coupled Mg/Ca and stable isotopes ($\delta^{18}\text{O}$ and $\delta^{13}\text{C}$) measurement, ~35 specimens were used. The shells were gently fractured between two methanol-cleaned microscope glass plates to open the chambers, mixed with a brush to homogenize the sample to minimize error from sample heterogeneity, and then split in subsamples for stable isotope analyses and Mg/Ca measurements.

Prior to the stable isotope analysis, the subsamples were ultrasonically cleaned with deionized water and methanol. The isotopic analyses were performed at GEOMAR, Kiel, using a MAT253 mass spectrometer coupled with a Kiel IV Carbonate device (Thermo Fisher Scientific, Germany). Results were referenced to the NBS19 standard and calibrated to the PDB scale. The analytical error was ± 0.06 ‰ for $\delta^{18}\text{O}$ and ± 0.04 ‰ for $\delta^{13}\text{C}$.

Numerous biological processes (e.g. symbiont activity, ontogeny) may affect the $\delta^{18}\text{O}$

fractionation processes in planktic foraminifera [Ravelo and Hillaire-Marcel, 2007]. Previous work suggests a large spread of disequilibria, ranging from negligible or zero offsets to -1‰ for *G. bulloides* and from -0.4‰ to +0.4‰ (*G. inflata*) [see Tapia et al., 2015 and references therein]. Consequently there is no consensus on possible oxygen isotopic disequilibrium. For this reason, and because non-symbiotic *G. inflata* is believed to calcify at or close to equilibrium, we do not consider any vital effect on the fractionation between foraminiferal $\delta^{18}\text{O}$ and seawater $\delta^{18}\text{O}$. The subsamples for Mg/Ca analysis were cleaned according to the protocol proposed by Barker et al. [2003], adding a reductive step. The analyses were performed on an ICP-OES (VARIAN 720 ES), which has a long-term analytical precision of $\pm 0.1 \text{ mmolmol}^{-1}$ for Mg/Ca on the ECRM752–1 standard. As clay contamination and post-depositional Mn-rich carbonate coatings can exert a significant control on Mg/Ca ratios [Barker et al., 2003], the efficiency of the cleaning was evaluated by monitoring the elements Fe, Al and Mn, which were measured alongside Mg. The Fe/Ca, Al/Ca and Mn/Ca ratios of our samples were $< 0.14 \text{ mmolmol}^{-1}$ with no evident linear correlation to Mg/Ca, suggesting that the associated Mg/Ca data were not biased by the aforementioned factors (see *supplementary material*).

The calculations of paleotemperature for *G. inflata* was conducted according to the calibration of Elderfield and Ganssen [2000] ($Mg/Ca = 0.52e^{0.1T}$) for temperatures between 0–19°C. Additional calibrations were also applied [e.g. Groeneveld and Chiessi, 2011], but ultimately rejected since the spread of calculated temperatures were larger than the thermal tolerance reported for *G. inflata* [Tolderlund and Bé, 1971]. In the case of *G. bulloides* the conversion to temperatures was conducted according to the calibration of Mashiotta et al. [1999] ($Mg/Ca = 0.474e^{0.107T}$).

To estimate the amplitude of temperature changes across each Marine Isotope Stage (MIS), we averaged the temperature estimates within each of the glacial and interglacial intervals. The intervals were defined according to the boundaries proposed by Lisiecki and Raymo [2005]. In order to evaluate glacial conditions without taking into account the deglaciation, we defined two glacial time windows, namely the Last Glacial Maximum (LGM) from ~29–17ka BP [Bostock et al., 2004] and the Penultimate Glacial Maximum (PGM) from ~180–150ka BP. The minimum carbon isotope values were used to define deglaciations [Spero and Lea, 2002]. Holocene time window was defined as < 8ka BP.

4.2.2 Seawater $\delta^{18}\text{O}$ and Relative Salinity Calculation

As the local sea water $\delta^{18}\text{O}$ ($\delta^{18}\text{O}_{\text{SW}}$) correlates linearly with seawater salinity on regional scales [LeGrande and Schmidt, 2006], we used the ice volume corrected seawater $\delta^{18}\text{O}_{\text{SW-IVC}}$ as a semi-quantitative proxy for local salinity changes. However, we refrained from

converting the $\delta^{18}\text{O}_{\text{SW-IVC}}$ signal into salinity, as the $\delta^{18}\text{O}_{\text{SW-IVC}}$ to salinity relationships are only regionally coherent and might have changed through time [LeGrande and Schmidt, 2006].

The ice volume corrected $\delta^{18}\text{O}_{\text{SW-IVC}}$ calculation firstly involves the subtraction of the temperature effect from the planktic $\delta^{18}\text{O}$ data ($\delta^{18}\text{O}_{\text{SW}}$ (VSMOW) = $\delta^{18}\text{O} + 0.27 - (4.38 - (4.38^2 - 4 \times 0.1 (16.9 - T_{\text{Mg/Ca}})^{1/2}) / (0.1 \times 2))$) [Shackleton, 1974]. This equation has been successfully used to reconstruct $\delta^{18}\text{O}_{\text{SW}}$ composition in Subantarctic and SO settings [e.g. Mashiotta et al., 1999]. This step is followed by the subtraction of the global mean ocean $\delta^{18}\text{O}_{\text{SW}}$ record of Waelbroeck et al. [2002], linearly interpolated at the time step of the core PS75/059-2 $\delta^{18}\text{O}$ records, from the reconstructed $\delta^{18}\text{O}_{\text{SW}}$ values.

4.3 Results

4.3.1 Planktic Foraminiferal Mg/Ca-Temperature

In the upper most sample of the core PS75/059-2 the Mg/Ca (temperature) values for *G. bulloides* and *G. inflata* are $1.17 \text{ mmolmol}^{-1}$ ($\sim 8.5^\circ\text{C}$) and $1.00 \text{ mmolmol}^{-1}$ ($\sim 6.6^\circ\text{C}$), respectively (Figure 2b). On the basis of an accuracy of $\pm 0.5\text{--}1^\circ\text{C}$ suggested for Mg/Ca-palaeothermometry [e.g. Mashiotta et al., 1999], the reconstructed Mg/Ca-temperature for *G. bulloides* ($\text{SST}_{\text{Mg/Ca } G.\text{bulloides}}$) and *G. inflata* ($\text{SubST}_{\text{Mg/Ca } G.\text{inflata}}$) are consistent with modern austral summer temperatures at water depths of $< 40 \text{ m}$ and $\sim 75 - \sim 400 \text{ m}$ (WOA09 and WOCE databases) (see supplementary material). Downcore, the Mg/Ca (temperature) values for *G. inflata* range from 0.58 to $1.45 \text{ mmolmol}^{-1}$ (~ 1 to $\sim 10^\circ\text{C}$), lower than the Mg/Ca (temperature) values of the surface-dwelling *G. bulloides* that vary between 0.88 and $2.02 \text{ mmolmol}^{-1}$ (~ 6 to $\sim 14^\circ\text{C}$). The Mg/Ca-temperature profiles from *G. inflata* and *G. bulloides* show a clear pattern of glacial-interglacial variability, also reflected in their $\delta^{18}\text{O}$ signal and in the $\delta^{18}\text{O}$ from *Cibicidoides* spp. (Figure 4.2a, b and c).

Overall, $\text{SubST}_{\text{Mg/Ca } G.\text{inflata}}$ suggest relatively variable interglacial temperatures: $\sim 6.4^\circ\text{C}$ (MIS 7), $\sim 7.6^\circ\text{C}$ (MIS 5), $\sim 5.2^\circ\text{C}$ (MIS 3), $\sim 8^\circ\text{C}$ (Holocene) (Figure 4.2b), respectively. On the other hand, the $\text{SST}_{\text{Mg/Ca } G.\text{bulloides}}$ suggest comparable interglacial temperatures of $\sim 9^\circ\text{C}$, with the exception of MIS 3 ($\sim 7^\circ\text{C}$) (Figure 4.2b). The selected glacial time windows consistently suggest stable glacial temperatures of $\sim 4.5^\circ\text{C}$ (PGM) and $\sim 5.2^\circ\text{C}$ (LGM) at subsurface and $\sim 7.8^\circ\text{C}$ (PGM) and $\sim 7.7^\circ\text{C}$ (PGM) at surface (Figure 4.2b).

The effects of dissolution on foraminiferal Mg/Ca is crucial to any temperature reconstruction [see Regenberg et al., 2014 and references therein] but is considered here negligible. Indeed, dissolution reduces the Mg/Ca content in planktic foraminifera, therefore the reconstructed temperatures may appear too low. By correcting the Mg/Ca for carbonate ion saturation state [ΔCO_3^{2-}] of the bottoms water ($0.1 - 0.2^\circ\text{C}$ and $0.4 - 0.6^\circ\text{C}$ per μmolkg^{-1} $\Delta[\text{CO}_3^{2-}]$ for surface and subsurface dwellers; Regenberg et al., 2014), unrealistic $\text{SubST}_{\text{Mg/Ca}}$

G. inflata are calculated, ~10 °C warmer than the modern temperatures of ~6 to ~5 °C at 75 – 400 m water depth. Dissolution also reduces the test-weights of foraminifera shells [e.g. *Regenberg et al.*, 2014]. The lack of correlation between Mg/Ca ratios and shell weights along core PS75/059-2 (see *supplementary material*), is an indication that the variations in our Mg/Ca records are not shaped by dissolution. Moreover, the effects of dissolution on Mg/Ca signal is species-specific, that is, some species experience a greater reduction in their Mg/Ca content than other [*Dekens et al.*, 2002]. Previous studies have pointed out that the Mg/Ca signal in the species considered here is highly robust even in dissolution prone-conditions [see *Tapia et al.*, 2015 and references therein].

4.3.2 Foraminiferal $\delta^{18}\text{O}$ and Relative Salinity at Surface and Subsurface

Along the core, the $\delta^{18}\text{O}$ in *G. inflata* displays a clear glacial-interglacial change, ranging from 2.27‰ to 4.17‰ (Figure 2c). Overall, $\delta^{18}\text{O}$ of *G. inflata* are slightly lighter than those of *G. bulloides* (2.1‰ to 4.2‰). The averaged $\delta^{18}\text{O}$ values from *G. inflata* during interglacial stages are 2.39‰ (Holocene), 3.65‰ (MIS 3), 2.96‰ (MIS 5) and 2.86‰ (MIS 7) (Figure 2b). Heavier $\delta^{18}\text{O}$ values are observed during PGM (3.67‰) and LGM (3.75‰).

The calculated $\delta^{18}\text{O}_{\text{SW-IVC}}$ values, with more positive (negative) values indicating saltier (fresher) conditions, range from ~0.8‰ to ~2.8‰ at surface (*G. bulloides*) and from ~-0.4‰ to ~1.9‰ at subsurface (*G. inflata*). The $\delta^{18}\text{O}_{\text{SW-IVC}}$ offset relative to the Holocene ($\Delta\delta^{18}\text{O}_{\text{SW-IVC}}$) is ~-0.15‰ at surface and ~-0.36‰ at subsurface during the LGM (Figure 4c). Notably, during the PGM the $\Delta\delta^{18}\text{O}_{\text{SW-IVC}}$ values suggest a different vertical salinity structure in comparison to the LGM, with values of ~+0.17‰ at surface and ~-0.35‰ at subsurface (Figure 4.3c, d and Figure 4.4a). Subsurface conditions are fresher during glacials than during interglacials, and the $\Delta\delta^{18}\text{O}_{\text{SW-IVC}}$ suggests a similar subsurface freshening during the LGM and the PGM (Figure 4.4a).

4.3.3 Planktic Foraminiferal $\delta^{13}\text{C}$

Although foraminiferal $\delta^{13}\text{C}$ reflects the carbon isotopic composition of the DIC in seawater during calcification, it is not in isotopic equilibrium with seawater [*Ravelo and Hillaire-Marcel*, 2007]. The foraminiferal $\delta^{13}\text{C}$ values were corrected assuming a constant disequilibrium offset from the $\delta^{13}\text{C}$ of dissolved inorganic matter DIC of 1.5‰ for *G. bulloides* and 0.3‰ for *G. inflata* [*Schiraldi et al.*, 2014]. The corrected $\delta^{13}\text{C}_{G.inflata}$ range from ~-0.24 to ~1.3‰ (Figure 4.2d), heavier than those in *G. bulloides* (~-0.13 to ~-1.91‰). The deep-dwelling *G. inflata* shows excursions of low $\delta^{13}\text{C}$ values, known as Carbon Isotope Minimum Events (CIME) [*Spero and Lea*, 2002], at ~14ka, ~81ka and ~130ka, roughly coincident with

$\delta^{13}\text{C}_{G. \textit{bulloides}}$ (Figure 4.2d). The amplitude of change in $\delta^{13}\text{C}_{G. \textit{bulloides}}$ is larger than that in the $\delta^{13}\text{C}_{G. \textit{inflata}}$.

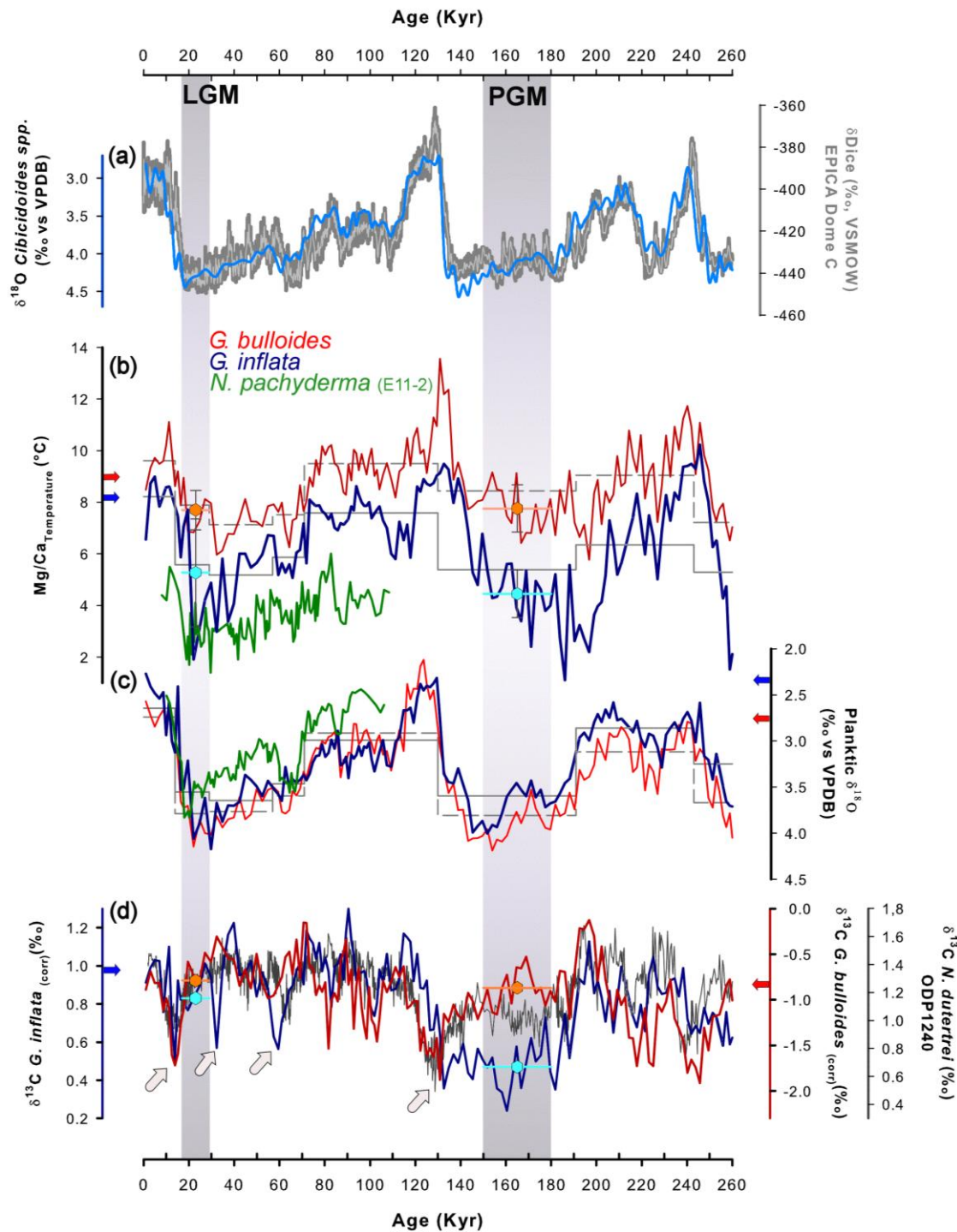


Figure 4.2 Foraminiferal proxy data of core PS75/059-2: (a) Benthic foraminiferal $\delta^{18}\text{O}$ record (blue) from core PS75/059-2 in comparison to the EPICA Dome C ice core Deuterium record (δD ; grey) displaying relative air temperature variations over East Antarctica (Antarctic Plateau) [Jouzel et al., 2007]. Records of planktic foraminifers *G. bulloides* (red) and *G. inflata* (blue): (b) Calculated Mg/Ca-temperatures, (c) $\delta^{18}\text{O}$ and (d) $\delta^{13}\text{C}$; $\delta^{13}\text{C}$ values were corrected according to Schiraldi et al. [2014]. For comparison Mg/Ca-temperatures and $\delta^{18}\text{O}$ values from *N. pachyderma* (green) at site E11-2 at 56°S are added [Mashiotta et al., 1999]. Shaded bars mark the Last Glacial Maximum (LGM, ~29–17 ka) and the Penultimate Last Glacial Maximum (PGM, ~180–150 ka). Dashed (*G. bulloides*) and continuous (*G. inflata*) grey lines denote averaged values per each isotopic stage; symbols denote

the averaged temperatures and $\delta^{13}\text{C}$ values during LGM and PGM for *G. bulloides* (orange) and *G. inflata* (light blue). Grey arrows denote $\delta^{13}\text{C}$ *G. inflata* minima. For comparison, the high resolution subsurface $\delta^{13}\text{C}$ record from the Equatorial Pacific [Pena et al., 2008] is provided (thin black line). The resemblance, timing and prominence of the CIMEs [Spero and Lea, 2002] suggest that the light $\delta^{13}\text{C}$ -signals in core PS75/059-2 represent large-scale water mass signatures. Coloured arrows on y-axes denote the averaged Holocene (0–8 ka) values for each species.

The $\delta^{13}\text{C}_{G.bulloides}$ suggest comparable values for Holocene (-0.8‰), LGM (-0.79‰) and PGM (-0.87‰) (Figure 4.2d). In contrast, the $\delta^{13}\text{C}_{G.inflata}$ is 0.83‰ during LGM and 0.47‰ during PGM; both values are lower than during the Holocene (0.99‰) (Figure 4.4b). The $\delta^{13}\text{C}$ difference between glacials at the subsurface is substantially larger than that at the sea surface (Figure 4.4b).

4.4. Discussion

4.4.1 Past Sea Surface Temperatures in the Central South Pacific

The glacial-interglacial $\text{SST}_{\text{Mg/Ca } G.bulloides}$ amplitude observed in core PS75/059-2 (~8 °C) is larger than that reported for core SO213-59-2 located further north in the subtropical South Pacific Gyre (SPG) at 45° S [-3 °C; Tapia et al., 2015]. Nonetheless, glacial-interglacial amplitudes of ~7 °C have been observed in other sectors of the South Pacific, for instance at site MD97-2120 in the SWP [45° S; Pahnke et al., 2003] and sites GeoB3327-5 (43° S) and PS75/034-2 (54° S) in the SEP [Ho et al., 2012]. Furthermore, the ~3 °C Holocene-LGM cooling suggested by our $\text{SubST}_{\text{Mg/Ca}}$ reconstruction (Figure 4.4a) is similar to the ~2 to ~4 °C of LGM-cooling previously reported for central South Pacific sites in the vicinity of the SAF between 115° and 120° W [Luz, 1977; Mashiotto et al., 1999; Loubere and Bennett, 2008].

Reconstructed temperature variations for site PS75/059-2, both in terms of the glacial-interglacial amplitude and the LGM cooling, are comparable to previously published temperature records from the central South Pacific derived from Mg/Ca at shallower sites [Mashiotto et al., 1999] i.e., core E11-2 (56° S 115° W, 3091 m water depth) and from independent proxies e.g., foraminifera census counting [RC12-225, E21-15, E11-1, E11-2; Luz 1977] or alkenones [PS75/034-2; Ho et al., 2012], supporting the assumption that our Mg/Ca-temperature reconstructions are not controlled by post-depositional overprint (e.g. dissolution).

Although our temperature reconstructions show similar trends than the Mg/Ca-derived sea surface temperatures based on *Neogloboquadrina pachyderma*(s) at site E11-2 [Mashiotto et al., 1999] (Figure 4.2b), the reconstructed absolute Mg/Ca-temperatures at site PS75/059-2 are warmer by ~3 °C. This difference may be explained by 1) the most southern position of the core E11-2, and 2) species-specific ecological preferences, in light of previous

findings suggesting that *N. pachyderma* tends to be associated to greater depths and the peak of *N. pachyderma* is seasonally displaced to the earliest part of the production season, therefore reflecting colder, late-winter/early-spring mixed waters [Ninnemann and Charles, 1997; Loubere and Bennett, 2008].

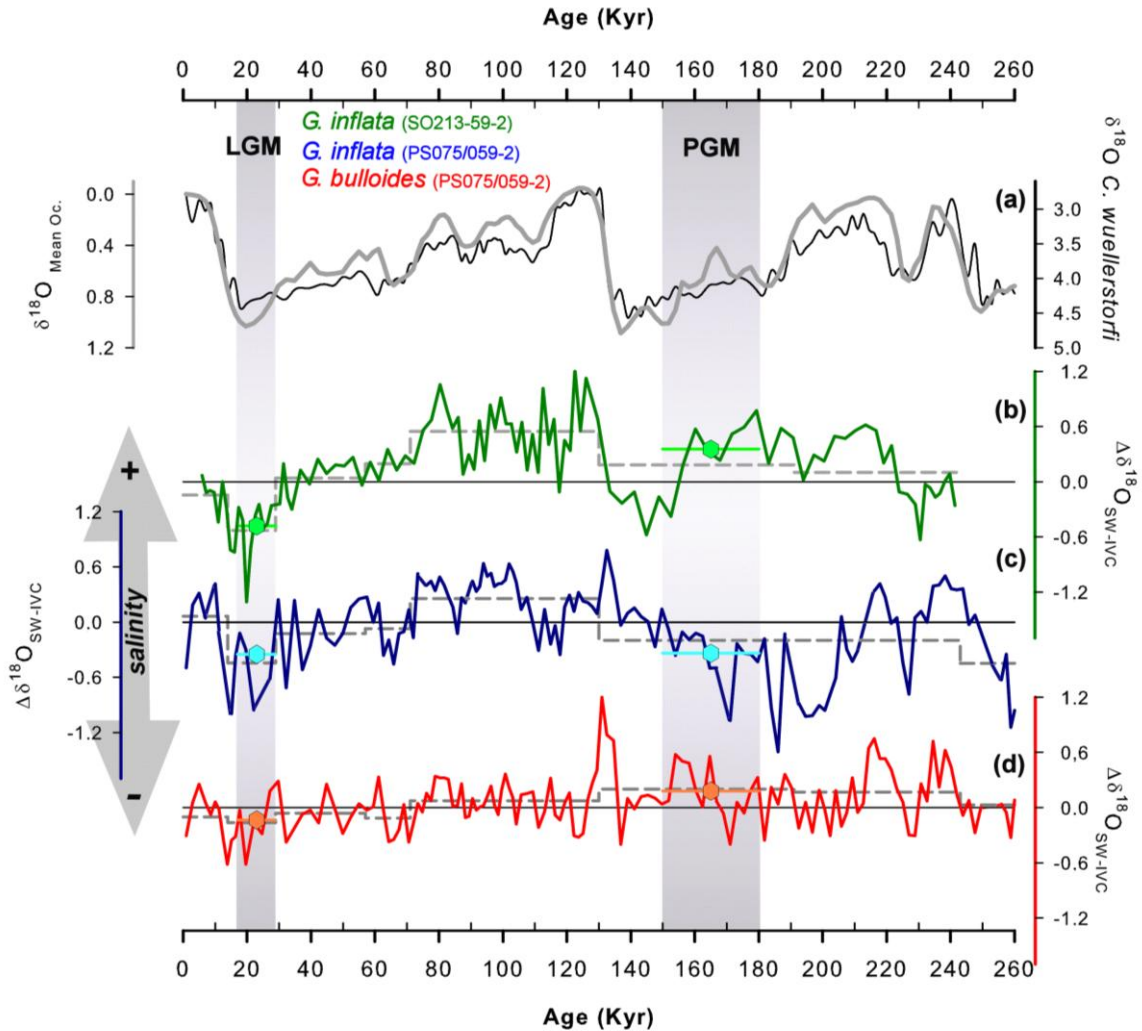


Figure 4.3 (a) Mean ocean $\delta^{18}\text{O}_{\text{SW}}$ (grey line) [Waelbroeck et al., 2002] in comparison to the benthic isotopic foraminiferal record at site PS75/059-2 (thin black line). Reconstructed local subsurface salinity anomaly ($\Delta\delta^{18}\text{O}_{\text{SW-IVC}}$) derived from *G. inflata* at the SPG (45° S) core site SO213-59-2 [Tapia et al., 2015] (b, green), and at the central south Pacific study site PS75/059-2 (54° S) (c, blue). In addition, the local surface $\Delta\delta^{18}\text{O}_{\text{SW-IVC}}$ record derived from *G. bulloides* (d, red) is shown. Shaded bars mark LGM (~29–17 ka) and PGM (~180–150 ka). Continuous black lines denote species-specific mean Holocene $\Delta\delta^{18}\text{O}_{\text{SW-IVC}}$ values for cores PS75/059-2 (< 8ka) and SO213-59-2 (< 10ka), dashed lines denoted averaged values per isotopic stage, averaged values during LGM and PGM are denoted by coloured symbols.

4.4.2 Vertical T and S Structure: Frontal Migration or Wind Intensity?

In general, our reconstructed temperature and salinity records suggest fresher/cooler glacial and more saline/warmer interglacial conditions (Figures 4.2 and 4.3). In the South Pacific, changes in SST and salinity at glacial-interglacial time-scales have been recurrently

related either to northward displacements of the oceanic frontal system [Ho *et al.*, 2012 and references therein]. The spatial variability in the displacement of the oceanic frontal system (SAF and PF) in the South Pacific at glacial-interglacial timescales, however, is regionally different. Studies focused on the SAF infer changes ranging from no displacement in the SWP (possibly forced by bottom topography) to a large northward progression in the SEP ($>9^\circ$ in latitude) [Kohfeld *et al.*, 2013]. At site PS75/059-2, in spite of its proximity to the modern SAF (Figure 4.1), the average reconstructed glacial $SST_{Mg/Ca}$ *G.bulloides* ($\sim 8^\circ\text{C}$) and $SubST_{Mg/Ca}$ *G.inflata* ($\sim 5^\circ\text{C}$) (see section 4.3.1 and Figure 4.2b) suggest higher temperatures along the water column than the isotherm typically associated with the SAF ($\sim 4^\circ\text{C}$) [Orsi *et al.*, 1995]. Further, contrasting patterns of change in physical properties during glacials (i.e. LGM-Holocene and PGM-Holocene; sections 4.3.1 and 4.3.2) at the sea surface and at depths argue against glacial-northward SAF migration as the main control of the upper ocean properties at the study site, as frontal displacement would affect the entire upper water column [see Tapia *et al.*, 2015]. These observations suggest that the study site remains northward of the SAF even during glacials. Our interpretation of a mean glacial-SAF located south of our study-site is in agreement with siliceous microfossils-based reconstructions that proposed a minor glacial northward displacement of the PF ($< 4^\circ$) during the LGM in the central south Pacific [Gersonde *et al.*, 2005; Benz *et al.*, submitted]. A latitudinally stationary oceanic frontal system is plausibly due to the presence of the East Pacific Rise in the region. Recent studies have emphasized the importance of bottom topography controlling the locations of oceanic fronts [e.g. Graham *et al.*, 2012]. Taken together, these observations reinforce the notion that at the central South Pacific in the vicinity of the EPR the Subantarctic Zone (SAZ) during glacials was in a similar position than today [Matsumoto *et al.*, 2001; Loubere and Bennett, 2008].

A main driver of temperature and salinity patterns at the study site, in addition, is wind intensity. Strong winds promote deeper mixed layers in the SO, which characterize the formation area of SAMW-AAIW [McCartney, 1977; Hartin *et al.*, 2011]. A strong relationship between the strength of the South Westerly Winds (SWW) and the formation of SOIW has been suggested by numerical experiments [e.g. Ribbe, 2001] and field observations [e.g. Ayers and Strutton, 2013]. Although a general consensus on glacial changes of the SWW is still lacking, intensified glacial SWW has been invoked as one of the factors controlling the dust fluxes in the South Pacific [Lamy *et al.*, 2014]. Consequently, several proxy reconstructions have invoked stronger glacial winds to explain enhanced AAIW presence at lower latitudes during glacial periods [Muratli *et al.*, 2010; Martínez-Méndez *et al.*, 2013].

Overall, our subsurface reconstruction is in agreement with the hypothesis of a stronger AAIW signal during glacials (Figure 4.2 and Figure 4.3). This is further supported by

the vertical thermal gradient as deduced from the difference between $\text{SST}_{\text{Mg/Ca } G. \textit{bulloides}}$ and $\text{SubSST}_{\text{Mg/Ca } G. \textit{inflata}}$. The vertical thermal gradient is substantially larger during glacial stages, namely ~ 3.3 °C during PGM and ~ 2.4 °C LGM, in comparison to the Holocene (~ 1.2 °C). As the $\text{SST}_{\text{Mg/Ca } G. \textit{bulloides}}$ is similar during both glacial time windows (see Section 4.3 and Figure 4.4a), vertical thermal gradient is mostly driven by subsurface temperatures. Also, the gradient of the reconstructed $\delta^{18}\text{O}_{\text{SW}}$ at surface and subsurface ($\Delta\delta^{18}\text{O}_{\text{SW } G. \textit{bulloides}-G. \textit{inflata}}$), i.e. a qualitative indicator of water mixing [Rohling and Cooke, 1999], is larger during PGM ($\sim 1.09\text{‰}$) and LGM ($\sim 0.8\text{‰}$) than during the Holocene (0.6‰). Larger vertical gradients in both vertical thermal gradient and $\Delta\delta^{18}\text{O}_{\text{SW } G. \textit{bulloides}-G. \textit{inflata}}$ imply shallower mixed layer depth (MLD) during glacials. As the MLD shallows, winds are more effective in entraining SO intermediate waters from just below the base of the mixed layer [Carranza and Gille, 2015], promoting the northward injection of fresher, southern sourced water (namely AAIW) that is being subducted at the SAF. This is in agreement with our reconstructed subsurface salinity that shows fresher-than-Holocene subsurface conditions during glacials (Figure 4.3c and Figure 4.4).

4.4.3 SOIWs Presence and Transport in the South Pacific During Glacials

Subsurface waters that are cooler and fresher relative to the Holocene conditions at site PS75/059-2 suggest an enhanced presence of AAIW during LGM (Figure 4.4). This is consistent with reconstructions from diverse oceanographic settings in the SEP, along the Chilean slope at sites ODP1233 and GeoB15016 [Muratli et al., 2010; Martínez-Méndez et al., 2013], and at site SO213-59-2 in the SPG [Tapia et al., 2015].

In contrast, subsurface conditions during the PGM seem to be more heterogenous in space, judging from contradictory findings in the literature. In the subtropical Pacific off Chile (27°S), the AAIW signal during the PGM is on average weaker than during the LGM, but still stronger than during the Holocene [GeoB15016; Martínez-Méndez et al., 2013]. Instead in the SPG (north of 45°S), a homogenous upper water column (from surface to deep-thermocline) occurs during the PGM, with saltier subsurface conditions relative to the Holocene, thereby suggesting a weaker SOIW signal [Tapia et al., 2015]. At site PS75/059-2 at 54°S , the PGM SOIW signal is weaker at the sea surface but stronger at depths relative to the Holocene condition; the PGM conditions at depth are comparable to the LGM conditions with similar temperatures and salinities (Figure 4.4a).

It has been suggested that the SOIWs might have transferred the climatic signal from high southern to low latitudes through “oceanic tunneling” [Pena et al., 2008; 2013]. If true, a vigorous SAMW-AAIW transport across latitudes will result in comparable subsurface physical properties between low and high latitudes. The subsurface latitudinal thermal

gradient, calculated from $\text{SubST}_{\text{Mg/Ca } G.\text{inflata}}$, between core sites SO213-59-2 (45° S) and PS75/059-2 (54° S), amounts to $\sim 6^\circ\text{C}$ during the PGM, which is twice as strong as those during the LGM and the Holocene (0–10ka) ($\sim 3^\circ\text{C}$) (Figure 4.5). The $\delta^{18}\text{O}_{\text{SW-IVC}}$, which behaves as a conservative tracer of transport (advection) and mixing of water masses for the subsurface ocean [Rohling and Cooke, 1999], also suggests a larger latitudinal gradient at subsurface depths during the PGM (1.26‰) than during the LGM (0.49‰) and the Holocene (0–10ka) (0.48‰) (Figure 4.5).

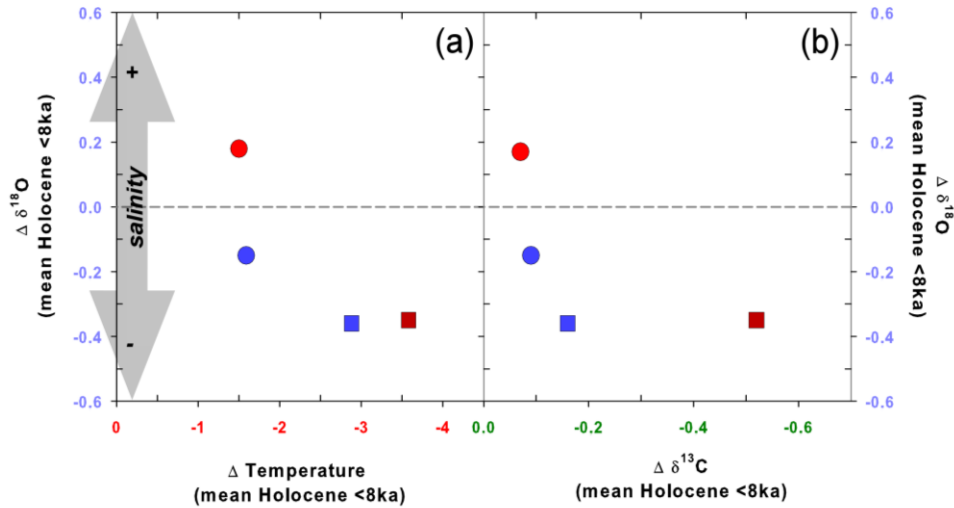


Figure 4.4 Surface (circle) and subsurface (square) differences in $\text{Mg/Ca}_{\text{Temperature}}$ (a) and $\delta^{13}\text{C}$ (b) relative to the Holocene (0–8 ka) versus salinity ($\Delta\delta^{18}\text{O}_{\text{SW-IVC}}$) at the core site PS75/059-2 during the LGM (blue) and PGM (red). The LGM and PGM time slices are characterized by colder- and fresher-than-Holocene subsurface waters. At surface LGM and PGM show comparable cooling and contrasting salinities. The $\Delta\delta^{13}\text{C}$ data during the LGM and the PGM are characterized by comparable values at surface and large discrepancy at subsurface.

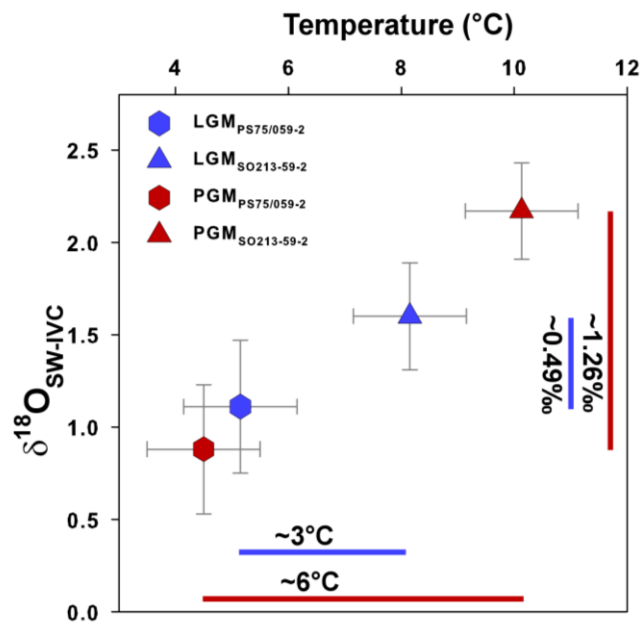


Figure 4.5 Subsurface temperatures and $\delta^{18}\text{O}_{\text{SW-IVC}}$ at cores SO213-59-2 (45°S; triangle) and PS75/059-2 (54°S;

hexagon) during the PGM (dark red) and the LGM (blue).

These results imply a similar subsurface ocean hydrography in the SO during both the Holocene and the LGM with similar advection and/or repartition routes of SOIW's into the SPG. Our interpretation is in accordance to the study of Matsumoto et al. [2001], which is based on evidence from foraminiferal $\delta^{18}\text{O}$. In contrast, the larger latitudinal gradients ($\delta^{18}\text{O}_{\text{sw}}$ and Mg/Ca-temperature) at depths during the PGM suggest a considerably reduced transport across latitudes in the central south Pacific. This is unlikely to be due to a cease in the production of SOIW's during the PGM, as at the southern site PS75/059-2 (54° S) SOIW is similarly present during both glacials as indicated by the reconstructed subsurface temperature and salinity (Section 3.2; Figure 4.4a). Rather, the strengthened gradients are probably caused by changes in the advection depth of the SOIW's into the SPG, as suggested by a deeper mixed layer in the SPG site SO213-59-2 during the PGM (see Figure 3.6).

4.4.4 Glacial Changes in Upwelling Strength Indicated by $\delta^{13}\text{C}$ Variability

At our study site, we observe a much larger $\delta^{13}\text{C}$ difference between LGM and PGM at the subsurface than at the sea surface (Section 4.3.3 and Figure 4.4b), with $\delta^{13}\text{C}$ being (0.36‰) lighter during PGM. The glacial $\delta^{13}\text{C}$ difference at the subsurface is unlikely to be driven by changes in productivity in the upper ocean because $\delta^{13}\text{C}_{G.bulloides}$ values are rather similar during the LGM (-0.72‰) and the PGM (-0.87‰). Air-sea exchange, which is a temperature-dependent process, can also increase (decrease) the $\delta^{13}\text{C}$ values of colder (warmer) water, but it is an unlikely cause for the subsurface glacial $\delta^{13}\text{C}$ difference given that both glacials are comparable in temperature, ~4.5 °C (LGM) and ~5.2 °C (PGM) (Section 4.3.2; Figure 4.2b and Figure 4.4a). Also ice coverage may affect the $\delta^{13}\text{C}$ signal by restricting air-sea equilibration but ice coverage differences between glacial time windows (LGM vs PGM) are considered negligible. Alternatively, the $\delta^{13}\text{C}$ of a water mass in the interior ocean might change due to the admixture of waters from greater depths depleted in $\delta^{13}\text{C}$ as a result of the preferential incorporation of light carbon isotopes released by the remineralization of organic matter with depth. Hence, lower subsurface $\delta^{13}\text{C}$ values at site PS75/059-2 during the PGM (on average 0.47‰) than those during LGM (on average 0.83‰) can be attributed to the presence of deeper water with low $\delta^{13}\text{C}$ values during the PGM. Changes in the source of upwelled $\delta^{13}\text{C}$ -depleted water between PGM and LGM are possible if the strength of the Ekman pumping varies over time.

Stronger Ekman pumping during the PGM is further supported by the comparison of

$\delta^{13}\text{C}$ between the glacial mean and the respective Carbon Isotope Minimum Events (CIME, [Figure 4.2d](#)). These prominent negative $\delta^{13}\text{C}$ excursions during the onset of deglaciations reflect renewed upwelling in the Southern Ocean, which brings “old”, low $\delta^{13}\text{C}$ CDW to the surface south of the PF. These waters were supposedly advected from the SO to the different ocean basins by SOIWs [*Spero and Lea, 2002; Bostock et al., 2004; Pena et al., 2008; 2013*]. We observe a smaller $\delta^{13}\text{C}$ difference (~23%) between the PGM (on average 0.47‰) and its respective CIME (0.36‰) than the $\delta^{13}\text{C}$ difference (~40%) between the LGM (on average 0.83‰) and its respective CIME (0.5‰) ([Figure 4.2d](#)). According our interpretation, comparable $\delta^{13}\text{C}$ values between PGM and both CIMEs at site PS75/059-2 can be taken as evidence for the presence of the same deep water mass as that causing the CIMEs, namely CDW. Our notion is supported by the synchrony to CIMEs reported from the equatorial Pacific’s thermocline i.e., site ODP2140 [*Pena et al., 2008*] ([Figure 4.2d](#)) suggesting that the light $\delta^{13}\text{C}$ -signals in core PS75/059-2 represent a true water mass signals.

4.4.5 Southern Annular Mode–like during LGM and PGM?

Taken together, our results suggest dissimilar subsurface conditions during PGM and LGM with more $\delta^{13}\text{C}$ depleted subsurface waters ([Section 4.4.4, Figure 4.4b](#)), a weakened SOIW signal at the sea surface ([Section 4.4.3, Figure 4.4a](#)), and steeper subsurface latitudinal gradients in temperature and salinity during the PGM ([Section 4.3, Figure 4.5](#)). The different glacial oceanographic patterns are most likely caused by a change in the intensity of the SWW, as we rule out a large-scale latitudinal migration of the SO frontal system at our core location during the PGM ([section 4.4.2](#); see also [section 3.4.3](#)). Considering that (1) the Southern Annular Mode (SAM) is the main climatic mode controlling the winds in the Southern Hemisphere [*Thompson et al., 2011*], and (2) a close coupling between SAM and the physical properties (temperature and salinity) and nutrients contents of the SOIWs in the Pacific Basin (160° E to 80° W) exist [*Ayers and Strutton, 2013*], SAM-like processes may be used as an analogy to illustrate the oceanographic response at our study site to changes in wind intensity. We are aware, that the SAM processes are on a much shorter time-scale unresolvable by our proxy records. Nonetheless, at present, the SAM alters 1) the strength of northward Ekman Flow, 2) the upwelling along the Antarctic Continent, 3) the vertical tilt of the surface of density, and 4) the strength of the Antarctic Circumpolar Current (ACC) that results in changes in MLD and oceanic heat transport [*Lenton and Matear, 2007; Thompson et al., 2011*].

In a glacial scenario wherein an intensified SWW is located at similar latitude than today, it is conceivable that SAM-like changes in SWW intensity drive the glacial differences

of subsurface $\delta^{13}\text{C}$, temperature and salinity conditions in our study area. Wind-conditions akin to the positive phase of the SAM result in positive wind stress curl anomalies north of the maximum wind stress ($\sim 55^\circ$ S). Negative wind stress curl anomalies south of the maximum wind stress, instead, lead to surface divergences and convergences that strengthens both the upwelling south of the maximum wind stress and convergence to the north of maximum wind stress (e.g. downwelling at $\sim 45^\circ$ S) [Lenton and Matear, 2007; Thompson et al., 2011]. At the same time, positive SAM also causes greater Ekman transport throughout the region of the SWW (Figure 4.6). Amplified Ekman pumping south of the SAF increases the contribution of deeper, low $\delta^{13}\text{C}$ CDW to intermediate waters, thereby altering the “preformed” characteristic of the AAIW. Further, stronger pumping results in an enhanced northward Ekman transport, which may increase the transport of AAIW to site PS75/059-2 (54° S), resulting in $\delta^{13}\text{C}$ -depleted subsurface waters during PGM. To the north of maximum wind stress, positive wind stress curl anomalies strengthen downwelling, which then leads to the deepening of the MLD. These processes promote the incorporation of salty/warm northern waters in the upper ocean; a scenario in agreement with previously reconstructed vertical thermal and $\delta^{18}\text{O}_{\text{SW}}$ gradients at 45° S (SO213-59-2) during MIS 6 [Tapia et al., 2015]. Positive wind stress curl anomalies also enhance the southward transport, bringing salty northern waters to our southern site at 54° S, as suggested by the higher salinity reconstructed from the mixed layer dwelling *G. bulloides* during the PGM (Figure 4.4a). On the other hand, opposite processes during the LGM, i.e. weaker upwelling and northward Ekman transport, would result in less contribution of low $\delta^{13}\text{C}$ waters to the newly formed AAIW, as suggested by $\delta^{13}\text{C}_{G.inflata}$ at site PS75/059-2. Weaker positive wind stress curl anomalies to the north of maximum wind stress would reduce the downwelling intensity, leading to a shallower MLD, as is suggested by the vertical gradients (thermal and $\delta^{18}\text{O}_{\text{SW}}$) at 45° S (SO213-59-2) during the LGM [Tapia et al., 2015].

Ultimately, the foregoing diverging scenarios between LGM and PGM modify the tilt of the density surface associated with the SOIWs, which may explain the subsurface latitudinal gradients ($\delta^{18}\text{O}_{\text{SW}}$ and temperature) between 54° S and 45° S (Figure 4.5). An increase in the tilt of the density surfaces implies a deepening of the injection depth of the SOIWs, therefore reducing their influence on the thermocline in the SPG (Figure 4.6). Such scenario is reflected in our proxy reconstructions: a larger subsurface latitudinal gradient exists between 54° S and 45° S during PGM, probably as a result of a weakened SOIW signal at the subsurface of the SPG (Figure 4.5).

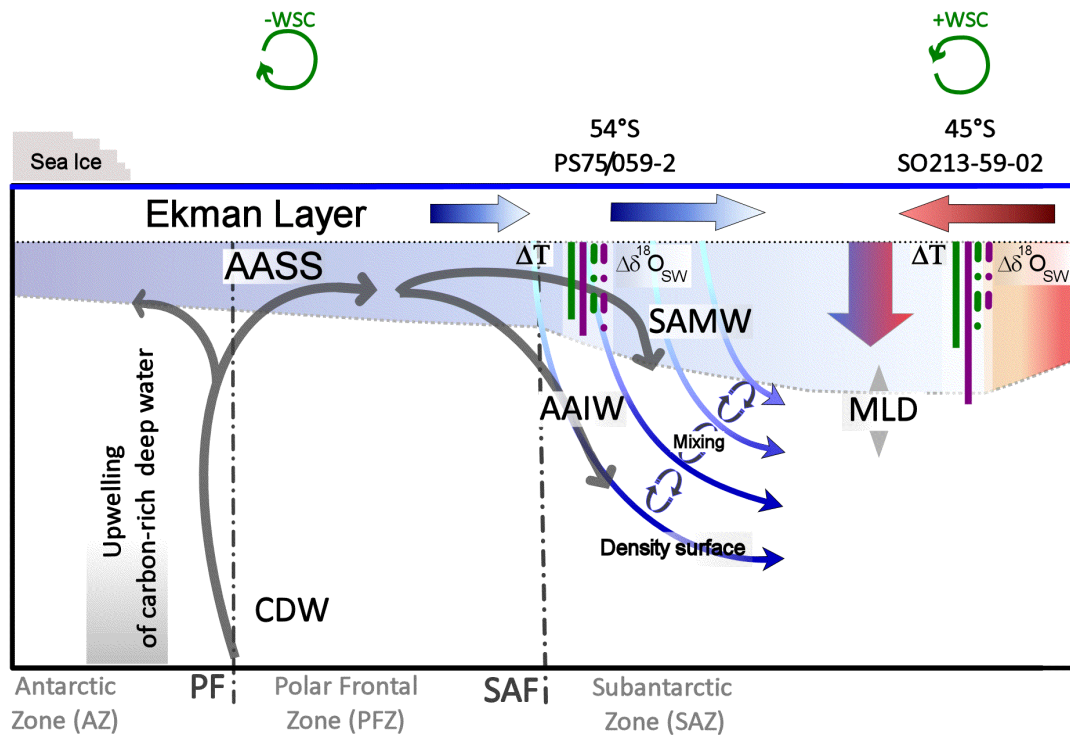


Figure 4.6 Schematic diagram showing the response of the ocean to the high index-polarity of the Southern Annular Mode [Thompson et al., 2011; Ayers and Strutton, 2013; Tapia et al., 2015]. The past change in mixed-layer depth (MLD) is inferred from the vertical thermal gradient (ΔT , continuous lines) between Mg/Ca-temperatures from *G. bulloides* ($SST_{Mg/Ca, G. bulloides}$) and *G. inflata* ($SubST_{Mg/Ca, G. inflata}$) and inferred surface- and subsurface- $\delta^{18}O_{SW}$ ($\Delta\delta^{18}O_{SW}$, dashed lines) (see text for details), differentiated for the LGM (green) and the PGM (pink) at 45° S and 54° S, respectively. Arrows indicate inferred horizontal and vertical water mass migration. Colour coding (red to blue) corresponds to either increased or decreased temperatures/heat content.

4.5 Summary

In this study we analyzed Mg/Ca, $\delta^{18}O$ and $\delta^{13}C$ on deep and shallow dwelling foraminifera to infer past changes in the water column structure at site PS75/059-2 in the CSP (54° S). Our Mg/Ca-derived ocean temperature records suggest a LGM-Holocene subsurface cooling of ~ 3 °C; this value is within the range of previously reported surface LGM-cooling (~ 4 °C) for the area. Freshening at the subsurface during glacials suggests a stronger influence of cold-fresh southern sourced waters (namely AAIW). The reconstructed temperature and $\delta^{18}O_{SW-IVC}$ (approximating salinities) suggest no substantial northward migration of the SAF during glacial stages. This argues against frontal displacement as the main mechanism controlling the water column properties at our study site in the CSP (54°S). Instead, an intensification of SWW is a more likely cause.

We further find substantial differences in the subsurface $\delta^{13}C$ signature of the AAIW between the PGM and the LGM. In the absence of large changes in productivity and air-sea exchange, the lower $\delta^{13}C$ values during the PGM (relative to the LGM) are likely due to the

deepening of the upwelling depth, resulting in a larger contribution of deep low $\delta^{13}\text{C}$ waters. This notion is further supported by the similarity in $\delta^{13}\text{C}$ values between the PGM and the CIMEs; the latter are caused by the reallocation of “old” low $\delta^{13}\text{C}$ deep waters from the ocean interior toward the surface during glacial terminations.

The larger latitudinal gradient at subsurface between the CSP (54° S) and the SPG (45° S) during the PGM suggest a reduced influence of SOIWs at thermocline depths in the SPG. In addition, glacial vertical gradients at these localities suggest glacial differences in the tilt of the surface densities associated with the SOIWs. Together, these observations point to glacial differences in the convection depth of AAIW injected into the SPG.

Dissimilarity in the upper ocean between the LGM and the PGM, in terms of upwelling depth, Ekman transport, downwelling, and surface densities, points to processes analogous to the effects, which the SAM has on the modern the ocean. SAM-like alterations of the southern hemisphere wind pattern are therefore a plausible explanation for glacial differences in the subsurface central Pacific, without invoking migrations of the oceanic frontal system.

4.6 Acknowledgments

This study was funded by the Federal Ministry of Education and Research (BMBF, Germany) through grant No. 03G0213B. Technical support and laboratory assistance from N. Gehre, L. Haxhijaj, and K. Werner (GEOMAR) are highly appreciated. Data presented in this study are available in the Pangaea database (www.pangaea.de).

4.7 References

- Anderson, R. F., S. Ali, L. I. Bradtmiller, S. H. H. Nielsen, M. Q. Fleisher, B. E. Anderson, and L. H. Burckle (2009), Wind-driven upwelling in the Southern Ocean and the deglacial rise in atmospheric CO_2 , *Science*, 323(5920), 1443–1448.
- Ayers, J. M., and P. G. Strutton (2013), Nutrient variability in Subantarctic Mode Waters forced by the Southern Annular Mode and ENSO, *Geophys. Res. Lett.*, 40, doi:10.1002/grl.50638.
- Barker, S., M. Greaves, and H. Elderfield (2003), A study of cleaning procedures used for foraminiferal Mg/Ca paleothermometry, *Geochem. Geophys. Geosyst.*, 4, doi:10.1029/2003GC000559.
- Bostock, H. C., B. N. Opdyke, M. K. Gagan, and L. K. Fifield (2004), Carbon isotope evidence for changes in Antarctic Intermediate Water circulation and ocean ventilation in the southwest Pacific during the last deglaciation, *Paleoceanography*, 19, PA4013, doi:10.1029/2004PA001047.
- Bostock, H. C., P. J. Sutton, M. Williams, and B. N. Opdyke (2013), Reviewing the circulation and mixing of Antarctic Intermediate Water in the South Pacific using evidence from

- geochemical tracers and Argo float trajectories, *Deep-Sea Res. Part I*, 73, 84–98, doi:10.1016/j.dsr.2012.11.007.
- Carranza, M. M., and S. T. Gille (2015), Southern Ocean wind-driven entrainment enhances satellite chlorophyll-a through the summer, *J. Geophys. Res. Oceans*, n/a–n/a, doi:10.1002/2014JC010203.
- Dekens, P. S., D. W. Lea, D. K. Pak, and H. J. Spero (2002), Core top calibration of Mg/Ca in tropical foraminifera: Refining paleotemperature estimation, *Geochem. Geophys. Geosyst.*, 3(4), doi:10.1029/2001GC000200.
- Elderfield, H., and G. Ganssen (2000), Past temperature and $\delta^{18}\text{O}$ of surface ocean waters inferred from foraminiferal Mg/Ca ratios, *Nature*, 405, 442–445, doi:10.1038/35013033.
- Gersonde, R., X. Crosta, A. Abelmann, and L. Armand (2005), Sea-surface temperature and sea ice distribution of the Southern Ocean at the EPILOG Last Glacial Maximum—a circum-Antarctic view based on siliceous microfossil records, *Quat. Sci. Rev.*, 24(7), 869–896, doi:10.1016/j.quascirev.2004.07.015.
- Graham, R. M., A. M. de Boer, K. J. Heywood, M. R. Chapman, and D. P. Stevens (2012), Southern Ocean fronts: Controlled by wind or topography? *J. Geophys. Res.*, 117, C08018, doi:10.1029/2012JC007887.
- Groeneveld, J., and C. M. Chiessi (2011), Mg/Ca of *Globorotalia inflata* as a recorder of permanent thermocline temperatures in the South Atlantic, *Paleoceanography*, 26(2), doi:10.1029/2010PA001940.
- Hartin, C. A., R. Fine, B. M. Sloyan, L. D. Talley, T. K. Chereskin, and J. Happell (2011), Formation rates of Subantarctic mode water and Antarctic intermediate water within the South Pacific, *Deep-Sea Res. Part I*, 58, 524–534, doi:10.1016/j.dsr.2011.02.010.
- Ho, S. L., G. Mollenhauer, F. Lamy, A. Martínez-García, M. Mohtadi, R. Gersonde, D. Hebbeln, S. Nuñez-Ricardo, A. Rosell-Melé, and R. Tiedemann (2012), Sea surface temperature variability in the Pacific sector of the Southern Ocean over the past 700 kyr, *Paleoceanography*, 27(4), PA4202, doi:10.1029/2012PA002317.
- Holte, J. W., L. D. Talley, T. K. Chereskin, and B. M. Sloyan (2013), Subantarctic mode water in the southeast Pacific: Effect of exchange across the Subantarctic Front, *J. Geophys. Res. Oceans*, 118(4), 2052–2066, doi:10.1002/jgrc.20144.
- Jouzel, J. et al. (2007), Orbital and millennial Antarctic climate variability over the past 800,000 years, *Science*, doi:10.1126/science.1141038.
- King, A. L., and W. R. Howard (2003), Planktonic foraminiferal flux seasonality in Subantarctic sediment traps: a test for paleoclimate reconstructions, *Paleoceanography*, 18(1), 1019, doi:10.1029/2002PA000839.
- Kohfeld, K. E., R. M. Graham, A. M. de Boer, L. C. Sime, E. W. Wolff, C. Le Quéré, and L. Bopp (2013), Southern Hemisphere westerly wind changes during the Last Glacial Maximum: paleo-data synthesis, *Quat. Sci. Rev.*, 68, 76–95, doi:10.1016/j.quascirev.2013.01.017.
- Lamy, F., R. Gersonde, G. Winckler, O. Esper, A. Jaeschke, G. Kuhn, J. Ullermann, A. Martínez-García, F. Lambert, and R. Kilian (2014), Increased dust deposition in the

- Pacific Southern Ocean during glacial periods, *Science*, 343(6169), 403–407.
- LeGrande, A. N., and G. A. Schmidt (2006), Global gridded data set of the oxygen isotopic composition in seawater, *Geophys. Res. Lett.*, 33(12), L12604, doi:10.1029/2006GL026011.
- Lenton, A., and R. J. Matear (2007), Role of the Southern Annular Mode (SAM) in Southern Ocean CO₂ uptake, *Global Biogeochem. Cycles*, 21(2), doi:10.1029/2006GB002714.
- Lisiecki, L. E., and M. E. Raymo (2005), A Pliocene-Pleistocene stack of 57 globally distributed benthic $\delta^{18}\text{O}$ records, *Paleoceanography*, 20(1), doi:10.1029/2004PA001071.
- Lisiecki, L. E., and P. A. Lisiecki (2002), Application of dynamic programming to the correlation of paleoclimate records, *Paleoceanography*, 17(4), 1–1–1–12, doi:10.1029/2001PA000733.
- Loubere, P., and S. Bennett (2008), Southern Ocean biogeochemical impact on the tropical ocean: Stable isotope records from the Pacific for the past 25,000 years, *Global and Planetary Change*, 63(4), 333–340, doi:10.1016/j.gloplacha.2008.08.001.
- Luz, B. (1977), Late Pleistocene paleoclimates of the South Pacific based on statistical analysis of planktonic foraminifers, *Palaeogeogr. Palaeoclimatol. Palaeoecol.*, 22(1), 61–78.
- Lynch-Stieglitz, J. (2003), Tracers of Past Ocean Circulation, in *Treatise on Geochemistry*, vol. 6, edited by H. D. Holland and K. K. Turekian, pp. 433–451, Elsevier, Oxford.
- Martínez-Méndez, G., D. Hebbeln, M. Mohtadi, F. Lamy, R. DePol-Holz, D. Reyes-Macaya, and T. Freudenthal (2013), Changes in the advection of Antarctic Intermediate Water to the northern Chilean coast during the last 970 kyr, *Paleoceanography*, 28, doi:10.1002/palo.20047.
- Mashiotta, T. A., D. W. Lea, and H. J. Spero (1999), Glacial–interglacial changes in Subantarctic sea surface temperature and $\delta^{18}\text{O}$ -water using foraminiferal Mg, *Earth Plan. Sci. Lett.*, 170, 417–432.
- Matsumoto, K., J. Lynch-Stieglitz, and R. F. Anderson (2001), Similar glacial and Holocene Southern Ocean hydrography, *Paleoceanography*, 16(5), 445–454.
- McCartney, M. S. (1977), Subantarctic Mode Water, in *A Voyage of Discovery, George Deacon 70th Anniversary Volume*, edited by M. Angel, pp. 103–119, Pergamon, New York.
- Mekik, F., R. François, and M. Soon (2007), A novel approach to dissolution correction of Mg/Ca–based paleothermometry in the tropical Pacific, *Paleoceanography*, 22(3), doi:10.1029/2007PA001504.
- Muratli, J. M., Z. Chase, A. C. Mix, and J. McManus (2010), Increased glacial-age ventilation of the Chilean margin by Antarctic Intermediate Water, *Nat. Geosci.*, 3, 23–26, doi:10.1038/ngeo715.
- Ninnemann, U. S., and C. D. Charles (1997), Regional differences in Quaternary Subantarctic nutrient cycling: Link to intermediate and deep water ventilation, *Paleoceanography*, 12(4), 560–567.

- Orsi, A. H., T. Whitworth, and W. D. Nowlin (1995), On the meridional extent and fronts of the Antarctic Circumpolar Current, *Deep-Sea Res. Part I*, 42(5), 641–673.
- Pahnke, K., R. Zahn, H. Elderfield, and M. Schulz (2003), 340,000-year centennial-scale marine record of Southern Hemisphere climatic oscillation, *Science*, 301(5635), 948–952, doi:10.1126/science.1084451.
- Pena, L. D., I. Cacho, P. Ferretti, and M. A. Hall (2008), El Niño–Southern Oscillation–like variability during glacial terminations and interlatitudinal teleconnections, *Paleoceanography*, 23, PA3101, doi:10.1029/2008PA001620.
- Pena, L. D., S. L. Goldstein, S. R. Hemming, K. M. Jones, E. Calvo, C. Pelejero, and I. Cacho (2013), Rapid changes in meridional advection of Southern Ocean intermediate waters to the tropical Pacific during the last 30 kyr, *Earth Plan. Sci. Lett.*, 368, 20–32, doi:10.1016/j.epsl.2013.02.028.
- Ravelo, A. C., and C. Hillaire-Marcel (2007), The Use of Oxygen and Carbon Isotopes of Foraminifera in Paleoceanography, in *Proxies in Late Cenozoic Paleoceanography*, vol. 1 of Developments in Marine Geology, edited by C. Hillaire-Marcel and A. De Vernal, pp. 735–764, Elsevier.
- Regenberg, M., A. Regenberg, D. Garbe-Schönberg, and D. W. Lea (2014), Global dissolution effects on planktonic foraminiferal Mg/Ca ratios controlled by the calcite-saturation state of bottom waters, *Paleoceanography*, doi:10.1002/2013PA002492.
- Ribbe, J. (2001), Intermediate water mass production controlled by southern hemisphere winds, *Geophys. Res. Lett.*, 28(3), 535–538, doi:10.1029/2000GL012242.
- Rohling, E. J., and S. Cooke (1999), Stable oxygen and carbon isotopes in foraminiferal carbonate shells, in *Modern Foraminifera*, edited by B. K. Sen Gupta, pp. 239–258, Kluwer Academic Publishers, Dordrecht.
- Ronge, T. A., S. Steph, R. Tiedemann, M. Prange, U. Merkel, D. Nürnberg, and G. Kuhn (2015), Pushing the boundaries: Glacial/Interglacial variability of intermediate- and deep-waters in the southwest Pacific over the last 350,000 years, *Paleoceanography*, 30, 23–38, doi:10.1002/2014PA002727.
- Schiraldi, B., E. L. Sikes, A. C. Elmore, M. S. Cook, and K. A. Rose (2014), The Southwest Pacific subtropics responds to the last deglacial warming with changes in shallow water sources, *Paleoceanography*, doi:10.1002/2013PA002584.
- Schneider, W., and L. Bravo (2006), Argo profiling floats document Subantarctic Mode Water formation west of Drake Passage, *Geophys. Res. Lett.*, 33, doi:10.1029/2006GL026463.
- Shackleton, N. J. (1974), Attainment of isotopic equilibrium between ocean water and the benthonic foraminifera genus *Uvigerina*: isotopic changes in the ocean during the last glacial, *Cent. Nat. Rech. Sci. Colloq. Int.* (219), 203–209.
- Spero, H. J., and D. W. Lea (2002), The cause of carbon isotope minimum events on glacial terminations, *Science*, 296(5567), 522–525.
- Tapia, R., D. Nürnberg, T. Ronge, and R. Tiedemann (2015), Disparities in glacial advection of Southern Ocean Intermediate Water to the South Pacific Gyre, *Earth Plan. Sci. Lett.*, 410, 152–164, doi:10.1016/j.epsl.2014.11.031.

- Thompson, D. W. J., S. Solomon, P. J. Kushner, M. H. England, K. M. Grise, and D. J. Karoly (2011), Signatures of the Antarctic ozone hole in Southern Hemisphere surface climate change, *Nat. Geosci.*, *4*(11), 741–749, doi:10.1038/ngeo1296.
- Tolderlund, D. S., and A. Bé (1971), Seasonal distribution of planktonic foraminifera in the western North Atlantic, *Micropaleontology*, *17*(3), 297–329.
- Ullermann, J. (2015), Glacial-interglacial oceanic changes in the central Pacific sector of the Southern Ocean during the past 500 ka, PhD Thesis, 135 pp., Bremen University, Bremen, Germany.
- Waelbroeck, C., L. Labeyrie, E. Michel, J. C. Duplessy, J. McManus, K. Lambeck, E. Balbon, and M. Labracherie (2002), Sea-level and deep water temperature changes derived from benthic foraminifera isotopic records, *Quat. Sci. Rev.*, *21*, 295–305.

Supplementary Material

S1. Age Model and Chronology

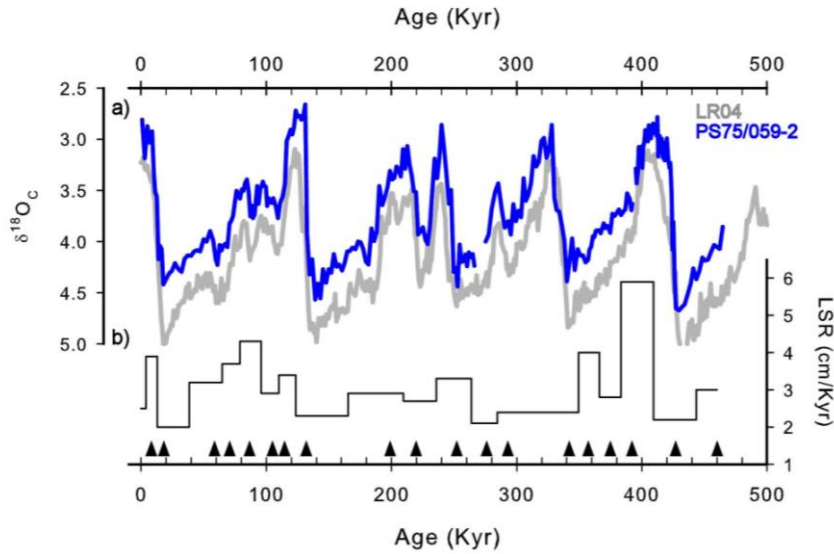


Figure S1 Stratigraphic framework of core PS75/059-2. (a) The $\delta^{18}O$ record of the benthic foraminifer *Cibicidoides* spp (blue curve) was correlated to the benthic $\delta^{18}O$ reference stack LR04 of Lisiecki and Raymo [2005](grey curve) using the program using the software “Match” [Lisiecki and Lisiecki, 2002]. Black triangles mark the stratigraphic tie lines between both records. (b) Linear sedimentation rates of sediment core PS75/059-2, ranging between 2 and 6 cm per 1000 years [Ullermann, 2015].

S2. Assessing cleaning efficiency

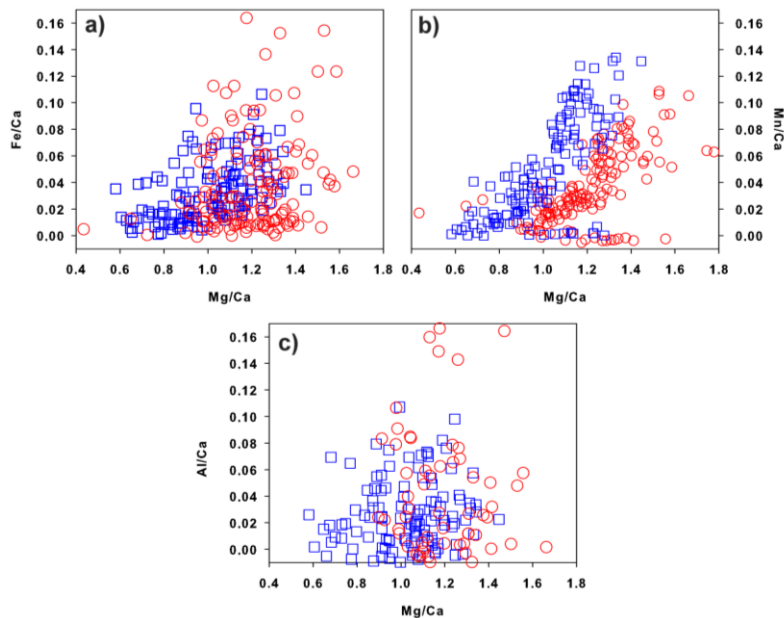


Figure S2 Mg/Ca plotted against (a) Fe/Ca, (b) Mn/Ca and (c) Al/Ca, low values (<0.14 mmolmol⁻¹) and lack of evident correlation with Mg/Ca ($R^2 < 0.3$) suggest that contamination has not controlled Mg/Ca variability in *G. bulloides* (red) and *G. inflata* (blue).

S3. Assessing the impact of dissolution on Mg/Ca-derived temperatures

Dissolution reduces the Mg/Ca and the test-weight of foraminifera [Brown and Elderfield, 1996; Dekens et al., 2002; Regenberg et al., 2006; 2014]. The lack of correlation between the shell weight and Mg/Ca ratios suggest that our Mg/Ca records are not shaped by dissolution. Furthermore, the amount of loss in Mg/Ca caused by dissolution varies between species [Dekens et al., 2002], studies comparing Mg/Ca-derived temperatures against dissolution proxies [Mekik et al., 2007], laboratory experiments [Marr et al., 2013] and reconstructions [Tapia et al., 2015] have suggested that the Mg/Ca signal of the species considered in this study poses a high fidelity even in dissolution prone environments.

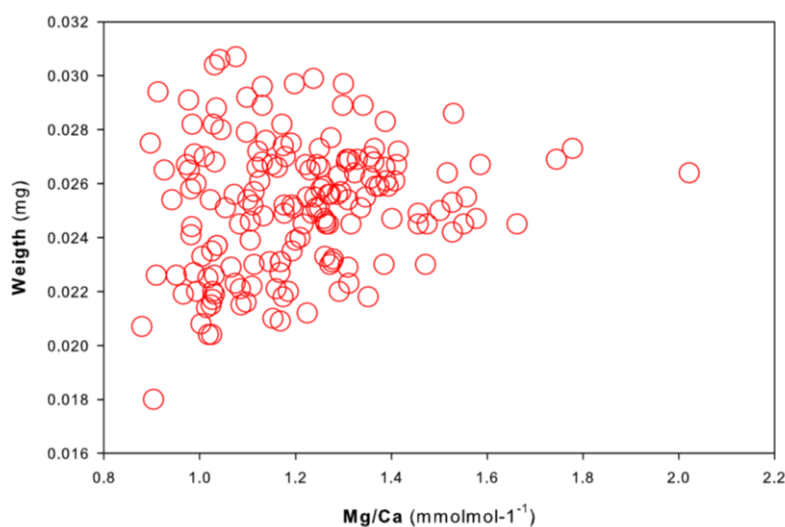


Figure S3 Shell weights plotted against Mg/Ca in *G. bulloides*, the coefficient of correlation (R^2) is <0.1 , discards dissolution as the main factor controlling Mg/Ca variability.

S4. Estimated vertical distribution of *G. bulloides* and *G. inflata*

The Mg/Ca (temperature) values of *G. bulloides* and *G. inflata* in upper most sediment from the core PS75/059-2 are $1.17 \text{ mmolmol}^{-1}$ ($\sim 8.5^\circ\text{C}$, circle) and $1.00 \text{ mmolmol}^{-1}$ ($\sim 6.6^\circ\text{C}$, square), respectively. On basis of the typical error associated to the Mg/Ca-paleothermometry of ± 0.5 to $\pm 1.0^\circ\text{C}$ [Mashiotta et al., 1999; Nürnberg and Groeneveld, 2006], suggest that the reconstructed Mg/Ca surface temperatures are identical to the summer temperatures i.e., World Ocean Atlas 2009 [Locarnini et al., 2010], CTD cast at station PS75/058-1 [Gersonde, 2011] and historical data from WOCE transect P17E between 54° and 55° (stations 139 to 144) (Figure S4). Moreover, Mg/Ca values at core site PS75/059-2 are consistent with Mg/Ca values from the core PS75/056-1 ($55^\circ 09' \text{ S}$; $114^\circ 47' \text{ W}$; 3581 m), i.e. $1.08 \text{ mmolmol}^{-1}$ ($\sim 7.73^\circ\text{C}$) for *G. bulloides* (Ullermann et al., in prep) [Ullermann, 2015] and $0.97 \text{ mmolmol}^{-1}$ ($\sim 6.2^\circ\text{C}$) for *G. inflata* [Tapia et al. in prep]. Based on

the correlation with temperature (i.e. climatological, in situ and historical data), we interpret these species as reflecting surface and subsurface water temperatures.

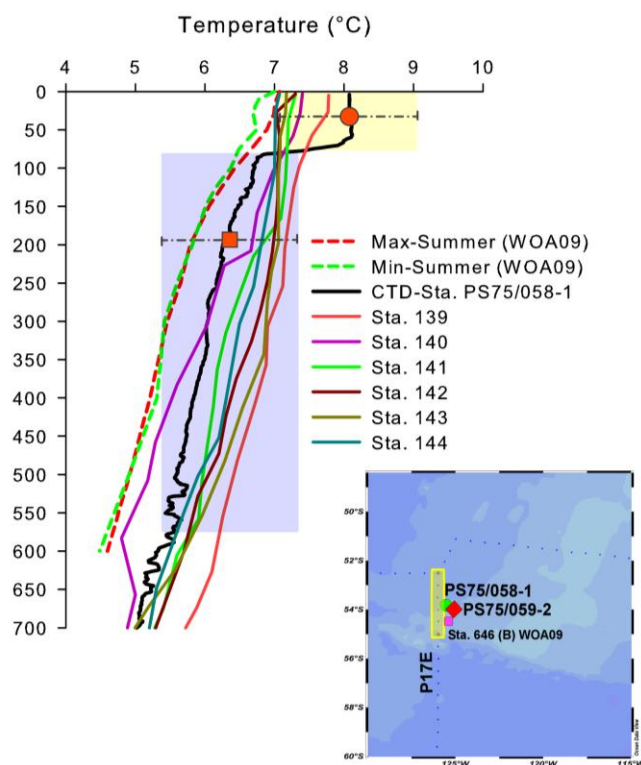


Figure S4 Vertical profile of the minimum and the maximum summer temperature WOA09, CTD cast and WOCE P17E of the upper 600 – 700 m of the water column; averaged Mg/Ca-temperature for *G. bulloides* (circle) and *G. inflata* (square) from upper most sediment sites PS75/059-2 and PS75/056-1. Colored boxes mark inferred vertical distribution assuming an error of $\pm 1^\circ\text{C}$. The inlet shows detail of the selected water column station WOA09 (pink square), CTD cast (green circle) and WOCE stations cruise P17E (yellow box) and study site (red diamond).

S. References

- Brown, S. J., and H. Elderfield (1996), Variations in Mg/Ca and Sr/Ca ratios of planktonic foraminifera caused by postdepositional dissolution: Evidence of shallow Mg-dependent dissolution, *Paleoceanography*, 11(5), 543–551.
- Dekens, P. S., D. W. Lea, D. K. Pak, and H. J. Spero (2002), Core top calibration of Mg/Ca in tropical foraminifera: Refining paleotemperature estimation, *Geochem. Geophys. Geosyst.*, 3(4), doi:10.1029/2001GC000200.
- Gersonde, R. (2011), The expedition of the research vessel “Polarstern” to the polar South Pacific in 2009/2010 (ANT-XXVI/2 - BIPOMAC) / Ed. by Rainer Gersonde with contributions of the participants, *EPIC3Berichte zur Polar- und Meeresforschung (Reports on Polar and Marine Research)*, Bremerhaven, Alfred Wegener Institute for Polar and Marine Research, 632, 330 p., ISSN: 1866-3192, 330.
- Lisiecki, L. E., and M. E. Raymo (2005), A Pliocene-Pleistocene stack of 57 globally distributed benthic $\delta^{18}\text{O}$ records, *Paleoceanography*, 20(1), doi:10.1029/2004PA001071.

- Lisiecki, L. E., and P. A. Lisiecki (2002), Application of dynamic programming to the correlation of paleoclimate records, *Paleoceanography*, 17(4), 1–1–1–12, doi:10.1029/2001PA000733.
- Locarnini, R. A., A. V. Mishonov, J. I. Antonov, T. P. Boyer, H. E. Garcia, O. K. Baranova, M. M. Zweng, and D. R. Johnson (2010), World Ocean Atlas 2009, vol. 1, *Temperature*, NOAA Atlas NESDIS, 68.
- Marr, J. P., H. C. Bostock, L. Carter, A. Bolton, and E. Smith (2013), Differential effects of cleaning procedures on the trace element chemistry of planktonic foraminifera, *Chemical Geology*, 351, 310–323, doi:10.1016/j.chemgeo.2013.05.019.
- Mashiotta, T. A., D. W. Lea, and H. J. Spero (1999), Glacial–interglacial changes in Subantarctic sea surface temperature and $\delta^{18}\text{O}$ -water using foraminiferal Mg, *Earth Plan. Sci. Lett.*, 170, 417–432.
- Mekik, F., R. François, and M. Soon (2007), A novel approach to dissolution correction of Mg/Ca–based paleothermometry in the tropical Pacific, *Paleoceanography*, 22(3), doi:10.1029/2007PA001504.
- Nürnberg, D., and J. Groeneveld (2006), Pleistocene variability of the Subtropical Convergence at East Tasman Plateau: evidence from planktonic foraminiferal Mg/Ca (ODP Site 1172A), *Geochem. Geophys. Geosyst.*, 7, Q04P11, doi:10.1029/2005GC000984.
- Regenberg, M., A. Regenberg, D. Garbe-Schönberg, and D. W. Lea (2014), Global dissolution effects on planktonic foraminiferal Mg/Ca ratios controlled by the calcite-saturation state of bottom waters, *Paleoceanography*, doi:10.1002/2013PA002492.
- Regenberg, M., D. Nürnberg, S. Steph, J. Groeneveld, D. Garbe-Schönberg, R. Tiedemann, and W.-C. Dullo (2006), Assessing the effect of dissolution on planktonic foraminiferal Mg/Ca ratios: Evidence from Caribbean core tops, *Geochem. Geophys. Geosyst.*, 7, doi:10.1029/2005GC001019.
- Tapia, R., D. Nürnberg, T. Ronge, and R. Tiedemann (2015), Disparities in glacial advection of Southern Ocean Intermediate Water to the South Pacific Gyre, *Earth Plan. Sci. Lett.*, 410, 152–164, doi:10.1016/j.epsl.2014.11.031.
- Ullermann, J. (2015), Glacial-interglacial oceanic changes in the central Pacific sector of the Southern Ocean during the past 500 ka, PhD Thesis, 135 pp., Bremen University, Bremen.



Evolution of the South Pacific Gyre's Thermocline during the last ~600 kyr

R. Tapia and D. Nürnberg

In preparation to be submitted to Paleoceanography

Abstract

The Intermediate Waters formed in the Southern Ocean, such as Subantarctic Mode Water (SAMW) and Antarctic Intermediate Water (AAIW), transport climatic signals from high to low latitudes and ventilate the thermocline in the Southern Hemisphere Gyres. Reconstructions of the SAMW-AAIW in the south Pacific suggest regional differences regarding their advection toward lower latitudes, but information of its impact on the South Pacific Gyre (SPG)'s thermocline on time scale longer than the last glacial-interglacial cycle is virtually unknown.

Here, we present a ~600 ka record of paired Mg/Ca ratios and stable oxygen isotope of surface- and deep-dwelling planktic foraminifera from the SPG. The reconstructed sea surface temperature characterized by the small glacial-interglacial amplitude, exceptionally warmer conditions are observed during MIS 15, MIS 13 and MIS 11. The evolution of the temperature and paleosalinity records at subsurface suggests two main stages of the advection of SAMW-AAIW to the SPG, shifting from colder/fresher to warmer/saltier conditions at 320–360 kyr, this substantially differs from the typical SAMW-AAIW glacial-interglacial cyclicity associated to the air-sea forcing. We discuss several possible mechanisms that could lead to this difference. The most likely explanation is a shift in the rotational speed of the SPG due to the decreasing intensity of the easterly winds from the Mid-Pleistocene Transition to the present.

CHAPTER 5

5.1 Introduction

The subtropical gyre dominates the circulation of the South Pacific Ocean. The counter clockwise rotation of the South Pacific gyre (SPG), driven by the interplay of low-latitude easterlies trade winds and high-latitude westerlies [Mata *et al.*, 2000; Wijffels *et al.*, 2001; Roemmich, 2007], involves the equatorward Humboldt Current System (HCS), the westward South Equatorial Current (SEC), the poleward East Australian current (EAC), and the eastward South Pacific Current (SPC) (Figure 5.1). The HCS and EAC play a vital role in the transport of heat and salt in the south Pacific by advecting southern cooler/fresher and tropical warmer/saltier waters, respectively [Tsimplis *et al.*, 1998; Wijffels *et al.*, 2001; Zilberman *et al.*, 2014]. In the SPG between 94° and 180° W, the meridional circulation at intermediate depths is dominated by the equatorward transport of the Southern Ocean Intermediate waters (SOIWs), consisted of the cold and fresh Subantarctic Mode Water (SAMW) and Antarctic Intermediate Water (AAIW) [Bostock *et al.*, 2010; Sloyan *et al.*, 2010; Herraiz-Borreguero and Rintoul, 2011b; Bostock *et al.*, 2013; Zilberman *et al.*, 2014]. The SAMW and AAIW return poleward as saltier and warmer waters in the EAC region (>180°W) [Bostock *et al.*, 2010; 2013; Zilberman *et al.*, 2014]. The SOIWs are responsible for renewing the water at thermocline depth in the subtropical South Pacific Gyre (SPG) [Bostock *et al.*, 2010; Hartin *et al.*, 2011; Herraiz-Borreguero and Rintoul, 2011a; Holte *et al.*, 2012; Bostock *et al.*, 2013].

In the literature, SOIWs are often considered as “the bridge” connecting high and low latitudes, via processes such as “oceanic tunnelling”, allowing the south-north transport of climatic signals (e.g. temperature and salinity) as well as nutrients [Liu *et al.*, 2002; Spero and Lea, 2002; Liu and Herbert, 2004; Sarmiento *et al.*, 2004; Liu and Alexander, 2007; Pena *et al.*, 2008; 2013]. The active participation of SAMW-AAIW in the heat, freshwater and carbon transports at global scale renders their role relevant in climate modulation [Spero and Lea, 2002; Bostock *et al.*, 2004; Pahnke and Zahn, 2005; Pena *et al.*, 2008; Ziegler *et al.*, 2013].

The formation of the modern SAMW-AAIW occurs in several hotspot across the south Pacific [Sloyan *et al.*, 2010; Hartin *et al.*, 2011; Herraiz-Borreguero and Rintoul, 2011b], but its principal formation area lays in the southeast Pacific (SEP) [Sallée *et al.*, 2006; Bostock *et al.*, 2010; Hartin *et al.*, 2011; Hasson *et al.*, 2011; Bostock *et al.*, 2013; Holte *et al.*, 2013]. The SAMW is formed equatorward of AAIW formation area, north of the subantarctic Front (SAF) [Hartin *et al.*, 2011; Holte *et al.*, 2013] (Figure 5.1), via deepening of mixed layers during wintertime convection [Sloyan *et al.*, 2010; Hartin *et al.*, 2011; Holte *et al.*, 2013]. Equatorward of the Polar Front (PF), the AAIW is formed from Antarctic Surface

Waters (AASW) by air-sea fluxes [Hartin et al., 2011]. McCartney [1977] argued that the formation of AAIW is related to SAMW, as they share similar temperature and salinity properties in the SEP, indeed the AAIW is often considered in the literature as the coldest and densest variety of SAMW [McCartney, 1977].

Although the mean state of the Pacific's thermocline have been reconstructed [e.g Patrick and Thunell, 1997; de Garidel-Thoron et al., 2005; Pena et al., 2008; Ford et al., 2015; Regoli et al., 2015] by pairing sea surface and subsurface proxies, a large spatio-temporal gap still remains. This is because most of the thermocline reconstructions are located in at equatorial Pacific and/or cover only the Last Glacial Maximum to the present. Given that the SPG has received little attention, the response of the SPG's thermocline to the SAMW-AAIW at time scales larger than the last glacial-interglacial (G-IG) cycle is virtually unknown. Here we present paired Mg/Ca and $\delta^{18}\text{O}$ records of planktic foraminifera covering the last ~600 kyr at site SO213-60-1 in the SPG (~44° S). In order to reconstruct the water column structure and the influence of the SAMW-AAIW on the SPG's thermocline water depth, we selected two species of planktic foraminifera with well-known habitat depths, namely the surface dweller *Globigerina bulloides* and the deep dweller *Globorotalia inflata*.

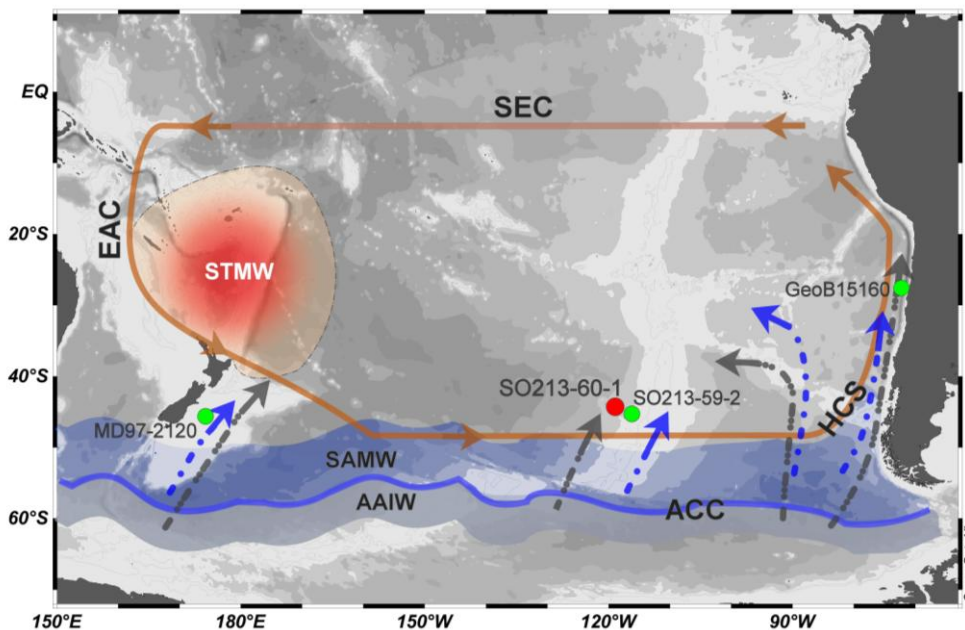


Figure 5.1 Circulation pattern in the South Pacific and location of the sediment core site SO213-60-1 as well as the reference cores discussed in this study. Surface water circulation includes Antarctic Circumpolar Current (ACC); Humboldt Current System (HCS), South Equatorial Current (SEC), East Australian Current (EAC). Shaded areas show the location of the Subtropical Mode Water (STMW), Subantarctic Mode Water (SAMW) and Antarctic Intermediate Water (AAIW). Subantarctic front (SAF; blue line) [Orsi et al., 1995] divides the Arrows denote the flow of the SAMW and AAIW.

5.2 Material and Methods

The age model of the gravity core SO213-60-1 (44°57.83' S; 119°33.07' W, 3471 m water depth, 670 cm length) (Figure 5.2), retrieved from the East Pacific Rise during R/V *Sonne* cruise SOPATRA [Tiedemann et al., 2014], is based on the visual correlation of its $\delta^{18}\text{O}$ benthic foraminiferal record (*Uvigerina peregrina*, >300 μm) and that of the ODP1123 (41° S) [Elderfield et al., 2012] using the software package AnalySeries 6.0 [Paillard et al., 1996]. The age model is further supported by biostratigraphic and paleomagnetic data [Tiedemann et al., 2014]. We note that the LR04 stack [Lisiecki and Raymo, 2005] is widely used to build age models, but opted for ODP1123 because of the following reasons. Firstly, the ODP1123 is the only site from the south Pacific in the area-not-weighted LR04 compilation [Lisiecki and Raymo, 2005; Elderfield et al., 2012], and secondly, a mean seawater $\delta^{18}\text{O}$ ($\delta^{18}\text{O}_{\text{SW}}$) reconstruction for the last 1.4 ma [Elderfield et al., 2012] is already available at ODP1123, which is an advantage since the mean $\delta^{18}\text{O}_{\text{SW}}$ data is necessary to reconstruct changes in local salinity (see section 2.2). The uppermost sediment (0–1 cm) from multicore SO213-60-2 (same location as the gravity core) was radiocarbon dated [see Molina-Kescher et al., 2014; Table 2].

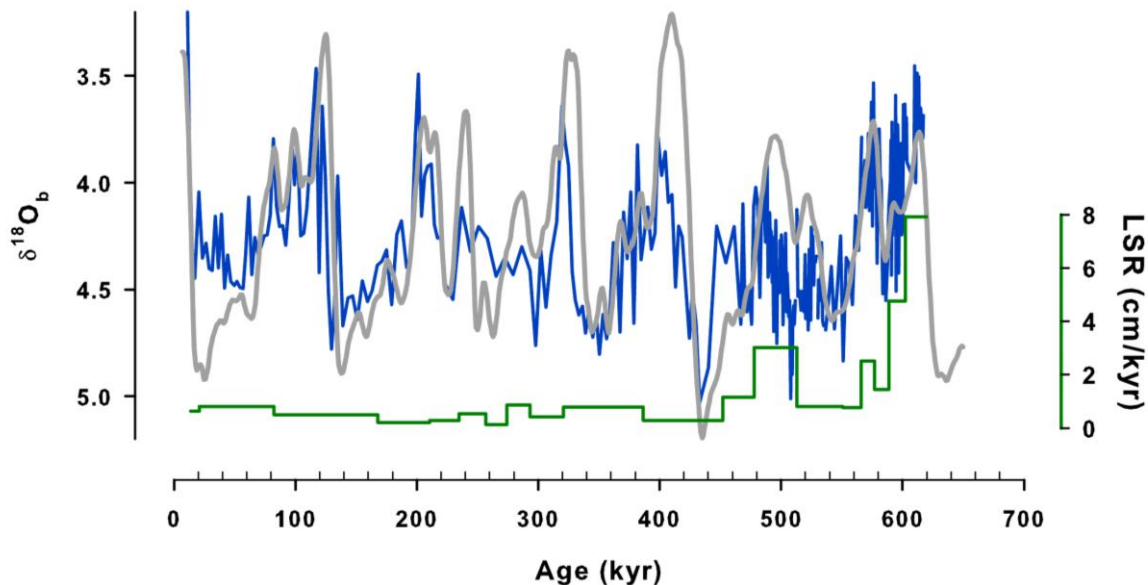


Figure 5.2 Correlation of benthic $\delta^{18}\text{O}$ signal from the core SO213-60-1 (*U. peregrina*) (blue) and the core ODP 1123 (gray). The linear sedimentation rate (green) is on average is 1.78 cm kyr^{-1} ; ranging from 0.2 to 7.9 cm kyr^{-1} .

5.2.2 Foraminiferal Mg/Ca-temperatures and salinity approximation

The planktic foraminifers *G. bulloides* and *G. inflata* have been used to reconstruct the upper ocean structure, from surface (mixed layer) to thermocline [e.g. Mortyn et al., 2002;

Thornalley et al., 2008; Farmer et al., 2011; Tapia et al., 2015]. *G. bulloides* is known to calcify above the thermocline in upper part of the water column (< 60 m) [Schiebel et al., 1997; Peeters et al., 2002; Mekik et al., 2007], whereas the deep dweller *Globorotalia inflata* calcifies at water depths of ~300–800 m water depth [Elderfield and Ganssen, 2000; Lončarić et al., 2006; Cléroux et al., 2007; Groeneveld and Chiessi, 2011]. Previous Mg/Ca-based studies in the SPG suggest that *G. bulloides* and *G. inflata* match with the modern water temperatures at sea surface (< 50 m water depth) and thermocline-depth (> 75 m), respectively [Tapia et al., 2015]. Here our interpretations are built on the working assumption that the selected foraminiferal species did not change their calcification depths during the time period investigated and they are representative of the modern depth-succession.

Foraminiferal sampling was conducted at 2 cm intervals. The samples were washed, dried and picked for *G. bulloides* and *G. inflata* (315–400 μm size fraction). To minimize artifacts related to age/depth uncertainties, the geochemical analysis were performed on material from the same sediment horizon. Visually detectable heavily encrusted specimens of *G. inflata* were excluded, since an inverse relationship between encrustation state and Mg/Ca content that results in artificially lower temperatures was found for this species [Hathorne et al., 2009; Groeneveld and Chiessi, 2011]. Approximately 35 specimens were gently crushed between two methanol-cleaned microscope glass plates, homogenized and then split in subsamples for stable isotope analyses and Mg/Ca measurements.

Prior to the stable isotope analysis, the subsamples were ultrasonically cleaned with deionized water and methanol. The isotopic measurements were performed at GEOMAR-Kiel, using a MAT 253 mass spectrometer coupled with a Kiel IV Carbonate device (Thermo Fisher Scientific, Germany). Results were referenced to the NBS19 standard and the isotope values are reported on the VPDB (Vienna PDB) scale. Analytical standard deviations were $\pm 0.05\text{‰}$ for $\delta^{18}\text{O}$.

The $\delta^{18}\text{O}$ fractionation processes in planktic foraminifera may be affected by biological processes known as vital effect. The vital effect varies between species and is difficult to estimate in species with a large vertical distribution [Rohling and Cooke, 1999; Ravelo and Hillaire-Marcel, 2007]. In this study we assume no vital effect on the fractionation between foraminiferal $\delta^{18}\text{O}$ and seawater $\delta^{18}\text{O}$, because there is no consensus on oxygen isotopic disequilibrium of the species considered here, ranging from negligible or zero offset to -1‰ for *G. bulloides* and from -0.4‰ to $+0.4\text{‰}$ for *G. inflata* [King and Howard, 2005; Lončarić et al., 2006; Steph et al., 2009; Wilke et al., 2009; Sagawa et al., 2013].

The Mg/Ca cleaning step was according to the protocol proposed by Barker et al. [2003] with an additional reductive cleaning step. Analyses were performed on an ICP OES (VARIAN 720-ES, GEOMAR-Kiel), the long-term analytical precision ($\pm 0.1 \text{ mmolmol}^{-1}$ for

Mg/Ca) was monitored by ECRM752-1 standard. Fe/Ca, Al/Ca and Mn/Ca ratios were determined in conjunction with Mg/Ca as clay contamination and post-depositional Mn-rich carbonate coatings can exert a significant control on Mg/Ca ratios [Barker *et al.*, 2003]. We discard this possibility since for all our samples the Fe/Ca, Al/Ca and Mn/Ca ratios were $<0.14 \text{ mmol mol}^{-1}$ with no evident correlation to Mg/Ca (Figure 5.3).

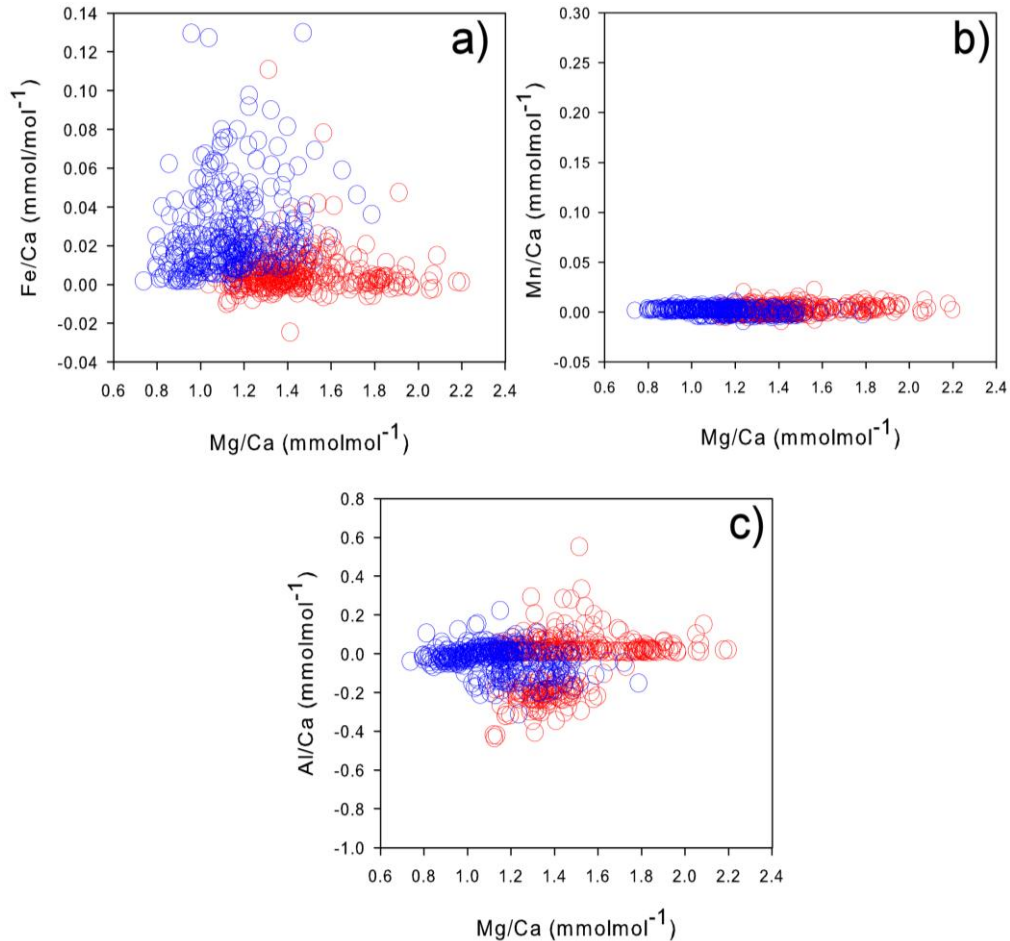


Figure 5.3 Mg/Ca plotted against (a) Fe/Ca, (b) Mn/Ca and (c) Al/Ca, low values and lack of covariance indicates that contamination has not controlled Mg/Ca variability of *G. bulloides* (red) and *G. inflata* (blue).

The conversion of Mg/Ca values to temperatures was conducted using the calibrations of Mashiotta *et al.* [1999] ($\text{Mg/Ca} = 0.474 e^{0.107T}$) for *G. bulloides* and Groeneveld and Chiessi [2011] ($\text{Mg/Ca} = 0.72e^{0.076T}$) for *G. inflata*.

The seawater $\delta^{18}\text{O}_{\text{SW}}$ correlates linearly with seawater salinity [LeGrande and Schmidt, 2006; 2011], therefore we used it as a semi-quantitative proxy of local salinity changes. However, we refrain from transforming the $\delta^{18}\text{O}_{\text{SW}}$ into salinity since the $\delta^{18}\text{O}_{\text{SW}}$ -salinity relationships are only regionally coherent [LeGrande and Schmidt, 2011]. To

calculate the $\delta^{18}\text{O}_{\text{SW}}$, we removed the temperature effect from the foraminiferal calcite $\delta^{18}\text{O}$ ($\delta^{18}\text{O}_{\text{C}}$) record using the equation of Shackleton [1974] ($\delta^{18}\text{O}_{\text{SW}}$ (SMOW) = $\delta^{18}\text{O}_{\text{C}}$ + 0.27 – (4.38 – (4.38² – 4 × 0.1 (16.9 – $T_{\text{Mg/Ca}}$))^{1/2})/(0.1 × 2)) and then the global ice volume component (IVC) [Elderfield et al., 2012] was subtracted from the reconstructed the seawater $\delta^{18}\text{O}$.

5.3 Results

5.3.1 Planktic foraminiferal Mg/Ca-temperature

The Mg/Ca (temperature) values of *G. bulloides* and *G. inflata* in surface sediments (top 1 cm of multicore) are 1.55 mmolmol⁻¹ (~11 °C) and 1.44 mmolmol⁻¹ (~9 °C), respectively. Downcore, the Mg/Ca (temperature) values range between 1.04 – 2.2 mmolmol⁻¹ (~7.3 – ~14.3 °C) for *G. bulloides* and 0.74 – 2.09 mmolmol⁻¹ (~3 – ~10 °C) for *G. inflata* (Figure 5.4). As shown in Figure 5.5a, Mg/Ca-temperatures (SST_{Mg/Ca}) are relatively stable throughout the record with G-IG oscillations of ~2 °C. Exceptionally warm conditions (> ~11 °C) are suggested by the SST_{Mg/Ca} for the marine isotopic stages (MIS) 11, 13 and 15. In contrast, the subsurface Mg/Ca-temperature (subST_{Mg/Ca}) does not show consistent G-IG cycles, but is characterized by a drastic shift from cold conditions (~5 °C) to warmer subST_{Mg/Ca} (~8 °C) circa ~350 kyr (see Figure 5.5a).

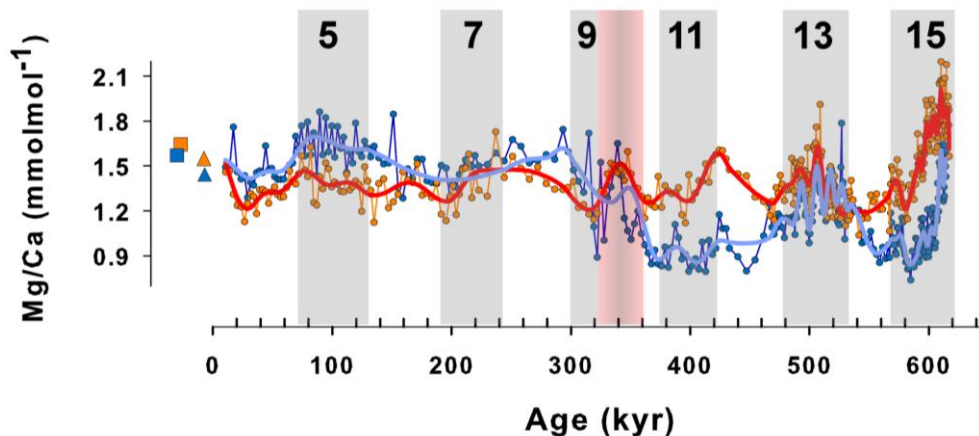


Figure 5.4 Foraminiferal Mg/Ca ratios for *G. bulloides* (orange) and *G. inflata* (blue) for the core SO213-60-1 (circle), surface samples SO213-60-2 (triangle) and SO213-59-1 (square) [Tapia et al., 2015]. Shaded bars indicate glacial intervals; black numbers in the bars represent the Marine Isotope Stages (MIS).

5.3.2 Oxygen stable isotopes in planktic foraminifera and relative salinity reconstructions.

The $\delta^{18}\text{O}$ values from the top 1 cm of multicore SO213-60-2 are 2.06‰ for *G. bulloides* and 2.6‰ for *G. inflata*. Downcore, the $\delta^{18}\text{O}$ values range from 3.88 to 2.5‰ at

surface and from 3.71 to 2.3‰ at subsurface. The most striking feature in [Figure 5b](#) is the divergence in the G-IG amplitudes of $\delta^{18}\text{O}$ at surface and thermocline water depth. At surface, the G-IG amplitude ($\sim 0.7\%$) is relatively constant across the record, but the range in the $\delta^{18}\text{O}_{G. \textit{bulloides}}$ values shift from 3.6 – 2.9‰ (MIS 15 to MIS 12) to 3.4 – 2.7‰ (MIS 10 to the present) ([Figure 5.5b](#)). In contrast, at thermocline depth the G-IG amplitude steadily increases from the older part of the record to the present ([Figure 5.5b](#)).

The calculated $\delta^{18}\text{O}_{\text{SW-IVC}}$ values at surface (*G. bulloides*) range from -0.94 to 2.61‰ suggesting saltier conditions during interglacial than glacial stages ([Figure 5.5c](#)). Interestingly, MIS 6 is the saltiest glacial stage with values comparable to interglacial stages ([Figure 5.5c](#)). At subsurface, the reconstructed $\delta^{18}\text{O}_{\text{SW-IVC}}$ (*G. inflata*) values range from -2.0 to 1.3 ‰ ([Figure 5.5c](#)), suggest the prevalence of fresher conditions between ~ 600 and ~ 330 kyr in comparison to the period between ~ 300 kyr and the present.

5.4. Discussion

5.4.1 Assessing the sea surface and subsurface Mg/Ca-temperature reconstructions in the SPG.

The effect of dissolution on the foraminiferal Mg/Ca is well documented and it is a key point to consider in any Mg/Ca-temperature reconstruction. However, the factors controlling the dissolution susceptibility remain poorly understood. The amount of loss in Mg caused by dissolution varies between species, with some species showing larger decrease in their Mg/Ca ratios than others [*Dekens et al.*, 2002]. It has been suggested to be related to preferential dissolution of high-Mg/Ca calcite [*Brown and Elderfield*, 1996], as well as the exposed surface area of the organisms. However, the Mg/Ca signal in the species considered in this study (*G. bulloides* and *G. inflata*) are generally considered to be resilient to environments prone to dissolution and capable of preserving reliably past sea water temperatures, as suggested by Mg/Ca and proxy-dissolution comparisons [*Mekik et al.*, 2007], dissolution experiments [*Marr et al.*, 2013] and reconstructions [*Tapia et al.*, 2015].

Previous studies on surface sediments (core tops) in the SPG have reported Mg/Ca values of $1.66 \text{ mmolmol}^{-1}$ for *G. bulloides* and $1.59 \text{ mmolmol}^{-1}$ for *G. inflata* (site SO213-59-2; ~ 3100 m water depth) [*Tapia et al.*, 2015], values slightly higher than the $1.55 \text{ mmolmol}^{-1}$ for *G. bulloides* and $1.44 \text{ mmolmol}^{-1}$ for *G. inflata* observed in surface sediments (0 – 1 cm) at the deeper site SO213-60-1 (~ 3400 m water depth) ([see section 5.3.1 and Figure 5.4](#)). At the sea floor, the dissolution is controlled by the carbonate ion saturation state ($\Delta[\text{CO}_3^{2-}]$) of the bottom water, that is, the difference between in situ carbonate ion concentration ($[\text{CO}_3^{2-}]_{in \textit{ situ}}$) and the saturation carbonate ion concentration ($[\text{CO}_3^{2-}]_{sat}$), the latter a function of depth/pressure and temperature. Lower Mg/Ca values observed at core site SO213-60-1

could therefore be related to depth-enhanced dissolution. However, the Mg/Ca-correction of $0.1 - 0.2 \text{ }^\circ\text{C}$ per $\mu\text{molkg}^{-1} \Delta[\text{CO}_3^{2-}]$ for surface and $0.4 - 0.6 \text{ }^\circ\text{C}$ per $\mu\text{molkg}^{-1} \Delta[\text{CO}_3^{2-}]$ for subsurface dwellers [Regenberg *et al.*, 2014], translates into water temperatures of ~ 4 to $\sim 12 \text{ }^\circ\text{C}$ warmer than the modern values. This incongruity suggests that the lower Mg/Ca values observed at the core site SO213-60-1 are unlikely to be controlled by dissolution. Alternatively, the Mg/Ca differences between the sites might be reflecting different time intervals, as radiocarbon dating of the surface sediments suggests ~ 3 kyr of discrepancy between the surface sediments from the core site SO213-60-1 ($\sim 11\text{ka}$) [see Table 4; Molina-Kescher *et al.*, 2014] and core site SO213-59-2 ($\sim 8\text{ka}$) [see Table 4; Tapia *et al.*, 2015].

Although the aforementioned observations argue against dissolution as the main driver of the Mg/Ca variability, the possibility of a dissolution-related bias cannot be completely eliminated. Therefore, in order to circumvent any possible bias, our interpretation is based on the relative changes in downcore $\text{Mg/Ca}_{\text{Temperature}}$ instead of absolute reconstructed values.

5.4.2 Past surface conditions at the South Pacific

The relatively stable temperatures suggested by the reconstructed $\text{SST}_{\text{Mg/Ca}}$ with $\sim 3 \text{ }^\circ\text{C}$ of G-IG amplitude (Figure 5.5a) is in agreement with previous Holocene-LGM reconstructions in the SPG i.e. site SO213-59-2 ($\sim 4 \text{ }^\circ\text{C}$) [Tapia *et al.*, 2015], DWBG-70 ($\sim 3.4 \text{ }^\circ\text{C}$) and E25-10 ($\sim 4.9 \text{ }^\circ\text{C}$) [Luz, 1977]. Traditionally, G-IG variations in SSTs and salinity in the south Pacific are explained as results of the interplay between the oceanic frontal system and westerly winds [e.g. Kaiser *et al.*, 2005; Nürnberg and Groeneveld, 2006; Sikes *et al.*, 2009; Verleye and Louwye, 2010; Ho *et al.*, 2012]. However, in contrast to the southeast Pacific, large glacial-latitudinal displacements of the oceanic frontal system are an unlikely scenario in the central south Pacific. Various proxy reconstructions support the idea of a relatively stationary latitudinal frontal system, located at similar latitude than their modern analogue [Matsumoto *et al.*, 2002; Gersonde *et al.*, 2005; Loubere and Bennett, 2008; Tapia *et al.*, 2015].

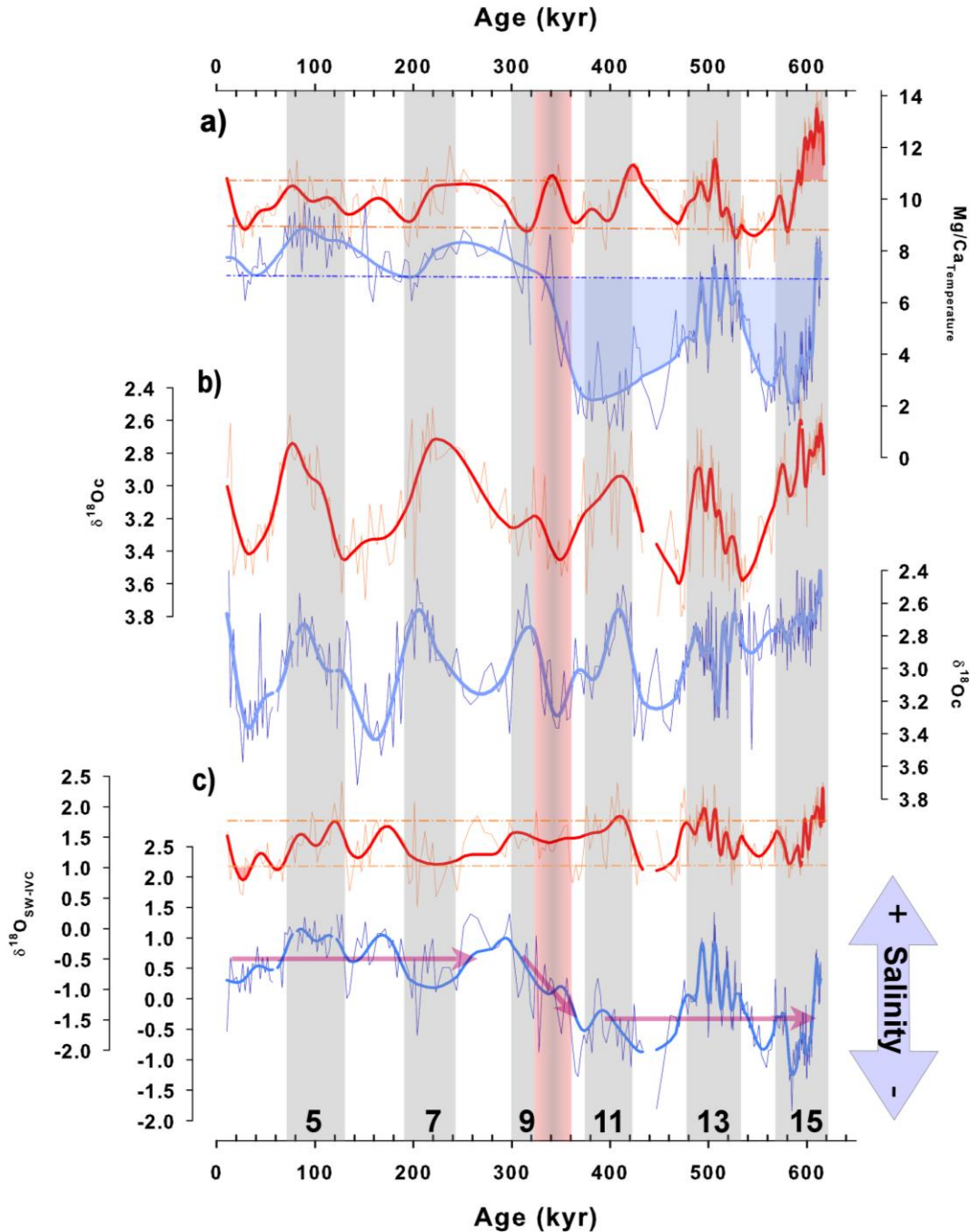


Figure 5.5a) Calculated seawater Mg/Ca-temperatures at sea surface (orange) and subsurface (blue). Red dashed lines denote the G-IG amplitude (~3 °C) at surface; blue dashed line highlights two main stages of the subsurface temperatures (warmer/colder than ~7 °C). b) Stable isotopic ($\delta^{18}\text{O}$) record of *G. bulloides* (red) and *G. inflata* (blue). The subsurface dweller *G. inflata* displays an increasing $\delta^{18}\text{O}$ -amplitude toward present, although surface dweller *G. bulloides* shows a relatively constant $\delta^{18}\text{O}$ -amplitude (~0.7‰) along the core, the section prior to 320-360 ka is characterized by heavier values than the younger section. c) Paleosalinity reconstructions (expressed as $\delta^{18}\text{O}_{\text{SW-IVC}}$) are characterized by low amplitude at surface (red), on the other hand at subsurface (blue) the $\delta^{18}\text{O}_{\text{SW-IVC}}$ suggest two stages shifting from fresher conditions to saltier conditions at ~300-360 kyr (reddish bar). Shaded bars indicate glacial intervals; black numbers in the bars represent the Marine Isotope Stages (MIS).

The presence of particularly warm surface waters during MIS 15 is the most striking feature along the record. Although not as warm, interglacial stages such MIS 11 and MIS 13 also show above average temperatures (Figure 5.5a and c). These findings are in agreement with previous studies that suggest a greater presence of tropical water i.e. south Pacific Subtropical Mode Water (STMW) off New Zealand during the Mid Pleistocene Transition (MPT). To the west of New Zealand, the presence of STW expand during the entire Mid Pleistocene Transition (MPT) (~500 – 1200 kyr) and some post-MPT interglacials (e.g. MIS 11 and MIS 5.5) [Hayward *et al.*, 2012]. At the eastern flank of New Zealand the SST reconstructions suggest larger and relatively permanent presence of STMW prior to MIS 13 [Hayward *et al.*, 2012], but after MIS13 its presence was restricted to only interglacial stages [Bostock *et al.*, 2015]. The agreement between our findings and previous studies suggest larger southward transport of tropical waters as a plausible explanation for the warmer/saltier surface ocean during MIS 15, 13 and 11. This idea is further reinforced by studies that suggest intensified Trade winds blowing on tropics and subtropical latitudes during the MPT [Marlow *et al.*, 2000; McClymont and Rosell-Melé, 2005], which could strengthen the southward wind-driven transport of Subtropical Mode Water (STMW) [Roemmich and Cornuelle, 1992; Tsubouchi *et al.*, 2007; Zilberman *et al.*, 2014].

5.4.3 Subsurface south Pacific and SAMW-AAIW variability

The SPG's thermocline is influenced by the northward advection of SAMW-AAIW [Sallée *et al.*, 2010; Hartin *et al.*, 2011; Bostock *et al.*, 2013; Zilberman *et al.*, 2014], therefore past changes in the advection of these fresh/cold southern waters has been often invoked to explain the glacial cooling in the tropical Pacific's thermocline [Liu *et al.*, 2002; Spero and Lea, 2002; Sarmiento *et al.*, 2004; Pena *et al.*, 2008; 2013]. Assuming that no change in the habitat depth preferences of the selected species occurred during the time interval analyzed, we calculated the vertical thermal gradient ($\Delta T_{\text{SST-subST}}$), defined as the difference between $\text{Mg/Ca}_{\text{SST}}$ and $\text{Mg/Ca}_{\text{subST}}$, to reconstruct the upper ocean structure (from mixed layer to thermocline). The $\Delta T_{\text{SST-subST}}$ record suggests two relatively well-defined section characterized by mean temperatures of ~6 °C and ~2 °C (see section 3, and Figure 6). The comparable mean $\text{Mg/Ca}_{\text{SST}}$ for both sections, i.e. 9.9 ± 0.76 °C vs 9.9 ± 1.1 °C, suggests that surface variability had minimal influence on the thermal gradient; consequently the $\Delta T_{\text{SST-subST}}$ is being shaped by $\text{Mg/Ca}_{\text{subST}}$. The vertical gradient of reconstructed surface and subsurface seawater isotopic composition ($\Delta \delta^{18}\text{O}_{\text{SW } G.\text{bulloides-G.inflata}}$) also suggests a shift in salinity, shifting from fresher to saltier conditions (Figure 5.6). The synchronous variations in temperature and salinity at thermocline depths in the SPG area suggest a general reduction in the presence of SAMW-AAIW at ~300–360 kyr.

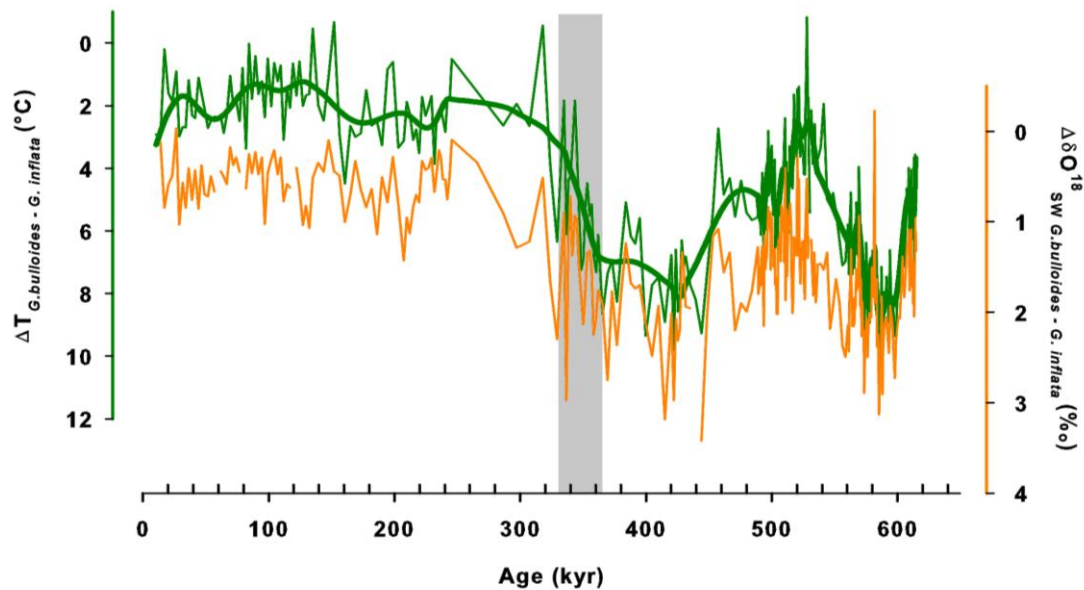


Figure 5.6 Vertical gradients in the water column in green thermal ($\Delta T_{SST-SubST}$) and in orange the seawater isotopic composition ($\Delta \delta^{18}O_{SW\ G.bulloides-G.inflata}$).

In recent years, two main scenarios regarding the variability of SAMW-AAIW have been proposed for the Pacific basin. While in the southwest Pacific benthic foraminiferal $\delta^{13}C$ records suggest stronger presence of AAIW during interglacial stages [Pahnke and Zahn, 2005; Elmore et al., 2015; Ronge et al., 2015], the opposite, i.e. stronger AAIW-signal during glacial stages have been proposed for the southeast Pacific [Martínez-Méndez et al., 2013]. Similarly, at the equatorial east Pacific temperature-salinity reconstructions based on deep dwelling planktic foraminifera also support the idea of an enhanced AAIW-signal during cold stages (i.e. LGM) [Pena et al., 2008; 2013]. In contrast, in the SPG (45° S) temperature-salinity reconstructions suggest a more complex scenario with contrasting presence of SAMW-AAIW during glacial stages (relative to present day), i.e. enhanced presence of SAMW-AAIW (colder/fresher conditions than today) during LGM and reduced presence of SAMW-AAIW (warmer/saltier conditions than today) during MIS 6 [Tapia et al., 2015]. In spite of differences in proxies and time coverage, taken together the aforementioned reconstructions do imply spatial variability in the presence of SAMW-AAIW through time.

5.4.4 Air-sea forcing and SAMW-AAIW formation

Among the processes involved in the formation of the SAMW-AAIW, the air-sea forcing has received considerable attention [McCartney, 1977; Dong et al., 2008; Hartin et al., 2011; Holte et al., 2012]. In fact, in the literature the breaking down of the ocean stratification and the development of a deep mixed layer is often considered synonymous

with the formation region of SAMW-AAIW [McCartney, 1977; Dong et al., 2008; Qu et al., 2008; Hartin et al., 2011; Holte et al., 2012]. Several studies have underlined the relationship between the intensity of Southern Westerly Winds (SWWs) over the SO and the SAMW-AAIW formation [England et al., 2000; Ribbe, 2001; Sloyan and Rintoul, 2001a; 2001b; Schneider and Bravo, 2006; Dong et al., 2008; Hartin et al., 2011; Holte et al., 2012; 2013]; as well as the physical properties (e.g. salinity, temperature, nutrients, chl-a) of SAMW-AAIW [Oke and England, 2004; Lovenduski and Gruber, 2005; Cai, 2006; Roemmich, 2007; Roemmich et al., 2007; Ayers and Strutton, 2013; Domingues et al., 2014; Loveday et al., 2015; Xue et al., 2015].

Although a consensus on the past changes in SWWs is still lacking, and multiple scenarios have been proposed regarding its intensity and/or latitudinal position [Kohfeld et al., 2013], the literature agrees in the notion that glacial conditions of the SWWs, in terms of intensity and/or latitudinal position, differed from its present day situation. This hypothesis have been used by some proxy studies to explain the G-IG variability of the SAMW-AAIW signal at lower latitudes in the southeast Pacific during cold stages [Martínez-Méndez et al., 2013; Pena et al., 2013]. However, variability displayed by our reconstructed temperature and salinity at subsurface does not fit with the typical G-IG cyclicity associated with the SWWs' variability. Consequently, it seems unlikely that salinity and temperature are a direct expression of the air-sea forcing i.e., intensified SWWs during Glacial stages. Further, it has been suggested that the precondition of the water column can significantly affect the final temperature-salinity properties of the newly formed SAMW-AAIW [Holte et al., 2012]. Indeed, a water column with low heat storage is prone to form the cold-dense varieties of SAMW (namely AAIW) [Holte et al., 2012]. In order to reduce the heat content of the water column in the SAMW-AAIW area a larger amount of cold water i.e. AASW is necessary. However, the amount of AASW exported further north to the SAMW-AAIW area depends of the Ekman transport and is therefore ultimately controlled by the SWWs' intensity, but as mentioned previously (see section 4.3) the variability of our subsurface records argue against a direct link to the SWWs' variability. Instead, changes in the rotational speed of the SPG can offer a better explanation to a larger presence of fresher southern water further north.

The circulation of the SPG is driven by easterly winds and westerly winds, the northward transport is balanced by the southward transport and vice versa. Changes in the rotational speed of the gyre have been linked to increased counter clockwise circulation at mid-depth, downward displacement of the surface densities, and amplified presence of warmer/saltier water in the SWP and colder/fresher water in the SEP [Roemmich, 2007; Roemmich et al., 2007; Schneider et al., 2007]. Scenario of faster rotational speed of the SPG may explain the warmer SSTs in the SWP [Hayward et al., 2012] and the SPG (this

study) via an increased southward transport of STMW. Furthermore, such scenario may cause the observed subsurface differences in temperature-salinity in the SPG, by amplifying the presence of AASW in the SAMW-AAIW region and promoting the advection of SAMW-AAIW into the subsurface SPG due to the associated mid-depth acceleration that imply the acceleration of the SPG [Roemmich, 2007; Roemmich et al., 2007; Schneider et al., 2007].

5.5 Conclusions

We presented the longest water column (surface to thermocline) reconstruction in the SPG. The small variability suggested by the reconstructed sea surface temperature agrees with early findings of a low sensitivity of the surface central south Pacific. Exceptionally warmer conditions are observed during MIS 15, MIS 13 and MIS 11. Considering the role of the SOIWs in ventilating the subtropical thermocline at the central south Pacific, the large changes in temperature and salinity suggest important changes in the presence of SOIWs in the SPG. However, the variability displayed by subsurface records does not fit with the typical G-IG cyclicity associated with the SWWs' variability.

As the circulation of the SPG is propelled by the interplay between easterly winds and westerly winds, a higher rotational speed of the SPG due to the stronger easterly winds during the MPT is a plausible scenario. Higher rotational speed of the SPG offer common a explanation to warmer SSTs in the SWP [Hayward et al., 2012] and the SPG (this study) during the MPT and a physical mechanism to explain the large subsurface differences in temperature-salinity in the SPG via larger formation of colder varieties of intermediate water (namely AAIW) as well as by a larger advection advection of SAMW-AAIW due to mid-depth acceleration. This scenario imply low-latitude forcing in the advection of Southern Intermediate Waters.

5.6. Acknowledgments

This study was funded by the Federal Ministry of Education and Research (BMBF; Germany) through grant No. 03G0213B. We thank to B. Hayward and M. Saavedra-Pellitero for their generous assistance in biostratigraphy. Technical support and laboratory assistance from N. Gehre and L. Haxhiaj (GEOMAR) are highly appreciated.

5.7 References

Ayers, J. M., and P. G. Strutton (2013), Nutrient variability in Subantarctic Mode Waters forced by the Southern Annular Mode and ENSO, *Geophys. Res. Lett.*, *40*, doi:10.1002/grl.50638.

Barker, S., M. Greaves, and H. Elderfield (2003), A study of cleaning procedures used for

- foraminiferal Mg/Ca paleothermometry, *Geochem. Geophys. Geosyst.*, **4**, doi:10.1029/2003GC000559.
- Bertrand, S., K. Hughen, J. Sepúlveda, and S. Pantoja (2014), Quaternary Science Reviews, *Quat. Sci. Rev.*, **105(C)**, 195–208, doi:10.1016/j.quascirev.2014.09.021.
- Bostock, H. C., B. N. Opdyke, and M. J. M. Williams (2010), Characterising the intermediate depth waters of the Pacific Ocean using $\delta^{13}\text{C}$ and other geochemical tracers, *Deep-Sea Res. Part I*, **57(7)**, 847–859, doi:10.1016/j.dsr.2010.04.005.
- Bostock, H. C., B. N. Opdyke, M. K. Gagan, and L. K. Fifield (2004), Carbon isotope evidence for changes in Antarctic Intermediate Water circulation and ocean ventilation in the southwest Pacific during the last deglaciation, *Paleoceanography*, **19**, PA4013, doi:10.1029/2004PA001047.
- Bostock, H. C., P. J. Sutton, M. Williams, and B. N. Opdyke (2013), Reviewing the circulation and mixing of Antarctic Intermediate Water in the South Pacific using evidence from geochemical tracers and Argo float trajectories, *Deep-Sea Res. Part I*, **73**, 84–98, doi:10.1016/j.dsr.2012.11.007.
- Bostock, H., B. W. Hayward, H. Neil, A. T. Sabaa, and G. H. Scott (2015), Changes in the position of the Subtropical Front south of New Zealand since the last glacial period, *Paleoceanography*, n/a–n/a, doi:10.1002/2014PA002652.
- Bova, S. C., T. Herbert, Y. Rosenthal, J. Kalansky, M. Altabet, C. Chazen, A. Mojarro, and J. Zech (2015), Links between Eastern Equatorial Pacific Stratification and Atmospheric CO₂ Rise during the last Deglaciation, *Paleoceanography*, doi:10.1002/2015PA002816.
- Brown, S. J., and H. Elderfield (1996), Variations in Mg/Ca and Sr/Ca ratios of planktonic foraminifera caused by postdepositional dissolution: Evidence of shallow Mg-dependent dissolution, *Paleoceanography*, **11(5)**, 543–551.
- Cai, W. (2006), Antarctic ozone depletion causes an intensification of the Southern Ocean super-gyre circulation, *Geophys. Res. Lett.*, **33(3)**, L03712, doi:10.1029/2005GL024911.
- Cléroux, C., E. Cortijo, J.-C. Duplessy, and R. Zahn (2007), Deep-dwelling foraminifera as thermocline temperature recorders, *Geochem. Geophys. Geosyst.*, **8(4)**, doi:10.1029/2006GC001474.
- de Garidel-Thoron, T., Y. Rosenthal, F. Bassinot, and L. Beaufort (2005), Stable sea surface temperatures in the western Pacific warm pool over the past 1.75 million years, *Nature*, **433(7023)**, 294–298, doi:10.1038/nature03189.
- Dekens, P. S., D. W. Lea, D. K. Pak, and H. J. Spero (2002), Core top calibration of Mg/Ca in tropical foraminifera: Refining paleotemperature estimation, *Geochem. Geophys. Geosyst.*, **3(4)**, doi:10.1029/2001GC000200.
- Domingues, R., G. Goni, S. Swart, and S. Dong (2014), Wind forced variability of the Antarctic Circumpolar Current south of Africa between 1993 and 2010, *J. Geophys. Res. Oceans*, n/a–n/a, doi:10.1002/2013JC008908.
- Dong, S., J. Sprintall, S. T. Gille, and L. Talley (2008), Southern Ocean mixed-layer depth from Argo float profiles, *J. Geophys. Res.*, **113(C6)**, doi:10.1029/2006JC004051.

- Elderfield, H., and G. Ganssen (2000), Past temperature and $\delta^{18}\text{O}$ of surface ocean waters inferred from foraminiferal Mg/Ca ratios, *Nature*, 405, 442–445, doi:10.1038/35013033.
- Elderfield, H., P. Ferretti, M. Greaves, and S. Crowhurst (2012), Evolution of Ocean Temperature and Ice Volume Through the Mid-Pleistocene Climate Transition, *Science*, doi:10.1126/science.1221294.
- Elmore, A. C., E. L. McClymont, H. Elderfield, S. Kender, M. R. Cook, M. J. Leng, M. Greaves, and S. Misra (2015), Earth and Planetary Science Letters, *Earth Plan. Sci. Lett.*, 428(C), 193–203, doi:10.1016/j.epsl.2015.07.013.
- England, M. H., S. McGregor, P. Spence, G. A. Meehl, A. Timmermann, W. Cai, A. Sen Gupta, M. J. McPhaden, A. Purich, and A. Santoso (2000), Recent intensification of wind-driven circulation in the Pacific and the ongoing warming hiatus, *Nature Climate Change*, –, doi:doi:10.1038/nclimate2106.
- Farmer, E. J., M. R. Chapman, and J. E. Andrews (2011), Holocene temperature evolution of the subpolar North Atlantic recorded in the Mg/Ca ratios of surface and thermocline dwelling planktonic foraminifers, *Global and Planetary Change*, 79(3-4), 234–243, doi:10.1016/j.gloplacha.2011.02.003.
- Fletcher, M. S., and P. I. Moreno (2012), Have the Southern Westerlies changed in a zonally symmetric manner over the last 14,000 years? A hemisphere-wide take on a controversial problem, *Quaternary International*, 253, 32–46, doi:10.1016/j.quaint.2011.04.042.
- Ford, H. L., A. C. Ravelo, P. S. Dekens, J. P. LaRiviere, and M. W. Wara (2015), The evolution of the equatorial thermocline and the early Pliocene El Padremean state, *Geophys. Res. Lett.*, 42(12), 4878–4887, doi:10.1002/2015GL064215.
- Gersonde, R., X. Crosta, A. Abelmann, and L. Armand (2005), Sea-surface temperature and sea ice distribution of the Southern Ocean at the EPILOG Last Glacial Maximum—a circum-Antarctic view based on siliceous microfossil records, *Quat. Sci. Rev.*, 24(7), 869–896, doi:10.1016/j.quascirev.2004.07.015.
- Groeneveld, J., and C. M. Chiessi (2011), Mg/Ca of *Globorotalia inflata* as a recorder of permanent thermocline temperatures in the South Atlantic, *Paleoceanography*, 26(2), doi:10.1029/2010PA001940.
- Hartin, C. A., R. A. Fine, and I. Kamenkovich (2013), Comparison of Subantarctic Mode Water and Antarctic Intermediate Water Formation Rates in the South Pacific Between Ncar- CCSM4 and observations, *Geophys. Res. Lett.*
- Hartin, C. A., R. Fine, B. M. Sloyan, L. D. Talley, T. K. Chereskin, and J. Happell (2011), Formation rates of Subantarctic mode water and Antarctic intermediate water within the South Pacific, *Deep-Sea Res. Part I*, 58, 524–534, doi:10.1016/j.dsr.2011.02.010.
- Hasson, A., A. Koch-Larrouy, R. Morrow, M. Juza, and T. Penduff (2011), The origin and fate of mode water in the southern Pacific Ocean, *Ocean Dynamics*, 62(3), 335–354, doi:10.1007/s10236-011-0507-3.
- Hathorne, E. C., R. H. James, and R. S. Lampitt (2009), Environmental versus biomineralization controls on the intratest variation in the trace element composition of the planktonic foraminifera *G. inflata* and *G. scitula*, *Paleoceanography*, 24(4), n/a–n/a,

doi:10.1029/2009PA001742.

- Hayward, B. W., A. T. Sabaa, A. Kolodziej, M. P. Crundwell, S. Steph, G. H. Scott, H. L. Neil, H. C. Bostock, L. Carter, and H. R. Grenfell (2012), Planktic foraminifera-based sea-surface temperature record in the Tasman Sea and history of the Subtropical Front around New Zealand, over the last one million years, *Marine Micropaleontology*, 82-83(C), 13–27, doi:10.1016/j.marmicro.2011.10.003.
- Herraiz-Borreguero, L., and S. R. Rintoul (2011a), Regional circulation and its impact on upper ocean variability south of Tasmania, *Deep Sea Research Part II: Topical Studies in Oceanography*, 58, 2071–2081, doi:10.1016/j.dsr2.2011.05.022.
- Herraiz-Borreguero, L., and S. R. Rintoul (2011b), Subantarctic mode water: distribution and circulation, *Ocean Dynamics*, 61(1), 103–126, doi:10.1007/s10236-010-0352-9.
- Ho, S. L., G. Mollenhauer, F. Lamy, A. Martínez-García, M. Mohtadi, R. Gersonde, D. Hebbeln, S. Nuñez-Ricardo, A. Rosell-Melé, and R. Tiedemann (2012), Sea surface temperature variability in the Pacific sector of the Southern Ocean over the past 700 kyr, *Paleoceanography*, 27(4), PA4202, doi:10.1029/2012PA002317.
- Holte, J. W., L. D. Talley, T. K. Chereskin, and B. M. Sloyan (2013), Subantarctic mode water in the southeast Pacific: Effect of exchange across the Subantarctic Front, *J. Geophys. Res. Oceans*, 118(4), 2052–2066, doi:10.1002/jgrc.20144.
- Holte, J. W., L. D. Talley, T. K. Chereskin, and B. M. Sloyan (2012), The role of air-sea fluxes in Subantarctic Mode Water formation, *J. Geophys. Res.*, 117, C03040, doi:10.1029/2011JC007798.
- Kaiser, J., F. Lamy, and D. Hebbeln (2005), A 70-kyr sea surface temperature record off southern Chile (Ocean Drilling Program Site 1233), *Paleoceanography*, 20(4), doi:10.1029/2005PA001146.
- King, A. L., and W. R. Howard (2005), $\delta^{18}\text{O}$ seasonality of planktonic foraminifera from Southern Ocean sediment traps: latitudinal gradients and implications for paleoclimate reconstructions, *Marine Micropaleontology*, 56(1-2), 1–24, doi:10.1016/j.marmicro.2005.02.008.
- Kohfeld, K. E., R. M. Graham, A. M. de Boer, L. C. Sime, E. W. Wolff, C. Le Quéré, and L. Bopp (2013), Southern Hemisphere westerly wind changes during the Last Glacial Maximum: paleo-data synthesis, *Quat. Sci. Rev.*, 68, 76–95, doi:10.1016/j.quascirev.2013.01.017.
- Lambert, F., B. Delmonte, J. R. Petit, M. Bigler, P. R. Kaufmann, M. A. Hutterli, T. F. Stocker, U. Ruth, J. P. Steffensen, and V. Maggi (2008), Dust-climate couplings over the past 800,000 years from the EPICA Dome C ice core, *Nature*, 452(7187), 616–619, doi:10.1038/nature06763.
- LeGrande, A. N., and G. A. Schmidt (2006), Global gridded data set of the oxygen isotopic composition in seawater, *Geophys. Res. Lett.*, 33(12), L12604, doi:10.1029/2006GL026011.
- LeGrande, A. N., and G. A. Schmidt (2011), Water isotopologues as a quantitative paleosalinity proxy, *Paleoceanography*, 26(3), PA3225, doi:10.1029/2010PA002043.

- Lisiecki, L. E., and M. E. Raymo (2005), A Pliocene-Pleistocene stack of 57 globally distributed benthic $\delta^{18}\text{O}$ records, *Paleoceanography*, 20(1), doi:10.1029/2004PA001071.
- Liu, Z., and M. Alexander (2007), Atmospheric bridge, oceanic tunnel, and global climatic teleconnections, *Rev. Geophys.*, 45(2), RG2005, doi:10.1029/2005RG000172.
- Liu, Z., and T. D. Herbert (2004), High-latitude influence on the eastern equatorial Pacific climate in the early Pleistocene epoch, *Nature*, doi:10.1038/nature02295.
- Liu, Z., S. I. Shin, B. Otto-Bliesner, J. E. Kutzbach, E. C. Brady, and D. E. Lee (2002), Tropical cooling at the last glacial maximum and extratropical ocean ventilation, *Geophys. Res. Lett.*, 29(10), 1409, doi:10.1029/2001GL013938.
- Lončarić, N., F. J. Peeters, D. Kroon, and G.-J. A. Brummer (2006), Oxygen isotope ecology of recent planktic foraminifera at the central Walvis Ridge (SE Atlantic), *Paleoceanography*, 21(3), doi:10.1029/2005PA001207.
- Loubere, P., and S. Bennett (2008), Southern Ocean biogeochemical impact on the tropical ocean: Stable isotope records from the Pacific for the past 25,000 years, *Global and Planetary Change*, 63(4), 333–340, doi:10.1016/j.gloplacha.2008.08.001.
- Loveday, B. R., P. Penven, and C. J. C. Reason (2015), Southern Annular Mode and westerly-wind-driven changes in Indian-Atlantic exchange mechanisms, *Geophys. Res. Lett.*, 42(12), 4912–4921, doi:10.1002/2015GL064256.
- Lovenduski, N. S., and N. Gruber (2005), Impact of the Southern Annular Mode on Southern Ocean circulation and biology, *Geophys. Res. Lett.*, 32, L11603, doi:10.1029/2005GL022727.
- Luz, B. (1977), Late Pleistocene paleoclimates of the South Pacific based on statistical analysis of planktonic foraminifers, *Palaeogeogr. Palaeoclimatol. Palaeoecol.*, 22(1), 61–78.
- Marlow, J. R., C. B. Lange, G. Wefer, and A. Rosell-Melé (2000), Upwelling intensification as part of the Pliocene-Pleistocene climate transition, *Science*.
- Marr, J. P., H. C. Bostock, L. Carter, A. Bolton, and E. Smith (2013), Differential effects of cleaning procedures on the trace element chemistry of planktonic foraminifera, *Chemical Geology*, 351, 310–323, doi:10.1016/j.chemgeo.2013.05.019.
- Martínez-Méndez, G., D. Hebbeln, M. Mohtadi, F. Lamy, R. DePol-Holz, D. Reyes-Macaya, and T. Freudenthal (2013), Changes in the advection of Antarctic Intermediate Water to the northern Chilean coast during the last 970 kyr, *Paleoceanography*, 28, doi:10.1002/palo.20047.
- Mata, M. M., M. Tomczak, S. Wijffels, and J. A. Church (2000), East Australian Current volume transports at 30 degrees S: Estimates from the World Ocean Circulation Experiment hydrographic sections PR11/P6 and the PCM3 current meter array, *J. Geophys. Res.*, 105(C12), 28509–28526.
- Matsumoto, K., T. Oba, and J. Lynch-Stieglitz (2002), Interior hydrography and circulation of the glacial Pacific Ocean, *Quaternary Science*
- McCartney, M. S. (1977), Subantarctic Mode Water, in *A Voyage of Discovery, George*

Deacon 70th Anniversary Volume, edited by M. Angel, pp. 103–119, Pergamon, New York.

- McClymont, E. L., and A. Rosell-Melé (2005), Links between the onset of modern Walker circulation and the mid-Pleistocene climate transition, *Geol.*, 33(5), 389, doi:10.1130/G21292.1.
- Mekik, F., R. François, and M. Soon (2007), A novel approach to dissolution correction of Mg/Ca-based paleothermometry in the tropical Pacific, *Paleoceanography*, 22(3), doi:10.1029/2007PA001504.
- Molina-Kescher, M., M. Frank, and E. C. Hathorne (2014), Nd and Sr isotope compositions of different phases of surface sediments in the South Pacific: Extraction of seawater signatures, boundary exchange, and detrital/dust provenance, *Geochem. Geophys. Geosyst.*, doi:10.1002/2014GC005443.
- Moreno, P. I., I. Vilanova, and R. Villa-Martínez (2014), Southern Annular Mode-like changes in southwestern Patagonia at centennial timescales over the last three millennia, *Nature*, doi:10.1038/ncomms5375.
- Mortyn, P. G., C. D. Charles, and D. A. Hodell (2002), Southern Ocean upper water column structure over the last 140 kyr with emphasis on the glacial terminations, *Global and Planetary Change*, 34(3), 241–252.
- Naveira Garabato, A. C., L. Jullion, D. P. Stevens, K. J. Heywood, and B. A. King (2009), Variability of Subantarctic Mode Water and Antarctic Intermediate Water in the Drake Passage during the Late-Twentieth and Early-Twenty-First Centuries, *J. Climate*, 22(13), 3661–3688, doi:10.1175/2009JCLI2621.1.
- Nürnberg, D., and J. Groeneveld (2006), Pleistocene variability of the Subtropical Convergence at East Tasman Plateau: evidence from planktonic foraminiferal Mg/Ca (ODP Site 1172A), *Geochem. Geophys. Geosyst.*, 7, Q04P11, doi:10.1029/2005GC000984.
- Oke, P. R., and M. H. England (2004), Oceanic response to changes in the latitude of the Southern Hemisphere subpolar westerly winds, *J. Climate*, 17(5), 1040–1054.
- Orsi, A. H., T. Whitworth, and W. D. Nowlin (1995), On the meridional extent and fronts of the Antarctic Circumpolar Current, *Deep-Sea Res. Part I*, 42(5), 641–673.
- Pahnke, K., and R. Zahn (2005), Southern Hemisphere water mass conversion linked with North Atlantic climate variability, *Science*, 307, 1741–1746, doi:10.1126/science.1102163.
- Paillard, D., L. Labeyrie, and P. Yiou (1996), Macintosh Program performs time-series analysis, *EOS, Transactions American Geophysical Union*, 77(39), 379–379, doi:10.1029/96EO00259.
- Patrick, A., and R. C. Thunell (1997), Tropical Pacific sea surface temperatures and upper water column thermal structure during the last glacial maximum, *Paleoceanography*.
- Peeters, F. J. C., G.-J. A. Brummer, and G. Ganssen (2002), The effect of upwelling on the distribution and stable isotope composition of *Globigerina bulloides* and *Globigerinoides ruber*(planktic foraminifera) in modern surface waters of the NW Arabian Sea, *Global and*

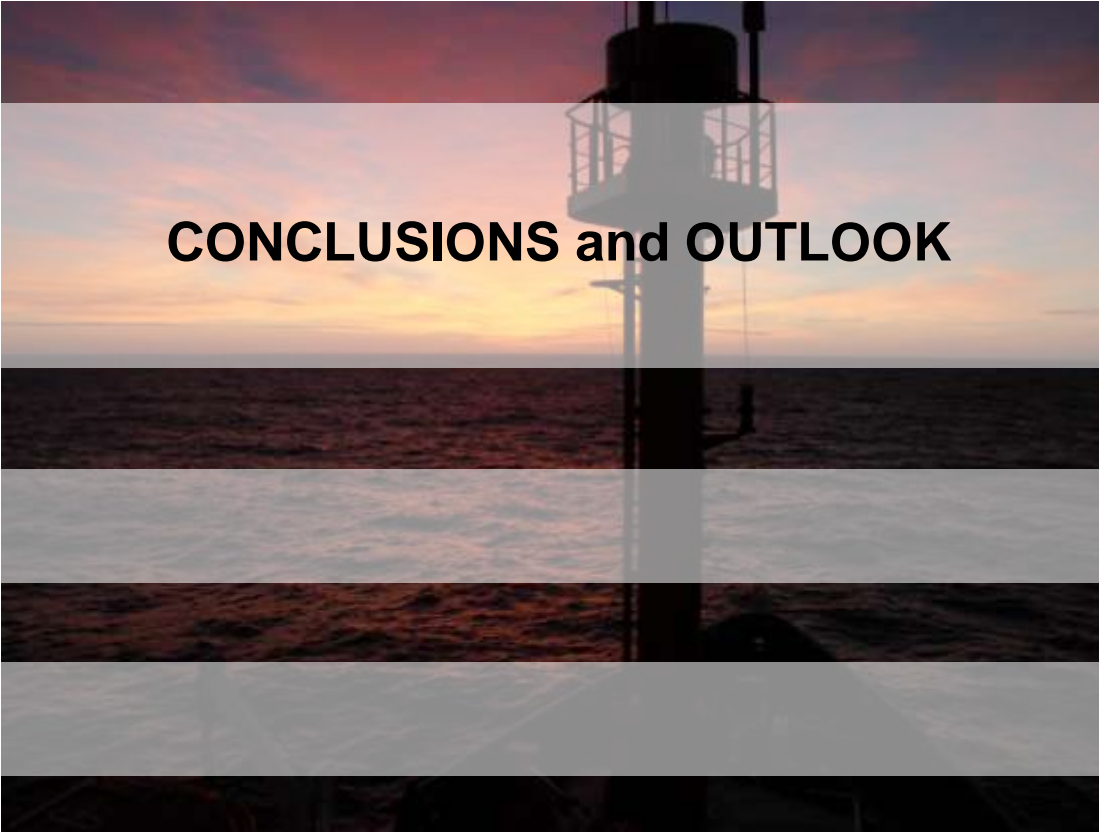
Planetary Change, 34(3), 269–291.

- Pena, L. D., I. Cacho, P. Ferretti, and M. A. Hall (2008), El Niño–Southern Oscillation–like variability during glacial terminations and interlatitudinal teleconnections, *Paleoceanography*, 23, PA3101, doi:10.1029/2008PA001620.
- Pena, L. D., S. L. Goldstein, S. R. Hemming, K. M. Jones, E. Calvo, C. Pelejero, and I. Cacho (2013), Rapid changes in meridional advection of Southern Ocean intermediate waters to the tropical Pacific during the last 30 kyr, *Earth Plan. Sci. Lett.*, 368, 20–32, doi:10.1016/j.epsl.2013.02.028.
- Qu, T., S. Gao, I. Fukumori, R. A. Fine, and E. J. Lindstrom (2008), Subduction of South Pacific waters, *Geophys. Res. Lett.*, 35(2), doi:10.1029/2007GL032605.
- Ravelo, A. C., and C. Hillaire-Marcel (2007), The Use of Oxygen and Carbon Isotopes of Foraminifera in Paleoceanography, in *Proxies in Late Cenozoic Paleoceanography*, vol. 1 of Developments in Marine Geology, edited by C. Hillaire-Marcel and A. De Vernal, pp. 735–764, Elsevier.
- Regenberg, M., A. Regenberg, D. Garbe-Schönberg, and D. W. Lea (2014), Global dissolution effects on planktonic foraminiferal Mg/Ca ratios controlled by the calcite-saturation state of bottom waters, *Paleoceanography*, doi:10.1002/2013PA002492.
- Regoli, F., T. de Garidel-Thoron, K. Tachikawa, Z. Jian, L. Ye, A. W. Droxler, G. Lenoir, M. Crucifix, N. Barbarin, and L. Beaufort (2015), Progressive shoaling of the equatorial Pacific thermocline over the last eight glacial periods, *Paleoceanography*, n/a–n/a, doi:10.1002/2014PA002696.
- Ribbe, J. (2001), Intermediate water mass production controlled by southern hemisphere winds, *Geophys. Res. Lett.*, 28(3), 535–538, doi:10.1029/2000GL012242.
- Roemmich, D. (2007), Super spin in the southern seas, *Nature*, 32(23), L23706, doi:10.1029/2005GL024701.
- Roemmich, D., and B. Cornuelle (1992), The subtropical mode waters of the South Pacific Ocean, *J. Phys. Oceanogr.*, 22(10), 1178–1187.
- Roemmich, D., J. Gilson, R. Davis, P. Sutton, S. Wijffels, and S. Riser (2007), Decadal Spinup of the South Pacific Subtropical Gyre, *J. Phys. Oceanogr.*, 37(2), 162–173, doi:10.1175/JPO3004.1.
- Rohling, E. J., and S. Cooke (1999), Stable oxygen and carbon isotopes in foraminiferal carbonate shells, in *Modern Foraminifera*, edited by B. K. Sen Gupta, pp. 239–258, Kluwer Academic Publishers, Dordrecht.
- Ronge, T. A., S. Steph, R. Tiedemann, M. Prange, U. Merkel, D. Nürnberg, and G. Kuhn (2015), Pushing the boundaries: Glacial/Interglacial variability of intermediate- and deep-waters in the southwest Pacific over the last 350,000 years, *Paleoceanography*, 30, 23–38, doi:10.1002/2014PA002727.
- Sagawa, T., A. Kuroyanagi, T. Irino, and M. Kuwae (2013), Seasonal variations in planktonic foraminiferal flux and oxygen isotopic composition in the western North Pacific: Implications for paleoceanographic reconstruction, *Mar. Micropaleontol.*, doi:10.1016/j.marmicro.2013.03.013.

- Sallée, J. B., K. Speer, S. Rintoul, and S. Wijffels (2010), Southern Ocean Thermocline Ventilation, *J. Phys. Oceanogr.*, *40*, 509–529, doi:10.1175/2009JPO4291.1.
- Sallée, J. B., N. Wienders, K. Speer, and R. Morrow (2006), Formation of subantarctic mode water in the southeastern Indian Ocean, *Ocean Dynamics*, *56*, 525–542, doi:10.1007/s10236-005-0054-x.
- Sarmiento, J. L., N. Gruber, M. A. Brzezinski, and J. P. Dunne (2004), High-latitude controls of thermocline nutrients and low latitude biological productivity, *Nature*, *427*, 56–60.
- Schiebel, R., J. Bijma, and C. Hemleben (1997), Population dynamics of the planktic foraminifer *Globigerina bulloides* from the eastern North Atlantic, *Deep Sea Research Part I: Oceanographic Research Papers*, *44*(9-10), 1701–1713, doi:10.1016/S0967-0637(97)00036-8.
- Schneider, W., and L. Bravo (2006), Argo profiling floats document Subantarctic Mode Water formation west of Drake Passage, *Geophys. Res. Lett.*, *33*, doi:10.1029/2006GL026463.
- Schneider, W., M. Fukasawa, J. Garcés-Vargas, L. Bravo, H. Uchida, T. Kawano, and R. Fuenzalida (2007), Spin-up of South Pacific subtropical gyre freshens and cools the upper layer of the eastern South Pacific Ocean, *Geophys. Res. Lett.*, *34*(24), doi:10.1029/2007GL031933.
- Shackleton, N. J. (1974), Attainment of isotopic equilibrium between ocean water and the benthonic foraminifera genus *Uvigerina*: isotopic changes in the ocean during the last glacial, *Cent. Nat. Rech. Sci. Colloq. Int.*, (219), 203–209.
- Sikes, E. L., W. R. Howard, C. R. Samson, T. S. Mahan, L. G. Robertson, and J. K. Volkman (2009), Southern Ocean seasonal temperature and Subtropical Front movement on the South Tasman Rise in the late Quaternary, *Paleoceanography*, *24*(2), doi:10.1029/2008PA001659.
- Sloyan, B. M., and S. R. Rintoul (2001a), Circulation, Renewal, and Modification of Antarctic Mode and Intermediate Water*, *J. Phys. Oceanogr.*, *31*, 1005–1030.
- Sloyan, B. M., and S. R. Rintoul (2001b), The Southern Ocean limb of the global deep overturning circulation, *J. Phys. Oceanogr.*, *31*(1), 143–173.
- Sloyan, B. M., L. D. Talley, T. K. Chereskin, R. Fine, and J. Holte (2010), Antarctic Intermediate Water and Subantarctic Mode Water formation in the Southeast Pacific: the role of turbulent mixing, *J. Phys. Oceanogr.*, *40*, 1558–1574, doi:10.1175/2010JPO4114.1.
- Speer, K., S. R. Rintoul, and B. Sloyan (2000), The Diabatic Deacon Cell*, *J. Phys. Oceanogr.*, *30*(12), 3212–3222, doi:10.1175/1520-0485(2000)030<3212:TDDC>2.0.CO;2.
- Spero, H. J., and D. W. Lea (2002), The cause of carbon isotope minimum events on glacial terminations, *Science*, *296*(5567), 522–525.
- Steph, S., M. Regenberg, R. Tiedemann, S. Mulitza, and D. Nürnberg (2009), Stable isotopes of planktonic foraminifera from tropical Atlantic/Caribbean core-tops: Implications for reconstructing upper ocean stratification, *Marine Micropaleontology*, *71*(1-2), 1–19, doi:10.1016/j.marmicro.2008.12.004.

- Talley, L. D., G. L. Pickard, W. J. Emery, and J. H. Swift (2011), *Descriptive physical oceanography: an introduction*, Academic press.
- Tapia, R., D. Nürnberg, T. Ronge, and R. Tiedemann (2015), Disparities in glacial advection of Southern Ocean Intermediate Water to the South Pacific Gyre, *Earth Plan. Sci. Lett.*, *410*, 152–164, doi:10.1016/j.epsl.2014.11.031.
- Thornalley, D. J. R., H. Elderfield, and I. N. McCave (2008), Holocene oscillations in temperature and salinity of the surface subpolar North Atlantic, *Nature*, *457*(7230), 711–714, doi:10.1038/nature07717.
- Tiedemann, R., F. Lamy, M. Molina-Kescher, R. Tapia, D. Poggemann, D. Nürnberg, and C. participants (2014), FS Sonne Fahrtbericht/Cruise Report SO213-SOPATRA: South Pacific Paleoceanographic Transects Geodynamic and Climatic Variability in Space and Time, Leg 1: Valparaiso/Chile - Valparaiso/Chile, 27.12.2010 - 12.01.2011 and Leg 2: Valparaiso/Chile - Wellington/New Zealand, 12.01.2011 - 07.03.2011,, 111, doi:10.2312/cr_so213.
- Toggweiler, J. R., J. L. Russell, and S. R. Carson (2006), Midlatitude westerlies, atmospheric CO₂, and climate change during the ice ages, *Paleoceanography*, *21*(2), doi:10.1029/2005PA001154.
- Tsimplis, M., S. Bacon, and H. Bryden (1998), The circulation of the subtropical South Pacific derived from hydrographic data, *J. Geophys. Res.*, *103*(C10), 21443–21–468.
- Tsubouchi, T., T. Suga, and K. Hanawa (2007), Three Types of South Pacific Subtropical Mode Waters: Their Relation to the Large-Scale Circulation of the South Pacific Subtropical Gyre and Their Temporal Variability, *J. Phys. Oceanogr.*, *37*(10), 2478–2490, doi:10.1175/JPO3132.1.
- Verleye, T. J., and S. Louwye (2010), Late Quaternary environmental changes and latitudinal shifts of the Antarctic Circumpolar Current as recorded by dinoflagellate cysts from offshore Chile (41° S), *Quat. Sci. Rev.*, *29*, 1025–1039, doi:10.1016/j.quascirev.2010.01.009.
- Vivier, F., D. Iudicone, F. Busdraghi, and Y. H. Park (2010), Dynamics of sea-surface temperature anomalies in the Southern Ocean diagnosed from a 2D mixed-layer model, *Clim. Dyn.*, *34*(2), 153–184.
- Wijffels, S. E., J. M. Toole, and R. Davis (2001), Revisiting the South Pacific subtropical circulation: A synthesis of World Ocean Circulation Experiment observations along 32°S, *J. Geophys. Res.*, *106*(C9), 19481–19513, doi:10.1029/1999JC000118.
- Wilke, I., H. Meggers, and T. Bickert (2009), Depth habitats and seasonal distributions of recent planktic foraminifers in the Canary Islands region (29° N) based on oxygen isotopes, *Deep-Sea Res. Part I*, *56*(1), 89–106, doi:doi:10.1016/j.dsr.2008.08.001.
- Xue, L., L. Gao, W. J. Cai, W. Yu, and M. Wei (2015), Response of sea surface fugacity of CO₂ to the SAM shift south of Tasmania: Regional differences, *Geophys. Res. Lett.*, *42*(10), 3973–3979, doi:10.1002/2015GL063926.
- Ziegler, M., P. Diz, I. R. Hall, and R. Zahn (2013), Millennial-scale changes in atmospheric CO₂ levels linked to the Southern Ocean carbon isotope gradient and dust flux, *Nat. Geosci.*, *6*(6), 457–461, doi:10.1038/ngeo1782.

Zilberman, N. V., D. H. Roemmich, and S. T. Gille (2014), Meridional volume transport in the South Pacific: Mean and SAM-related variability, *J. Geophys. Res. Oceans*, 119(4), 2658–2678, doi:10.1002/2013JC009688.



CONCLUSIONS and OUTLOOK

CHAPTER 6

6.1 General Conclusions

This thesis contributes to reducing the spatio-temporal gap in our understanding of past oceanographic changes in the data-sparse central South Pacific. Paired Mg/Ca- $\delta^{18}\text{O}_c$ analyses on multispecies planktic foraminifera used in this thesis allow us to provide the first surface and subsurface Mg/Ca-temperatures and paleosalinity (expressed as $\delta^{18}\text{O}_{\text{SW-IVC}}$) records from the central south Pacific Gyre (SPG) across various timescales, spanning the Holocene back to 600 kyr. The multiproxy approach (combining planktic foraminiferal Mg/Ca, $\delta^{18}\text{O}$ and $\delta^{13}\text{C}$) allow us draw lines between the evolution of the upper water column structure (from surface to thermocline) at the SPG's thermocline and the northward advection of the intermediate waters formed at the Southern Ocean through different timescales.

Here I briefly summarize the main conclusions presented in the different chapters that compose this thesis as well as present some perspectives for future studies.

Chapter 3. The comparison of climatological (e.g. World Ocean Atlas), oceanographic (e.g. World Ocean Circulation Experiment, Global Ocean Data Analysis Project, Carbon dioxide In the Atlantic Ocean) and Mg/Ca data from surface sediments presented in this thesis support the idea that the Mg/Ca analysis on planktic foraminiferal calcite can provide reliable results even in unfavorable environments such as the deep Pacific, where the calcite dissolution may affect the initial Mg/Ca signal. The reconstructed downcore sea surface temperatures (Mg/Ca_{SST}) reinforce early suggestions of a low sensitivity of central South Pacific (~44°S) to glacial-interglacial changes. In contrast, the subsurface at the SPG is characterized by large glacial-interglacial variations in temperature and paleosalinity. The large variability highlights the major role played by the intermediate water formed in the Southern Ocean in ventilating the SPG's thermocline.

In the eastern Pacific, enhanced presence of intermediate water at the lower latitudes during glacial stages is a scenario widely accepted in the literature. However, our results suggest variable presence of intermediate waters at the SPG's thermocline during glacial, with colder- and fresher-than-Holocene subsurface waters during LGM, versus warmer- and saltier-than-Holocene subsurface waters during MIS 6. These findings underline the spatial heterogeneity in the glacial advection of intermediate waters in the Pacific basin.

Chapter 4. The reconstructed water column structure further south (~54° S) reinforces the initial suggestions presented in Chapter 3. There the subsurface freshening during glacial stages suggests a stronger influence of cold-fresh southern sourced waters (namely AAIW) without discernible glacial differences between LGM and MIS 6. Since the intermediate waters formed in the Southern Ocean play a major role in ventilating the SPG's

thermocline, the observed glacial differences further north (44° S) (Chapter 3) are more likely a result of changes in the advection of the intermediate waters rather than a ceasing in their formation. At 54°S the reconstructed temperature and salinity at surface and subsurface suggest no substantial northward migration of the subantarctic front (SAF) during glacial stages, which argues against previous suggestion of a frontal displacement as the main mechanism controlling the formation/advection of intermediate water toward lower latitudes.

The reconstructed subsurface $\delta^{13}\text{C}$ signatures of the AAIW show substantial differences between the time windows selected to characterize glacial conditions, PGM (~29 – ~17ka BP) and LGM (~180 – ~150ka BP). Assuming no large changes in productivity and air-sea exchange caused by changes in temperature and/or ice coverage, the lower $\delta^{13}\text{C}$ values during PGM (relative to LGM) is likely due to a deepening of the upwelling depth, since the contribution of deep low $\delta^{13}\text{C}$ waters can affect the $\delta^{13}\text{C}$ values. A larger contribution of deep low $\delta^{13}\text{C}$ waters is further supported by the similarity in $\delta^{13}\text{C}$ values between the PGM and Carbon Isotope Minimum Events (CIMEs); the latter are caused by the reallocation of “old” low $\delta^{13}\text{C}$ deep waters from the ocean interior toward the surface during glacial terminations.

Subsurface latitudinal gradient between the central South Pacific (54° S) and the SPG (45° S) during PGM suggest a reduced influence of intermediate waters on the thermocline in the SPG. Additionally, glacial vertical gradients ($\text{Mg}/\text{Ca}_{\text{Temperature}}$ and $\delta^{18}\text{O}_{\text{SW}}$) at these localities imply glacial differences in the tilt of the surface densities associated with the intermediate waters. Together, these observations point to glacial differences in the convection depth of AAIW injected into the SPG. The contrasting upper ocean' structure between LGM and PGM, in terms of thermal gradient, upwelling depth, Ekman transport, downwelling, and latitudinal gradients (surface densities) resembles the effects that the different phases of the modern Southern Annular Mode (SAM) have on the present day's ocean. SAM-like alterations of the southern hemisphere wind patterns (e.g. wind intensification) offers a plausible explanation for inferred dissimilar glacial scenarios in the subsurface central Pacific in the absence of oceanic frontal migrations.

Chapter 5 On longer time scales (~600 kyr), the reconstructed $\text{Mg}/\text{Ca}_{\text{SST}}$ at SPG (~44° S) agrees with the finding of a relatively small glacial-interglacial amplitude (~3 °C) (Chapter 3). Exceptionally warm temperatures are observed in MIS 15, MIS 13 and MIS 11. At subsurface, the evolution in the temperature and paleosalinity records show/demonstrate a drastic step change likely linked to the influence/presence of intermediate waters, shifting from colder/fresher to warmer/saltier conditions at 320–360 kyr. This drastic shift differs substantially from previously observed intermediate waters' glacial-interglacial variability associated with the Southern Ocean air-sea forcing (e.g. westerly wind intensity), suggesting

that it is controlled by a different factor than air-sea forcing. It probably has to do with the water column conditions before the formation of intermediate waters, for instance a water column with lower heat storage can generate a deeper mixed layer, which in turn results in a colder mode of intermediate waters.

6.2 Future perspectives for future works

To date, two opposing scenarios regarding the AAIW's evolution in the South Pacific have been proposed, i.e., a stronger AAIW signal during glacial stages in the southeast Pacific (SEP) [Martínez-Méndez et al., 2013] versus weaker presence of AAIW during glacial stages in the southwest Pacific (SWP) [Pahnke and Zahn, 2005; Ronge et al., 2015], which are explained by invoking regional differences. Since four types of AAIW have been defined in the modern Pacific with each type originating from a specific formation area [Bostock et al., 2013], it is possible that the abovementioned SWP-SEP dichotomy reflects differences in their contribution to the "intermediate water complex" (SAMW-AAIW). Further, Chapter 3/4 also demonstrates the spatial variability in the presence of intermediate waters. Therefore, future studies should focus on not only the temporal evolution of the intermediate water but also increasing the spatial coverage to better understand the processes and the influence of intermediate waters in the South Pacific.

In the east Pacific, the evolution of intermediate water has been inferred from records at intermediate latitudes and the equatorial Pacific. Evolution build on the assumption that changes at intermediate depths depend of the northward transport of the Antarctic Intermediate Water (AAIW) formed between the Subantarctic Front (SAF) and the Antarctic Polar Front (APF) in the southeast Pacific. In fact, the large glacial migration of the oceanic fronts in the SEP has been invoked to support a plausible northward migration of the AAIW's formation center, hence allowing a further northward penetration of this water mass. Recently, it has been proposed that during the LGM the AAIW flowed at greater depths and presented a smaller vertical coverage (shorter distance between its upper and lower boundary) [Bova et al., 2015]. Although this scenario agree with the larger signal of AAIW observed by Martínez-Méndez et al., [2013], this certainly disagree with other studies located at similar latitude in the equatorial Pacific that suggest a larger presence of intermediate water at thermocline depths, therefore larger presence at shallower depths [e.g. Pena et al., 2008; Pena et al., 2013]. It is evident that studies in the AAIW's formation are necessary, in order to validate the different scenarios that have been proposed during the last decades.

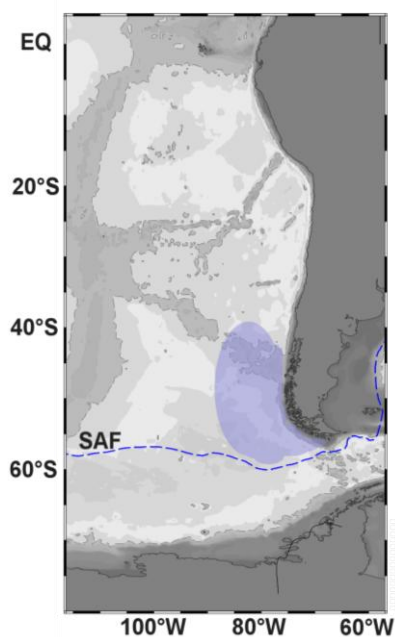


Figure 6.1 Bathymetric chart showing (shaded area) a possible area of interest to future studies regarding the evolution of the intermediate water formed at SEP.

6.3 Data handling

All data presented in this thesis will be available on the Pangaea ® database (www.pangaea.de) once the respective article are published online, i.e. data presented in Chapter 3 is available in <http://doi.pangaea.de/10.1594/PANGAEA.841469>

6.4 References

- Bostock, H. C., S. E. Mikaloff Fletcher, and M. J. M. Williams (2013), Estimating carbonate parameters from hydrographic data for the intermediate and deep waters of the Southern Hemisphere oceans, *Biogeosciences*, 10(10), 6199–6213, doi:10.5194/bg-10-6199-2013.
- Bova, S. C., T. Herbert, Y. Rosenthal, J. Kalansky, M. Altabet, C. Chazen, A. Mojarro, and J. Zech (2015), Links between Eastern Equatorial Pacific Stratification and Atmospheric CO₂ Rise during the last Deglaciation, *Paleoceanography*, doi:10.1002/2015PA002816.
- Martínez-Méndez, G., D. Hebbeln, M. Mohtadi, F. Lamy, R. DePol-Holz, D. Reyes-Macaya, and T. Freudenthal (2013), Changes in the advection of Antarctic Intermediate Water to the northern Chilean coast during the last 970 kyr, *Paleoceanography*, 28, doi:10.1002/palo.20047.
- Pahnke, K., and R. Zahn (2005), Southern Hemisphere water mass conversion linked with North Atlantic climate variability, *Science*, 307, 1741–1746, doi:10.1126/science.1102163.
- Pena, L. D., I. Cacho, P. Ferretti, and M. A. Hall (2008), El Niño–Southern Oscillation–like variability during glacial terminations and interlatitudinal teleconnections, *Paleoceanography*, 23, PA3101, doi:10.1029/2008PA001620.
- Pena, L. D., S. L. Goldstein, S. R. Hemming, K. M. Jones, E. Calvo, C. Pelejero, and I. Cacho (2013), Rapid changes in meridional advection of Southern Ocean intermediate

waters to the tropical Pacific during the last 30 kyr, *Earth Plan. Sci. Lett.*, 368, 20–32, doi:10.1016/j.epsl.2013.02.028.

Ronge, T. A., S. Steph, R. Tiedemann, M. Prange, U. Merkel, D. Nürnberg, and G. Kuhn (2015), Pushing the boundaries: Glacial/Interglacial variability of intermediate- and deep-waters in the southwest Pacific over the last 350,000 years, *Paleoceanography*, 30, 23–38, doi:10.1002/2014PA002727.

Appendix 1

Evolution of the sea surface temperature and $\delta^{18}\text{O}$ in the central South Pacific during the past 500 ka: Implications on ocean circulation

J. Ullermann¹, **R. Tapia**², F. Lamy¹, D. Nürnberg², R. Gersonde¹, R. Tiedemann¹

¹ Alfred Wegener Institute Helmholtz Centre for Polar and Marine Research, Am Alten Hafen 26, D – 27568, Bremerhaven, Germany

² GEOMAR – Helmholtz Centre for Ocean Research Kiel, Wischhofstr. 1–3, D–24148, Kiel, Germany.

In preparation

Abstract

Despite the Southern Ocean is central to understand past climate change, the long term paleoceanographic evolution of its Pacific sector remains largely unknown. Here, we present orbital scale surface water temperature (Mg/Ca-based) and $\delta^{18}\text{O}$ records of planktic foraminiferal species *G. bulloides*. The records from sediment cores collected in the Subantarctic and Polar Frontal Zone, central South Pacific (~55° S), at both sides of the East Pacific Rise and at the Pacific Antarctic Ridge, reach back to ~500 ka. Our results indicate that commonly used Mg/Ca calibration equations systematically overestimate temperatures by ~3 °C for the central South Pacific study area, whereas the amplitude ranges are correctly reflected. Further our results reveal that sea surface temperatures co-varied with Antarctic air temperatures showing similar relative strengths of glacials and interglacials, with amplitude changes ranging from 2.5 °C to 6.5 °C. The surface water $\delta^{18}\text{O}$ values show no glacial-interglacial modulation after ice volume correction, implying rather stable sea surface salinity. In consistence to previous studies, larger glacial-interglacial surface water temperature and $\delta^{18}\text{O}$ variations off New Zealand and Chile may imply surface circulation changes linked to the Antarctic Circumpolar Current and subtropical South Pacific gyre systems - an inference, which is partly supported by Earth System model simulations.

Appendix 2

Reduced admixture of North Atlantic Deep Water to the deep central South Pacific during the last two glacial periods

M. Molina-Kescher¹, M. Frank¹, **R. Tapia**¹, T. A. Ronge², D. Nürnberg¹, R. Tiedemann²

¹ GEOMAR – Helmholtz Centre for Ocean Research Kiel, Wischhofstr. 1–3, D–24148, Kiel, Germany.

² Alfred Wegener Institute Helmholtz Centre for Polar and Marine Research, Am Alten Hafen 26, D – 27568, Bremerhaven, Germany

In revision in Paleooceanography

Abstract

The South Pacific is a sensitive location for the variability of the global oceanic thermohaline circulation given that deep waters from the Atlantic Ocean, the Southern Ocean, and the Pacific basin are exchanged. Here we reconstruct the deep-water circulation of the central South Pacific for the last two glacial cycles (from 240,000 years ago to the Holocene) based on radiogenic neodymium (Nd) and lead (Pb) isotope records complemented by benthic stable carbon data obtained from two sediment cores located on the flanks of the East Pacific Rise. The records show small but consistent glacial/interglacial changes in all three isotopic systems with interglacial average values of -5.8 and 18.757 for ϵ_{Nd} and $^{206}\text{Pb}/^{204}\text{Pb}$, respectively, whereas glacial averages are -5.3 and 18.744. Comparison of this variability of Circumpolar Deep Water (CDW) to previously published records along the pathway of the global thermohaline circulation is consistent with reduced admixture of North Atlantic Deep Water (NADW) to CDW during cold stages. The absolute values and amplitudes of the benthic $\delta^{13}\text{C}$ variations are essentially indistinguishable from other records of the Southern Hemisphere and confirm that the low central South Pacific sedimentation rates did not result in a reduction of the amplitude of any of the measured proxies. In addition, the combined detrital Nd and strontium ($^{87}\text{Sr}/^{86}\text{Sr}$) isotope signatures imply that Australian and New Zealand dust has remained the principal contributor of lithogenic material to the central South Pacific.

Appendix 3

Data Compilation

Here I summarize the unpublished data presented in the different chapters that compose this thesis.

Glacial Signature of Antarctic Intermediate Water at the Central South Pacific: Implications for Subsurface Transfer of Climatic Signal

Table PS75/059-2 bulk data

Depth (cm)	Age (Kyr)	<i>G. bulloides</i>			<i>G. inflata</i>		
		<i>Mg/Ca</i> <i>mmolmol</i> ⁻¹	$\delta^{18}\text{O}$ ‰	$\delta^{13}\text{C}$ ‰	<i>Mg/Ca</i> <i>mmolmol</i> ⁻¹	$\delta^{18}\text{O}$ ‰	$\delta^{13}\text{C}$ ‰
2.5	0.971	1.17	2.57	0.61	1.00	2.27	1.21
7.5	2.972	1.29	2.72	0.81	1.25	2.41	1.29
12.5	4.973	1.34	2.84	0.68	1.28	2.48	1.33
17.5	6.974	1.31	2.73	0.69	1.14	2.54	1.33
22.5	8.721	1.32	2.67	0.38		2.47	1.06
27.5	10.010	1.41	2.78	0.52	1.23	2.94	1.23
32.5	11.298	1.56	2.63	0.41	1.23	2.58	1.40
37.5	12.587	1.37	2.76	-0.11		3.00	1.00
42.5	13.876	1.19	2.96	-0.22		3.13	0.80
47.5	15.164	1.27	3.20	-0.10	1.09	2.41	1.22
52.5	16.453	1.10	3.66	0.24	0.94	3.53	1.12
57.5	17.742	1.23	3.73	0.39	1.05	3.52	0.85
62.5	19.643	0.99	3.70	0.92	1.12	3.21	1.07
67.5	22.168	0.98	4.15	0.77	0.63	4.06	1.13
72.5	24.692	1.03	3.85	0.71		3.89	1.20
77.5	27.217	1.13	4.00	1.01	0.79	3.62	1.31
82.5	29.741	1.11	4.01	0.91	0.85	4.17	1.24
87.5	32.266	0.90	3.82	1.20	0.70	3.67	0.87
92.5	34.790	0.91	3.94	1.08	0.93	3.88	1.28
97.5	37.315	0.98	3.85	0.95	0.73	3.70	1.46
102.5	39.839	0.98	3.83	0.95	0.78	3.70	1.52
107.5	42.364	1.04	3.61	0.65	0.95	3.66	1.25
112.5	44.888	1.13	3.85	0.83	0.95	3.37	1.26
117.5	47.413	1.03	3.80	0.63	0.90	3.42	1.33
122.5	49.937	1.03	3.52	1.00	0.91	3.49	1.14
127.5	52.462	1.01	3.65	0.67	0.94	3.60	1.27
132.5	54.986	1.10	3.53	0.52	1.02	3.43	1.18
137.5	57.511	1.11	3.50	0.55	1.02	3.52	0.93
142.5	59.549	1.07	3.56	0.66	0.87	3.58	0.86
147.5	61.135	1.11	3.77	0.75	0.91	3.65	1.02

152.5	62.720	0.99	3.79	0.97	0.88	3.28	1.07
157.5	64.305	0.93	3.75	1.03	0.91	3.50	1.17
162.5	65.891	1.03	3.55	0.78	0.86	3.41	1.20
167.5	67.476	1.04	3.59	1.16	0.95	3.45	1.27
172.5	69.062	1.20	3.52	0.74	0.96	3.42	1.32
177.5	70.647	1.08	3.34	1.35	1.07	3.37	1.20
182.5	72.022	1.12	3.40	1.34	0.91	3.43	1.49
187.5	73.396	1.24	3.26	0.86	1.17	3.36	1.44
192.5	74.770	1.19	3.16	0.85		3.23	1.42
197.5	76.145	1.33	3.07	0.55	1.14	3.16	1.34
202.5	77.519	1.25	3.09	0.66	1.14	3.16	1.42
207.5	78.893	1.41	3.00	0.59	1.12	3.04	1.27
212.5	80.267	1.36	3.03	0.69	1.11	3.17	1.34
217.5	81.641	1.40	2.96	-0.04	1.08	3.13	1.27
222.5	83.015	1.41	2.94	0.49	1.11	2.99	1.08
227.5	84.389	1.31	2.90	0.57	1.05	3.08	1.30
232.5	85.763	1.29	3.01	0.48	1.04	2.89	1.31
237.5	87.114	1.24	3.40	0.93	1.07	3.27	1.36
242.5	88.253	1.16	3.20	1.01	1.06	3.24	1.23
247.5	89.393	1.15	3.24	1.16		3.17	1.47
252.5	90.532	1.31	3.13	0.67	1.09	3.41	1.60
257.5	91.672	1.22	3.13	0.83	1.14	3.15	1.44
262.5	92.811	1.39	2.82	0.18	1.12	3.19	1.35
267.5	93.951	1.37	2.82	0.64	1.23	3.15	1.22
272.5	95.090	1.27	3.04	0.86	1.19	3.06	1.27
277.5	96.229	1.36	2.99	0.42	1.16	3.16	1.26
282.5	97.369	1.30	2.90	0.21	1.14	3.06	1.27
287.5	98.508	1.25	2.88	0.07	1.14	3.08	1.23
292.5	99.648	1.34	2.96	0.64	1.16	3.02	1.12
297.5	100.787	1.39	3.03	0.28	1.09	3.20	1.07
302.5	101.927	1.24	3.14	0.22	1.11	3.33	1.04
307.5	103.066	1.28	2.99	0.04	1.12	3.23	1.10
312.5	104.205	1.18	2.94	0.29	1.14	3.12	1.28
317.5	105.700	1.25	3.15	0.71	1.08	2.99	1.22
322.5	107.533	1.31	3.11	0.58	1.05	3.27	1.36
327.5	109.366	1.23	3.32	0.70	0.95	3.28	1.17
332.5	111.198	1.14	3.09	0.86	0.93	3.01	1.18
337.5	113.031	1.27	2.88	0.75	1.07	2.96	1.23
342.5	114.864	1.29	3.11	0.87	1.00	2.67	1.47
347.5	116.396	1.46	2.38	0.40	1.06	2.67	1.45
352.5	117.853	1.30	2.55	0.44	0.93	2.64	1.43
357.5	119.309	1.46	2.43	0.49	1.06	2.80	1.22
362.5	120.766	1.52	2.44	0.48	1.23	2.53	1.36
367.5	122.222	1.36	2.19	-0.06	1.21	2.38	1.18
372.5	123.679	1.39	2.12	0.20	1.27	2.45	1.18

Appendix

377.5	125.135	1.26	2.39	-0.10	1.24	2.40	1.22
382.5	126.592	1.39	2.55	-0.03	1.23	2.42	0.96
387.5	128.048	1.59	2.45	-0.13	1.25	2.38	0.97
392.5	129.505	1.53	2.76	0.08	1.28	2.32	1.10
397.5	130.961	2.02	3.07	-0.38	1.29	2.76	0.94
402.5	132.558	1.74	3.31	0.34	1.34	3.36	0.66
407.5	134.700	1.78	3.56	0.26	1.31	3.45	0.76
412.5	136.841	1.22	3.47	0.45	1.15	3.46	0.84
417.5	138.982	1.32	3.75	0.32	1.27	3.30	0.79
422.5	141.124	1.22	3.75	0.28	1.18	3.47	0.89
427.5	143.265	1.08	4.08	0.57	1.03	3.64	0.74
432.5	145.406	1.10	4.06	0.49	0.88	3.99	0.71
437.5	147.548	1.12	4.06	0.29	0.84	3.92	0.87
442.5	149.689	1.13	4.03	0.42	1.02	3.87	0.81
447.5	151.830	1.18	3.96	0.61	0.89	4.01	0.77
452.5	153.971	1.26	4.19	0.36	0.80	3.91	0.82
457.5	156.113	1.18	4.07	0.34	0.80	3.93	0.66
462.5	158.254	1.17	4.09	0.63	0.83	3.79	0.64
467.5	160.395	1.05	4.03	0.77	0.91	3.60	0.54
472.5	162.537	1.02	3.88	0.46	0.91	3.53	0.68
477.5	164.678	1.26	3.77	0.86	0.77	3.46	0.88
482.5	166.819	0.94	3.89	0.84	0.73	3.53	0.66
487.5	168.961	0.98	3.75	0.97	0.89	3.60	0.79
492.5	171.102	0.98	3.53	0.75	0.66	3.43	0.92
497.5	173.243	1.11	3.73	0.57	0.85	3.61	0.80
502.5	175.385	0.98	3.84	0.63	0.82	3.53	0.83
507.5	177.526	1.04	3.94	0.44	0.76	3.72	1.03
512.5	179.667	1.13	3.96	0.60	0.78	3.68	0.74
517.5	181.809	0.97	3.69	0.48	0.88	3.66	0.65
522.5	183.950	1.17	3.82	0.82	0.68	3.57	0.86
527.5	186.091	1.07	3.78	0.81	0.58	3.46	1.05
532.5	188.232	1.27	3.56	0.29	0.91	3.41	0.82
537.5	190.374	1.03	3.74	0.79	0.68		
542.5	192.515	0.97	3.32	1.28	0.72	2.96	1.23
547.5	194.656	1.02	3.42	1.27	0.68	2.91	1.21
552.5	196.798	0.88	3.39	1.37	0.65	3.00	1.43
557.5	198.924	1.16	3.26	1.20	0.75	2.80	1.16
562.5	200.645	1.22	2.98	0.71	0.77	2.71	1.22
567.5	202.366	1.02	3.09	1.08	0.79	2.80	1.13
572.5	204.086	1.17	3.21	0.72	0.87	2.66	1.01
577.5	205.807	1.11	2.91	0.50	1.08	2.75	1.17
582.5	207.527	1.15	2.96	0.28	0.99	2.58	0.95
587.5	209.248	1.35	2.95	0.61	0.87	2.78	1.12
592.5	210.968	1.19	2.85	0.45	0.91	2.76	1.30
597.5	212.689	1.21	2.90	0.53			

602.5	214.410	1.50	2.98	0.09			
607.5	216.130	1.35	3.34	0.08	1.10	2.91	1.04
612.5	217.851	1.26	3.29	-0.23	1.20	2.78	0.98
617.5	219.571	1.47	2.98	0.07	1.07	2.97	1.10
622.5	221.418	1.13	3.54	0.41	0.95	3.07	0.96
627.5	223.291	1.26	3.26	-0.18	1.10	2.92	1.26
632.5	225.163	1.31	3.33	-0.23	1.01	2.95	1.35
637.5	227.036	1.03	3.58	0.45	0.86	3.07	1.19
642.5	228.909	1.20	3.09	0.37	1.04	3.29	1.15
647.5	230.782	1.47	3.10	0.48	1.19	2.93	1.16
652.5	232.655	1.24	3.10	0.72	1.08	2.86	1.22
657.5	234.527	1.53	3.09	0.30	1.20	2.80	1.23
662.5	236.400	1.38	2.82	0.18	1.17	2.89	1.14
667.5	238.273	1.58	3.03	0.06	1.33	2.76	1.29
672.5	240.146	1.66	2.79	-0.30	1.33	2.69	1.02
677.5	242.019	1.53	2.81	-0.16	1.34	2.78	0.94
682.5	243.891	1.25	3.21	-0.24	1.32	3.02	0.98
687.5	245.764	1.55	3.09	-0.41	1.45	2.59	0.95
692.5	247.637	1.36	3.15	0.19	1.25	3.16	1.08
697.5	249.510	1.27	3.62	-0.05	1.16	3.21	1.00
702.5	251.383	0.43	3.84	0.32	0.97	3.42	1.05
707.5	252.913	0.65	4.02	0.33	1.00	3.14	1.03
712.5	254.404	0.72	4.05	0.34			
717.5	255.896	1.11	3.81	0.48	0.80	3.50	0.88
722.5	257.388	1.01	3.93	0.66	0.83	3.66	1.06
727.5	258.880	0.95	3.79	0.73	0.61	3.70	0.89

Table PS75/059-2 data temperature and water isotopic composition

Depth (cm)	Age (Kyr)	<i>G. bulloides</i>		<i>G. inflata</i>	
		Temperature (°C)	$\delta^{18}\text{O}_{\text{SW-IVC}}$	Temperature (°C)	$\delta^{18}\text{O}_{\text{SW-IVC}}$
2.5	0.971	8.5	0.82	6.56	0.04
7.5	2.972	9.3	1.19	8.73	0.72
12.5	4.973	9.7	1.39	8.99	0.85
17.5	6.974	9.5	1.18	7.83	0.58
22.5	8.721	9.6	1.06		
27.5	10.010	10.2	1.19	8.58	0.95
32.5	11.298	11.1	1.11	8.61	0.45
37.5	12.587	9.9	0.80		
42.5	13.876	8.6	0.51		
47.5	15.164	9.2	0.78	7.43	-0.46
52.5	16.453	7.9	0.82	5.87	0.18
57.5	17.742	8.9	1.10	7.05	0.42

Appendix

62.5	19.643	6.9	0.51	7.72	0.24
67.5	22.168	6.8	0.97	1.91	-0.42
72.5	24.692	7.3	0.85		
77.5	27.217	8.1	1.31	4.21	-0.08
82.5	29.741	8.0	1.42	4.88	0.78
87.5	32.266	6.0	0.76	2.98	-0.18
92.5	34.790	6.1	0.91	5.82	0.77
97.5	37.315	6.8	1.06	3.38	0.02
102.5	39.839	6.8	1.11	4.07	0.27
107.5	42.364	7.4	0.97	6.01	0.67
112.5	44.888	8.1	1.39	6.00	0.36
117.5	47.413	7.3	1.12	5.47	0.28
122.5	49.937	7.2	0.85	5.65	0.41
127.5	52.462	7.1	1.03	5.97	0.69
132.5	54.986	7.9	1.17	6.72	0.79
137.5	57.511	7.9	1.10	6.69	0.81
142.5	59.549	7.6	1.14	5.17	0.53
147.5	61.135	8.0	1.47	5.63	0.74
152.5	62.720	6.9	1.10	5.27	0.17
157.5	64.305	6.3	0.76	5.59	0.34
162.5	65.891	7.3	0.79	5.07	0.08
167.5	67.476	7.4	0.89	6.04	0.41
172.5	69.062	8.7	1.17	6.16	0.43
177.5	70.647	7.7	0.76	7.18	0.67
182.5	72.022	8.0	0.96	5.63	0.37
187.5	73.396	9.0	1.18	8.10	1.06
192.5	74.770	8.6	1.08		
197.5	76.145	9.6	1.29	7.86	0.94
202.5	77.519	9.1	1.21	7.87	0.98
207.5	78.893	10.2	1.47	7.65	0.87
212.5	80.267	9.8	1.46	7.55	1.02
217.5	81.641	10.1	1.46	7.34	0.93
222.5	83.015	10.2	1.44	7.55	0.82
227.5	84.389	9.5	1.15	7.01	0.70
232.5	85.763	9.4	1.15	6.92	0.41
237.5	87.114	9.0	1.39	7.19	0.80
242.5	88.253	8.4	1.02	7.13	0.74
247.5	89.393	8.3	1.04		
252.5	90.532	9.5	1.23	7.36	0.98
257.5	91.672	8.8	1.11	7.84	0.87
262.5	92.811	10.0	1.14	7.68	0.92
267.5	93.951	9.9	1.16	8.62	1.17
272.5	95.090	9.2	1.25	8.29	1.03
277.5	96.229	9.9	1.37	8.00	1.07
282.5	97.369	9.4	1.16	7.86	0.92

287.5	98.508	9.1	1.06	7.87	0.95
292.5	99.648	9.7	1.32	8.00	0.95
297.5	100.787	10.1	1.50	7.37	0.99
302.5	101.927	9.0	1.35	7.56	1.17
307.5	103.066	9.3	1.24	7.71	1.08
312.5	104.205	8.5	0.95	7.83	0.97
317.5	105.700	9.1	1.27	7.30	0.67
322.5	107.533	9.5	1.28	6.99	0.80
327.5	109.366	8.9	1.30	6.01	0.52
332.5	111.198	8.2	0.92	5.79	0.23
337.5	113.031	9.2	1.09	7.24	0.67
342.5	114.864	9.4	1.45	6.52	0.30
347.5	116.396	10.5	1.05	7.14	0.50
352.5	117.853	9.4	1.00	5.85	0.18
357.5	119.309	10.5	1.18	7.08	0.70
362.5	120.766	10.9	1.29	8.60	0.83
367.5	122.222	9.9	0.83	8.42	0.65
372.5	123.679	10.0	0.81	8.89	0.86
377.5	125.135	9.1	0.85	8.71	0.76
382.5	126.592	10.0	1.23	8.65	0.75
387.5	128.048	11.3	1.40	8.74	0.70
392.5	129.505	10.9	1.54	9.03	0.63
397.5	130.961	13.6	2.33	9.12	0.95
402.5	132.558	12.2	1.92	9.48	1.32
407.5	134.700	12.4	1.86	9.26	0.99
412.5	136.841	8.9	0.73	7.97	0.50
417.5	138.982	9.5	1.23	8.92	0.63
422.5	141.124	8.8	1.12	8.19	0.69
427.5	143.265	7.7	1.25	6.88	0.59
432.5	145.406	7.8	1.27	5.28	0.54
437.5	147.548	8.0	1.24	4.79	0.27
442.5	149.689	8.1	1.17	6.78	0.68
447.5	151.830	8.5	1.21	5.38	0.45
452.5	153.971	9.2	1.71	4.28	0.17
457.5	156.113	8.5	1.63	4.34	0.43
462.5	158.254	8.5	1.62	4.71	0.35
467.5	160.395	7.5	1.32	5.61	0.42
472.5	162.537	7.2	1.14	5.62	0.38
477.5	164.678	9.1	1.69	3.92	0.03
482.5	166.819	6.4	1.20	3.40	0.04
487.5	168.961	6.8	1.07	5.34	0.54
492.5	171.102	6.8	0.73	2.40	-0.53
497.5	173.243	7.9	1.19	4.94	0.30
502.5	175.385	6.8	1.07	4.61	0.19
507.5	177.526	7.3	1.33	3.79	0.18

Appendix

512.5	179.667	8.1	1.46	4.00	0.10
517.5	181.809	6.7	0.78	5.21	0.36
522.5	183.950	8.5	1.35	2.73	-0.40
527.5	186.091	7.6	1.17	1.11	-0.88
532.5	188.232	9.2	1.49	5.56	0.41
537.5	190.374	7.2	1.34	2.62	
542.5	192.515	6.7	0.91	3.23	-0.35
547.5	194.656	7.1	1.19	2.70	-0.49
552.5	196.798	5.8	0.86	2.20	-0.48
557.5	198.924	8.4	1.32	3.63	-0.37
562.5	200.645	8.9	1.11	3.97	-0.42
567.5	202.366	7.1	0.83	4.14	-0.25
572.5	204.086	8.4	1.32	5.17	-0.07
577.5	205.807	8.0	0.93	7.30	0.59
582.5	207.527	8.3	1.08	6.48	0.24
587.5	209.248	9.8	1.46	5.20	0.11
592.5	210.968	8.6	1.08	5.63	0.22
597.5	212.689	8.8	1.18		
602.5	214.410	10.8	1.78		
607.5	216.130	9.8	1.88	7.45	0.87
612.5	217.851	9.2	1.66	8.33	0.95
617.5	219.571	10.6	1.66	7.23	0.81
622.5	221.418	8.1	1.55	5.98	0.52
627.5	223.291	9.1	1.33	7.49	0.58
632.5	225.163	9.5	1.19	6.66	0.09
637.5	227.036	7.2	0.84	5.01	-0.25
642.5	228.909	8.6	0.82	6.89	0.58
647.5	230.782	10.6	1.39	8.27	0.65
652.5	232.655	9.0	1.20	7.28	0.53
657.5	234.527	10.9	1.85	8.36	0.92
662.5	236.400	10.0	1.35	8.09	0.94
667.5	238.273	11.2	1.76	9.38	1.04
672.5	240.146	11.7	1.57	9.40	0.90
677.5	242.019	10.9	1.27	9.49	0.88
682.5	243.891	9.1	1.05	9.29	0.90
687.5	245.764	11.1	1.21	10.23	0.51
692.5	247.637	9.8	0.86	8.79	0.61
697.5	249.510	9.2	1.14	8.02	0.43
702.5	251.383			6.26	0.24
707.5	252.913	2.9		6.51	0.09
712.5	254.404	4.0			
717.5	255.896	7.9	1.17	4.28	-0.09
722.5	257.388	7.1	1.08	4.73	0.18
727.5	258.880	6.5	0.81	1.52	-0.61

Table PS75/059-2 Contamination control

Depth (cm)	Age (Kyr)	<i>G. bulloides</i>			<i>G. inflata</i>		
		Mn/Ca <i>mmolmol</i> ⁻¹	Fe/Ca <i>mmolmol</i> ⁻¹	Al/Ca <i>mmolmol</i> ⁻¹	Mn/Ca <i>mmolmol</i> ⁻¹	Fe/Ca <i>mmolmol</i> ⁻¹	Al/Ca <i>mmolmol</i> ⁻¹
2.5	0.971	-0.005	0.003	-0.019	0.00	0.05	0.03
7.5	2.972	-0.004	0.024	0.004	0.01	0.11	0.10
12.5	4.973	-0.002	0.017	0.011	0.00	0.04	-0.05
17.5	6.974	-0.003	0.000	0.012	0.00	0.05	0.04
22.5	8.721	-0.003	0.006	-0.010	0.00	0.14	0.13
27.5	10.010	-0.004	0.008	0.000	0.00	0.07	0.63
32.5	11.298	-0.003	0.042	0.057	0.00	0.06	0.27
37.5	12.587	-0.002	0.011	0.026	0.00	0.12	0.16
42.5	13.876	-0.003	0.008	0.016	0.00	0.11	0.10
47.5	15.164	-0.004	0.026	0.003	0.00	0.07	0.07
52.5	16.453	-0.004	0.005	-0.002	0.00	0.02	-0.02
57.5	17.742	-0.002	0.060	0.079	0.00	0.02	0.00
62.5	19.643	-0.001	0.033	0.015	0.00	0.05	0.07
67.5	22.168	0.004	0.065	0.091	0.00	0.01	-0.03
72.5	24.692	0.002	0.012	0.040	0.01	0.16	0.15
77.5	27.217	0.003	0.029	0.055	0.01	0.04	0.03
82.5	29.741	0.004	0.030	0.059	0.01	0.05	0.04
87.5	32.266	0.005	0.002	0.024	0.00	0.02	0.01
92.5	34.790	0.005	0.017	0.083	0.01	0.07	0.05
97.5	37.315	0.004	0.006	0.106	0.00	0.01	0.01
102.5	39.839	0.009	0.011	0.079	0.01	0.02	0.00
107.5	42.364	0.010	0.006	0.085	0.02	0.07	0.06
112.5	44.888	0.016	0.012	0.160	0.04	0.01	0.01
117.5	47.413	0.014	0.010	0.002	0.02	0.03	0.03
122.5	49.937	0.014	0.003	-0.023	0.02	0.02	0.00
127.5	52.462	0.016	0.005	-0.014	0.03	0.10	0.07
132.5	54.986	0.016	0.015	0.005	0.03	0.02	0.01
137.5	57.511	0.017	0.028	0.001	0.02	0.07	0.05
142.5	59.549	0.012	0.015	-0.004	0.03	0.01	0.03
147.5	61.135	0.025	0.190	0.204	0.03	0.01	0.02
152.5	62.720	0.013	0.018	0.012	0.02	0.04	0.04
157.5	64.305	0.006	0.016	0.022	0.02	0.07	0.04
162.5	65.891	0.016	0.034	0.031	0.01	0.01	-0.03
167.5	67.476	0.021	0.077	0.084	0.04	0.01	-0.02
172.5	69.062	0.030	0.025	0.004	0.05	0.03	0.00
177.5	70.647	0.026	0.014	-0.016	0.05	0.01	0.01
182.5	72.022	0.034	0.008	-0.028	0.04	0.02	-0.01
187.5	73.396	0.040	0.094	0.066	0.09	0.02	0.00
192.5	74.770	0.049	0.051	-0.021	0.08	0.15	0.05
197.5	76.145	0.047	0.152	0.054	0.08	0.07	0.05
202.5	77.519	0.068	0.016	-0.020	0.08	0.03	0.00

Appendix

207.5	78.893	0.070	0.090	0.050	0.09	0.05	0.07
212.5	80.267	0.082	0.009	-0.025	0.08	0.05	0.03
217.5	81.641	0.060	0.063	-0.010	0.09	0.04	0.02
222.5	83.015	0.069	0.068	0.032	0.09	0.03	0.01
227.5	84.389	0.061	0.012	-0.036	0.08	0.02	0.00
232.5	85.763	0.063	0.036	-0.003	0.08	0.03	0.02
237.5	87.114	0.050	0.020	-0.035	0.07	0.03	0.02
242.5	88.253	0.037	0.010	-0.074	0.07	0.02	0.00
247.5	89.393	0.026	0.021	-0.016	0.08	0.17	0.14
252.5	90.532	0.055	0.054	0.012	0.07	0.05	0.03
257.5	91.672	0.042	0.007	-0.040	0.07	0.04	0.02
262.5	92.811	0.084	0.013	-0.037	0.09	0.02	0.01
267.5	93.951	0.081	0.047	-0.032	0.13	0.05	0.02
272.5	95.090	0.064	0.039	-0.025	0.11	0.06	0.04
277.5	96.229	0.099	0.067	-0.011	0.10	0.04	0.03
282.5	97.369	0.069	0.011	-0.056	0.10	0.02	0.01
287.5	98.508	0.073	0.033	-0.056	0.11	0.03	0.01
292.5	99.648	0.081	0.016	-0.054	0.11	0.02	0.00
297.5	100.787	0.086	0.107	0.024	0.10	0.02	0.00
302.5	101.927	0.072	0.018	-0.060	0.10	0.04	0.01
307.5	103.066	0.076	0.011	-0.077	0.10	0.07	0.07
312.5	104.205	0.069	0.006	-0.065	0.11	0.06	0.05
317.5	105.700	0.060	0.008	-0.010	0.08	0.01	-0.01
322.5	107.533	0.048	0.012	-0.067	0.08	0.02	0.02
327.5	109.366	0.060	0.009	-0.054	0.06	0.01	-0.01
332.5	111.198	0.030	0.009	-0.049	0.04	0.01	0.00
337.5	113.031	0.044	0.034	0.068	0.05	0.04	0.02
342.5	114.864	0.035	0.038	-0.024	0.03	0.04	0.02
347.5	116.396	0.056	0.014	-0.023	0.07	0.03	0.02
352.5	117.853	0.055	0.002	-0.077	0.05	0.03	0.01
357.5	119.309	0.054	0.054	-0.031	0.07	0.02	0.00
362.5	120.766	0.071	0.006	-0.072	0.10	0.08	0.06
367.5	122.222	0.052	0.007	-0.079	0.11	0.09	0.07
372.5	123.679	0.068	0.023	1.816	0.07	0.07	0.04
377.5	125.135	0.049	0.008	-0.094	0.08	0.04	0.02
382.5	126.592	0.073	0.011	-0.084	0.07	0.06	0.02
387.5	128.048	0.052	0.123	-0.016	0.09	0.03	0.00
392.5	129.505	0.055	0.154	0.048	0.08	0.02	0.00
397.5	130.961	0.063	0.510	0.408	0.09	0.06	0.02
402.5	132.558	0.064	0.284	0.198	0.09	0.06	0.03
407.5	134.700	0.063	0.363	0.337	0.08	0.05	0.03
412.5	136.841	0.036	0.054	-0.056	0.06	0.02	0.00
417.5	138.982	0.034	0.031	-0.046	0.07	0.05	0.04
422.5	141.124	0.025	0.057	-0.038	0.05	0.03	0.03
427.5	143.265	0.023	0.107	-0.005	0.03	0.03	0.03

432.5	145.406	0.019	0.021	-0.033	0.02	0.01	-0.02
437.5	147.548	0.023	0.113	0.009	0.04	0.00	-0.02
442.5	149.689	0.028	0.009	-0.005	0.06	0.02	0.01
447.5	151.830	0.032	0.014	0.062	0.03	0.01	0.05
452.5	153.971	0.025	0.136	0.076	-0.08	0.02	-0.49
457.5	156.113	0.022	0.164	0.166	0.03	0.01	-0.02
462.5	158.254	0.025	0.171	0.149	0.02	0.01	-0.04
467.5	160.395	0.017	0.029	-0.054	0.04	0.01	0.06
472.5	162.537	0.016	0.073	0.025	0.02	0.05	0.02
477.5	164.678	0.023	0.173	0.143	0.02	0.04	0.06
482.5	166.819	0.005	0.026	-0.036	0.02	0.02	0.02
487.5	168.961	0.022	0.029	-0.055	0.02	0.06	0.08
492.5	171.102	0.010	0.011	-0.087	0.01	0.01	-0.01
497.5	173.243	0.028	0.090	0.049	0.03	0.02	0.01
502.5	175.385	0.032	0.021	-0.028	0.04	0.01	-0.01
507.5	177.526	0.039	0.024	-0.070	0.04	0.01	-0.01
512.5	179.667	0.037	0.063	-0.021	0.01	0.01	-0.02
517.5	181.809	0.037	0.087	-0.054	0.05	0.01	-0.01
522.5	183.950	0.028	0.094	0.027	0.04	0.04	0.01
527.5	186.091	0.016	0.047	-0.046	0.00	0.04	0.03
532.5	188.232	0.046	0.005	-0.082	0.04	0.01	1.46
537.5	190.374	0.027	0.045	-0.095	0.02	0.01	0.02
542.5	192.515	0.019	0.056	-0.042	0.01	0.04	0.49
547.5	194.656	0.009	0.065	-0.023	0.01	0.01	0.07
552.5	196.798	0.009	0.025	-0.118	0.01	0.01	0.02
557.5	198.924	0.022	0.074	-0.042	0.01	0.02	0.02
562.5	200.645	0.020	0.070	-0.115	0.01	0.00	-0.01
567.5	202.366	0.025	0.031	-0.112	0.01	0.00	-0.01
572.5	204.086	0.031	0.019	-0.119	0.04	0.03	0.04
577.5	205.807	0.027	0.087	-0.060	0.04	0.07	0.06
582.5	207.527	0.029	0.010	-0.107	0.04	0.06	0.11
587.5	209.248	0.031	0.019	-0.098	0.02	0.01	-0.01
592.5	210.968	0.028	0.080	-0.031	0.04	0.03	0.02
597.5	212.689	0.028	0.094	-0.137	0.05	0.14	0.14
602.5	214.410	0.078	0.123	0.004	0.06	0.12	0.13
607.5	216.130	0.073	0.044	-0.038	0.07	0.02	0.00
612.5	217.851	0.054	0.060	-0.051	0.10	0.03	0.02
617.5	219.571	0.060	0.060	-0.041	0.07	0.04	0.01
622.5	221.418	0.036	0.058	-0.010	0.05	0.01	0.01
627.5	223.291	0.032	0.061	-0.055	0.06	0.04	0.05
632.5	225.163	0.044	0.106	0.027	0.05	0.04	0.04
637.5	227.036	0.021	0.013	-0.088	0.03	0.03	0.02
642.5	228.909	0.024	0.041	-0.051	0.04	0.07	0.07
647.5	230.782	0.042	0.234	0.164	0.06	0.08	0.08
652.5	232.655	0.058	0.041	-0.054	0.09	0.04	0.03

Appendix

657.5	234.527	0.109	0.206	-0.016	0.10	0.03	0.02
662.5	236.400	0.077	0.047	-0.067	0.13	0.02	0.00
667.5	238.273	0.091	0.037	-0.053	0.10	0.08	0.06
672.5	240.146	0.105	0.048	0.002	0.13	0.03	0.01
677.5	242.019	0.106	0.047	-0.072	0.12	0.04	0.03
682.5	243.891	0.054	0.007	-0.105	0.13	0.04	0.03
687.5	245.764	0.091	0.039	-0.057	0.13	0.03	0.02
692.5	247.637	0.059	0.047	-0.044	0.09	0.02	0.00
697.5	249.510	0.030	0.044	-0.058	0.07	0.04	0.04
702.5	251.383	0.017	0.005	-0.129	0.03	0.00	-0.05
707.5	252.913	0.022	0.013	-0.104	0.03	0.01	-0.01
712.5	254.404	0.027	0.000	-0.105			
717.5	255.896	0.022	0.000	-0.159	0.01	0.02	0.01
722.5	257.388	0.017	0.061	-0.043	0.02	0.02	0.03
727.5	258.880	0.004	-0.001	-0.159	0.00	0.01	0.00

Evolution of the South Pacific Gyre's thermocline during the last 600 kyr

Table SO213-60-1

Depth (cm)	Age (Kyr)	<i>G. bulloides</i>			<i>G. inflata</i>		
		Mg/Ca mmolmol ⁻¹	$\delta^{18}\text{O}$ ‰	$\delta^{13}\text{C}$ ‰	Mg/Ca mmolmol ⁻¹	$\delta^{18}\text{O}$ ‰	$\delta^{13}\text{C}$ ‰
0.5	10.7	1.46	2.96	0.94	1.49	1.55	1.20
2.5	13.9	1.47	2.62	0.67	1.49	3.24	1.20
4.5	17.2	1.31	3.55	1.07	1.76	2.76	1.29
6.5	20.4	1.24	3.43	0.93	1.46	3.25	1.14
8.5	23.6	1.23	3.32	0.89	1.41	3.30	1.25
10.5	26.6	1.13	3.32	0.79	1.44	3.58	1.18
12.5	29.1	1.25	3.51	1.27	1.29	3.24	1.38
14.5	31.6	1.32	3.33	1.15	1.39	3.44	1.41
16.5	34.1	1.30	3.36	1.28	1.37	3.19	1.24
18.5	36.6	1.18	3.55	1.38	1.46	3.44	1.09
20.5	39.2	1.34	3.38	0.94	1.47	3.20	0.92
22.5	41.7	1.34	3.24	0.60	1.46	3.41	1.31
24.5	44.2	1.33	3.24	0.59	1.63	2.66	0.74
26.5	46.7	1.25	3.34	0.80	1.47	3.37	1.21
28.5	49.2	1.33	3.23	0.52	1.48	3.06	1.06
30.5	51.7	1.36	3.47	0.24	1.43	3.43	0.85
32.5	54.3	1.31	3.15	0.74	1.41	3.28	1.29
34.5	56.8	1.29	3.31	0.82	1.41	3.24	1.33
36.5	59.3	1.29	3.10	0.99	1.41		
38.5	61.8	1.36	3.12	1.01	1.48	3.27	1.48
40.5	64.3	1.47	2.86	0.68	1.51	3.07	1.31
42.5	66.8	1.40	2.89	0.73	1.52	2.89	1.28
44.5	69.4	1.38	2.90	0.81	1.70	2.99	1.31
46.5	71.9	1.45	2.73	0.44	1.62	2.86	1.58
48.5	74.4	1.57	2.56	0.66	1.77	2.72	1.12
50.5	76.9	1.47	2.82	0.77	1.57	2.99	1.55
52.5	79.4	1.43	2.84	0.71	1.79		
54.5	81.9	1.63	2.79	0.48	1.57	2.99	1.45
56.5	84.4	1.26	2.79	0.41	1.72	2.54	1.31
58.5	87.0	1.24	2.88	0.64	1.44	2.87	1.33
60.5	89.5	1.43	2.82	0.99	1.86	2.69	1.25
62.5	92.0	1.35	3.00	0.75	1.57	2.93	1.50
64.5	94.5	1.52	2.80	0.76	1.82	2.81	1.35
66.5	97.0	1.48	3.12	0.69	1.59	2.68	1.19
68.5	99.5	1.36	3.15	0.75	1.77	2.81	1.06
70.5	102.1	1.39	2.75	0.50	1.56	2.95	1.38
72.5	104.6	1.38	2.90	0.29	1.76	2.85	1.12
74.5	107.1	1.33	3.05	0.27	1.62	2.88	1.31
76.5	109.6	1.33	3.06	0.50	1.69	2.94	1.01
78.5	112.1	1.45	3.11	0.55	1.45	3.11	1.44

Appendix

80.5	114.6	1.34	3.07	0.46	1.59	2.85	1.09
82.5	117.2	1.36	3.36	0.55	1.52	3.26	1.10
84.5	119.7	1.40	3.44	0.48	1.79		
86.5	122.2	1.38	3.35	0.35	1.60	3.37	1.18
88.5	124.7	1.20	3.30	0.13	1.56	2.81	0.96
90.5	127.2	1.50	3.66	0.61	1.67	3.12	0.85
92.5	129.7	1.40	3.37	0.64	1.62	2.96	0.27
94.5	132.2	1.34	3.37	0.29	1.56	2.71	0.89
96.5	135.1	1.12	3.42	0.41	1.63	2.79	0.60
98.5	139.1	1.38	3.20	-0.09	1.55	3.35	1.11
100.5	143.2	1.41	3.54	-0.24	1.51	3.71	1.18
102.5	147.2	1.22	3.30	0.48	1.52	3.47	1.17
104.5	151.2	1.26	3.70	0.36	1.85	3.09	0.90
106.5	155.2	1.31	3.11	0.05	1.35	3.36	1.04
108.5	159.3	1.46	3.30	0.33	1.28	3.43	0.60
110.5	163.3	1.41	3.36	0.73	1.48	3.32	1.13
112.5	167.3	1.39	3.11	0.53	1.42	3.54	0.72
114.5	171.3	1.51	3.32	0.07	1.55	3.39	0.88
116.5	175.4	1.31	3.49	0.36	1.54	3.03	0.65
118.5	179.4	1.32	3.46	0.24	1.40	3.48	0.87
120.5	183.4	1.29	3.22	0.61	1.39	2.71	0.73
122.5	187.4	1.39	3.03	0.61	1.38	3.34	0.91
124.5	191.5	1.18	3.32	0.49	1.50	2.75	1.17
126.5	195.5	1.13	2.84	0.33	1.49	2.71	1.32
128.5	198.6	1.30	2.60	0.67	1.29	2.64	1.22
130.5	201.3	1.37	3.58	0.91	1.38	2.95	1.21
132.5	203.9	1.17	2.92	0.65	1.36	2.45	1.09
134.5	206.5	1.31	3.16	0.39	1.44	2.60	1.06
136.5	209.2	1.48	2.66	0.71	1.48	2.60	0.86
138.5	211.8	1.49	2.80	0.41	1.54	2.78	1.12
140.5	214.4	1.58	2.55	0.27	1.51	2.64	0.97
142.5	217.0	1.29	2.86	0.45	1.50	2.97	1.29
144.5	219.7	1.45	2.52	0.34	1.57	2.67	1.16
146.5	222.9	1.34	2.84	0.50	1.50	2.95	1.34
148.5	230.0	1.30	2.82	0.61	1.51	2.95	1.04
150.5	237.0	1.73	2.77	0.72	1.59	3.05	1.03
152.5	244.1	1.42	2.76	0.43	1.53	2.88	1.36
154.5	251.2	1.56	2.79	0.46	1.68	3.17	0.98
156.5	258.2	1.48	2.98	0.33	1.63	3.22	0.98
158.5	265.3	1.41	3.11	0.10	1.52	3.18	0.88
160.5	272.4	1.49	2.85	0.44	1.54	3.02	0.84
162.5	279.4	1.38	3.26	0.44	1.58	2.97	0.83
164.5	286.5	1.34	3.17	0.16	1.54	3.14	1.21
166.5	293.5	1.34	3.01	0.01	1.74	3.05	0.95
168.5	297.8	1.36	3.36	-0.02	1.59	3.40	0.99

170.5	302.1	1.40	3.18	-0.22	1.47	2.93	0.61
172.5	306.5	1.22	3.43	0.69	1.40	2.64	0.80
174.5	310.8	1.24	3.30	0.68	1.32	2.76	0.99
176.5	315.2	1.18	3.13	0.41	1.72	2.48	1.12
178.5	319.3	1.14	3.40	0.56	1.09	2.74	0.91
180.5	322.2	1.18	2.88	0.78	0.89	2.86	1.15
182.5	325.0	1.33	3.24	0.73	1.52	2.80	1.00
184.5	327.8	1.32	3.32	0.78	1.00	2.88	0.93
186.5	330.7	1.45	3.22	0.66	1.29	3.20	1.22
188.5	333.5	1.52	2.94	0.53	1.36	3.29	1.18
190.5	336.4	1.50	3.51	0.60	1.48	2.96	0.90
192.5	339.2	1.45	3.43	0.78	1.65	2.95	0.85
194.5	342.0	1.48	3.42	0.71	1.44	3.30	0.99
196.5	344.9	1.40	3.48	0.56	1.15	3.36	1.14
198.5	347.7	1.60	3.34	0.54	1.07	3.37	1.26
200.5	350.6	1.45	3.56	0.96	1.01	3.20	1.19
202.5	353.4	1.36	3.46	1.03	1.11	3.02	1.37
204.5	356.2	1.35	3.53	1.03	1.20	3.32	1.18
206.5	359.1	1.30	3.21	0.87	1.05	3.30	1.24
208.5	361.9	1.15	3.28	0.81	0.97	3.10	1.31
210.5	364.8	1.29	3.30	1.02	0.92	2.82	1.32
212.5	367.6	1.24	3.17	0.81	0.85	3.03	1.36
214.5	370.4	1.23	3.20	1.06	0.94	3.04	1.34
216.5	373.3	1.43	2.83	0.75	0.84	3.16	1.06
218.5	376.1	1.22	3.67	0.86	0.83	2.85	1.30
220.5	379.0	1.37	3.05	0.59	0.96	3.08	1.24
222.5	381.8	1.33	3.38	0.93	0.82	3.19	1.42
224.5	384.6	1.32	3.04	0.86	0.95	2.99	1.34
226.5	387.5	1.32	2.92	1.03	1.11	2.99	1.30
228.5	390.3	1.36	3.10	0.91	1.02	3.01	1.35
230.5	393.2	1.17	3.02	0.83	0.88	2.96	1.42
232.5	396.0	1.12	2.95	0.64	0.91	2.72	1.33
234.5	398.8	1.44	2.61	0.97	0.80	2.93	1.73
236.5	401.7	1.27	3.31	0.73	0.83	2.85	1.51
238.5	404.5	1.32	2.79	1.16	0.88	2.81	1.50
240.5	407.4	1.40	3.39	0.78	0.81	2.54	1.61
242.5	410.2	1.40	2.97	0.71	0.99	2.69	1.43
244.5	413.0	1.51	2.90	0.55	0.79	2.49	1.62
246.5	415.9	1.39	2.96	0.69	1.00	2.59	1.47
248.5	418.7	1.54	2.93	0.74	0.91	2.83	1.28
250.5	421.6	1.58	2.66	0.70	0.95	2.59	1.43
252.5	424.4	1.61	3.16	0.88	1.17	3.42	1.21
254.5	427.2	1.60	3.00	0.62	1.08	3.30	1.31
256.5	430.1	1.55	3.23	0.58	1.08	3.02	1.36
258.5	432.9	1.48	3.41	0.41	0.95	3.45	1.29

Appendix

260.5	440.1	1.45			0.89	3.10	1.11
262.5	447.2	1.43	3.88	0.80	0.80	2.88	1.38
264.5	454.4	1.29	3.45	0.82	0.87	3.32	1.14
266.5	461.6	1.26	3.15	0.66	1.03	3.39	0.99
268.5	466.9	1.17	3.45	0.66	1.24	3.07	1.53
270.5	468.6	1.26	3.39	0.82	1.09	3.07	1.46
272.5	470.4	1.14	3.44	0.80	1.04	3.22	1.36
274.5	472.1	1.36	3.87	0.77	1.09	3.09	1.50
276.5	473.9	1.32	3.73	0.57	1.18	2.95	1.83
278.5	475.6	1.44	3.76	0.49	1.16	3.14	1.46
280.5	477.3	1.38	3.17	1.05	1.09	2.85	1.86
282.5	479.1	1.27	2.84	1.25	1.02	2.99	1.80
284.5	480.8	1.34	3.53	1.23	1.15	2.96	1.84
286.5	482.6	1.34	3.28	1.27	1.15	2.82	1.86
288.5	484.3	1.35	2.97	1.02	1.13	2.79	1.78
290.5	485.2	1.55	2.89	0.88	1.16	2.74	1.82
292.5	485.9	1.35	2.87	0.61	1.13	2.78	1.87
294.5	486.5	1.25	2.94	1.22	1.15	2.74	1.82
296.5	487.2	1.33	3.01	0.17	1.15	2.72	1.65
298.5	487.9	1.52	3.14	0.58	1.04	2.80	1.62
300.5	488.5	1.44	2.65	1.32	1.18	2.84	1.65
302.5	489.2	1.52	2.78	0.91	1.15	2.77	1.62
304.5	489.9	1.48	3.00	0.74	1.23	2.82	1.34
306.5	490.5	1.47	3.09	0.88	1.31	2.79	1.73
308.5	491.2	1.49	2.85	0.69	1.30	2.96	1.47
310.5	491.8	1.38	2.90	0.19	1.44	2.77	1.48
312.5	492.5	1.51	2.66	0.15	1.28	2.88	1.36
314.5	493.2	1.54	3.02	0.79	1.41	2.93	1.32
316.5	493.8	1.44	2.78	0.44	1.41	2.75	1.31
318.5	494.5	1.40	3.56	0.72	1.36	2.90	1.23
320.5	495.2	1.37	3.17	0.53	1.36	3.04	1.31
322.5	495.8	1.47	3.05	0.84	1.29	2.90	1.31
324.5	496.5	1.46	2.99	0.96	1.17	3.05	1.49
326.5	497.1	1.44	3.02	0.50	1.19	2.82	1.04
328.5	497.8	1.34	3.06	0.47	1.28	2.70	1.16
330.5	498.5	1.62	3.04	0.50	1.16	3.00	1.22
332.5	499.1	1.34	3.16	0.85	1.06	3.01	1.46
334.5	499.8	1.19	3.21	0.58	0.99	2.59	1.09
336.5	500.5	1.44	3.02	0.47	1.05	2.66	1.25
338.5	501.1	1.38	3.00	0.80	1.19	3.01	1.18
340.5	501.8	1.31	2.99	0.68	1.18	2.89	1.36
342.5	502.4	1.40	2.76	0.51	1.13	3.02	0.98
344.5	503.1	1.44	2.75	0.65	1.23	2.53	1.33
346.5	503.8	1.63	2.90	0.10	1.46	3.13	1.29
348.5	504.4	1.61	2.83	0.42	1.43	3.03	1.10

350.5	505.1	1.66	2.91	0.56	1.47	2.87	1.01
352.5	505.8	1.76	3.28	0.13	1.59	3.32	0.87
354.5	506.4	1.47	3.56	0.11	1.45	2.95	0.98
356.5	507.1	1.41	3.10	0.48	1.52	3.30	0.96
358.5	507.7	1.54	3.39	0.68	1.35	2.63	0.92
360.5	508.4	1.47	3.11	0.55	1.38	3.20	0.92
362.5	509.1	1.91	3.24	0.12	1.32	3.30	0.76
364.5	509.7	1.56	3.01	-0.30	1.38	3.16	0.81
366.5	510.4	1.60	2.85	0.05	1.19	3.30	0.90
368.5	511.1	1.27	3.30	0.64	1.27	3.30	0.79
370.5	511.7	1.26	3.10	0.64	1.25	3.18	0.88
372.5	512.4	1.35	3.02	0.34	1.22	3.10	0.84
374.5	513.1	1.34	3.19	0.46	1.18	2.81	1.27
376.5	513.7	1.29	3.54	0.92	1.13	2.72	1.42
378.5	514.4	1.32	3.59	1.02	1.22	2.73	1.39
380.5	515.0	1.16	3.46	0.82	1.37	2.71	1.41
382.5	515.7	1.29	3.29	0.72	1.41	2.70	1.18
384.5	516.4	1.37	3.37	1.00	1.43	2.72	1.16
386.5	517.0	1.38	3.39	0.54	1.48	2.67	1.35
388.5	517.7	1.50	3.19	0.72	1.43	2.72	1.31
390.5	518.4	1.24	3.16	0.60	1.48	3.26	0.95
392.5	519.0	1.31	3.48	0.97	1.46	2.65	1.32
394.5	519.7	1.16	3.48	0.95	1.40	3.31	1.03
396.5	520.3	1.38	3.29	0.71	1.36	2.87	0.98
398.5	521.0	1.43	3.65	0.73	1.37	2.87	1.24
400.5	521.7	1.24	3.33	0.42	1.27	2.82	1.30
402.5	522.3	1.32	3.38	0.98	1.33	2.77	1.29
404.5	523.0	1.22	3.23	0.72	1.24	2.84	1.05
406.5	523.7	1.16	3.05	0.36	1.13	2.80	0.95
408.5	524.3	1.30	3.42	0.80	1.19	2.82	1.12
410.5	525.0	1.20	3.55	0.86	1.11	2.77	1.20
412.5	525.6	1.21	3.22	0.42	1.33	2.66	1.02
414.5	526.3	1.15	3.14	0.60	1.49	2.63	1.17
416.5	527.0	1.20	3.24	0.72	1.79	2.51	1.24
418.5	527.6	1.19	3.48	0.96	1.37	2.57	1.15
420.5	528.3	1.19	3.52	0.94	1.39	2.80	1.32
422.5	529.0	1.22	3.39	0.44	1.19		
424.5	529.6	1.24	3.53	0.57	1.01		
426.5	530.3	1.10	3.54	1.06	1.21		
428.5	531.0	1.18	3.46	0.64	1.32	2.81	1.00
430.5	531.6	1.21	3.52	0.82	1.25	2.87	1.11
432.5	532.3	1.26	3.53	0.86	1.19	2.87	1.09
434.5	532.9	1.14	3.62	0.94	1.16	2.64	0.97
436.5	533.6	1.33	3.44	0.78	1.32	2.94	1.13
438.5	534.3	1.17	3.57	0.55	1.26	2.66	1.08

Appendix

440.5	534.9	1.40	3.55	0.62	1.28	2.71	1.02
442.5	535.6	1.24	3.70	0.68	1.19	2.82	0.92
444.5	536.6	1.27	3.42	0.87	1.22	2.89	0.98
446.5	539.1	1.20	3.65	1.00	1.20	3.04	0.97
448.5	541.5	1.04	3.62	0.84	1.20	2.60	1.21
450.5	544.0	1.15	3.54	0.83	0.99	3.50	1.00
452.5	546.5	1.19	3.49	0.68	1.00	2.65	1.22
454.5	548.9	1.15	3.51	0.85	1.01	2.82	0.74
456.5	551.4	1.31	3.19	0.64	1.06	2.95	0.94
458.5	553.9	1.26	3.19	0.78	0.94	2.94	1.15
460.5	556.4	1.31	3.25	0.77	0.91	2.73	0.88
462.5	558.8	1.21	3.30	0.58	0.85	2.64	1.03
464.5	561.3	1.21	3.24	1.03	0.96	2.61	1.00
466.5	564.0	1.31	3.42	1.13	0.88	2.92	0.98
468.5	566.5	1.26	3.17	0.76	0.97	2.83	0.91
470.5	567.3	1.07	3.01	0.27	0.89	2.74	0.96
472.5	568.1	1.38	3.01	0.52	1.19	2.92	0.96
474.5	568.9	1.49	2.89	0.71	1.12	2.73	1.17
476.5	569.7	1.47	3.10	0.68	0.98	2.85	1.08
478.5	570.5	1.40	2.87	0.64	1.02	2.69	1.15
480.5	571.3	1.39	3.06	0.98	0.97	2.70	1.08
482.5	572.1	1.35	3.01	0.67	0.92	2.75	1.07
484.5	572.8	1.25	2.97	0.96	0.91	2.85	0.98
486.5	573.6	1.54	2.82	0.74	1.09	2.57	1.15
488.5	574.4	1.29	2.93	0.57	1.08	2.72	1.05
490.5	575.2	1.46	2.93	0.60	1.03	2.90	1.11
492.5	576.0	1.26	2.89	0.64	0.99	2.69	1.08
494.5	576.8	1.38	2.77	0.54	0.97	2.81	1.29
496.5	577.6	1.22	2.67	0.62	1.15	2.76	1.13
498.5	578.4	1.35	3.02	0.44	1.12	2.83	0.91
500.5	579.2	1.26	3.05	0.40	0.94	2.77	1.02
502.5	580.0	1.14	3.12	0.46	0.91	3.01	1.00
504.5	580.8	1.24	3.18	0.91	0.86	2.78	1.03
506.5	581.6	1.15	2.95	0.60	0.87	2.73	1.07
508.5	582.4	1.15	3.04	0.80	0.81	2.71	1.23
510.5	583.6	1.37	2.93	0.59	0.82	2.96	1.27
512.5	584.9	1.33	3.02	0.50	0.74	2.68	1.41
514.5	586.3	1.45	3.07	0.86	0.93	2.84	1.04
516.5	587.7	1.28	3.04	0.68	0.82	2.89	1.34
518.5	589.1	1.38	3.07	0.88	1.02	2.64	1.17
520.5	590.3	1.56	2.74	0.78	1.01	2.33	1.18
522.5	590.7	1.72	2.76	0.90	0.96	2.57	1.44
524.5	591.1	1.51	2.83	0.68	0.88	2.85	1.20
526.5	591.5	1.48	2.82	1.20	0.97	2.75	1.13
528.5	592.0	1.50	2.64	1.03	0.86	2.87	1.47

530.5	592.4	1.49	2.67	0.60	0.90	2.78	1.09
532.5	592.8	1.44	2.71	1.03	0.95	2.57	0.89
534.5	593.2	1.47	2.47	0.95	1.01	2.79	1.25
536.5	593.6	1.62	2.74	0.90	1.15	2.68	1.34
538.5	594.1	1.58	2.54	0.87	1.10	2.74	1.22
540.5	594.5	1.54	2.46	0.99	0.95	2.70	1.21
542.5	594.9	1.41	--	0.66	1.15	2.44	0.96
544.5	595.3	1.45	2.69	1.21	0.98	2.67	1.08
546.5	595.7	1.59	2.74	1.19	1.15	2.73	1.20
548.5	596.1	1.52	2.83	0.91	1.08	2.89	1.23
550.5	596.6	1.58	2.85	1.23	0.93	2.68	1.01
552.5	597.0	1.70	2.86	1.28	1.04	2.68	1.43
554.5	597.4	1.62	2.89	1.12	0.89	2.66	1.28
556.5	597.8	1.94	3.00	1.10	0.96	2.44	1.30
558.5	598.2	1.80	2.94	1.11	0.98	2.68	1.24
560.5	598.7	1.90	2.93	1.26	1.00	2.83	1.37
562.5	599.1	1.82	2.96	0.83	1.21	2.93	1.23
564.5	599.5	1.79	2.92	1.03	1.02	2.97	1.14
566.5	599.9	1.64	3.25	0.63	0.89	2.74	0.95
568.5	600.3	1.61	2.85	0.96	0.93	2.68	1.21
570.5	600.8	1.72	2.98	1.08	1.07	2.80	1.33
572.5	601.2	1.60	2.75	0.71	0.96	2.79	1.31
574.5	601.6	1.76	2.86	0.92	1.03	2.89	1.27
576.5	602.0	1.68	2.92	1.00	1.10	2.75	1.06
578.5	602.4	1.94	2.75	0.82	1.17	2.56	1.17
580.5	602.9	1.78	2.67	0.83	1.00	2.49	1.04
582.5	603.3	1.73	2.73	0.89	1.22	2.46	1.11
584.5	603.7	1.85	2.80	0.99	1.05	2.99	1.37
586.5	604.1	1.90	2.80	1.24	1.15	2.68	1.20
588.5	604.5	1.81	2.92	0.96	1.05	2.71	1.29
590.5	605.0	1.77	2.80	1.17	0.96	2.45	1.08
592.5	605.4	1.76	2.83	0.99	0.95	2.88	1.03
594.5	605.8	1.59	2.72	0.95	0.99	2.64	1.11
596.5	606.2	1.83	2.87	0.73	1.18	2.69	1.42
598.5	606.6	1.82	2.86	0.78	1.13	2.77	1.13
600.5	607.1	1.63	2.86	0.70	1.15	2.72	1.24
602.5	607.5	1.81	2.66	0.53	1.38	2.70	1.22
604.5	607.9	1.69	2.71	0.71	1.28	2.48	1.26
606.5	608.3	1.79	2.71	1.01	1.20	2.66	1.37
608.5	608.7	2.05	2.84	0.53	1.52	2.76	1.18
610.5	609.2	1.90	2.86	1.05	1.60	2.76	0.97
612.5	609.6	1.80	2.59	1.07	1.49	2.53	1.40
614.5	609.8	1.82	2.84	0.83	1.64	2.73	1.19
616.5	610.1	2.07	2.63	0.94	1.51	2.63	1.31
618.5	610.4	2.20	2.82	0.86	1.60	2.52	1.35

Appendix

620.5	610.6	1.93	2.73	1.00	1.46	2.63	1.38
622.5	610.9	1.95	2.67	0.87	1.53	2.53	1.43
624.5	611.1	1.81	2.58	1.25	1.63	2.48	1.56
626.5	611.4	2.07	2.66	1.11	1.52	2.64	1.23
628.5	611.6	2.05	2.90	1.05	1.55	2.58	1.48
630.5	611.9	1.84	2.74	1.15	1.48	2.61	1.56
632.5	612.1	1.71	2.80	0.97	1.44	2.49	1.60
634.5	612.4	1.69	2.70	1.20	1.26	2.45	1.49
636.5	612.6	1.77	2.76	1.05	1.29	2.41	1.66
638.5	612.9	1.77	2.79	1.07	1.36	2.60	1.58
640.5	613.1	1.97	2.72	1.11	1.30	2.45	1.61
642.5	613.4	2.09	2.58	1.13	1.54	2.48	1.37
644.5	613.6	1.74	2.57	1.18	1.64	2.49	1.59
646.5	613.9	1.84	2.65	1.28	1.60	2.45	1.52
648.5	614.1	1.85	2.62	0.91	1.50	2.77	1.49
650.5	614.4	1.81	2.59	1.29	1.43	2.60	1.43
652.5	614.6	1.85	2.70	1.14			
654.5	614.9	2.18	2.50	1.00			
656.5	615.1	1.70	2.73	1.17			
658.5	615.4	1.83	2.66	1.18			
660.5	615.7	1.86	2.70	1.26			
662.5	615.9	1.74	2.84	1.14			
664.5	616.2	1.90	2.89	1.12			
666.5	616.4	1.96	2.75	0.95			
668.5	616.7	1.77	2.87	0.82			
670.5	616.9	1.87	2.83	1.12			
672.5	617.2	1.56	2.80	1.24			

Evolution of the sea surface temperature and $\delta^{18}\text{O}$ in the central South Pacific during the past 500 ka: Implications on ocean circulation

Table PS75/059-2

Depth (cm)	Age (Kyr)	<i>G. bulloides</i>	
		Mg/Ca	$\delta^{18}\text{O}$
2.5	0.971	1.17	2.57
7.5	2.972	1.29	2.72
12.5	4.973	1.34	2.84
17.5	6.974	1.31	2.73
22.5	8.721	1.32	2.67
27.5	10.010	1.41	2.78
32.5	11.298	1.56	2.63
37.5	12.587	1.37	2.76
42.5	13.876	1.19	2.96
47.5	15.164	1.27	3.20
52.5	16.453	1.10	3.66
57.5	17.742	1.23	3.73
62.5	19.643	0.99	3.70
67.5	22.168	0.98	4.15
72.5	24.692	1.03	3.85
77.5	27.217	1.13	4.00
82.5	29.741	1.11	4.01
87.5	32.266	0.90	3.82
92.5	34.790	0.91	3.94
97.5	37.315	0.98	3.85
102.5	39.839	0.98	3.83
107.5	42.364	1.04	3.61
112.5	44.888	1.13	3.85
117.5	47.413	1.03	3.80
122.5	49.937	1.03	3.52
127.5	52.462	1.01	3.65
132.5	54.986	1.10	3.53
137.5	57.511	1.11	3.50
142.5	59.549	1.07	3.56
147.5	61.135	1.11	3.77
152.5	62.720	0.99	3.79
157.5	64.305	0.93	3.75
162.5	65.891	1.03	3.55
167.5	67.476	1.04	3.59
172.5	69.062	1.20	3.52
177.5	70.647	1.08	3.34
182.5	72.022	1.12	3.40
187.5	73.396	1.24	3.26
192.5	74.770	1.19	3.16

197.5	76.145	1.33	3.07
202.5	77.519	1.25	3.09
207.5	78.893	1.41	3.00
212.5	80.267	1.36	3.03
217.5	81.641	1.40	2.96
222.5	83.015	1.41	2.94
227.5	84.389	1.31	2.90
232.5	85.763	1.29	3.01
237.5	87.114	1.24	3.40
242.5	88.253	1.16	3.20
247.5	89.393	1.15	3.24
252.5	90.532	1.31	3.13
257.5	91.672	1.22	3.13
262.5	92.811	1.39	2.82
267.5	93.951	1.37	2.82
272.5	95.090	1.27	3.04
277.5	96.229	1.36	2.99
282.5	97.369	1.30	2.90
287.5	98.508	1.25	2.88
292.5	99.648	1.34	2.96
297.5	100.787	1.39	3.03
302.5	101.927	1.24	3.14
307.5	103.066	1.28	2.99
312.5	104.205	1.18	2.94
317.5	105.700	1.25	3.15
322.5	107.533	1.31	3.11
327.5	109.366	1.23	3.32
332.5	111.198	1.14	3.09
337.5	113.031	1.27	2.88
342.5	114.864	1.29	3.11
347.5	116.396	1.46	2.38
352.5	117.853	1.30	2.55
357.5	119.309	1.46	2.43
362.5	120.766	1.52	2.44
367.5	122.222	1.36	2.19
372.5	123.679	1.39	2.12
377.5	125.135	1.26	2.39
382.5	126.592	1.39	2.55
387.5	128.048	1.59	2.45
392.5	129.505	1.53	2.76
397.5	130.961	2.02	3.07
402.5	132.558	1.74	3.31
407.5	134.700	1.78	3.56
412.5	136.841	1.22	3.47
417.5	138.982	1.32	3.75

422.5	141.124	1.22	3.75
427.5	143.265	1.08	4.08
432.5	145.406	1.10	4.06
437.5	147.548	1.12	4.06
442.5	149.689	1.13	4.03
447.5	151.830	1.18	3.96
452.5	153.971	1.26	4.19
457.5	156.113	1.18	4.07
462.5	158.254	1.17	4.09
467.5	160.395	1.05	4.03
472.5	162.537	1.02	3.88
477.5	164.678	1.26	3.77
482.5	166.819	0.94	3.89
487.5	168.961	0.98	3.75
492.5	171.102	0.98	3.53
497.5	173.243	1.11	3.73
502.5	175.385	0.98	3.84
507.5	177.526	1.04	3.94
512.5	179.667	1.13	3.96
517.5	181.809	0.97	3.69
522.5	183.950	1.17	3.82
527.5	186.091	1.07	3.78
532.5	188.232	1.27	3.56
537.5	190.374	1.03	3.74
542.5	192.515	0.97	3.32
547.5	194.656	1.02	3.42
552.5	196.798	0.88	3.39
557.5	198.924	1.16	3.26
562.5	200.645	1.22	2.98
567.5	202.366	1.02	3.09
572.5	204.086	1.17	3.21
577.5	205.807	1.11	2.91
582.5	207.527	1.15	2.96
587.5	209.248	1.35	2.95
592.5	210.968	1.19	2.85
597.5	212.689	1.21	2.90
602.5	214.410	1.50	2.98
607.5	216.130	1.35	3.34
612.5	217.851	1.26	3.29
617.5	219.571	1.47	2.98
622.5	221.418	1.13	3.54
627.5	223.291	1.26	3.26
632.5	225.163	1.31	3.33
637.5	227.036	1.03	3.58
642.5	228.909	1.20	3.09

647.5	230.782	1.47	3.10
652.5	232.655	1.24	3.10
657.5	234.527	1.53	3.09
662.5	236.400	1.38	2.82
667.5	238.273	1.58	3.03
672.5	240.146	1.66	2.79
677.5	242.019	1.53	2.81
682.5	243.891	1.25	3.21
687.5	245.764	1.55	3.09
692.5	247.637	1.36	3.15
697.5	249.510	1.27	3.62
702.5	251.383	0.43	3.84
707.5	252.913	0.65	4.02
712.5	254.404	0.72	4.05
717.5	255.896	1.11	3.81
722.5	257.388	1.01	3.93
727.5	258.880	0.95	3.79
732.5	260.372	1.02	4.14
737.5	261.863	1.02	3.79
742.5	263.355	1.03	4.04
747.5	264.847	1.04	3.73
752.5	266.339	1.00	3.94
757.5	267.831	1.10	4.06
762.5	269.323	1.03	4.00
767.5	270.814	1.17	4.17
772.5	272.306	1.17	3.59
777.5	273.798		3.93
782.5	275.290	0.90	3.35
787.5	277.676	1.17	3.30
792.5	280.249	1.20	3.29
797.5	282.821	1.28	3.26
802.5	285.394	1.31	3.34
807.5	287.966	1.29	3.35
812.5	290.539	1.15	3.53
817.5	293.111	1.00	3.82
822.5	295.236	0.91	3.62
827.5	297.284	1.07	3.31
832.5	299.332	1.18	3.64
837.5	301.380	0.99	3.58
842.5	303.429	0.99	3.73
847.5	305.477	1.05	3.59
852.5	307.525	1.05	3.29
857.5	309.573	1.09	3.34
862.5	311.621	1.12	3.17
867.5	313.669	1.04	3.16

872.5	315.717	1.17	2.76
877.5	317.765	1.19	2.57
882.5	319.813	1.08	3.09
887.5	321.861	1.38	3.08
892.5	323.909	1.36	2.92
897.5	325.957	1.47	2.69
902.5	328.005	1.47	2.64
907.5	330.053	1.62	2.81
912.5	332.101	1.57	3.24
917.5	334.149	1.61	3.91
922.5	336.198	1.34	3.19
927.5	338.246	1.53	3.41
932.5	340.294	1.45	3.59
937.5	342.359	1.15	3.74
942.5	344.469	1.40	3.61
947.5	346.579	1.17	3.72
952.5	348.690	1.13	3.86
957.5	350.800	1.13	3.89
962.5	352.910	1.13	3.96
967.5	355.021	1.17	3.96
972.5	357.048	1.09	3.99
977.5	358.326	1.13	3.76
982.5	359.603	0.95	3.86
987.5	360.881	1.08	3.56
992.5	362.159	1.10	3.65
997.5	363.436	1.06	3.62
1002.5	364.714	1.06	3.73
1007.5	365.992	1.23	3.61
1012.5	367.270	1.04	3.34
1017.5	368.547	1.04	3.27
1022.5	369.825	1.13	3.22
1027.5	371.103	1.02	3.20
1032.5	372.381	1.07	3.35
1037.5	373.658	1.17	3.30
1042.5	374.936	1.04	3.52
1047.5	376.550	1.07	3.39
1052.5	378.250	0.99	3.30
1057.5	379.950	1.18	3.32
1062.5	381.650	1.19	3.36
1067.5	383.350	1.26	3.21
1072.5	385.050	1.16	3.44
1077.5	386.750	1.14	3.15
1082.5	388.450	1.15	3.16
1087.5	390.150	1.14	3.12
1092.5	391.684	1.34	3.47

1097.5	392.550	1.31	3.26
1107.5	394.282	1.26	2.99
1112.5	395.148	1.51	2.81
1117.5	396.015	1.59	3.01
1122.5	396.881	1.89	2.83
1127.5	397.747	1.70	2.86
1132.5	398.613	1.64	2.78
1137.5	399.479	1.70	3.02
1142.5	400.345	1.74	2.68
1147.5	401.211	1.66	2.82
1152.5	402.077	1.56	2.71
1157.5	402.943	1.71	2.68
1162.5	403.809	1.66	2.83
1167.5	404.675	1.67	2.63
1172.5	405.541	1.71	2.68
1177.5	406.408	1.60	2.55
1182.5	407.274	1.61	2.48
1187.5	408.140	1.28	3.26
1192.5	409.006	1.57	2.43
1197.5	409.872	1.72	2.57
1207.5	411.604	1.84	2.40
1212.5	412.470	1.69	
1217.5	413.336	1.55	2.30
1222.5	414.202	1.66	2.43
1227.5	415.068	1.44	2.33
1232.5	415.935	1.44	2.73
1237.5	416.801	1.45	2.47
1242.5	417.667	1.43	2.64
1247.5	418.533	1.31	2.43
1252.5	419.399	1.49	2.83
1257.5	420.265	1.37	2.80
1262.5	421.131	1.53	2.74
1267.5	421.997	1.54	2.68
1272.5	422.863	1.53	2.71
1277.5	423.729	1.60	2.66
1282.5	424.595	1.47	3.02
1287.5	425.461	1.75	3.03
1292.5	426.328	1.50	2.90
1297.5	427.296	1.52	3.24
1302.5	429.630	1.29	3.98
1307.5	431.964	1.18	4.23
1312.5	434.298	1.25	3.53
1317.5	436.632	1.43	4.14
1322.5	438.966	1.32	3.78
1327.5	441.300	1.32	4.03

1332.5	443.634	1.26	3.95
1337.5	445.968	0.93	4.02
1342.5	448.303	1.11	3.99
1347.5	450.637	0.89	4.00
1352.5	452.971	0.98	3.87
1357.5	455.305	1.04	3.82
1362.5	457.639	1.15	3.56
1367.5	459.973	1.05	3.77
1372.5	462.307	0.98	3.73
1377.5	464.641	1.11	3.81
1382.5	466.975	1.09	3.30
1387.5	469.309	1.63	3.35

Table PS75/056-2

Depth (cm)	Age (Kyr)	<i>G. bulloides</i>	
		<i>Mg/Ca</i>	$\delta^{18}\text{O}$
0.5	0.57	1.08	2.59
5.5	6.3	1.23	2.53
10.5	7.87	1.40	2.55
15.5	9.45	1.36	2.48
20.5	11.02	1.41	2.62
25.5	12.59	1.41	2.70
30.5	13.88	1.35	3.03
35.5	15.18	1.28	3.27
40.5	16.47	1.55	3.19
45.5	17.76	1.30	3.58
50.5	18.52	1.04	4.09
55.5	19.25	1.10	4.34
60.5	19.99	1.21	4.17
65.5	20.73	1.04	4.27
70.5	21.46	1.10	4.27
75.5	22.2	0.96	4.28
80.5	22.93	0.90	4.17
85.5	23.73	1.23	4.16
90.5	25.02	1.21	4.25
95.5	26.3	0.95	4.12
100.5	27.54	0.89	4.21
105.5	28.15	0.92	4.01
110.5	28.76	0.92	3.88
115.5	29.36	0.99	4.18
120.5	29.97	0.87	3.92
125.5	30.57	0.99	4.14
130.5	31.23	0.89	4.15

135.5	31.9	0.96	4.04
140.5	32.56	0.93	4.16
145.5	33.22	1.19	3.99
150.5	33.88	0.96	3.91
155.5	34.55	1.00	3.98
160.5	35.21	1.12	4.04
165.5	35.87	1.17	3.82
170.5	36.53	1.10	3.83
175.5	37.19	1.02	3.85
180.5	37.86	1.02	3.86
185.5	38.52	1.05	3.85
190.5	39.18	0.96	3.82
195.5	40.32	1.16	3.78
200.5	41.62	1.06	3.73
205.5	42.92	1.07	3.67
210.5	44.23	1.09	3.82
215.5	45.53	1.02	3.54
220.5	46.24	1.11	3.57
225.5	46.94	1.09	3.38
230.5	47.65	1.30	3.60
235.5	48.36	1.24	3.80
240.5	49.07	1.11	3.70
245.5	49.78	1.35	3.70
250.5	50.49	1.11	3.62
255.5	51.2	1.29	3.54
260.5	51.91	1.14	3.73
265.5	52.62	1.14	3.71
270.5	53.33	1.20	3.69
275.5	54.04	1.04	3.68
280.5	55.32	1.13	3.76
285.5	56.68	1.07	3.74
290.5	58.04	1.14	3.59
295.5	58.85	1.16	3.59
300.5	59.65	1.05	3.63
305.5	60.46	1.24	3.65
310.5	61.27	1.19	3.75
315.5	62.07	1.07	4.00
320.5	62.88	1.05	3.97
325.5	63.68	0.98	4.07
330.5	64.49	0.99	3.94
335.5	65.3	0.98	3.95
340.5	66.1	1.09	3.95
345.5	66.91	0.98	3.74
350.5	67.72	1.00	3.67
355.5	68.52	1.03	3.87

360.5	69.33	1.07	
365.5	70.13	1.07	3.61
370.5	70.94	1.07	3.50
375.5	71.75	1.11	3.63
380.5	72.55	1.18	
385.5	73.36	1.21	3.54
390.5	74.47	1.15	
395.5	75.65	1.28	3.27
400.5	76.83	1.11	3.41
405.5	78.01	1.18	3.40
410.5	79.08	1.12	3.51
415.5	79.6	1.16	3.36
420.5	80.11	1.12	3.43
425.5	80.63	1.25	3.41
430.5	81.14	1.31	3.30
435.5	81.65	1.26	3.31
440.5	82.17	1.36	
445.5	82.68	1.39	3.05
450.5	83.2	1.35	3.11
455.5	83.71	1.31	3.20
460.5	84.53	1.25	
465.5	85.37	1.31	3.13
470.5	86.22	1.24	3.25
475.5	87.06	1.18	3.48
480.5	87.91	1.27	3.46
485.5	88.75	1.20	3.41
490.5	89.6	1.07	3.50
495.5	90.44	1.12	3.45
500.5	91.29	1.25	3.36
505.5	92.13	1.27	3.35
510.5	92.98	1.35	3.36
515.5	93.82	1.31	3.02
520.5	94.67	1.33	3.16
525.5	95.51	1.23	3.00
530.5	96.36	1.29	3.01
535.5	97.2	1.26	3.06
540.5	98.05	1.35	3.02
545.5	98.9	1.28	3.05
550.5	99.74	1.16	3.07
555.5	100.59	1.21	2.90
560.5	101.43	1.15	3.15
565.5	102.28	1.23	3.16
570.5	103.12	1.18	3.06
575.5	103.97	1.37	3.24
580.5	104.81	1.17	3.13

585.5	105.66	1.27	3.15
590.5	106.5	1.26	3.10
595.5	107.35	1.09	3.10
600.5	108.19	1.25	3.15
605.5	109.04	1.19	3.10
610.5	109.88	1.22	3.26
615.5	111.18	1.41	3.29
620.5	112.6	1.17	3.09
625.5	114.02	1.19	2.86
630.5	115.44	1.07	2.59
635.5	116.85	1.25	2.61
640.5	118.27	1.37	2.46
645.5	119.69	1.53	2.49
650.5	120.96	1.39	2.30
655.5	122.13	1.44	2.22
660.5	123.29	1.57	2.18
665.5	124.46	1.36	2.39
670.5	125.63	1.43	2.47
675.5	126.8	1.48	2.65
680.5	127.96	1.48	2.53
685.5	129.13	1.48	2.72
690.5	130.3	1.49	2.88
695.5	131.51	1.36	2.94

Table PS75/076-2

Depth (cm)	Age (Kyr)	<i>G. bulloides</i>	
		<i>Mg/Ca</i>	$\delta^{18}\text{O}$
12.5	20.96	1.16	2.79
22.5	27.39	1.02	2.93
207.5	109.27	1.00	3.48
217.5	113.72		3.65
227.5	118.18	1.17	2.69
237.5	122.64	0.89	3.08
242.5	124.86	1.44	3.02
247.5	127.09	0.97	2.77
252.5	129.32	1.02	2.59
257.5	131.55	1.18	2.62
262.5	133.78	1.20	2.60
267.5	135.66	1.11	2.57
272.5	137.50	1.10	2.72
277.5	139.34	0.90	3.48
287.5	143.03	1.21	2.83
297.5	146.71	1.00	3.58

477.5	206.89	0.81	3.20
482.5	209.11	0.96	3.11
487.5	211.33	0.91	3.05
492.5	213.56	1.01	3.08
497.5	215.78	1.12	3.05
502.5	218.00	1.03	2.93
507.5	220.22	1.02	3.28
517.5	224.67	1.02	3.24
527.5	229.16	1.01	3.20
537.5	233.64	0.99	3.07
547.5	238.12	1.12	3.26
552.5	240.36	1.22	3.04
557.5	242.60	1.24	3.09
562.5	244.84	1.37	3.07
567.5	247.09	1.32	2.89
572.5	249.33	1.34	3.18
577.5	251.40	1.38	3.06
587.5	255.40	1.27	2.82
597.5	259.40	0.92	3.08
817.5	326.59		
827.5	331.02	0.92	2.85
837.5	335.46	1.17	2.80
842.5	337.67	1.14	3.00
847.5	339.89	1.15	3.12
852.5	341.88	1.08	3.28
857.5	343.64	0.96	3.61
862.5	345.40	1.17	3.13
867.5	347.16	1.09	3.24
877.5	350.68	1.01	3.06
887.5	354.19	1.17	2.92
1027.5	384.87		
1037.5	386.89	0.99	3.42
1047.5	388.90	1.31	3.09
1052.5	390.62	1.16	3.09
1057.5	392.42	1.20	3.62
1061.5	393.86	1.30	3.51
1067.5	396.03	1.24	3.11
1072.5	397.83	1.28	3.01
1077.5	399.63	1.41	3.01
1082.5	401.43	1.32	3.07
1087.5	403.23	1.48	3.05
1092.5	405.04	1.34	3.11
1097.5	406.84	1.39	3.01
1102.5	408.64	1.53	2.92
1107.5	410.44	1.34	2.74

1112.5	412.24	1.38	2.79
1117.5	414.05	1.34	2.76
1122.5	415.85	1.23	2.70
1127.5	417.65	1.28	2.94
1132.5	419.45	1.09	2.88
1137.5	421.25	1.03	3.08
1142.5	423.05	1.26	3.20
1147.5	424.86	1.11	3.10
1152.5	426.66	1.19	3.14
1157.5	428.46	1.18	3.16
1162.5	430.34	1.26	3.00
1167.5	432.25	0.90	3.97
1172.5	434.16	1.00	3.51
1177.5	436.07	0.91	3.52
1187.5	439.90	0.99	3.70

Table PS75/079-2

Depth (cm)	Age (Kyr)	<i>G. bulloides</i>	
		<i>Mg/Ca</i>	$\delta^{18}\text{O}$
2.5	15.06	1.03	3.13
7.5	16.38	0.95	3.34
12.5	17.70	1.18	3.52
17.5	19.02	0.95	3.96
22.5	20.34	0.71	3.68
462.5	115.90	0.88	2.76
472.5	121.84	0.99	2.74
477.5	124.81	1.04	3.08
482.5	127.78	1.00	2.77
487.5	130.75	1.31	2.84
492.5	133.73	1.17	2.59
497.5	135.21	1.42	2.14
502.5	136.09	1.21	2.98
507.5	136.97	1.37	2.81
512.5	137.85	1.43	3.01
517.5	138.73	1.00	2.91
857.5	210.56		
862.5	211.95	0.93	3.45
867.5	213.35	0.87	3.34
872.5	214.74	0.96	3.39
877.5	216.14		3.49
952.5	238.61	0.92	3.19
957.5	240.16	0.99	3.10
962.5	241.71	1.11	2.95

967.5	243.27	1.14	2.89
972.5	244.82	1.21	2.93
977.5	246.37	1.19	2.79
982.5	247.92	1.15	3.29
1352.5	335.30	0.96	3.01
1357.5	336.75	1.01	3.13
1362.5	338.19	1.15	2.87
1367.5	339.64	1.30	3.21
1377.5	342.38	1.22	2.84
1592.5	388.42		
1597.5	389.95		3.13
1602.5	391.47	1.13	3.34
1607.5	393.19	1.09	3.49
1612.5	396.85	1.21	3.09
1617.5	400.51	1.16	3.39
1622.5	404.17	1.14	3.21
1627.5	407.83	1.18	3.05
1632.5	411.50	1.21	3.10
1637.5	415.16	1.30	3.00
1642.5	418.82	1.16	2.88
1646.5	421.75	1.16	2.83
1652.5	426.11	1.02	3.16
1657.5	427.30	1.08	3.33
1662.5	428.49	1.00	3.41
1667.5	429.69	1.12	3.37
1672.5	430.88	1.10	3.70
1676.5	431.84	1.02	3.71
1682.5	433.27	0.96	3.67
1687.5	434.46	0.78	3.84
